理學博士 學位 論文

Selective Syntheses of Molecular Knot and [3]Catenane via Coordination-Driven Self-Assembly

(배위결합이 원동력인 자체조립을 이용한 분자매듭과 [3]카테네인의 선택적 합성)

蔚 山 大 學 校 大 學 院

化 學 科

金 東 煥

Selective Syntheses of Molecular Knot and [3]Catenane via Coordination-Driven Self-Assembly

指 導 敎 授　池 起 煥

이 論文을 理學博士 學位 論文으로 제출함

2020年 2月

蔚 山 大 學 校 大 學 院

化 學 科

金 東 煥

金 東 煥의 理學博士 學位 論文을 認准함

審査委員 양 성 봉 印

審査委員 이 민 형 印

審査委員 정 재 훈 印

審査委員 조 양 래 印

審査委員 지 기 환 印

蔚 山 大 學 校 大 學 院

2020年 2月

국문요약

카테네인, 로택세인, 매듭 및 고리와 같은 복잡한 위상의 응용은 분자기계, 근육, 스마트 소재나 나노 장치 등으로 응용되거나 발견되고 있다. 이렇게 복잡한 구조를 효과적이고 선택적으로 합성하기엔 아직 해결해야 할 많은 과제가 있어 이들의 실용적 응용을 위해서는 효율적인 합성전략이 절실히 필요하다. 한편, 지난 30년 동안 배위결합이 원동력인 자체조립을 이용하여 다양한 형상, 크기 및 기하학적 구조를 갖는 2차원 또는 3차원 모양의 초분자 합성이 획기적으로 가능하였다. 이는 배위결합이 생성되는 반응의 가역적 특성 때문에 열역학적으로 가장 안정한 초분자가 주 생성물로 제조된다는 기본 원리에 따라 미리 설계된 주개와 금속 받개를 사용함으로써 선택적이고 정량적으로 특정 초분자가 합성된 것이다. 이러한 접근방식으로 제조된 초분자는 촉매작용, 약물전달, 주인-손님 화학 및 분자인식과 같은 다양한 분야에 활용되어 왔다. 최근, 배위결합을 원동력으로 하는 자체조립 반응에 중간 생성물인 고리 내부 또는 고리 사이의 다양한 비공유 상호작용이 최종 생성물의 열역학적 안정성에 상승적으로 적용되도록, 적절한 작용기가 도입된 주개와 금속 받개를 자체조립 반응에 사용함으로써 다른 합성법으론 접근하기 어려운 복잡한 위상을 갖는 초분자를 성공적으로 합성하고 있다. 본 논문에서는 이렇게 배위 결합과 비공유 상호작용이 원동력인 자체조립을 이용하여 서로 얽혀진 위상과 복잡한 구조를 갖는 초분자 화합물의 선택적, 정량적 합성방법에 관하여 연구한 내용과 결과를 서술하고 있다. "배위결합이 원동력인 자체조립을 이용한 분자 매듭 및 [3]카테네인의 선택적 합성"이란 제목의 본 논문은 주개와 금속 받개, 농도 또는 용매의 변화에 따라 합성되는 거대고리 초분자의 구조와 그 위상 및 물리, 화학적 특성을 네 단원으로 구분하여 서술하였다.

Chapter 1은 초분자 자체조립 및 그 응용 분야에 관한 일반적인 내용을 소개한 것으로 금속-리간드 배위결합과 수소결합, π-상호작용 등 같이 주요한 비공유 상호작용에 관하여도 서술하였다. 본 논문의 주제인 배위결합을 원동력으로 하는 자체조립 반응과 그 결과로 얻어지는 열역학적으로 안정한 생성물에 관하여 논의하였다. 또한 본 논문에 배위결합이 원동력인 자체조립으로 제조된 초분자의 위상에 관한 연구결과가 2장, 3장 그리고 4장에 서술되어 있으므로 이들 단원과 연관된 기존 문헌들에 대해서 논의하였다. 배위결합이 원동력인 자체조립 반응의 결과는 다양한 응용에 성공적으로 적용되어 왔으므로 이 자체조립 생성물의 응용에 관련된 내용 역시 이 장에서 소개하였다.

Chapter 2는 분자 매듭 8_{18}의 합성과 그 특성에 관해 서술하였다. 루테늄(Ⅱ) 기반의 테트라센 받개와 다이피리딜 다이싸이에노싸이오펜 주개 사이의 배위결합과 고리내부 비공유 상호작용이 원동력인 자체조립 결과로 독특하고 복잡한 위상을 갖는 분자매듭 8_{18} 초분자를 효과적으로 합성할 수 있었다. 이 분자 매듭은 다양한 분광학적 방법과 신크로트론 방사를 이용한 단결정 엑스선 회절 연구를 통하여 그 구조를 완벽하게 규명하였다. 한편, 낮은 농도에서는 [2+2] 거대고리가 형성되는 것 또한 관찰할 수 있었다.

Chaper 3은 배위결합과 고리사이에 존재하는 비공유 상호작용 두 가지 힘이 원동력인 자체조립에 의해 선형 [3]카테네인이 선택적이고 정량적으로 합성되는 연구결과를 서술하고 있다. 트리아졸 기반의 주개와 나프탈렌 기반의 루테니움 받개가 배위결합이 원동력인 자체조립 반응에 사용되었고, 반응 중 고리사이에 존재하는 비공유 상호작용이 상승적으로 작동됨으로써 독특한 위상을 갖는 선형 [3]카테네인이 최종 초분자로 생성되었다. 농도 효과 및 파이렌 첨가 실험은 비공유 상호작용이 최종 생성물의 구조와 위상을 결정하는데 중요한 요인임을 보여준다.

Chapter 4는 배위결합과 고리사이의 비공유 상호작용 두 구성요소에 의한 자체조립 반응으로 독특한 위상과 구조인 폐쇄된-삼연접-사슬 초분자의 선택적이고 정량적인 합성에 대해 서술하였다. 벤즈이미다졸 기반의 주개와 이 주개가 갖는 회전 유연성으로 야기된 고리사이의 비공유 상호작용이 독특하고 새로운 위상의 초분자가 성공적으로 제조되는 주요 요인이다. 엑스선을 이용한 폐쇄된-삼연접-사슬 초분자 단결정의 위상 규명은 물론이고 더불어 폐쇄된-삼연접-사슬 초분자의 선택적이고 정량적인 합성법에 관한 세계 최초의 연구결과이다.

결론적으로, 배위결합과 고리내부 혹은 고리사이의 비공유 상호작용이 원동력인 새로운 자체조립 반응으로 복잡한 구조와 위상의 초분자가 선택적이고 정량적으로 만들어질 수 있다는 것을 증명하였다. 이 실험결과들은 주개와 금속 받개에 다양한 작용기를 적절한 조합으로 장착시킴으로써 고리내부 또는 고리사이의 비공유 상호작용이 상승적으로 작동하게 함이 복잡하고 독특한 구조와 위상을 갖는 초분자를 합성하는데 중요한 조건임을 말해주고 있다.

Abstract

Applications for non-trivial topologies, such as catenanes, rotaxanes, knots and links, have been found in molecular machines and muscles, smart materials and nanoscale devices. However, the selective synthesis of these complex structures still represents a great challenge. Therefore, strategies that are more efficient are highly desired for their practical applications. Over the past three decades, the use of coordination-driven self-assembly has simplified the production of 2D and 3D supramolecular architecture of various shapes, sizes and geometry. Due to the reversibility of the coordination bond, more thermodynamic products tend to favor, and thus give rise to selective and quantitative formation of the pre-designed product. The supramolecules obtained by using this approach have been utilized for various applications, such as catalysis, drug delivery, host-guest chemistry and molecular recognition. Recently, the concept of coordination-driven self-assembly along with inter- or intra-cycler NCIs has been successfully applied for the construction of various complex molecular topologies. Selective and quantitative syntheses of interlocked compounds via coordination-driven self-assembly present some important advantages in supramolecular chemistry. The thesis entitled “Selective Synthesis of Molecular Knot and [3]Catenane via Coordination-Driven Self-Assemblies” presents the results obtained from the research work carried out on the synthesis, characterization and exploration of the chemistry of metal-based acceptors, ditopic donors and their corresponding supramolecular metallomacrocycles. The accompanied research work has been divided into the following four chapters:

Chapter 1 gives a general introduction on the supramolecular self-assembly and its applications. A general introduction on important non-covalent interactions (NCIs) is provided, such as hydrogen bonding, π-interactions and metal-ligand coordination. As the work carried out in this thesis encompasses a coordination-driven self-assembly and corresponding thermodynamic stable product, the introduction on these topics have been covered. Since the second, third and fourth chapters of this thesis include work on the formation of molecular topology via coordination driven self-assembly, the related literature is discussed in this chapter. The concept of coordination-driven self-assembly has been successfully applied in various applications. Therefore, a related introduction on the applications of self-assembled products is also provided in this chapter.

Chapter 2 describes the synthesis and characterization of a molecular knot 8_{18}. A coordination-driven self-assembly of Ru(II)-based tetracene acceptor and dipyridyl dithienothiophene donor along with intracycler NCIs results in the isolation of the unique and novel supramolecular topology. We also observed the formation of [2+2] macrocycle at lower concentrations. The molecular knot obtained was fully characterized by various spectroscopic techniques, including single-crystal X-ray diffractions study via the use of synchrotron radiations.

Chapter 3 describes the selective and quantitative syntheses of a linear [3]catenane by two component coordination-driven self-assembly and intercycler NCIs. Triazole-based donors and naphthalene-based acceptors were used for the coordination-driven self-assembly reaction, which enabled the formation of a linear [3]catenane topology

through synergistic non-covalent intercycler interactions. The concentration-based and/or pyrene addition experiments show the importance of synergistic NCIs.

Chapter 4 describes the selective and quantitative syntheses of a closed three-linked chain by two component coordination-driven self-assembly and intercycler NCIs. Moderate flexibility of the benzimidazole–based donor was utilized along with intercycler NCIs to synthesize the novel topology. This is the first example of selective and quantitative synthesis, along with the first X-ray characterization of the topology of the closed three-linked chain.

In conclusion, a new approach that utilizes the coordination-driven self-assembly and inter or intra cycler NCIs for the construction of complex supramolecular topologies has been demonstrated. The experimental results show that the right combination of functional groups in combining units facilitating inter- and/or intra-cycler NCIs is an important requirement for the selective synthesis of supramolecules with complex and higher-order topologies.

Index

Scheme index

Table index

Figure index

Chapter 1 General introduction

1.1 Supramolecular chemistry and self-assembly

Supramolecular chemistry[1] has mainly found its inspiration in biological systems, such as nucleic acids, protein complexes, enzymes and viruses, etc.[2] The design and synthesis of supramolecular systems have received immense attention because of their importance in mimicking sophisticated biological functions.[3] A supramolecular complex is a result of self-assembly between multiple small components that are held together by various intermolecular interactions.[4] In nature, supramolecular self-assembly via non-covalent interactions determined the structure and functions of biological systems, such as DNA, proteins, enzymes, viruses, biological ribosomes and mitochondria.[5] Therefore, an understanding of supramolecular self-assembly and intermolecular interactions is crucial for the design and synthesis of novel biomolecules. In contrast to molecular synthesis by forming covalent bonds that require human intervention, self-assembly is a bottom-up approach that combines individual components through molecular recognition to generate a single thermodynamically favored product. The self-assembly of multiple components generate well-defined supramolecular architectures under the given set of conditions, such as metal-ion templating, non-covalent interactions driven and coordination driven, among others.[6] The concept of supramolecular chemistry and self-assembly has been successfully applied to molecular recognition, host–guest chemistry, molecular self-assembly, mechanically interlocked or intertwined compounds, molecular folding and dynamic covalent chemistry.[7] Recent advances in this field have led to the development of a vast variety of supramolecular systems, which found application in catalysis, drug-delivery, Nano-chemistry, Nano-medicine, crystal engineering and so on.[8] Supramolecular self-assembly has emerged as a multidisciplinary area providing opportunities to scientists working in diverse areas, such as chemistry, physics, biology, mathematics, polymer chemistry, material science, Nano-chemistry and so on. Recently, the concept of supramolecular self-

assembly has been applied in the construction of interlocked and intertwined compounds, such as catenanes, rotaxanes, knots and links.[9] These complex supramolecules due to their unique intercycler moments found application in molecular muscles and machine and Nano devices. Recent advances in the field of supramolecular self-assembly and the availability of powerful synchrotron X-ray diffraction analysis has attracted the interest of chemists of all disciplines.

1.2 Metal-ligand coordination

Some important examples of metal-ligand coordination[10] in biology include; hemoglobin in human blood, chlorophyll in green plants and vitamin B-12 etc. Metal-ligand coordination has been extensively used in all disciplines of chemistry, including organometallic chemistry, inorganic chemistry, organic catalysis and supramolecular chemistry.[11] It is well known that novel materials and unique properties can be obtained from metal complexes obtained by the metal-ligand coordination. As compared to organic counterparts, these metal complexes can exhibit different properties due to the presence of metal, metal-ligand coordination and other NCIs. Metal ions are positively charged species. However, depending on the coordination environment delivered by ligands it can be cationic, anionic or neutral.[12]

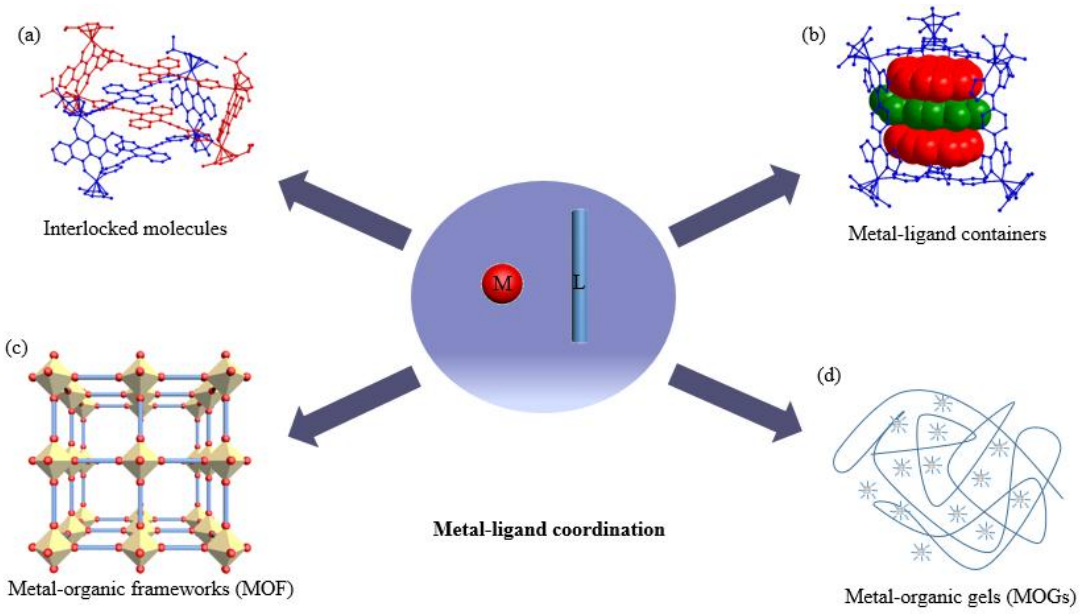

Figure 1.1 Utilization of metal-ligand coordination for various applications.

Interactions between metal ions and ligands are selective and reversible, and the overall properties of the resulting complexes are unique from the individual metal or ligand. In case of transition metals, the presence of d-orbitals provides interesting properties to the resulting complexes. Apart from their structures, the metal-ligand complexes can be used in acid−base catalysis, ligand exchange, electron transfer and redox reactions, etc. In addition, properties of certain metals ions, such as luminescence and magnetic resonance radioactivity, have been utilized in various applications, such as subcellular imaging agents, metal-responsive MRI imaging, PET imaging etc. Metal coordination has found important role in material chemistry, reticular chemistry, supramolecular topology, polymer chemistry and biochemistry. Metal ions–ligand interactions have been widely explored for the synthesis of metal coordination networks, metal-organic frameworks and self-assembling 2D and 3D supramolecular complexes.[13]

NCIs also play a vital role in the construction of complex supramolecular topologies.[14] Interlocked or intertwined compounds (e.g. catenanes, rotaxanes and knots) have had attractive and extensive attention in the recent years due to their

unique ability to molecular motion, as well as their promising application in smart materials and nanoscale devices.[15] Since these complex topologies would not have been feasible through traditional routes, chemists have developed various methodologies to realize these interlocked or intertwined species. Among all the reported strategies, the metal-ion template followed by ring closing and electron deficient/electron-rich π—π template have been sucessfully employed for the production of a number of complex topologies, such as catenenes, rotaxanes, knots etc. In these aformentioned methods, NCIs play a crucial role in bringing two moieties together by inter- or intra-cycler interactions, such as π— π and CH— π etc.[16]

1.3 Non-covalent interactions

Non-covalent interactions (NCIs) refer to the attractive force between the molecules or functionalities that are not covalent in nature.[17] These NCIs are strong enough to hold the molecules or structures in a particular orientation or conformation. The common types of NCIs include hydrogen bonding, dipole-dipole interactions, π-interactions, van der Waals interactions, and coordination bond.[18] Biological molecules utilize multiple NCIs (such as hydrogen bonding, electrostatic and hydrophobic interactions) to carry out various important functions with reversibility, specificity and flexibility. NCIs have much weaker strength and distances (2-20 kcal, >2 Å) as compared to covalent bonds (100-120 kcal, < 2 Å). However, the strength of NCIs lies in unity (synergy) and large numbers, which help them to govern important biological and chemical processes.[19] Table 1.1 shows the comparison of a covalent bond with non-covalent interactions.

Interaction	Strength
Covalent Bond	200–400 kJ mol^{-1}
Hydrogen Bonding	4–120 kJ mol^{-1}

Dipole-Dipole	5–50 kJ mol^{-1}
Cation-π	5–80 kJ mol^{-1}
π–π	0–50 kJ mol^{-1}
van der Waals	< 5 kJ mol^{-1}

Table 1.1: Comparison of strength and bond distance between covalent bond and non-covalent interactions

As a result of these NCIs, only four types of bases construct the whole double helix structure of a DNA, which contain all the genetic information of an organism. The structures of proteins, specific binding in enzymatic reactions and aggregations of four polypeptides to form hemoglobin are some few but important examples of the summation of multiple intermolecular NCIs. Inspired by biological processes, chemists have utilized weak but pivotal NCIs in supramolecular chemistry for catalysis, host-guest chemistry and molecular recognition.[20] In catalysis, the NCIs provide stability to the transition state by lowering the free energy of catalyst-substrate complex. NCIs between host-guest molecules can change the characteristics of the encapsulated species. Molecular recognition by inter- or intra-molecular NCIs, such as π— π and CH— π, can influence the structural outcome and molecular topology. As a consequence, properties of new material can differ from the individual components. All different types of non-covalent interactions, such as hydrogen bonding, van der Waals forces, coulombic interactions, charge transfer complexes, and hydrophobic effect strongly affect the structure and function of supramolecular systems.

1.3.1 Hydrogen bonding

One of the most important non-covalent interactions is the hydrogen bonding between an electronegative atom (A) attached to a hydrogen atom (H) and another nearby electronegative atom (X) having lone pair of electrons.[21] Hydrogen bonding is generally denoted by A–H···X, where the solid line denotes a fully covalent bond,

while the dotted or dashed line indicates the hydrogen bond. Intermolecular and intramolecular hydrogen bonding are two types of dipole-dipole interactions between molecules or within molecules. The bond enthalpy of a hydrogen bond varies according to the electronegative values of the attached atoms. For example, the bond enthalpy of a typical hydrogen bond is 3-7 kcal mol^{-1}, while its value is 38.6 kcal mol^{-1} for F-H--F^-. Table 1.2 shows the bond enthalpies of common hydrogen bonds.

Hydrogen bond	**Bond enthalpy**
N—H···O	1.9 kcal mol^{-1}
N—H···N	3.1 kcal mol^{-1}
HO—H···OH_3^+	4.3 kcal mol^{-1}
O—H···O	5.0 kcal mol^{-1}
O—H···N	6.9 kcal mol^{-1}

Table 1.2: Comparison of hydrogen bond strengths

Due to the NCIs, water molecules attract each other and the formation of hydrogen bonds occur, and due to these interactions water has its high boiling point and surface tension. Although the strength of the hydrogen bond is much weaker than a covalent bond, large numbers give characteristics to these interactions. Conversely, a hydrogen bond is almost 10 times stronger as compared to other NCIs. Particularly, hydrogen bonding has great importance in biology. Most of the biological molecules involve these hydrogen bonding interactions. For example, two strands of DNA are held together because of the hydrogen bond between the corresponding nucleotides: where adenine binds with thymine (A&T), while guanine binds with cytidine (G&C).[22],[23]

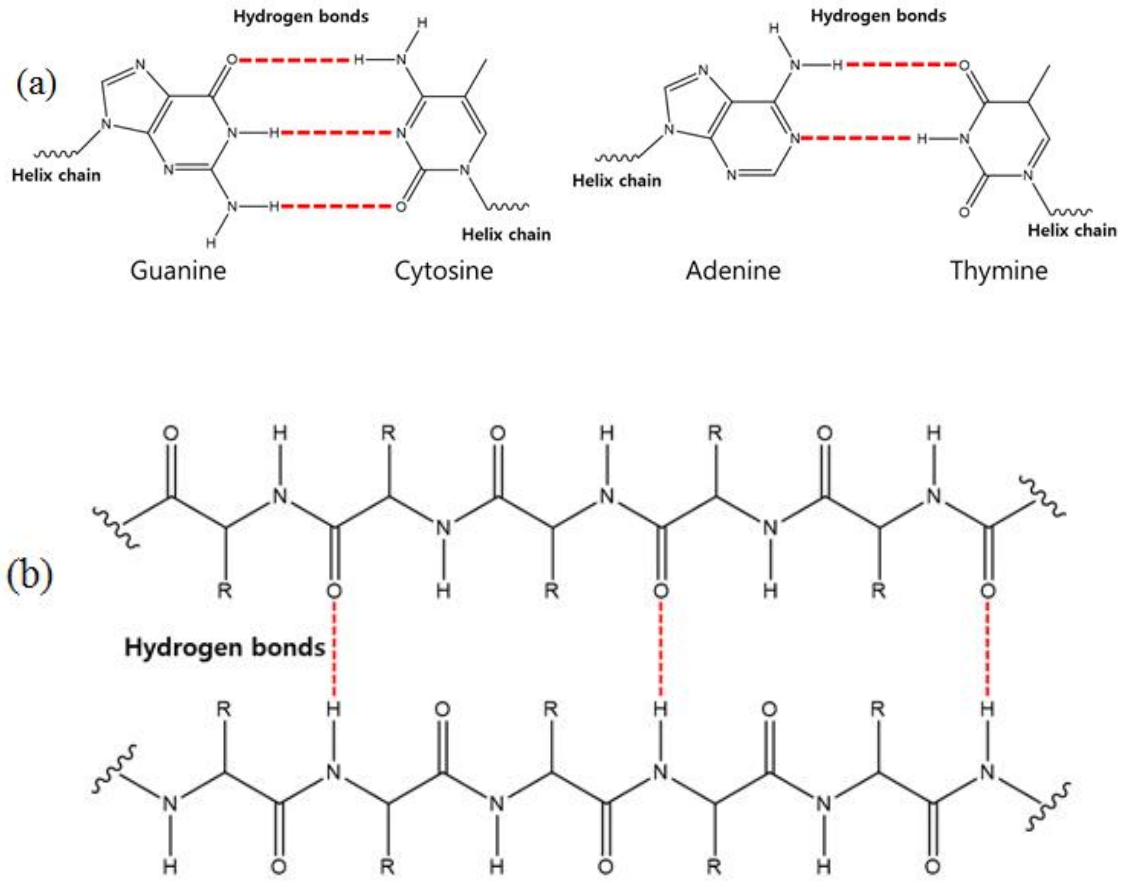

Figure 1.2 Hydrogen bonding interactions in biomolecules (a) DNA (b) Proteins (α-Helices β-Sheets)

The secondary, tertiary and quaternary structures of proteins exist due to intermolecular hydrogen bonding. These interactions between amino acids determine the configuration of the protein molecules. Apart from their biological importance, hydrogen bonds have an important role in supramolecular chemistry. Most importantly, their strength and directionality have been utilized in the construction of supramolecular architectures. These supramolecular complexes can be selectively constructed via the self-assembly of simple building blocks exploiting hydrogen bonding interactions and other NCIs. Self-assembly through multiple hydrogen bonding interactions has been utilized in various fields, such as material, supramolecular and polymer chemistry, crystal growth, metal-organic frameworks and molecular topology. Particularly, host-guest chemistry and molecular sensing

through these interactions has been utilized in recent years. In contrast to traditional bonds, such as the covalent bond, the reversibility of hydrogen bonds results in the formation of a thermodynamic stable product with higher selectivity. By utilizing the strength, directionality and reversibility of hydrogen bonds, the design and synthesis of complex biomolecules is the main goal of supramolecular chemists.[24],[25]

1.3.2 π-interactions and various π interactions

In biology and chemistry, π-π interactions are another important class of NCIs that involve the attraction between π-systems.[26],[27] These interactions are the result of intermolecular overlapping of p-orbitals between the π-electron containing conjugated systems. Although these interactions are weaker in comparison to hydrogen bonding, there strength depends on the number of conjugated π-electrons.[28] For example, molecules with flat rings, such as naphthalene, anthracene, triphyelene and pyrene, etc., have strong π- π interactions. The common type of these π interactions involves: π-π stacking, metal-π, anion- π, cation- π and CH- π interactions.[29] The complication in understanding these interactions generates from different geometry and energies. However, the interactions involving π-systems are very important in biological functions, such as protein-ligand recognition, nucleobase stacking between DNA and RNA molecules and protein folding. π-interactions also play an important role in various chemical transformations.[30] For instance, π-metal bonding during a catalytic transformation plays an important role in pushing the reaction to completion. In addition, π-interactions lower the transitions state by lowering the free energy of ligand-metal complex. Some notable examples of reactions involving π-metal interactions are; Suzuki reaction, Sonogashira coupling, Negishi coupling and Heck reaction.[31] From the aforementioned reactions, the π-interactions with Pd catalysis are pivotal for the formation of coupling product. π-π interactions or π-stacking play an enormous role in supramolecular chemistry and are important building blocks for the constructions of 2D and 3D architectures.[32]

Specifically, π-stacking have been widely used in supramolecular self-assembly and molecular recognition. The syntheses of interlocked molecules, such as catenanes, are important examples of intercycler π-π interactions. Stoddart and co-workers extensively utilized π-π interactions for the construction of a variety of complex molecular topologies, and it was the subject of 2016 Noble prize in Chemistry.[33] ^{1}H-NMR spectroscopy was found to be helpful in the identification of these interactions as changes in the aromatic protons occurred, e.g. the upfield shift of phenyl protons due to the stacking interactions. A benzene dimer is an ideal system to describe the existence of π-interactions and a prototype for experimental and computational studies. The commonly observed π-interactions between aromatic systems are shown in figure 1.3.

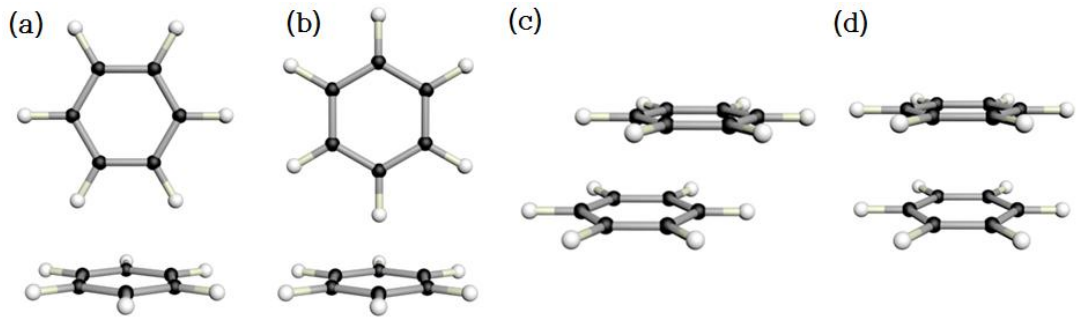

Figure 1.3 Diagram showing π-interactions in a benzene molecule (a) T-shaped (or edge-to-face) (b) T-shape tilted (c) Paralleled displaced (or off set) (d) stacking (face to face)

The parallel displaced π-interactions and CH- π interactions are commonly observed geometry in biology and chemistry. By taking the advantage of π-stacking, a large number of host-guest models have been developed in supramolecular chemistry. Therefore, the study and understanding of π-interactions can be utilized for drug delivery systems, biomolecules and biomedicines.[34] In addition, the self-assembling properties of these interactions can be used for the construction of supramolecular topologies in material science, which can find application in Nano-machines and Nano-devices.

1.4 Coordination-driven self-assembly

Recent years have seen a remarkable upsurge in the design, self-assembly and application of multifunctional supramolecules materials.[35] In this regard, bottom-up coordination-driven self-assembly[36], which combines metal-based acceptors and organic donors, emerged as a powerful approach for the construction of a vast variety of 2D and 3D supramolecular architectures of predetermined shapes, sizes and geometry.[37] For example, electron-deficient metals, such as Pd(II), Pt(II), Ru(II) and Ir(III), are often used in combination with electron-rich nitrogen-containing pyridyl moieties. This direction bonding approach has a range of potential applications in chemical and biological sciences. In the past few years, a vast variety of supramolecular complexes have been obtained, which found application in catalysis, host-guest chemistry, molecular recognition and drug-delivery.[38]

1.4.1 Coordination-driven self-assembly and thermodynamic product

The outcome of coordination-driven self-assembled products depends on the information coded in the components.[39] Bond strength and distance of a coordination bond is found in between covalent and non-covalent bonds. Due to the reversible nature of a coordinate bond, thermodynamically favored and stable products will appear despite the use of multicomponent species.[40] For example, the combination of a ditopic linear acceptor oriented at 90^{o}C and a ditopic donor oriented at 180^{o}C will result in the formation of [4+4] square.[41]

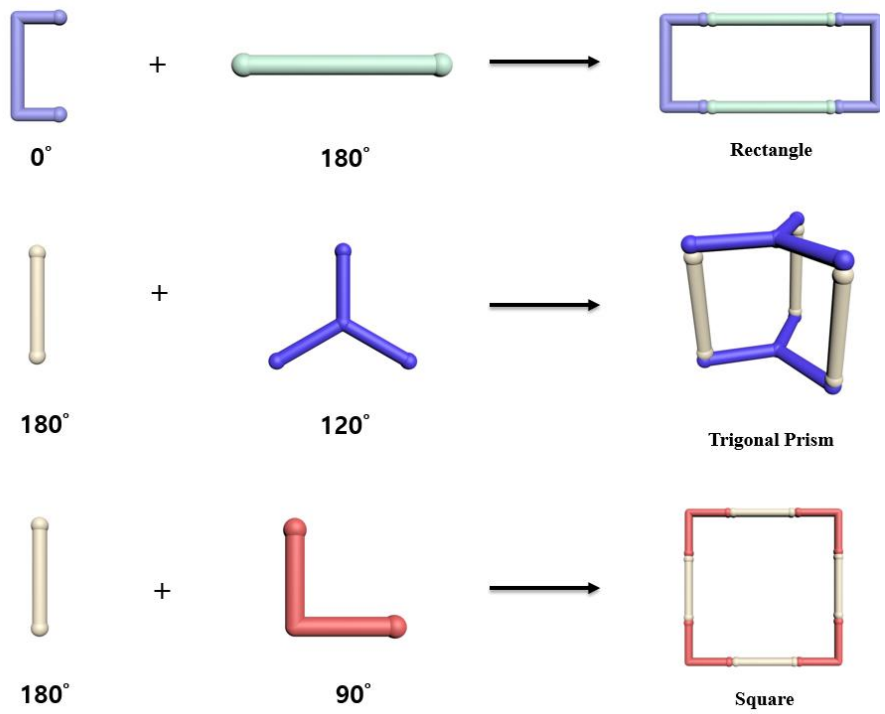

Figure 1.4: Coordination-driven self-assembly approach to the construction of 2D metallacycles from predesigned components of various shapes, size and geometry.

1.4.2 Design molecular architectures via coordination-driven self-assembly

Coordination-driven self-assembly of two or more components incorporated with multiple NCIs, such as π— π and CH— π, has been regarded as the most promising way of supramolecular topology production.[42]

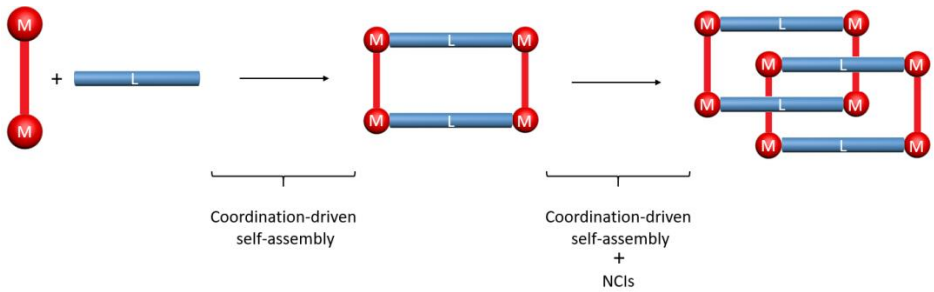

Figure 1.5 Supramolecular topologies by the synergistic use of coordination-driven self-assembly and intercycler NCIs

1.4.2.1 Topologies utilizing coordination-driven self-assembly and Intercycler NCIs:

1.4.2.1.1 Topology of [2] catenane

In 2015, Chi and coworker reported the first example of a [2]-catenane synthesized by coordination-driven self-assembly.[42] Tetracene-based dinuclear Ru(II) acceptor and anthracene-based ditopic pyridyl donor were utilized for the self-assembly reaction, which in nitromethane or methanol (0.5mM) resulted in the formation of a [2+2] monorectangle, Whereas, concentrated reaction mixtures in methanol result in the formation of the topology of [2]-catenane. (figure 1.6, a)

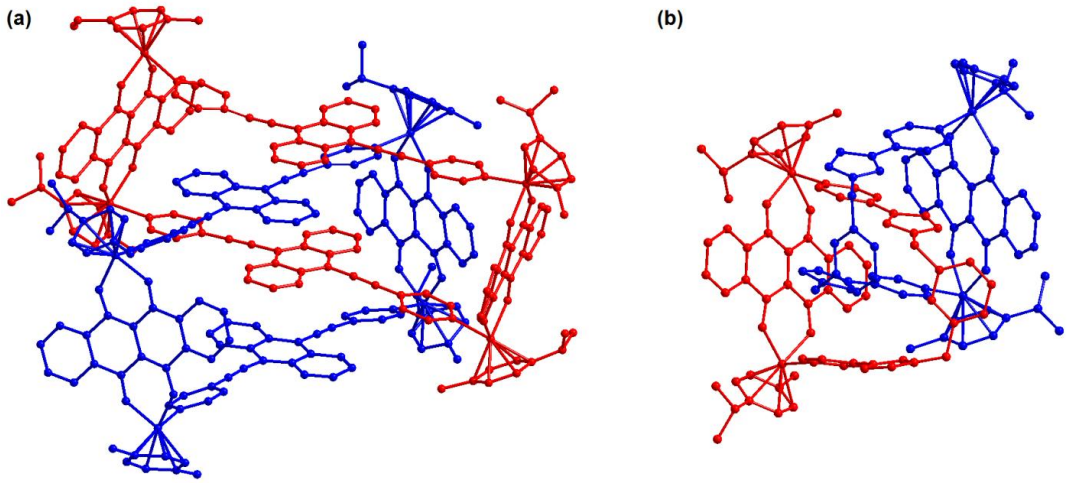

Figure 1.6 Molecular structures of [2] catenane topology obtained via the coordination-driven self-assembly and intercycler NCIs.

In a similar study, [2] catenane was obtained from the coordination-driven self-assembly of two [1+1] monorectangles using tetracene Ru(II) acceptor and dipyridyl donor.[43] The $[1+1]_2$ st were well established by ESI-MS, detailed NMR and single-crystal X-ray analyses.

1.4.2.1.2 Topology of Solomon link

In 2016, Chi and coworkers reported the first example of a Solomon link obtained by the coordination-driven self-assembly of two [2+2] monorectangles.[44] The appropriate geometry of a dipyridyl carbazole donor and synergistic intercycler NCIs arise from the presence of π—rich Ru(II) tetracene acceptor and results in the formation of this doubly interlocked topology. Detailed analysis of crystal structure revealed the presence of multiple strong π— π and CH—π interactions between donor and acceptor moieties.

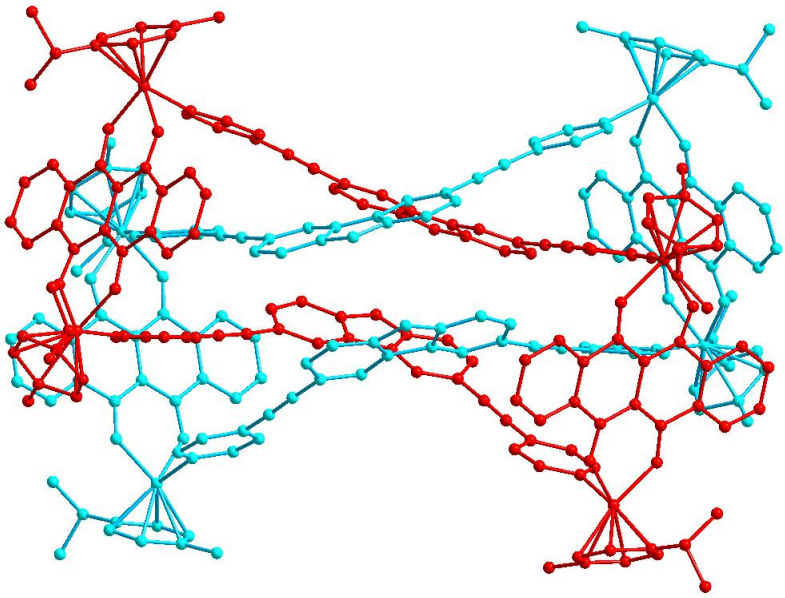

Figure 1.7 Molecular structure of Solomon link topology obtained via the coordination-driven self-assembly and intercycler NCIs.

1.4.2.1.3 Topology of "ring-in-ring" structure

In 2011, Stang, Chi and coworkers reported the formation of a non-catenane interlocked "ring-in-ring" topology by the coordination-driven self-assembly of tetracene Ru(II) acceptor and 1, 4-di(pyridine-4-yl)buta-1,3-diyne donor.[45]Appropriate length of the donor with respect to tetracene acceptor lead to

the intercycler π—π interactions, which results in the formation of the ring-in-ring topology. Similar "ring-in-ring" topology using Ir(III) acceptor and same donor was reported by Chi and coworkers in 2017.[46] Both examples show the same set of π—π interactions between the acceptor and donor moieties.

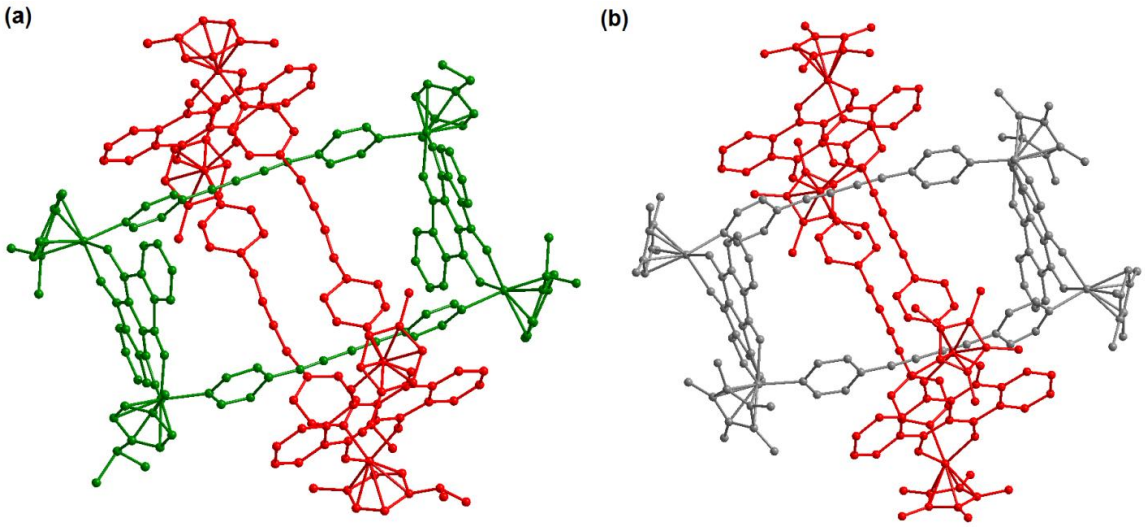

Figure 1.8 Molecular structure of "ring in ring" topology obtained via the coordination-driven self-assembly and intercycler NCIs.

1.4.2.1.4 Topology of Borromean rings (BRs)

Molecular BRs are interlocked molecules consisting of three chemically independent rings that are locked in such a way that no two of the three rings are attached to each other.[47] Chi and coworkers reported the formation of the Borromean ring using tetracene-based Ru and Ir acceptors and ditopic pyridyl donors.[48] Compounds were characterized by various spectroscopic techniques, including single-crystal X-ray diffraction studies. Concentration based titration experiments show sequential transformation of a fully characterized monomeric rectangle to molecular BRs and vice versa. Furthermore, the addition of π—rich pyrene hindered the formation of molecular BRs, which highlights the importance of intercycler NCIs.

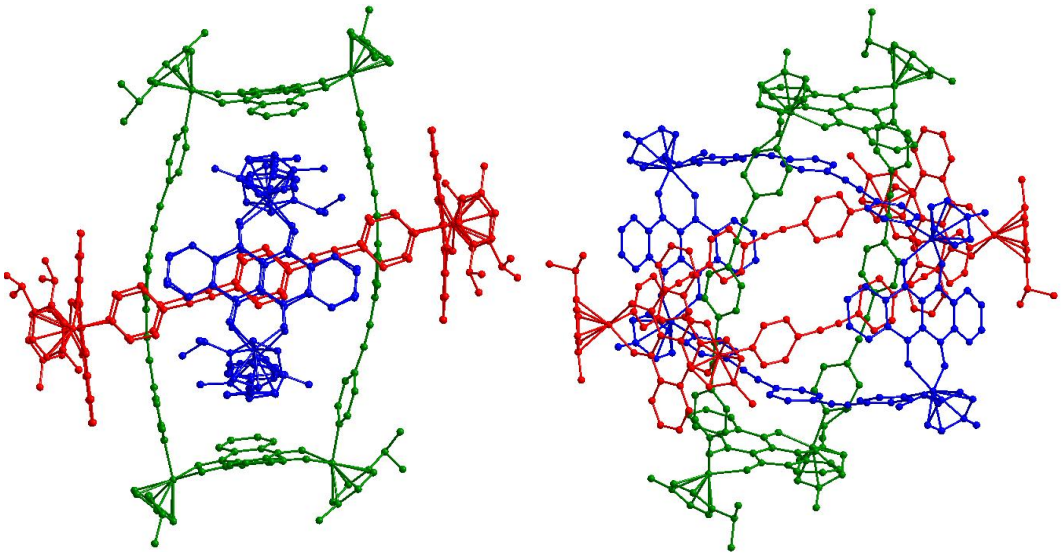

Figure 1.9 Molecular structure of Borromean ring topology obtained via the coordination-driven self-assembly and intercycler NCIs.

In addition to the aforementioned topologies, recent reports by our groups show the selective and quantitative formation of non-trivial topologies via corodination-driven self-assembly and intercycler NCIs. In this thesis, we will discuss the synthesis and application of the supramolecules obtained by our group via coordiantion-driven self-assembly.

1.4.3 Application

The concept of coordination-driven self-assembly has been successfully applied in the isolation of supramolecules of various shapes, sizes and geometry. Moreover, these 2D and 3D supramolecules have been successfully applied in various applications, such as host-guest chemistry, molecular recognition, catalysis and biological studies.[49]

1.4.3.1 Host-guest chemistry and molecular recognition

Supramolecular cage molecules that are capable of accommodating guest molecules have received tremendous attention owing to their various potential applications, such as containers for labile chemical species, molecular flasks for chemical reactions, drug delivery, stacking of aromatic molecules and sensing.[50] In this regard, coordination-driven self-assembly emerged as a powerful approach for the design and synthesis of container molecules of various shapes, sizes and geometry. Two components or multicomponent coordination-driven self-assembly of square planner metal [Pd(II) and Pt(II)] acceptors and multitopic pyridyl donor have been extensively used for the construction of polyhedras, spheres, cubes and prisms.[51] Recently, the two component self-assembly using Ru(II) or Ir(III) also gained attention due to their potential application in drug-delivery, catalysis, host-guest chemistry and molecular topology. Our group has made significant efforts for the selective and quantitative synthesis of 2D and 3D supramolecules by using the two component coordination-driven self-assembly. In 2008, Therrin and coworkers reported the coordination-driven self-assembly of a Ru(II)-based prismatic cage, which was able to accumulate $M(acac)_2$ (M=Pd, Pt; acac=acetylacetonate) inside its cavity to form "complex-in-a-complex" derivative.[52] In 2011, we reported the design and preparation of novel M_3L_2 trigonal cages by using coordination-driven self-assembly of pre-organized metalloligands containing octahedral aluminum(III), gallium(III) or ruthenium(II) centers along with ditopic or tritopic metalloligands.[53] Due to the presence of electron rich ethynyl functionalities and flourescent nature of these molecule, they have been utilized in the detection of nitro aromatics. In 2015, our group reported the template-free coordination-driven self-assembly of two components to form a large prismatic cage, which was capable of encapsulating three planar hetero-guests through π–π stacking (figure 1.10).[54] The supramolecular complex has been obtained in good yield and was characterized by various spectroscopic techniques, including the single-crystal X-ray diffraction analysis.

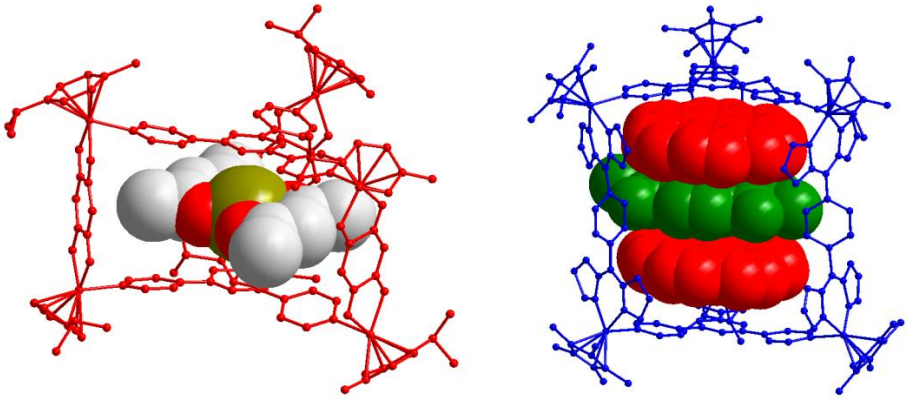

Figure 1.10 (a) coordination-driven self-assembly of a Ru(II)-based "complex-in-a-complex" derivative (b) **t**emplate-free coordination-driven self-assembly of two components to form a large prismatic cage which was capable of encapsulating three planar hetero-guests through π–π stacking

1.4.3.2 Biological studies

Since the success of a platinum-based drug, namely cisplatin, there has been increasing interest in the development of alternative metal-based drugs.[55] Due to their promising biological properties of Ru(II), there is great interest in developing new molecules for drug discovery programs. Ru-based coordination complexes that have anticancer activities provide promising alternatives to platinum-based drugs. NAMI-A and KP1019 are two Ru-based coordination complexes to enter clinical trials.[56]

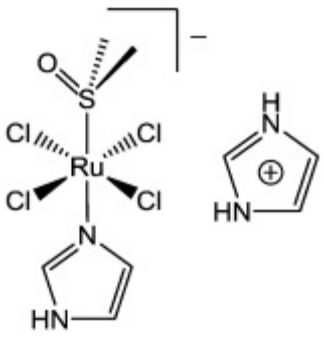

Figure 1.11: Chemical structure of NAMI-A (Imidazolium *trans*-imidazoledimethylsulfoxidetetrachloro-ruthenate)

Most of the ruthenium complexes are hexacoordinate or octahedral, and are capable of adopting oxidation states II, III and IV. In addition, the ligand exchange rate for ruthenium complexes is slow, which provides kinetic stability and minimize side reactions. In vivo, the Ru(III) complexes are reduced to corresponding Ru(II) complexes-a main reason for its antitumor properties. The exact mechanism action of Ru-based drugs is not known. However, data suggests that Ru(II) complexes are capable of binding DNA and RNA. Our group and others have extensively studied the antiproliferative properties of Ru(II)-based supramolecules obtained by the coordination-driven self-assembly.[57] Ruthenium-based 2D and 3D supramolecules, such as molecular rectangles and cages, are important because of their easy synthesis. In addition, these supramolecules have high nuclearity and synergic effects of incorporated functionalities. Till date, a number of Ru(II)-based metallomacrocycles have been reported for their anticancer activity.[58] In addition, the container molecules discussed in the previous section have been used in drug-delivery. Furthermore, recent reports use the characteristic green fluorescence of a BODIPY donor, which along with Ru(II) moieties are able to interact with DNA and protein molecules.[59] Some of the representative examples are shown in figure 1.12.

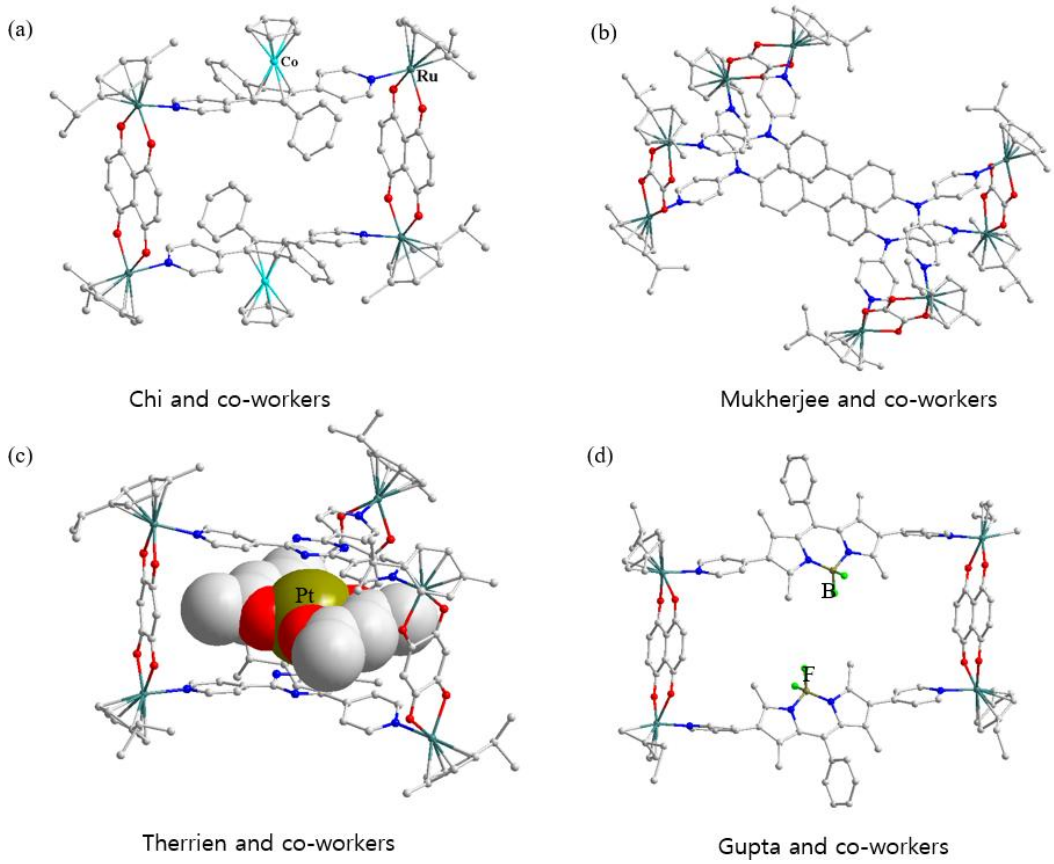

Figure 1.12 representative examples of Ru-based supramolecules used for biomedical applications.

1.5 Reference

1. Steed, J. W.; Atwood, J. L. *Supramolecular Chemistry;* Wiley, **2013**.

2. Hannon, M. J. *Chemical Society Reviews* **2007**, *36*, 280.

3. (a) Wilson, A. J. Supramolecular Chemistry. *Annu. Reports Sect. "B" (Organic Chem.* **2007**, *103*, 174. (b) Mattia, E.; Otto, S. *Nature Nanotechnology* **2015**, *10*, 111–119. (c) Sanders, J. K. *Angewandte Chemie International Edition* **1995**, *107*, 2617–2617.

4. (a) Sanders, J. K. *Angewandte Chemie International Edition* **1995,** *107,* 2617. (b) Philp, D.; Stoddart, J. F. *Angewandte Chemie International Edition* **1996**, *35*, 1154-1196. (c) Lehn, J.-M. *Proceedings of the National Academy of Sciences* **2002**, *99*, 4763-4768. (d) Whitesides, G. M.; Boncheva, M. *Proceedings of the National Academy of Sciences* **2002**, *99*, 4769-4774. (e) Hof, F.; Rebek, J. *Proceedings of the National Academy of Sciences* **2002**, *99*, 4775-4777.

5. (a) Lehn, J.-M. *Chemical Society Reviews* **2007**, *36*, 151. (b) Steed, J. W.; Turner, D. R.; Wallace, K. *Core Concepts in Supramolecular Chemistry and Nanochemistry; Wiley,* **2007**. (c) Cann, A. J. *Principles of Molecular Virology (Standard Edition); Elsevier Science*, **2001**. (d) Uchida, M.; Klem, M. T.; Allen, M.; Suci, P.; Flenniken, M.; Gillitzer, E.; Varpness, Z.; Liepold, L. O.; Young, M.; Douglas, T. *Advanced Materials* **2007**, *19*, 1025-1042.

6. (a) Zan do, E.; Casanova, M.; Alessio, E. *Chemical Reviews* **2008,** *108,* 4979-5013. (b) Fujita, M. *Chemical Society Reviews* **1998,** *27,* 417-425. (c) Cotton, F. A.; Lin, C.; Murillo, C. A. *Accounts of Chemical Research* **2001**, *34*, 759-771. (d) Li, S.-S.; Northrop, B. H.; Yuan, Q.-H.; Wan, L.-J.; Stang, P. J. *Accounts of Chemical Research* **2009**, *42*, 249-259.

7. (a) Whitesides, G. M.; Grzybowski, B. *Science* **2002,** *295,* 2418-2421. (b) Leininger, S.; Olenyuk, B.; Stang, P. J. *Chemical Reviews* **2000,** *100,* 853-908. (c) Holliday, B. J.; Mirkin, C. A. *Angewandte Chemie International Edition* **2001,** *40,* 2022-2043. (d) Seidel, S. R.; Stang, P. J. *Accounts of Chemical Research* **2002,** 35, 972-983. (e) Fujita, M.; Tominaga, M.; Hori, A.; Therrien, B. *Accounts of Chemical Research* **2005**, *38*, 369-378. (f) Oliveri, C. G.; Ulmann, P. A.; Wiester, M. J.; Mirkin, C. A. *Accounts of Chemical Research* **2008**, *41*, 1618-1629. (g) De, S.; Mahata, K.; Schmittel, M. *Chemical Society Reviews* **2010,** *39,* 1555-1575.

8. Kolesnichenko, I. V.; Anslyn, E. V. *Chemical Society Reviews* **2017**, *46*, 2385–2390.

9. Au-Yeung, H. Y.; Yee, C.-C.; Hung Ng, A. W.; Hu, K. Strategies To Assemble Catenanes with Multiple Interlocked Macrocycles. *Inorganic Chemistry* **2018**, *57*, 3475–3485.

10. Khusnutdinova, J. R.; Milstein, D. *Angewandte Chemie International Edition* **2015**, *54*, 12236-12273.

11. (a) McConnell, A. J.; Wood, C. S.; Neelakandan, P. P.; Nitschke, J. R. Stimuli-Responsive Metal–Ligand Assemblies. *Chemical Reviews* **2015**, *115*, 7729–7793. (b) Almeida Paz, F. A.; Klinowski, J.; Vilela, S. M. F.; Tomé, J. P. C.; Cavaleiro, J. A. S.; Rocha, *Chemical Society Reviews* **2012**, *41*, 1088–1110. (c) Eddaoudi, M.; Moler, D. B.; Li, H.; Chen, B.; Reineke, T. M.; O'Keeffe, M.; Yaghi, O. M. *Accounts of Chemical Research* **2001** *34*, 319-330. (d) Sabbatini, N.; Guardigli, M.; Lehn, J.-M. *Coordination Chemistry Reviews.* **1993**, *123*, 201–228. (e) Zeng, F.; Zimmerman, S. C. *Chemical Reviews* **1997**, *97*, 1681–1712.

12. Birk, J. P.; Foster, J. *Journal of Chemical Educations* **1993**, *70*, 460.

13. Furukawa, H.; Cordova, K. E.; O'Keeffe, M.; Yaghi, O. M. *Science* **2013**, *341*, 1230444–1230444.

14. Zhou, H. C.; Long, J. R.; Yaghi, O. M. *Chemical Reviews* **2012**, *112*, 673-674.

15. Neel, A. J.; Hilton, M. J.; Sigman, M. S.; Toste, F. D. *Nature* **2017**, *543*, 637–646.

16. Černý, J.; Hobza, P. *Physical Chemistry Chemical Physics*. **2007**, *9*, 5291–5303.

17. Waters, M. L. *Accounts of Chemical Research* **2013**, *46*, 873–873.

18. Claessens, C. G.; Stoddart, J. F. *Journal of Physical Organic Chemistry*. **1997**, *10*, 254–272.

19. Kim, K. S.; Tarakeshwar, P.; Lee, J. Y. *Chemical Reviews* **2000,** *100,* 4145-4186**.**

20. Jin, Y.; Yu, C.; Denman, R. J.; Zhang, W. Recent Advances in Dynamic Covalent Chemistry. *Chemical Society Reviews* **2013**, *42*, 6634.

21. Jeffrey, G. A. *An Introduction to Hydrogen Bonding; Oxford University Press*, **1997**.

22. Alberts, B.; Johnson, A.; Lewis, J.; Raff, M.; Roberts, K.; Walter, P. *Molecular Biology of the Cell, Fourth Edition; Garland Science,* **2002**.

23. Watson, J. D.; Crick, F. H. C. *Nature* **1953**, *171*, 737.

24. Lawson, D. M.; Artymiuk, P. J.; Yewdall, S. J.; Smith, J. M. A.; Livingstone, J. C.; Treffry, A.; Luzzago, A.; Levi, S.; Arosio, P.; Cesareni, G.; Thomas, C. D.; Shaw,W. V.; Harrison, P. M. *Nature* **1991**, *349*, 541.

25. Proulx-Curry, P. M.; Chasteen, N. D. *Coordination Chemistry Reviews* **1995**, *144*, 347.

26. Janiak, C. *Journal of the Chemical Society, Dalton Transactions* **2000**, 3885.

27. Neusser, H. J.; Krause, H. *Chemical Reviews* **1994**, *94*, 1829.

28. Jorgensen, W. L.; Severance, D. L. *Journal of the American Chemical Society* **1990**, 112, 4768.

29. Grimme, S. *Angewandte Chemie International Edition* **2008**, 47, 3430.

30. Pierre, V. C.; Kaiser, J. T.; Barton, J. K. *Proceedings of the National Academy of Sciences of the United States of America* **2007**, 104, 429.

31. Budiman, Y. P.; Friedrich, A.; Radius, U.; Marder, T. B. *ChemCatChem* **2019**.

32. Tiekink, E. R. T.; Zukerman-Schpector, J. *John Wiley & Sons, Ltd: Chichester, UK,* **2012**.

33. Leigh, D. A. *Angewandte Chemie International Edition* **2016**, *55*, 14506–14508.

34. Zhuang, W.-R.; Wang, Y.; Cui, P.-F.; Xing, L.; Lee, J.; Kim, D.; Jiang, H.-L.; Oh, Y.-K.. *Journal of Controlled Release* **2019**, *294*, 311–326.

35. (a) Zheng, Y.–R.; Yang, H.–B.; Ghosh, K.; Zhao, L.; Stang, P. J. *Chemistry - A European Journal* **2009**, *15*, 7203–7214. (b) Northrop, B. H.; Zheng, Y. R.; Ki–Whan, C. H. I.; Stang, P. J. *Accounts of Chemical Research* **2009**, *42*, 1554–1563. (c) Cook, T. R.; Stang, P. J. *Chemical Reviews* **2015**, *115*, 7001–7045. (d) Datta, S.; Saha, M. L.; Stang, P. J. *Accounts of Chemical Research* **2018**, *51*, 2047–2063. (e) Singh, N.; Singh, J.; Kim, D.; Kim, D. H.; Kim, E. H.; Lah, M. S.; Chi, K. W. *Inorganic Chemistry* **2018**, *57*, 3521–3528.

36. (a) Saha, R.; Devaraj, A.; Bhattacharyya, S.; Das, S.; Zangrando, E.; Mukherjee, P. S. *Journal of the American Chemical Society* **2019**, *141*, 8638–8645. (b) Howlader, P.; Mondal, B.; Purba, P. C.; Zangrando, E.; Mukherjee, P. S. *Journal of the American Chemical Society* **2018**, 140, 7952–7960. (c) Li, S.; Huang, J.; Zhou, F.; Cook, T. R.; Yan, X.; Ye, Y.; Zhu, B.; Zheng, B.; Stang, P. J. *Journal of the American Chemical Society* **2014**, *136*, 5908–5911. (d) Yan, X.; Wang, M.; Cook, T. R.; Zhang, M.; Saha, M. L.; Zhou, Z.; Li, X.; Huang, F.; Stang, P. J. *Journal of the American Chemical Society* **2016**, 138, 4580–4588.

37. (a) Fujita, M.; Tominaga, M.; Hori, A.; Therrien, B. *Accounts of Chemical Research* **2005**, *38*, 369–378. (b) Chakrabarty, R.; Mukherjee, P. S.; Stang, P. J. *Chemical Reviews* **2011**, *111*, 6810–6918. (c) Cook, T. R.; Stang, P. J. *Chemical Reviews* **2015**, 7001–7045. (d) Xu, L.; Wang, Y.-X.; Chen, L.-J.; Yang, H.-B. *Chemical Society Reviews* **2015**, *44*, 2148–2167.

38. (a) Howlader, P.; Das, P.; Zangrando, E.; Mukherjee, P. S. *Journal of the American Chemical Society* **2016**, *138*, 1668–1676. (b) Therrien, B. *Chemistry - A European Journal* **2013**, *19*, 8378–8386. (c) Shanmugaraju, S.; Mukherjee, P. S. *Chemistry - A European Journal* **2015**, *21*, 6656–6666. (d) Mishra, A.; Jung, H.; Lee, M. H.; Lah, M. S.; Chi, K. W. *Inorganic Chemistry* **2013**, *52*, 8573–8578.

39. Northrop, B. H.; Yang, H.-B.; Stang, P. J. *Chemical Communications* **2008**, *45*, 5896-5908

40. Debata, N. B.; Tripathy, D.; Sahoo, H. S. *Coordination Chemistry Review* **2019**, *387*, 273–298.

41. Chakrabarty, R.; Mukherjee, P. S.; Stang, P. J. *Chemical Reviews* **2011**, *111*, 6810–6918.

42. Lee, H.; Elumalai, P.; Singh, N.; Kim, H.; Lee, S. U.; Chi, K.–W. *Journal of the American Chemical Society* **2015**, *137*, 4674–4677.

43. Jo, J.–H.; Singh, N.; Kim, D.; Cho, S. M.; Mishra, A.; Kim, H.; Kang, S. C.; Chi, K.–W. *Inorganic Chemistry* **2017**, *56*, 8430–8438.

44. Song, Y. H.; Singh, N.; Jung, J.; Kim, H.; Kim, E.–H.; Cheong, H.–K.; Kim, Y.; Chi, K.–W. *Angewandte Chemie International Edition* **2016**, *55*, 2007–2011.

45. Vajpayee, V.; Song, Y. H.; Cook, T. R.; Kim, H.; Lee, Y.; Stang, P. J.; Chi, K.–W. *Journal of the American Chemical Society* **2011**, *133*, 19646–19649.

46. Singh, N.; Kim, D.; Kim, D. H.; Kim, E.-H.; Kim, H.; Lah, M. S.; Chi, K.-W. *Dalton Transactions* **2017**, *46*, 571–577.

47. (a) Chichak, K. S. *Science (80–.).* **2004**, *304*, 1308–1312. (b) Cantrill, S. J.; Chichak, K. S.; Peters, A. J.; Stoddart, J. F. *Accounts of Chemical Research* **2005**, *38*, 1–9. (c) Mao, C.; Sun, W.; Seeman, N. C. *Nature* **1997**, *386*, 137–138. (d) Schalley, C. A. *Angewandte Chemie International Edition* **2004**, *43*, 4399–4401. (e) Meyer, C. D.; Forgan, R. S.; Chichak, K. S.; Peters, A. J.; Tangchaivang, N.; Cave, G. W. V.; Khan, S. I.; Cantrill, S. J.; Stoddart, J. F. *Chemistry - A European Journal* **2010**, *16*, 12570–12581. (f) Chichak, K. S.; Cantrill, S. J.; Stoddart, J. F. *Chemical Communications* **2005**, 27, 3391.

48. Kim, T.; Singh, N.; Oh, J.; Kim, E.–H.; Jung, J.; Kim, H.; Chi, K.–W. *Journal of the American Chemical Society* **2016**, *138*, 8368–8371.

49. (a) Acharyya, K.; Bhattacharyya, S.; Sepehrpour, H.; Chakraborty, S.; Lu, S.; Shi, B.; Li, X.; Mukherjee, P. S.; Stang, P. J. *Journal of the American Chemical Society* **2019**, 141, 14565–14569. (b) Chang, X.; Zhou, Z.; Shang,

C.; Wang, G.; Wang, Z.; Qi, Y.; Li, Z. Y.; Wang, H.; Cao, L.; Li, X.; et al. *Journal of the American Chemical Society* **2019**, *141*, 1757–1765.

50. (*a*) Wiester, M. J.; Ulmann P. A.; Mirkin, C. A. *Angewandte Chemie International Edition* **2011**, *50,* 114-137. (*b*) Yoshizawa, M.; Klosterman J. K.; Fujita, M. *Angewandte Chemie International Edition* **2009**, *48,* 3418-3438. (*c*) Koblenz, T. S.; Wassenaar J.; Reek, J. N. H. *Chemical Society Reviews* **2008,** *37*, 247-262. (d) Kawano, M.; Kobayashi, Y.; Ozeki T.; Fujita, M. *Journal of the American Chemical Society* **2006**, *128*, 6558-6559. (e) Horiuchi, S.; Murase T.; Fujita, M. *Journal of the American Chemical Society* **2011**, *133*, 12445-12447. (f) Schmitt, F.; Freudenreich, J.; Barry, N. P. E.; Juillerat-Jeanneret, L.; Süss-Fink G.; Therrien, B. *Journal of the American Chemical Society* **2012**, *134*, 754-757.

51. Cook, T. R.; Vajpayee,V.; M. H. Lee, Stang, P. J.; and Chi, K.-W. *Accounts of Chemical Research* **2013**, *46*, 2464-2474.

52. Therrien, B.; Süss-Fink, G.; Govindaswamy, P.; Renfrew A. K.; Dyson, P. J.; *Angewandte Chemie International Edition* **2008**, *47*, 3773-3776.

53. Wang, M.; Vajpayee, V.; Shanmugaraju, S.; Zheng, Y.-R.; Zhao, Z.; Kim, H.; Mukherjee, P. S.; Chi, K.-W.; Stang, P. J. *Inorganic Chemistry* **2011**, *50*, 1506-1512.

54. Singh, N.; Jo, J.-H.; Song, Y. H.; Kim, H.; Kim, D.; Lah, M. S.; Chi, K.-W. *Chemical Communications* **2015**, *51*, 4492-4495.

55. (a) Kostova, I. *Current Medicinal Chemistry* **2006**, *13*, 1–22. (b) Bratsos, I.; Jedner, S.; Gianferrara, T. Alessio, E. *Chim. International Journal of Chemistry* **2007**, *61*, 692–697. (c) Renfrew, A. *Chim. International Journal of Chemistry* **2009**, *63*, 217–219. (d) Singh, A. K.; Pandey, D. S.; Xu

Q.; Braunstein, P. *Coordination Chemistry Review* **2014**, 31–56. (e) Nazarov, A. A.; Hartinger C. G.; Dyson, P. J. *J. Journal of Organometallic Chemistry* **2014**, *751*, 251–260.

56. (a) Trondl, R.; Heffeter, P.; Kowol, C. R.; Jakupec, M. A.; Berger W.; Keppler, B. K. *Chemical Science* **2014**, *5*, 2925–2932. (b) Trondl, R.; Heffeter, P.; Jakupec, M. A.; Berger W.; Keppler, B. K. *BMC Pharmacology and Toxicology* **2012**, *13*, A82. (c) Scolaro, C.; Bergamo, A.; Brescacin, L.; Delfino, R.; Cocchietto, M.; Laurenczy, G.; Geldbach, T. J.; Sava G.; Dyson, P. J. *J. Journal of Medicinal Chemistry* **2005**, *48*, 4161–4171. (d) Leijen, S.; Burgers, S. A.; Baas, P.; Pluim, D.; Tibben, M.; Van Werkhoven, E.; Alessio, E.; Sava, G.; Beijnen J. H.; Schellens, J. H. M. *Investigational New Drugs* **2015**, *33*, 201–214.

57. (a) Orhan, E.; Garci, A.; Therrien, B. *Inorganica Chimica Acta* **2017**, *461*, 78–83. (b) Dubey, A.; Min, J. W.; Koo, H. J.; Kim, H.; Cook, T. R.; Kang, S. C.; Stang, P. J.; Chi, K.-W. *Chemistry - A European Journal* **2013**, *19*, 11622–11628. (c) Vajpayee, V.; Lee, S.; Kim, S.-H.; Kang, S. C.; Cook, T. R.; Kim, H.; Kim, D. W.; Verma, S.; Lah, M. S.; Kim, I. S.; Wang, M.; Stang, P. J.; Chi, K.-W. *Dalton Transactions* **2013**, *42*, 466–475. (d) Shanmugaraju, S.; Vajpayee, V.; Lee, S.; Chi, K.-W.; Stang, P. J.; Mukherjee, P. S. *Inorganic Chemistry* **2012**, *51* (8), 4817–4823. (e) Mishra, A.; Kang, S. C.; Chi, K.-W. *European Journal of Inorganic Chemistry* **2013**, *2013*, 5222–5232. (f) Therrien, B.; Furrer, J. *Advanced Journal of Chemistry* **2014**, *2014*, 1–20. (g) Kim, T.; Song, H. S.; Singh, J.; Kim, D.; Kim, H.; Kang, S. C.; Chi, K.-W. *Inorganica Chimica Acta* **2018**, *482*, 179–186. (h) Therrien, B.; Süss-Fink, G.; Govindaswamy, P.; Renfrew, A. K.; Dyson, P. J. *Angewandte Chemie International Edition* **2008**, *47*, 3773–3776. (i) Vajpayee, V.; Yang, Y. J.; Kang, S. C.; Kim, H.; Kim, I. S.; Wang, M.; Stang, P. J.; Chi, K.-W. *Chemical Communications* **2011**, *47*, 5184–5186. (j) Mishra, A.; Jung, H.; Park, J. W.;

Kim, H. K.; Kim, H.; Stang, P. J.; Chi, K.-W. *Organometallics* **2012**, *31*, 3519–3526. (k) Vajpayee, V.; Song, Y. H.; Jung, Y. J.; Kang, S. C.; Kim, H.; Kim, I. S.; Wang, M.; Cook, T. R.; Stang, P. J.; Chi, K.-W. *Dalton Transactions* **2012**, *41*, 3046–3052. (l) Cook, T. R.; Vajpayee, V.; Lee, M. H.; Stang, P. J.; Chi, K.-W. *Accounts of Chemical Research* **2013**, *46*, 2464–2474.

58. (a) Garci, A.; Dobrov, A. A.; Riedel, T.; Orhan, E.; Dyson, P. J.; Arion, V. B.; Therrien, B. *Organometallics* **2014**, *33*, 3813–3822. (b) Mishra, A.; Jeong, Y. J.; Jo, J.-H.; Kang, S. C.; Kim, H.; Chi, K.-W. *Organometallics* **2014**, *33*, 1144–1151. (c) Therrien, B. *CrystEngComm* **2015**, *17*, 484–491. (p) Krishnamurthy, S.; Ke, X.; Yang, Y. Y. *Nanomedicine* **2015**, *10*, 143–160. (d) Orhan, E.; Garci, A.; Riedel, T.; Soudani, M.; Dyson, P. J.; Therrien, B. *J. Organomet. Chem.* **2016**, *803*, 39–44. (e) Singh, N.; Jang, S.; Jo, J.-H.; Kim, D. H.; Park, D. W.; Kim, I.; Kim, H.; Kang, S. C.; Chi, K.-W. *Chemistry - A European Journal* **2016**, *22*, 16157–16164. (f) Jo, J. H.; Singh, N.; Kim, D.; Cho, S. M.; Mishra, A.; Kim, H.; Kang, S. C.; Chi, K.-W. *Inorganic Chemistry* **2017**, *56*, 8430–8438. (g) Ajibola Adeyemo, A.; Shettar, A.; Bhat, I. A.; Kondaiah, P.; Mukherjee, P. S. *Inorganic Chemistry* **2017**, *56*, 608–617. (h) Gupta, G.; Oggu, G. S.; Nagesh, N.; Bokara, K. K.; Therrien, B. *CrystEngComm* **2016**, *18*, 4952–4957. (i) Orhan, E.; Garci, A.; Riedel, T.; Dyson, P. J.; Therrien, B. *Journal of Organometallic Chemistry* **2016**, *815–816*, 53–58. (j) Gupta, G.; Nowak-Sliwinska, P.; Herrero, N.; Dyson, P. J.; Therrien, B. *Journal of Organometallic Chemistry* **2015**, *796*, 59–64. (k) Adeyemo, A. A.; Shettar, A.; Bhat, I. A.; Kondaiah, P.; Mukherjee, P. S. *Dalton Transactions* **2018**, *47*, 8466–8475.

59. (a) Kostova, I. *Current Medicinal Chemistry* **2006**, *13*, 1–22. (b) Bratsos, I.; Jedner, S.; Gianferrara, T.; Alessio, E. *International Journal of Chemistry* **2007**, *61*, 692–697. (c) Renfrew, A. *International Journal of Chemistry* **2009**, *63*, 217–219. (d) Singh, A. K.; Pandey, D. S.; Xu, Q.; Braunstein, P.

Coordination Chemistry Reviews 2014, 31–56. (e) Nazarov, A. A.; Hartinger, C. G.; Dyson, P. J. *Journal of Organometallic Chemistry* **2014**, *751*, 251–260. (f) Han Ang, W.; Dyson, P. J. *Eur. J. Inorganic Chemistry* **2006**, *2006*, 4003–4018. (g) Antonarakis, E. S.; Emadi, A. *Cancer Chemotherapy and Pharmacology* **2010**, *66*, 1–9. (h) Amin, A.; Buratovich, M. *Mini-Reviews in Medicinal Chemistry* **2009**, *9*, 1489–1503. (i) Trondl, R.; Heffeter, P.; Kowol, C. R.; Jakupec, M. A.; Berger, W.; Keppler, B. K. *Chemical Science* **2014**, *5*, 2925–2932. (j) Trondl, R.; Heffeter, P.; Jakupec, M. A.; Berger, W.; Keppler, B. K. *BMC Pharmacology and Toxicology* **2012**, *13*, A82. (k) Scolaro, C.; Bergamo, A.; Brescacin, L.; Delfino, R.; Cocchietto, M.; Laurenczy, G.; Geldbach, T. J.; Sava, G.; Dyson, P. J. *J. journal of medicinal chemistry* **2005**, *48*, 4161–4171. (l) Leijen, S.; Burgers, S. A.; Baas, P.; Pluim, D.; Tibben, M.; Van Werkhoven, E.; Alessio, E.; Sava, G.; Beijnen, J. H.; Schellens, J. H. M. *Investigational New Drugs* **2015**, *33*, 201–214. (m) Barry, N. P. E.; Edafe, F.; Dyson, P. J.; Therrien, B. *Dalton Transactions* **2010**, *39*, 2816. (n) Mattsson, J.; Govindaswamy, P.; Renfrew, A. K.; Dyson, P. J.; Štěpnička, P.; Süss-Fink, G.; Therrien, B. *Organometallics* **2009**, *28* (15), 4350–4357. (o) Smith, G. S.; Therrien, B. *Dalton Transactions* **2011**, *40*, 10793.

Chapter 2. Coordination-driven self-assembly of a molecular knot 8_{18}

2.1 Introduction

The importance and prevalence of molecular knots and catenanes with recognizable entangled patterns have been increasingly highlighted by a number of scientists in the field of chemistry, biology, topological physics and mathematics.[1,2] Recent studies have found that a significant percentage of biomolecules including DNA, RNA and proteins are knotted,[2, 3] and that viruses and enzymes play crucial roles in the knotting and unknotting of DNA.[4] On the other hand, soft matter physicists have started establishing correlations between the topologies of nematic colloids and their dynamical and mechanical properties.[5] The on-line encyclopedia of integer sequences[6] describes the billions of theoretical knots developed and tabulated by mathematicians for more than 200 years.[7] Chemists have devoted considerable time to the knotting of small molecules together in laboratories using a series of chemical reactions in a controlled manner, but of the six billion possible prime knots,[6] only four singlestranded knots have been realized so far (Figures 1.1A to D).[8] Sauvage et al. synthesized the first molecular knot, the trefoil knot, using a metal-template strategy (Figure 1.1A)[8a] and this was followed by the figure-of-eight knot (Figure 1B)[8c] and the pentafoil knot (Figure 1.1C).[8d] Recently a fourth knot with eight non-alternating crossings, the 8_{19} knot, was successfully synthesized by Leigh using a multi-step process (Figure 1.1D).[8e] To date no molecular knot with more than eight crossings has been realized, and thus, the rational synthesis of such knots by self-assembly remains a challenge in the supramolecular chemistry field. Coordination-driven self-assembly [9] is a well-stablished efficient approach for the synthesis of molecular architectures of well-defined geometries and sizes including the largest supramolecule[10] reported to date. This approach has also produced a number of molecular topologies that include Borromean rings,[11] the Solomon's link,[12] Hopf's link,[13] and cyclic [3]catenane[14] using a metal-based acceptor and dipyridyl donors of various sizes and functionalities.

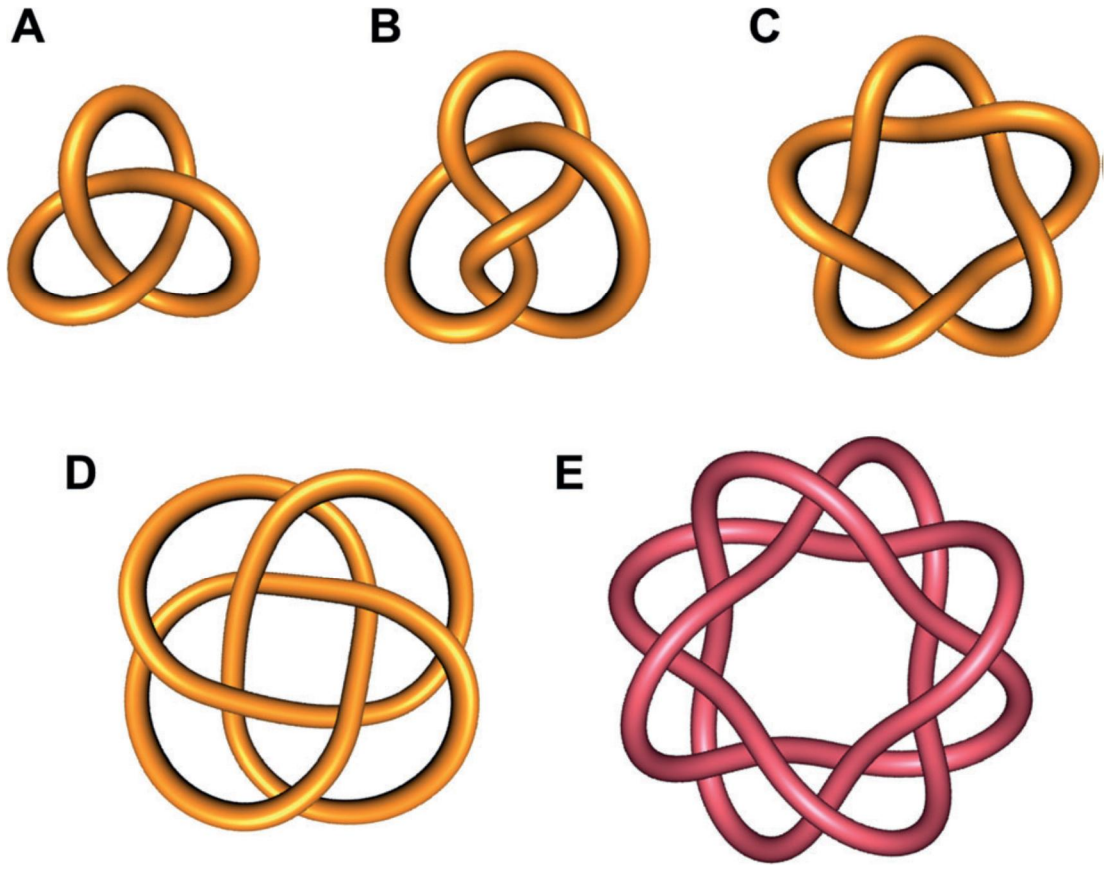

Figure 2.1 Topological images of synthesized molecular knots thus far. A) The trefoil knot [3_1] in Alexander-Briggs notation with three crossings. B) The Figure-of-eight knot [4_1], with four crossings. C) The pentafoil knot [5_1] with five crossings. D) The 8_{19} knot with eight crossings. E) The topological image of synthesized molecular knot in this study. (see Figure 2.2).

Herein we report the straightforward synthesis of a molecular knot with sixteen crossings by coordination-driven [8+8] self-assembly using eight strands each of arene Ru^{II} acceptor **A8** and slightly bent 2,6-bis(4-pyridyl)dithieno[3,2-b:2',3'-d]thiophene donor (L1), which is the first realized single stranded molecular knot with sixteen crossings (Figure 2.1E). The synthesized knot was unambiguously characterized by NMR spectroscopy, ESI-MS and single-crystal X-ray diffraction analysis.

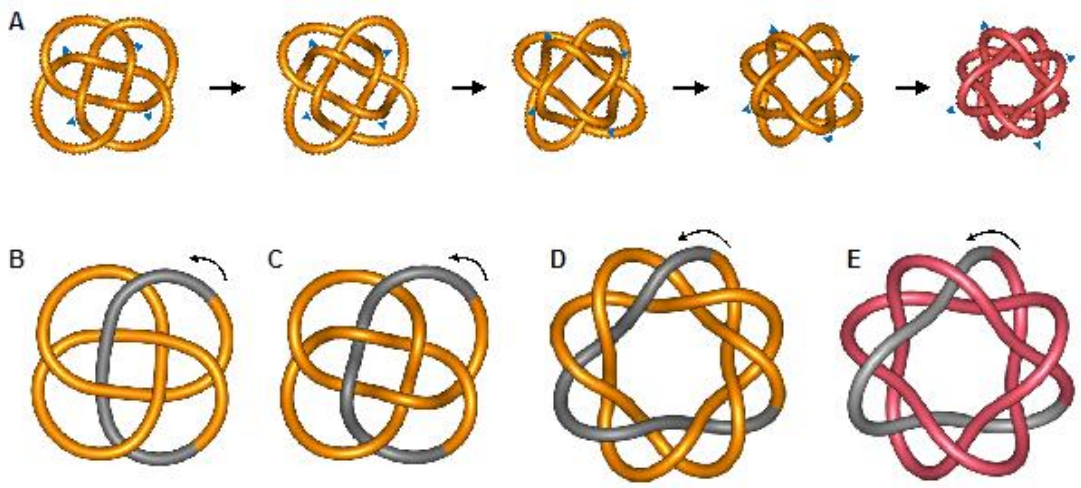

Figure 2.2 (A) Schematic procedure for the geometric folding of 8_{18} knot to form sixteen crossings, which indicates that the geometry of synthesized sixteen-crossings in this study can be artificially derived from geometric folding of carrick knot, 8_{18}, of eight crossings. Topology and crossing pattern of molecular knots of (B) the 8_{19} knot, (C) the 8_{18} knot, (D) the T(3,8) torus knot, and (E) the molecular knot 8_{18} synthesized in this study. While the 8_{19} and 8_{18} knots have eight crossings, the T(3,8) torus knot and the molecular knot synthesized in this study have sixteen crossings. However, each pair of eight- and sixteen-crossing knots have structural similarities but have different crossing patterns (*1*). The overpasses (O) and underpasses (U) of each knot along the gray-colored path are as follows: (B) O-O-U-U, (C) O-U-O-U, (D) O-O-U-U-O-O-U-U, and (E) U-O-O-O-O-U-U-U. Whereas the 8_{18} knot shows the perfect alternating pattern, the 8_{19} has a non-alternating pattern compared to that of 8_{18}. The topological information with crossing patterns of knots is easily described with the Dowker notation.[15] The Dowker notation of each knot is as follows: (B) 12 -14 16 -2 4 -6 8 -10, (C) 12 14 16 2 4 6 8 10, (D) 12 -14 16 -18 20 -22 24 -26 28 -30 32 -2 4 -6 8 -10, and (E) -12 14 16 18 -20 22 24 -26 -28 30 32 -2 -4 6 8 -10.

2.2 Material and methods

The arene-ruthenium acceptor A1-A4 were prepared according to the reported methods.[16] Deuterated NMR solvents were purchased from Cambridge Isotope Laboratory(Andover, MA, USA). NMR spectra were recorded on a Bruker 300, 800 and 900 MHz spectrometer (University of Ulsan and Korea Basic Science Institute, Ochang). ^{1}H NMR chemical shifts are reported relative to the residual protons of deuterated CD_3OD (3.31 ppm) and deuterated CD_3NO_2 (4.33 ppm). ESI-MS data of **1** and **2** was recorded on Synapt G2 quadrupole time-of flight (TOF) mass spectrometer equipped with an electrospray ion source (Waters, Milford, MA, USA) and analyzed with the MassLynx software suite system at the Korea Basic Science Institute, Ochang).

2.2.1 Crystallographic data collection and structure refinement

Diffraction data of **1** was collected at 100 K on an ADSC Quantum 210 CCD diffractometer with synchrotron radiation (λ = 0.70000 Å) at the Supramolecular Crystallography Beamline 2D, Pohang Accelerator Laboratory (PAL), Pohang, Korea. The raw data were processed and scaled using the program HKL3000. The structure was solved by direct methods, and the refinements were carried out with full-matrix least-squares on F^2 with appropriate software implemented in the SHELXTL program package.[17] All the non-hydrogen atoms were refined anisotropically, and hydrogen atoms were added to their geometrically ideal positions. The contributions of the most disordered solvent molecules were removed from the diffraction data using the SQUEEZE routine of PLATON software,[18] and then final refinements were carried out. X-ray crystallographic data is provided in Table 2.1.

2.2.2 Synthesis of dipyridyl dithienothiophene donor L1 2,6-bis(4-pyridyl)dithieno[3,2-b:2’,3’-d]thiophene

d]thiophene

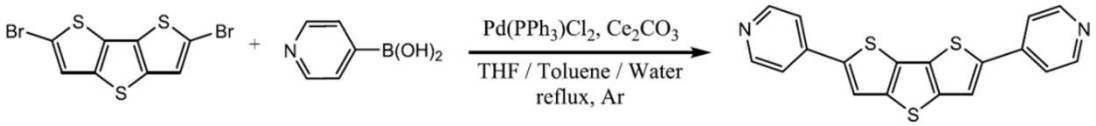

L1

A mixture of 2,6-dibromo-dithieno[3,2-b:2',3'-d]thiophene (200.0 mg, 0.58 mmol, 1eq), 4-pyridinylboronic acid (213.9 mg, 1.74 mmol, 3 eq), [1,1′-bis(diphenylphosphino)ferrocene]dichloropalladium(II) (70.0 mg, 0.10 mmol, 0.165eq) and cesium carbonate (3779.9 mg, 11.60 mmol, 20 eq, 2.0 mL in aqueous) in 20 mL solvent (toluene:THF = 1:1) was stirred at reflux for 24h. The resulting mixture was poured into water (100 mL) and extracted with CH_2Cl_2 (100 mL × 3). The combined extract was washed with brine (50 mL) and dried over sodium sulfate. The solution was concentrated and purified by silica gel column chromatography eluted with CH_2Cl_2/ethyl acetate (5:1 to 1:1) to obtain pure L in 82% yield (based on dibromide precursor). Mp: 298 ℃ (dec). ^{1}H NMR (300 MHz, $CDCl_3$) δ 8.63 (dd, J = 4.6, 1.6 Hz, 2H), 7.73 (s, 1H), 7.50 (dd, J = 4.6, 1.6 Hz, 2H). ^{13}C NMR (75 MHz, $CDCl_3$) δ 150.55, 142.97, 142.48, 141.31, 131.55, 119.51, 118.93. ESI-HRMS calcd for $[C_{18}H_{11}N_2S_3]^+$: 351.0084; found 351.0078; Analysis (Calcd., found for $C_{18}H_{10}N_2S_3$): C (61.68, 61.42), H (2.88, 2.89), N (7.99, 7.99), S (27.45, 27.44).

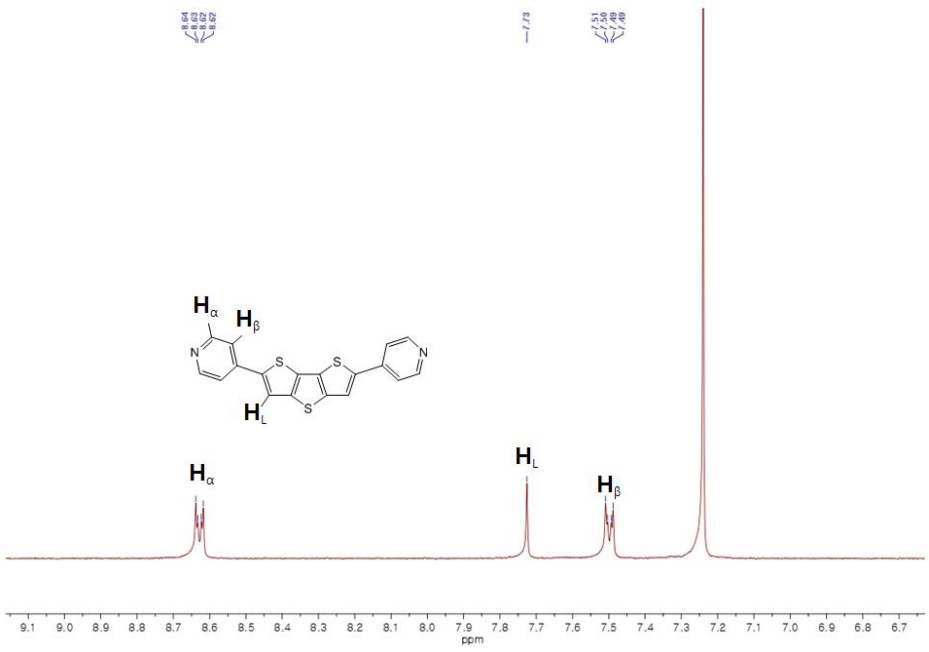

Figure 2.3 ^{1}H NMR spectrum of **L1** ($CDCl_3$, 300 MHz)

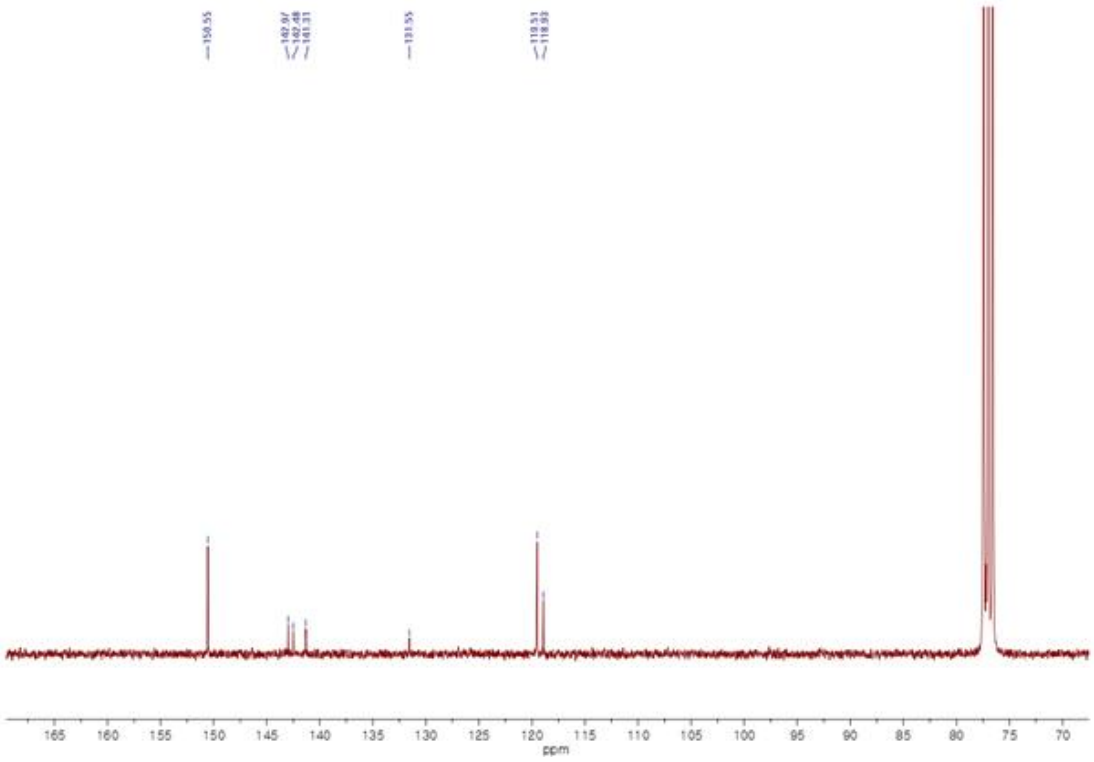

Figure 2.4 ^{13}C NMR spectrum of **L1** ($CDCl_3$, 75 MHz)

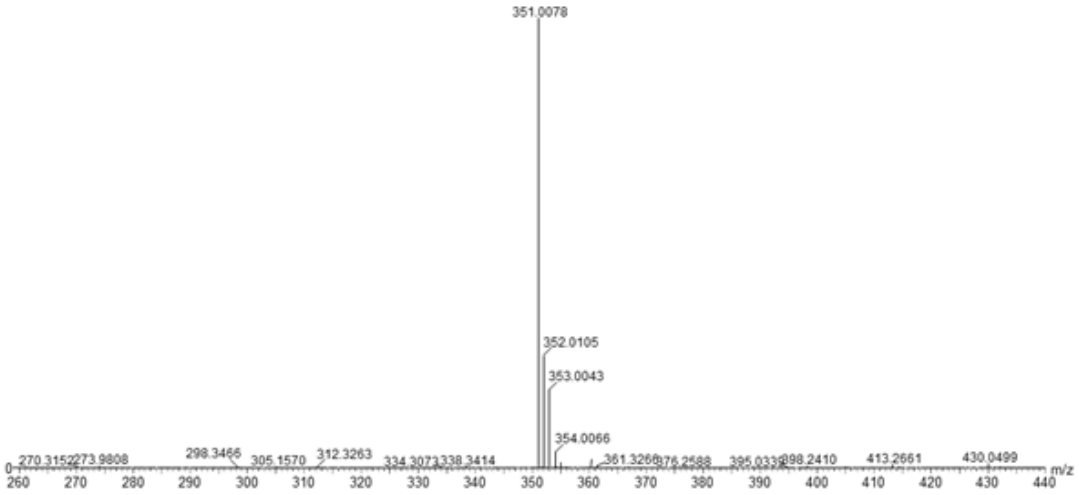

Figure 2.5 ESI mass spectrum of **L1** ($C_{18}H_{11}N_2S_3$ (L1+H^+))

2.2.3 General procedure for Ru(II) acceptor A5-A8

Arene-Ru(II) acceptor **A1-A4** and silver triflate(use aluminum foil) were stirred in methanol at room temperature for 12 h, then filtered. The solution was concentrated to small volume (5 mL). Ether was added and kept 1 day then filtered (washed with ether). The filtrate was dried in vacuum.

2.2.4 Synthesis of Ru(II) acceptor A5 Bis(trifluoromethanesulfonato)[μ-ethanedioato(2-)-κO^1,κO'^2:κO^2,κO'^1]bis[(1,2,3,4,5,6-η)-1-methyl-4-(1-methylethyl) benzene]diruthenium(II)

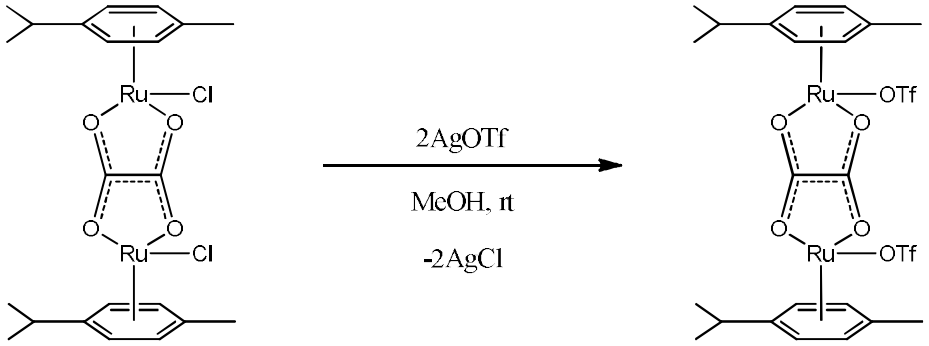

A1 A5

Ru(II) acceptor **A5** was made by the general procedure described above using Ru(II) acceptor **A1** (200 mg, 0.318 mmol, 1 eq) and silver triflate (163 mg, 0.636 mmol, 2 eq). The dark yellow colored powder was characterized as **A5**. Isolated yield: 77%. Anal. calcd. for $C_{24}H_{28}F_6O_{10}Ru_2S_2$: C, 33.65; H, 3.29. Found: C, 33.56; H, 3.30. ^{1}H NMR (300 MHz, CD_3OD) δ 6.01 (d, J = 6.2 Hz, 4H), 5.79 (d, J = 6.2 Hz, 4H), 2.90 (dt, J = 12.9, 6.4 Hz, 2H), 2.29 (s, 6H), 1.41 (d, J = 6.8 Hz, 12H). ^{13}C NMR (75 MHz, CD_3OD) δ 173.02, 101.56, 99.35, 81.09, 79.29, 32.80, 22.52, 18.43. ESI-MS for **A5** ($C_{24}H_{28}F_6O_{10}Ru_2S_2$): m/z = 708.9600 [**A5**-OTf]$^+$, 280.0046 [**A5**-2OTf] $^{2+}$.

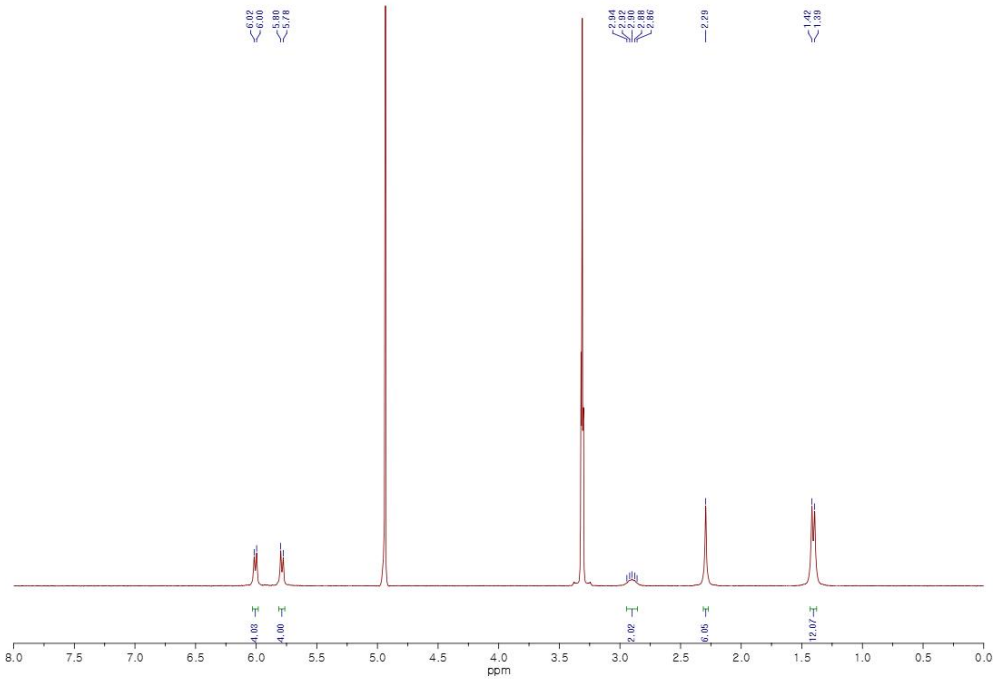

Figure 2.6 ^{1}H NMR spectrum of **A5** (CD_3OD [8.0 mM], 300 MHz)

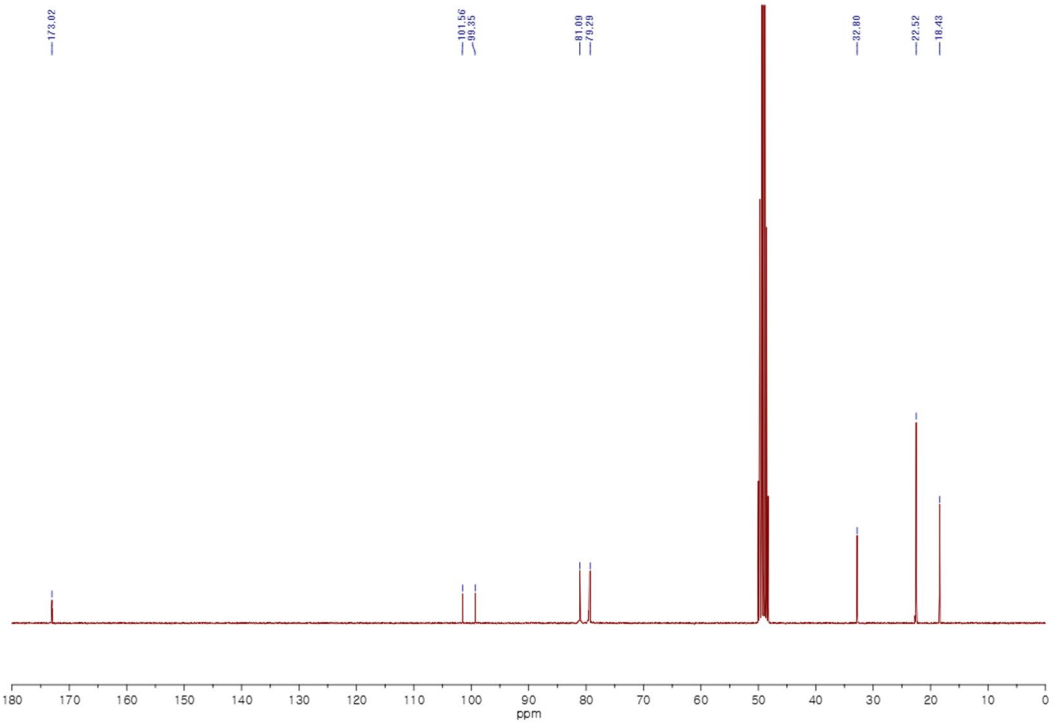

Figure 2.7 ^{13}C NMR spectrum of **A5** (CD_3OD [8.0 mM], 75 MHz)

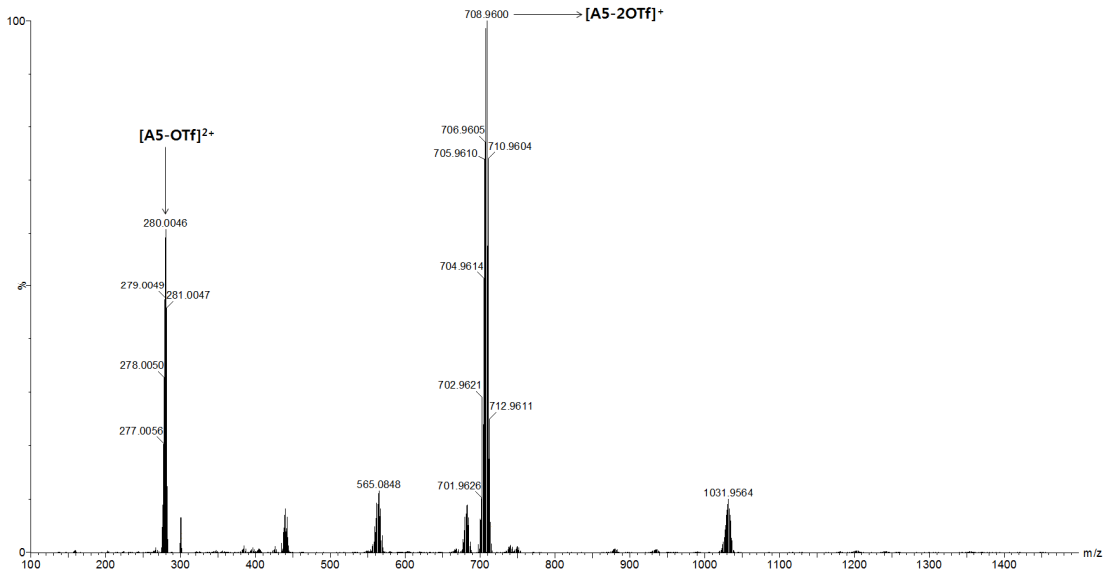

Figure 2.8 Full ESI mass spectrum of **A5** (Reaction in CD_3OD [8.0 mM])

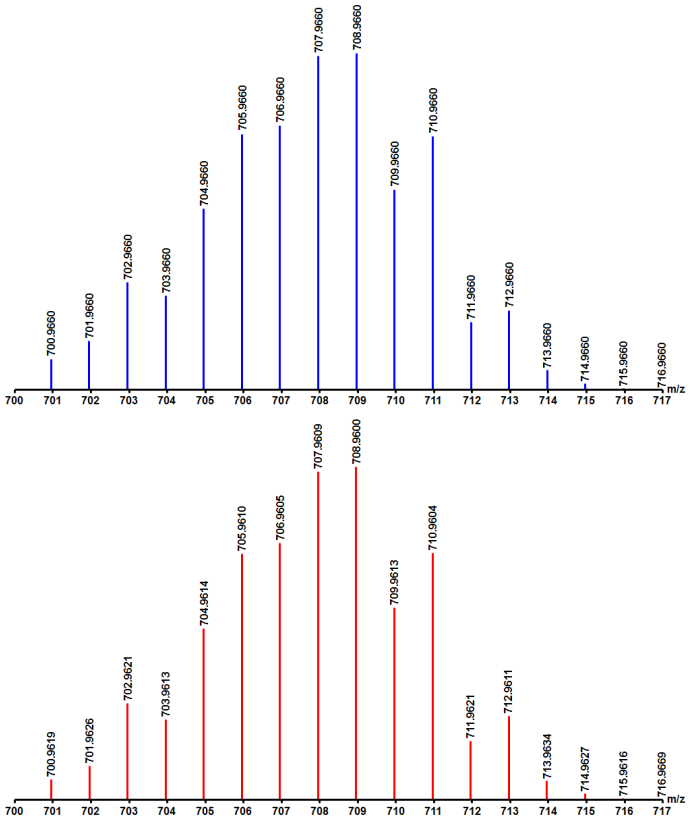

Figure 2.9 Calculated (blue) and experimental (red) ESI mass spectra of [**A5**-OTf]$^+$. (Reaction in CD_3OD [20 mM])

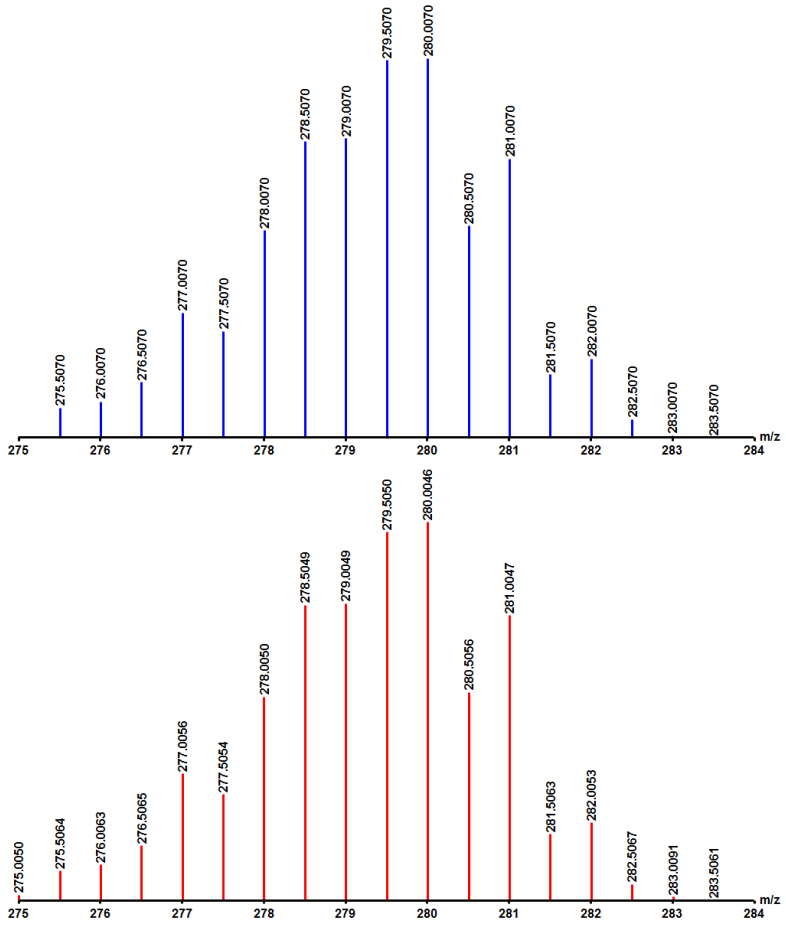

Figure 2.10 Calculated (blue) and experimental (red) ESI mass spectra of [**A5**-2OTf]$^{2+}$. (Reaction in CD_3OD [20 mM])

2.2.5 Synthesis of Ru(II) acceptor A6 Bis(trifluoromethanesulfonato)[μ-2,5-di(hydroxy-κ*O*)-2,5-cyclohexadiene-1,4-dionato(2-)-κO^1:κO^4]bis[(1,2,3,4,5,6-η)-1-methyl-4-(1-methylethyl)benzene]diruthenium(II)

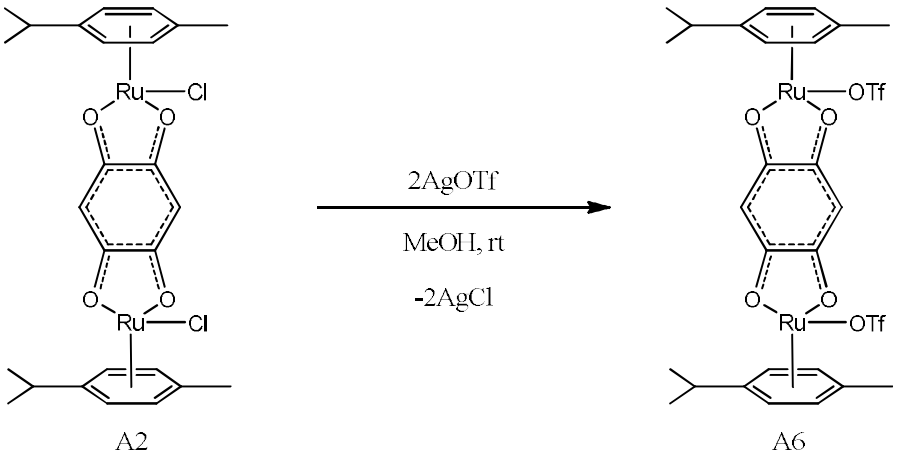

A2 A6

Ru(II) acceptor **A6** was made by the general procedure described above using Ru(II) acceptor **A2** (200 mg, 0.294 mmol, 1 eq) and silver triflate (151 mg, 0.588 mmol, 2 eq). The dark red colored powder was characterized as **A6**. Isolated yield: 75%. Anal. calcd. for $C_{28}H_{30}F_6O_{10}Ru_2S_2$: C, 37.09; H, 3.33. Found: C, 36.99; H, 3.34. ^{1}H NMR (300 MHz, CD_3OD) δ 6.03 (t, J = 5.8 Hz, 4H), 5.85 (d, J = 6.9 Hz, 2H), 5.80 (t, J = 5.8 Hz, 4H), 2.95 (dtd, J = 13.7, 6.9, 2.5 Hz, 2H), 2.36 (d, J = 2.5 Hz, 6H), 1.42 (dd, J = 6.9, 1.9 Hz, 12H). ^{13}C NMR (75 MHz, CD_3OD) δ 186.52, 103.01, 102.62, 98.93, 82.20, 80.37, 32.90, 22.68, 18.60. ESI-MS for **A6** ($C_{28}H_{30}F_6O_{10}Ru_2S_2$): m/z = 758.9769 [**A6**-OTf]$^+$, 305.0129 [**A6**-2OTf]$^{2+}$.

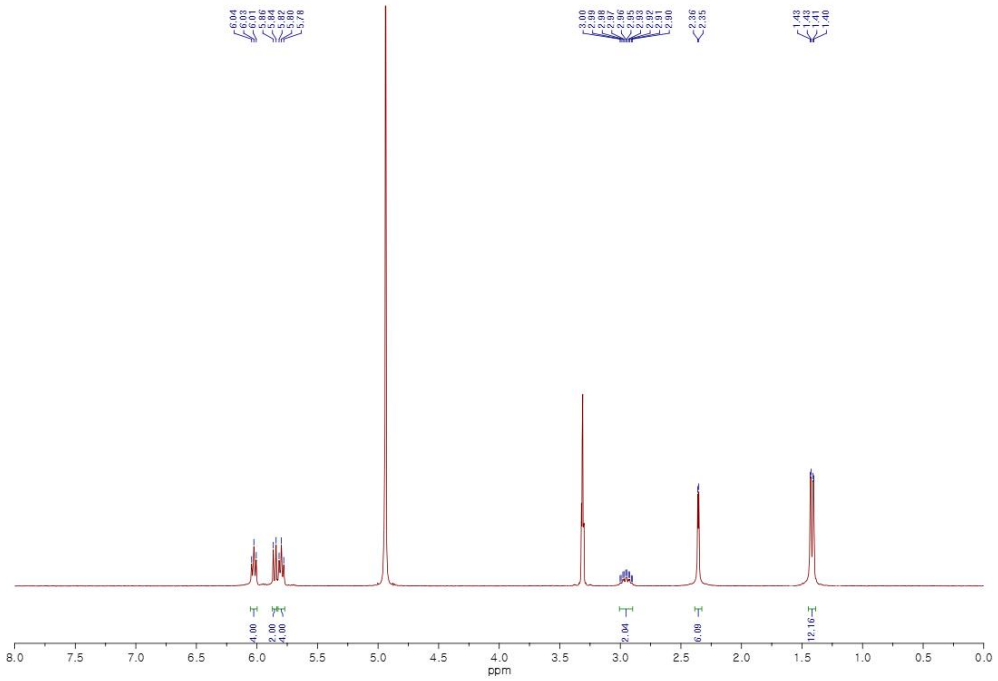

Figure 2.11 ^{1}H NMR spectrum of **A6** (CD_3OD [8.0 mM], 300 MHz)

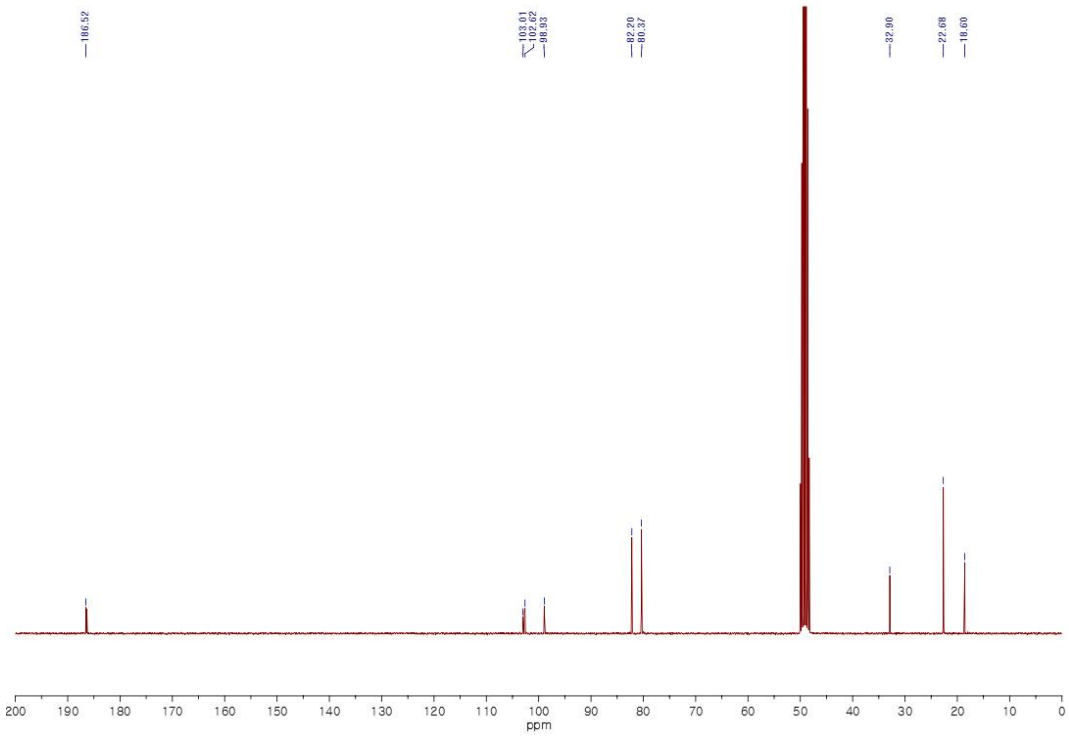

Figure 2.12 ^{13}C NMR spectrum of **A6** (CD_3OD [8.0 mM], 75 MHz)

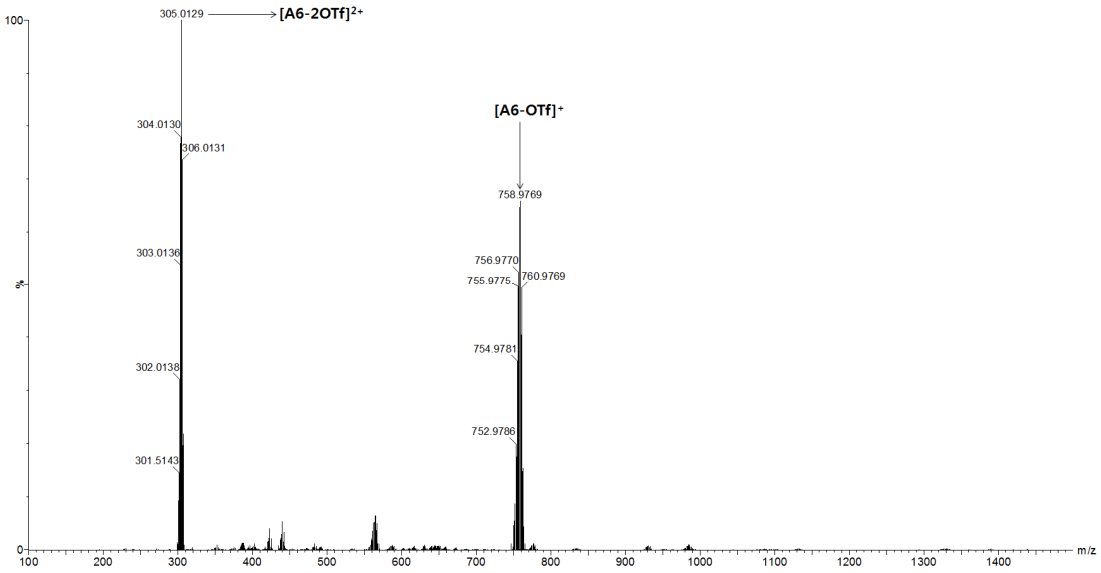

Figure 2.13 Full ESI mass spectrum of **A6** (Reaction in CD_3OD [8.0 mM])

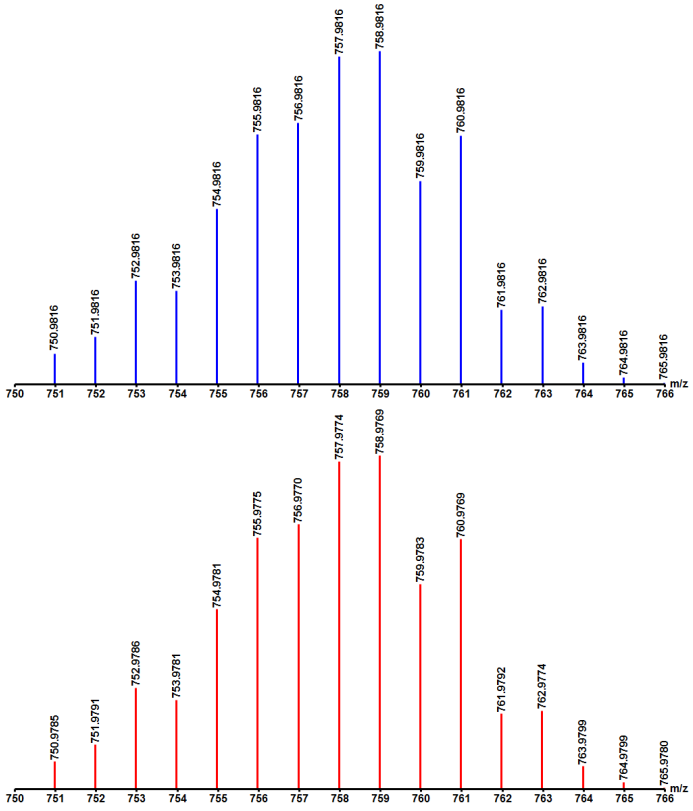

Figure 2.14 Calculated (blue) and experimental (red) ESI mass spectra of [**A6**-OTf]$^+$. (Reaction in CD_3OD [20 mM])

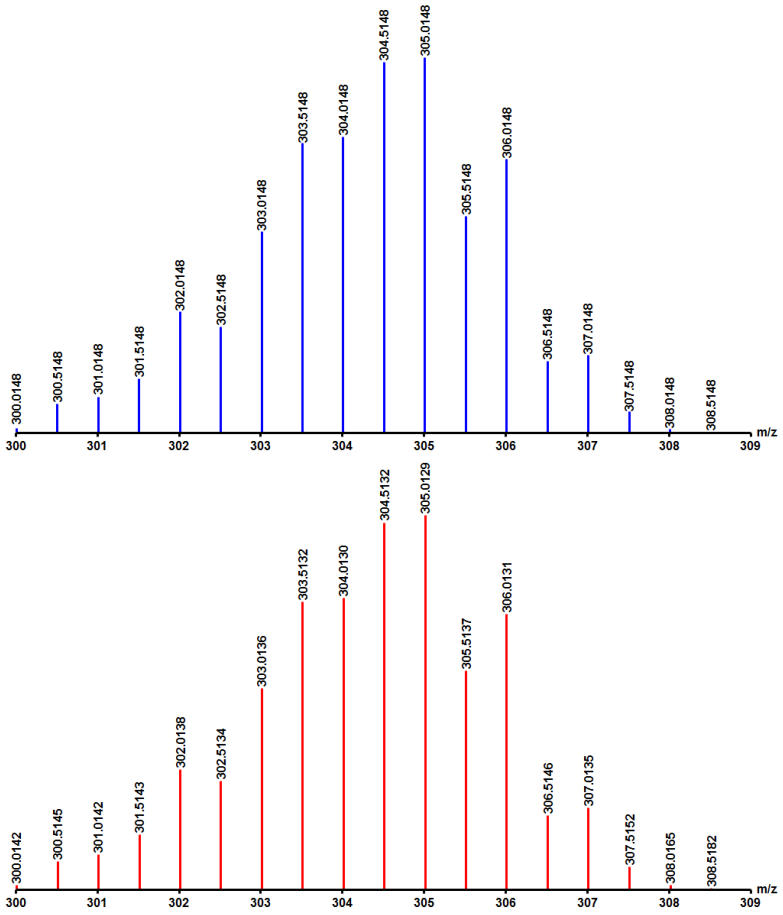

Figure 2.15 Calculated (blue) and experimental (red) ESI mass spectra of [**A6**-2OTf]$^{2+}$. (Reaction in CD_3OD [20 mM])

2.2.6 Synthesis of Ru(II) acceptor A7 Bis(trifluoromethanesulfonato)[μ-5,8-di(hydroxy-κ*O*)-1,4-naphthalenedionato(2-)-κO^1:κO^4]bis[(1,2,3,4,5,6-η)-1-methyl-4-(1-methylethyl)benzene]diruthenium(II)

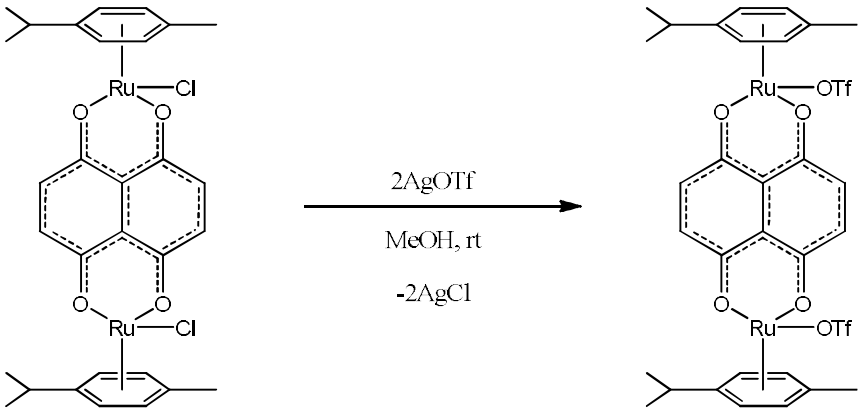

A3 A7

Ru(II) acceptor **A7** was made by the general procedure described above using Ru(II) acceptor **A3** (200 mg, 0.274 mmol, 1 eq) and silver triflate (141 mg, 0.548 mmol, 2 eq). The bright brown colored powder was characterized as **A7**. Isolated yield: 84%. Anal. calcd. for $C_{32}H_{32}F_6O_{10}Ru_2S_2$: C, 40.17; H, 3.37. Found: C, 40.15; H, 3.37. ^{1}H NMR (300 MHz, CD_3OD) δ 7.37 (s, 4H), 5.90 (d, J = 6.3 Hz, 4H), 5.66 (d, J = 6.3 Hz, 4H), 2.92 (dt, J = 13.9, 6.9 Hz, 2H), 2.29 (s, 6H), 1.41 (d, J = 6.9 Hz, 12H). ^{13}C NMR (75 MHz, CD_3OD) δ 172.35, 138.18, 111.24, 101.83, 99.37, 82.30, 79.78, 31.72, 21.92, 17.15. ESI-MS for **A7** ($C_{32}H_{32}F_6O_{10}Ru_2S_2$): m/z = 808.9923 [**A7**-OTf]$^+$, 330.0204 [**A7**-2OTf] $^{2+}$.

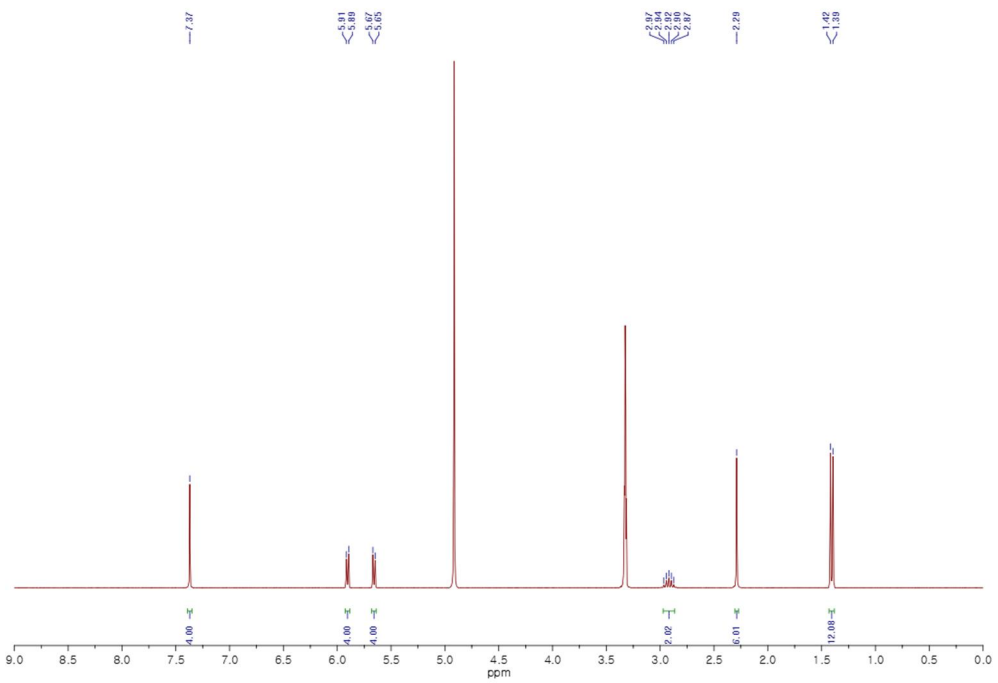

Figure 2.16 ^{1}H NMR spectrum of **A7** (CD_3OD [8.0 mM], 300 MHz)

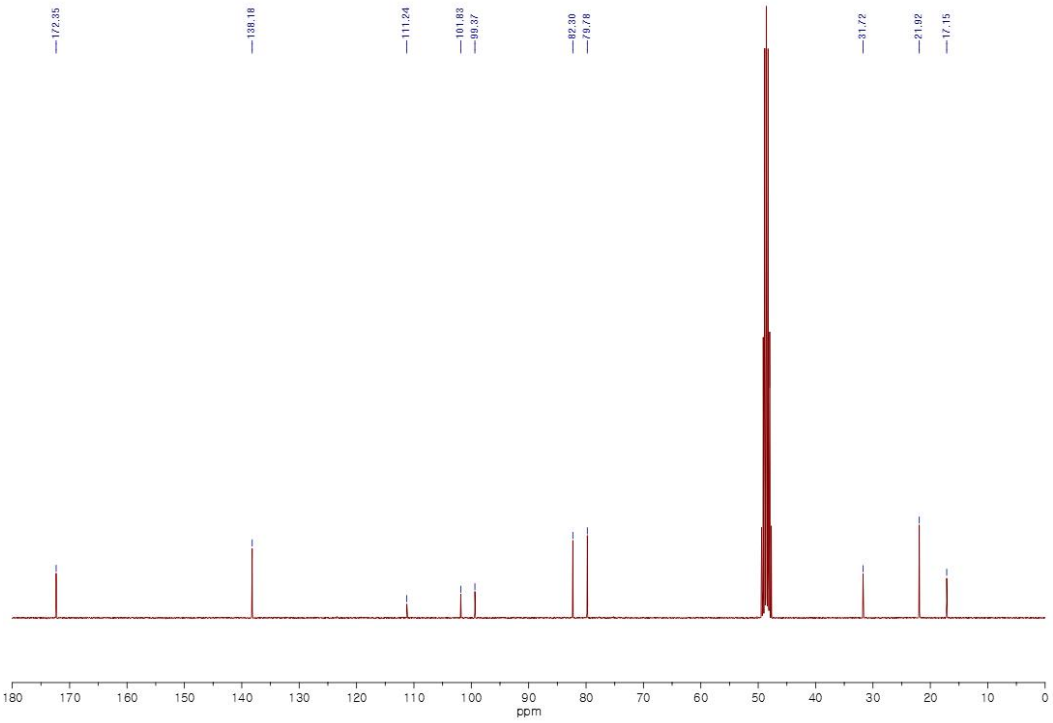

Figure 2.17 ^{13}C NMR spectrum of **A7** (CD_3OD [8.0 mM], 75 MHz)

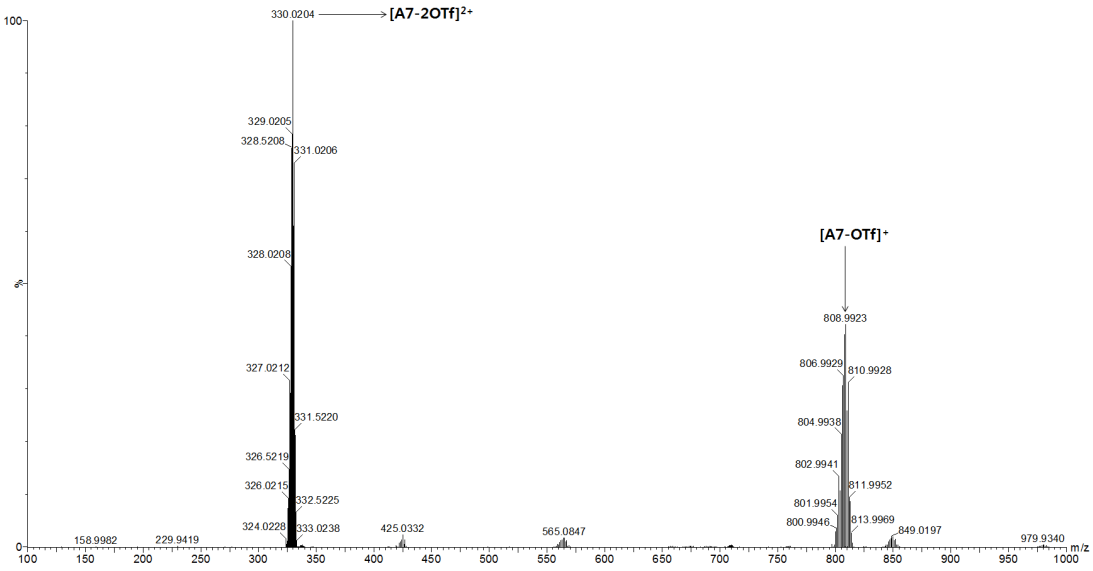

Figure 2.18 Full ESI mass spectrum of **A7** (Reaction in CD_3OD [8.0 mM])

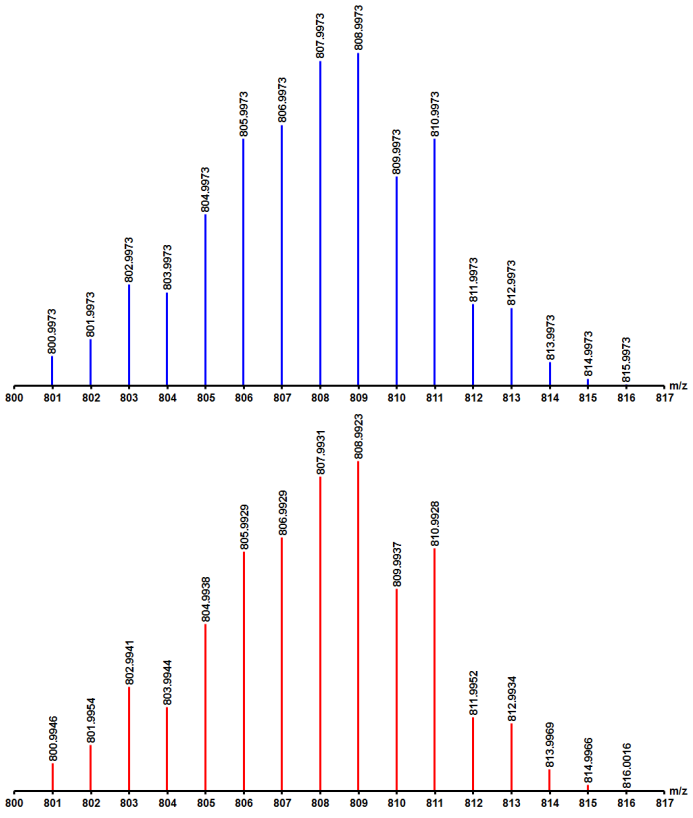

Figure 2.19 Calculated (blue) and experimental (red) ESI mass spectra of [**A7**-OTf]$^+$. (Reaction in CD_3OD [8.0 mM])

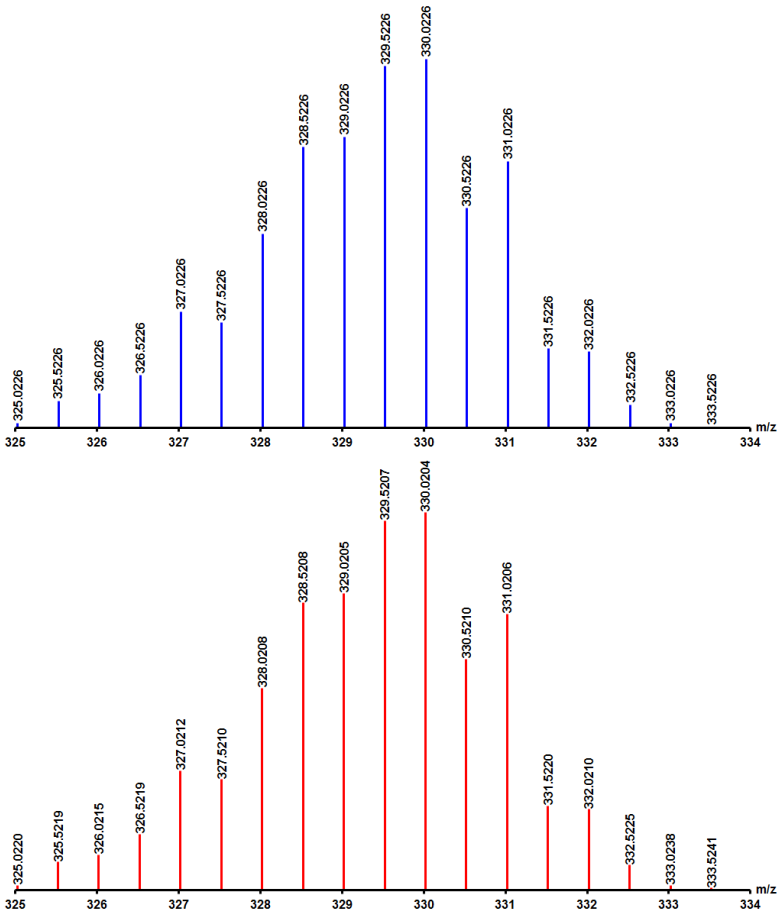

Figure 2.20 Calculated (blue) and experimental (red) ESI mass spectra of [**A7**-2OTf]$^{2+}$. (Reaction in CD_3OD [8.0 mM])

2.2.7 Synthesis of Ru(II) acceptor A8 Bis(trifluoromethanesulfonato)[μ-6,11-di(hydroxy-κ*O*)-5,12-naphthacenedionato(2-)-κO^5:κO^{12}]bis[(1,2,3,4,5,6-η)-1-methyl-4-(1-methylethyl)benzene]diruthenium(II)

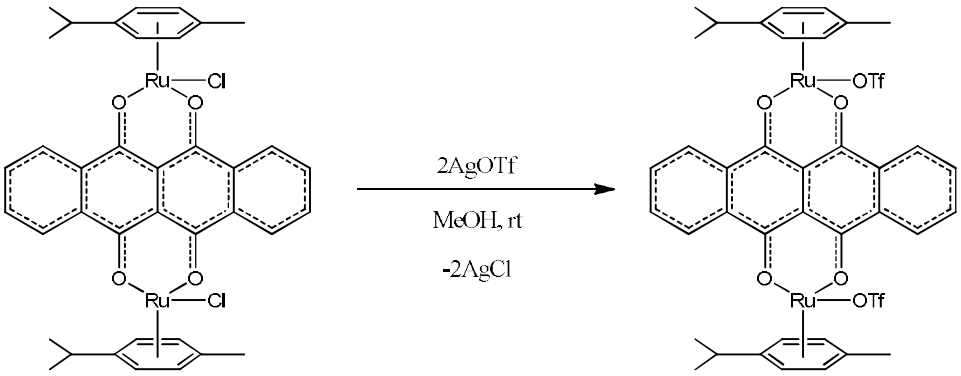

A4 A8

Ru(II) acceptor **A8** was made by the general procedure described above using Ru(II) acceptor **A4** (200 mg, 0.241 mmol, 1 eq) and silver triflate (124 mg, 0.482 mmol, 2 eq). The bright green colored powder was characterized as **A8**. Isolated yield: 81%. Anal. calcd. for $C_{40}H_{36}F_6O_{10}Ru_2S_2$: C, 45.45; H, 3.43. Found: C, 45.38; H, 3.44. ^{1}H NMR (300 MHz, CD_3OD) δ 8.75 (dd, J = 6.1, 3.4 Hz, 4H), 7.98 (dd, J = 6.0, 3.4 Hz, 4H), 6.06 (d, J = 6.2 Hz, 4H), 5.80 (d, J = 6.2 Hz, 4H), 3.07 (dt, J = 13.8, 6.9 Hz, 2H), 2.42 (s, 6H), 1.48 (d, J = 6.9 Hz, 12H). ^{13}C NMR (75 MHz, CD_3OD) δ 170.77 , 134.63, 133.66, 127.79, 106.92, 101.59, 99.45, 82.30, 79.42, 31.83, 22.12, 17.67. ESI-MS for **A8** ($C_{40}H_{36}F_6O_{10}Ru_2S_2$): m/z = 909.0208 [**A8**-OTf]$^+$, 380.0353 [**A8**-2OTf]$^{2+}$.

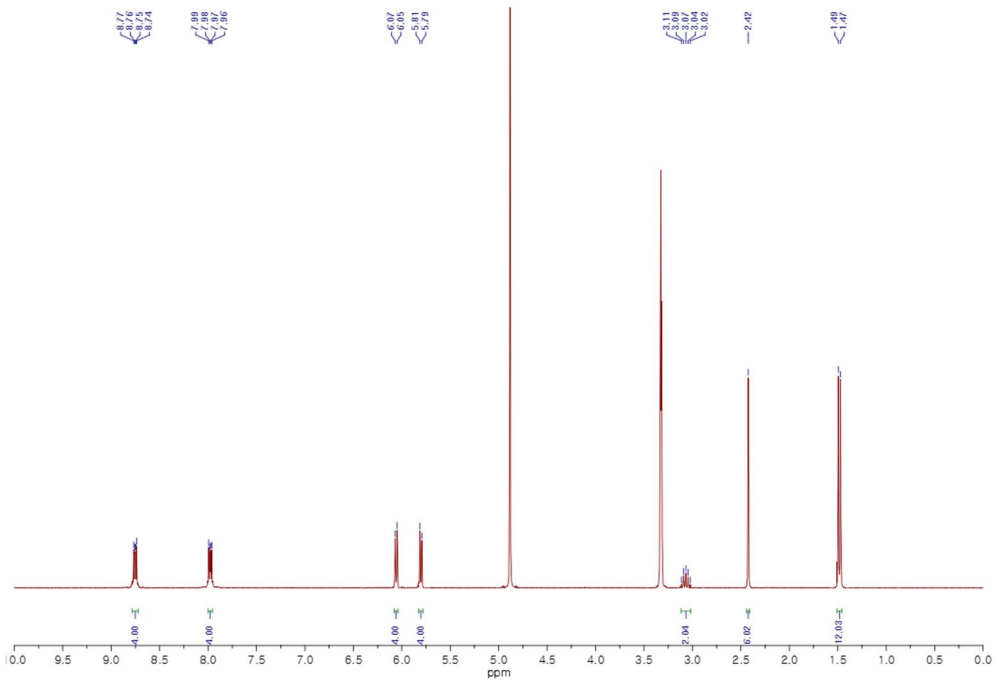

Figure 2.21 ^{1}H NMR spectrum of **A8** (CD_3OD [8.0 mM], 300 MHz)

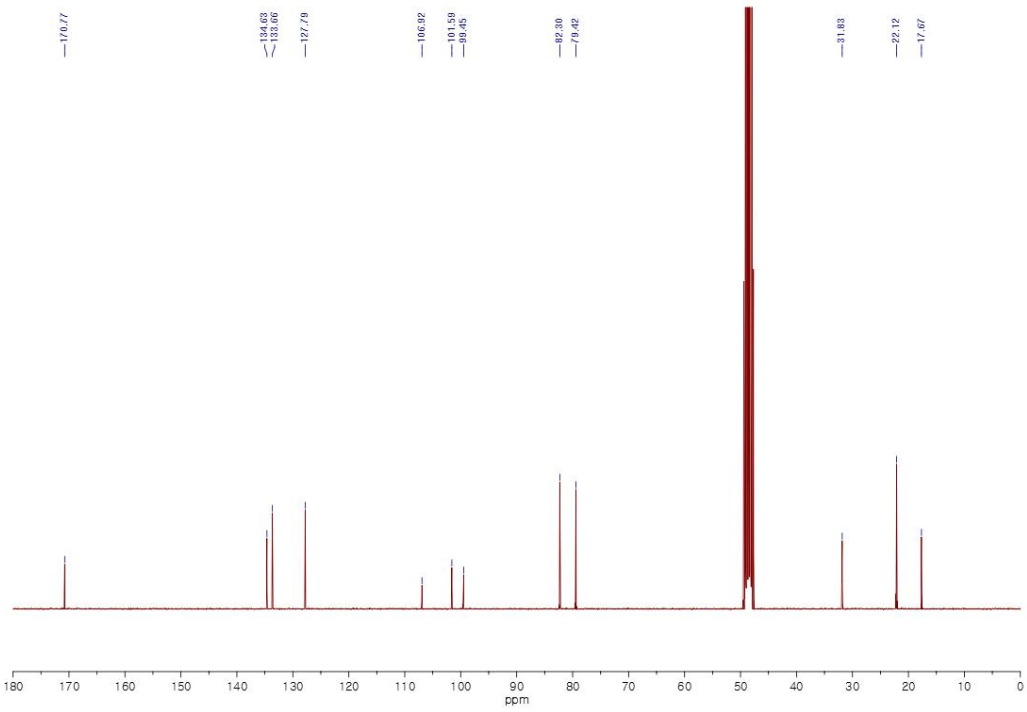

Figure 2.22 ^{13}C NMR spectrum of **A8** (CD_3OD [8.0 mM], 75 MHz)

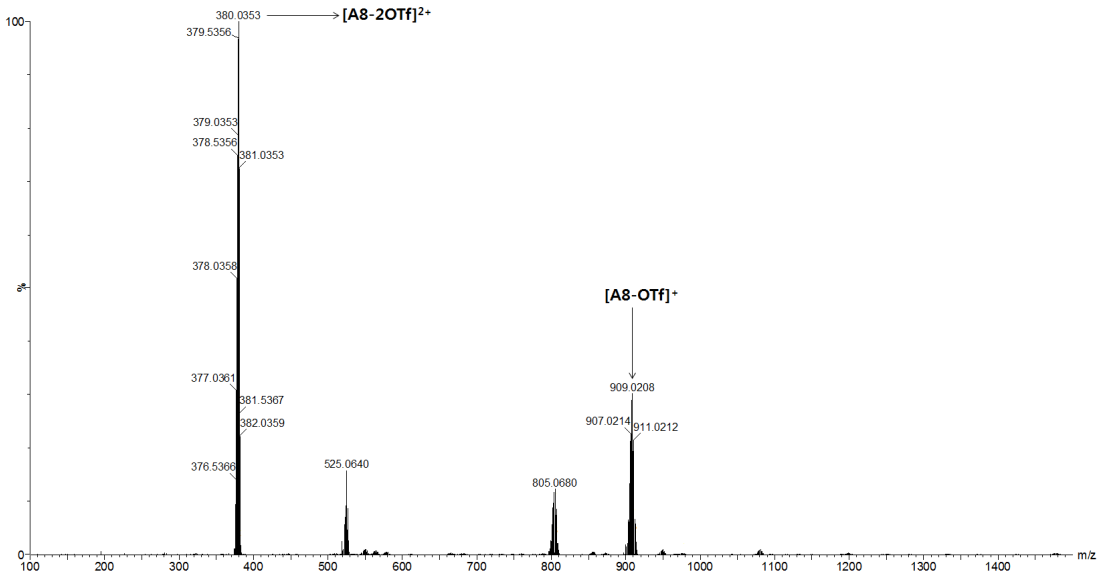

Figure 2.23 Full ESI mass spectrum of **A8** (Reaction in CD_3OD [8.0 mM])

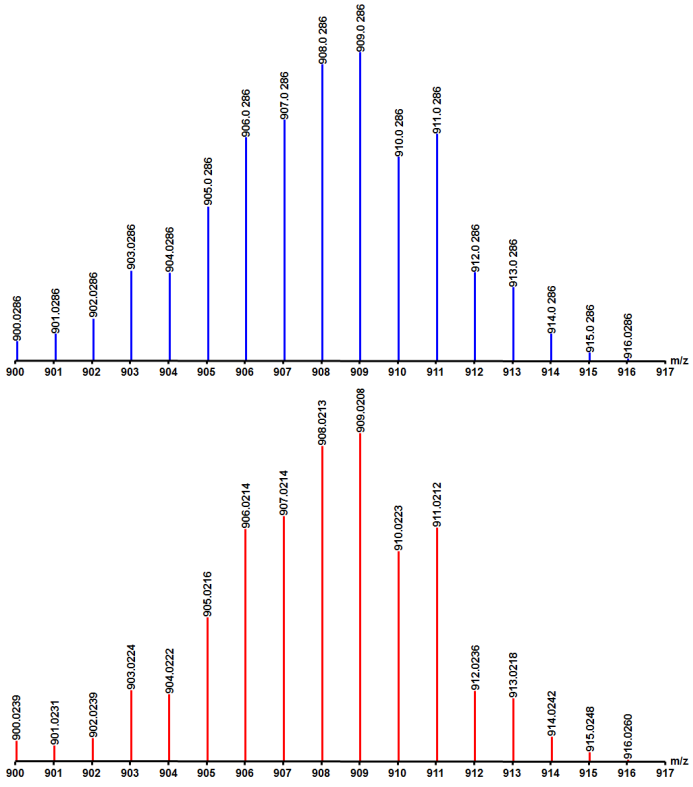

Figure 2.24 Calculated (blue) and experimental (red) ESI mass spectra of [**A8**-OTf]$^+$. (Reaction in CD_3OD [8.0 mM])

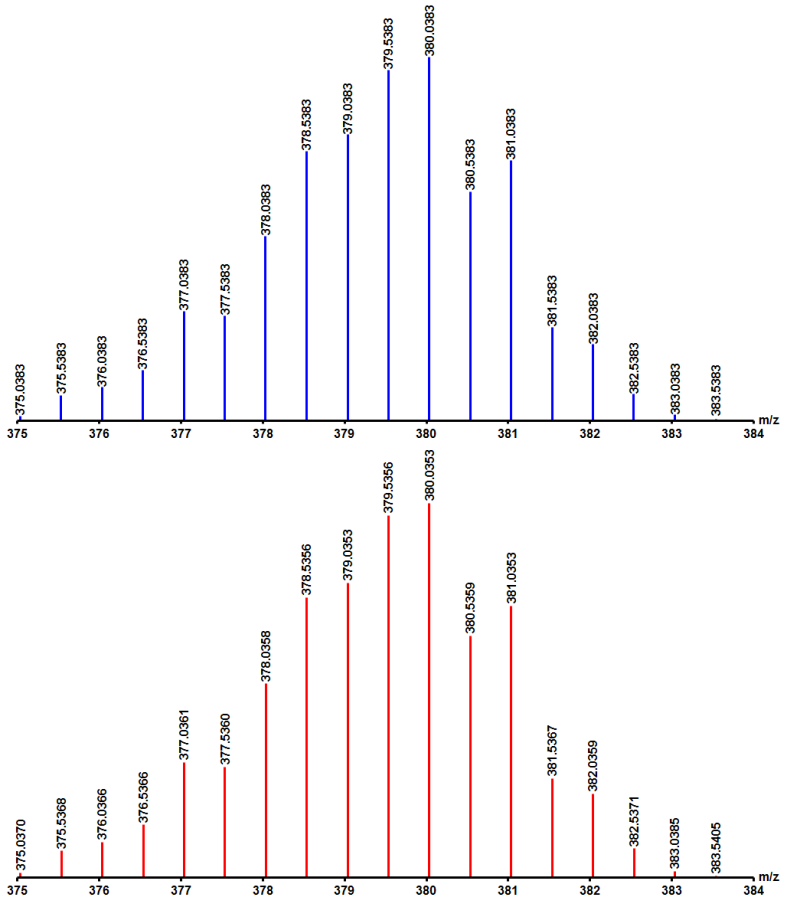

Figure 2.25 Calculated (blue) and experimental (red) ESI mass spectra of [**A8**-2OTf]$^{2+}$. (Reaction in CD_3OD [8.0 mM])

2.2.8 Coordination-driven self-assembly of a mixture of molecular knot 1 and macrocycle 2

The arene-Ru(II) acceptor **A8** (8.4 mg, 8.0 μmol) and donor **L1** (2.8 mg, 8.0 μmol) were stirred in CD_3OD (1.0 mL) at room temperature for 12 h to produce a greenish solution. The resulting solution was characterized as a mixture of products **1** and **2** (85:15 by ^1H NMR). The products were precipitated and isolated by dropwise addition of diethyl ether into this solution, and washed twice with diethyl ether using centrifugation method. The dark-green colored crystalline powders were dried to give a mixture of **1** and **2** in 87% yield. ^1H NMR (900 MHz, CD_3OD) knot **1**: δ 9.54 (d, J = 6.2 Hz, 8H), 9.38 (d, J = 6.3 Hz, 8H), 9.12 (d, J = 6.4 Hz, 8H), 8.88 (d, J = 8.5 Hz, 8H), 8.73 (d, J = 6.5 Hz, 8H), 8.62 (d, J = 8.6 Hz, 8H), 8.52 (d, J = 8.7 Hz, 8H), 8.20 (d, J = 5.8 Hz, 8H), 8.11 (d, J = 8.5 Hz, 8H), 7.89 (t, J = 8.2 Hz, 8H), 7.75 (d, J = 5.7 Hz, 8H), 7.64 (t, J = 7.8 Hz, 8H), 7.60 – 7.55 (m, 16H), 7.39 (d, J = 6.4 Hz, 8H), 7.31 (t, J = 8.1 Hz, 8H), 6.51 (s, 8H), 6.40 (s, 8H), 6.05 (d, J = 6.4 Hz, 12H), 6.04 (d, J = 5.9 Hz, 16H), 6.02 (d, J = 5.9 Hz, 12H), 5.97 (d, J = 6.1 Hz, 12H), 5.91 (d, J = 6.0 Hz, 12H), 5.88 (d, J = 6.2 Hz, 12H), 5.85 (d, J = 6.4 Hz, 12H), 5.82 (d, J = 6.1 Hz, 12H), 3.03 (dt, J = 14.4, 7.2 Hz, 8H), 2.88 (dt, J = 14.3, 7.2 Hz, 8H), 2.52 (s, 24H), 2.37 (s, 24H), 1.52 (d, J = 7.2 Hz, 24H), 1.43 (d, J = 7.2 Hz, 24H), 1.31 (d, J = 7.2 Hz, 24H), 1.27 (d, J = 7.2 Hz, 24H); macrocycle **2**: δ 8.91 (s, 3H), 8.85 (s, 3H), 8.41 (s, 3H), 8.25 (s, 3H), 8.16 (s, 3H), 8.07 (s, 3H), 5.77 (s, 3H), 2.97 (s, 3H), 2.20 (s, 8H), 1.37 (d, J = 7.2 Hz, 24H). ^{13}C NMR (225 MHz, CD_3OD) δ 170.13, 169.88, 169.57, 169.18, 169.14, 168.98, 161.82, 161,67, 161.52, 156.02, 153.71, 153.67, 151.51, 151.39, 150.14, 143.63, 143.18, 142.87, 142.17, 139.35, 138.77, 133.84, 133.71, 133.53, 133.42, 133.34, 133.06, 132.32, 132.21, 132.07, 131.81, 131.66, 129.28, 128.97, 127.64, 127.10, 126.71, 126.58, 126.52, 123.06, 122.58, 122.15, 121.81, 121.65, 120.42, 120.24, 120.12, 119.09, 118.82, 107.59, 107.27, 104.05, 103.76, 130.51, 130.45, 99.99, 99.87, 98.80, 98.54, 84.52, 84.35, 83.74, 83.24, 83.15, 83.01, 82.71, 82.54, 82.05, 82.01, 81.64, 65.48, 30.71, 30.61, 30.56, 29.26, 21.69, 21.60, 21.31, 21.24, 21.03, 20.68, 16.89, 16.87, 16.48, 14.01.

2.2.9 Coordination-driven self-assembly of molecular knot 1

The arene-Ru(II) acceptor **A8** (8.4 mg, 8.0 μmol) and donor **L1** (2.8 mg, 8.0 μmol) were stirred in CD_3OD (1.0 mL) at room temperature for 12 h to provide a greenish solution. To this solution, D_2O (1.0 mL) was added and stirred further for 2 h. The resulting dark-green colored solution was characterized as the only product **1** by ^1H NMR and ESI-MS analyses. The product was precipitated by dropwise addition of diethyl ether into the solution, and washed with diethyl ether. The dark-green colored crystalline powders were dried to give the molecular knot **1** in 83% yield. Anal. Calcd for $C_{464}H_{368}F_{48}N_{16}O_{80}Ru_{16}S_{40}\cdot 2H_2O$: C 49.34; H 3.32; N 1.98. Found: C 49.56; H 3.32; N 1.99. Mp: >300℃. ^1H NMR (900 MHz, 1:1 CD_3OD/D_2O) δ 9.43 (s, 8H), 9.25 (s, 8H), 9.05 (d, J = 24.0 Hz, 8H), 8.76 (s, 8H), 8.65 (s, 8H), 8.54 (s, 8H), 8.42 (s, 8H), 8.11 (s, 8H), 8.07 (d, J = 7.1 Hz, 8H), 7.85 (s, 8H), 7.66 (s, 8H), 7.58 (s, 8H), 7.52 (s, 8H), 7.41 (s, 8H), 7.34 (s, 8H), 7.24 (s, 8H), 6.47 (d, J = 11.4 Hz, 8H), 6.38 (s, 8H), 6.01 (d, J = 5.5 Hz, 10H), 5.97 (s, 12H), 5.93 (d, J = 5.7 Hz, 10H), 5.85 (s, 8H), 5.80 (d, J = 8.1 Hz, 16H), 5.73 (s, 8H), 2.87 – 2.84 (m, 8H), 2.70 – 2.68 (m, 8H), 2.45 (s, 24H), 2.33 (s, 24H), 1.39 (d, J = 6.6 Hz, 24H), 1.30 (d, J = 5.9 Hz, 24H), 1.18 (d, J = 6.5 Hz, 24H), 1.13 (d, J = 6.7 Hz, 24H); ESI-HRMS m/z calcd for $[C_{458}H_{368}F_{30}N_{16}O_{62}Ru_{16}S_{32}]^{6+}$: 1128.0229; found 1128.0045 [**1**-6OTf]$^{6+}$.

2.2.10 Coordination-driven self-assembly of monomeric macrocycle 2

The arene-Ru(II) acceptor **A8** (3.17 mg, 3.0 μmol) and donor **L1** (1.05 mg, 3.0 μmol) were stirred in CD_3NO_2 (1.0 mL) at room temperature for 12 h to produce a darkgreen solution. The resulting solution was characterized as the sole product **2** by ^1H, DOSY NMR and ESI-MS analyses. ^1H NMR (300 MHz, CD_3NO_2) δ 8.80 (dd, J = 6.0, 3.4 Hz, 8H), 8.49 (d, J = 6.6 Hz, 8H), 7.99 (dd, J = 6.0, 3.4 Hz, 8H), 7.65 (s, 4H), 7.38 (d, J = 5.9 Hz, 8H), 5.94 (d, J = 6.2 Hz, 8H), 5.73 (d, J = 6.2 Hz, 8H), 3.37 – 2.51 (m, 4H), 2.27 (s, 12H), 1.39 (d, J = 6.9 Hz, 24H). ^{13}C NMR (200 MHz,

CD_3NO_2) δ 169.23, 151.94, 144.33, 143.42, 141.63, 140.36, 133.77, 132.77, 132.12, 127.02, 121.84, 121.27, 120.46, 120.25, 118.65, 107.08, 103.91, 99.34, 83.70, 82.62, 30.54, 21.17, 16.59; ESI-HRMS m/z calcd for $[C_{113}H_{92}F_3N_4O_{11}Ru_4S_7]^{3+}$: 789.3688; found 789.3630 [**2**-3OTf]$^{3+}$.

2.2.11 Coordination-driven self-assembly of monomeric macrocycle 3

The arene-Ru(II) acceptor **A5** (6.85 mg, 8.0 μmol) and donor **L1** (2.80 mg, 8.0 μmol) were stirred in CD_3OD (1.0 mL) at room temperature for 12 h to produce a bright orange solution. The products were precipitated and isolated by dropwise addition of diethyl ether into this solution, and washed twice with diethyl ether using centrifugation method. The orange powder was characterized as **3**. Yield: (7.82 mg, Yield: 81 %), Anal. Calcd for $C_{84}H_{76}F_{12}N_4O_{20}Ru_4S_{10}\cdot 2H_2O$: C 41.17; H 3.29; N 2.29. Found: C 41.15; H 3.30; N 2.29. ^{1}H NMR (300 MHz, CD_3OD) δ 7.97 (d, J = 6.6 Hz, 8H), 7.92 (s, 4H), 7.60 (d, J = 6.6 Hz, 8H), 5.93 (d, J = 6.2 Hz, 8H), 5.75 (d, J = 6.2 Hz, 8H), 2.84 (dt, J = 13.8, 6.8 Hz, 5H), 2.22 (s, 12H), 1.37 (d, J = 6.9 Hz, 24H); ^{13}C NMR (75 MHz, CD_3OD) δ 170.98, 152.42, 145.24, 144.12, 132.60, 122.26, 120.69, 102.25, 97.37, 82.08, 81.48, 31.08, 21.07, 16.64. ESI-HRMS m/z calcd for $[C_{81}H_{76}F_3N_4O_{11}Ru_4S_7]^{3+}$: 655.9937; found 655.9904 [**3**-3OTf]$^{3+}$.

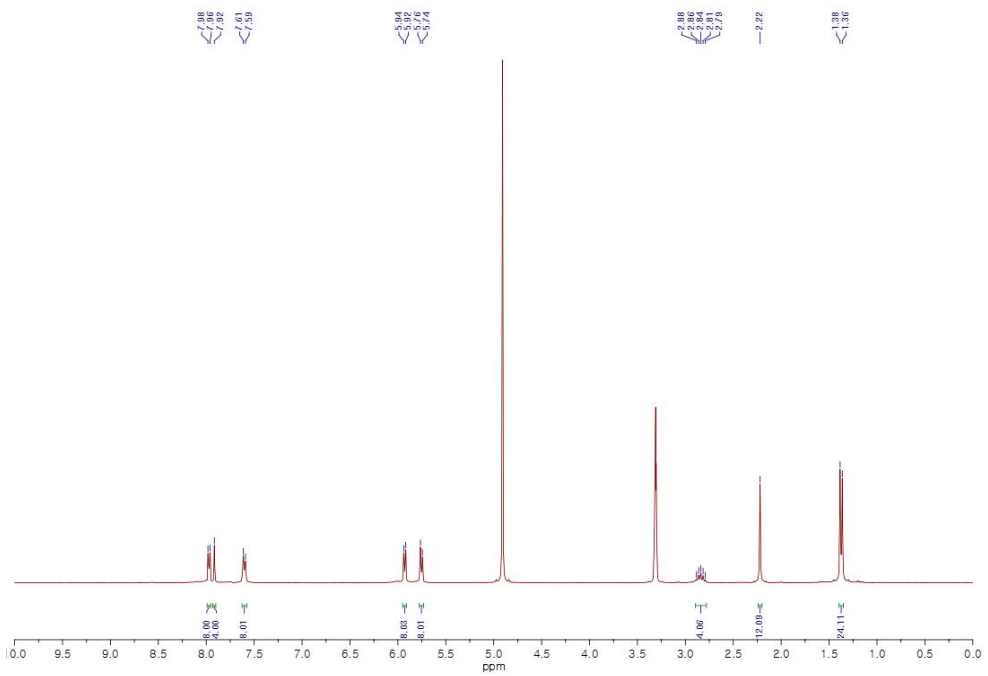

Figure 2.26 ^{1}H NMR spectrum of **3** (CD_3OD [8.0 mM], 300 MHz)

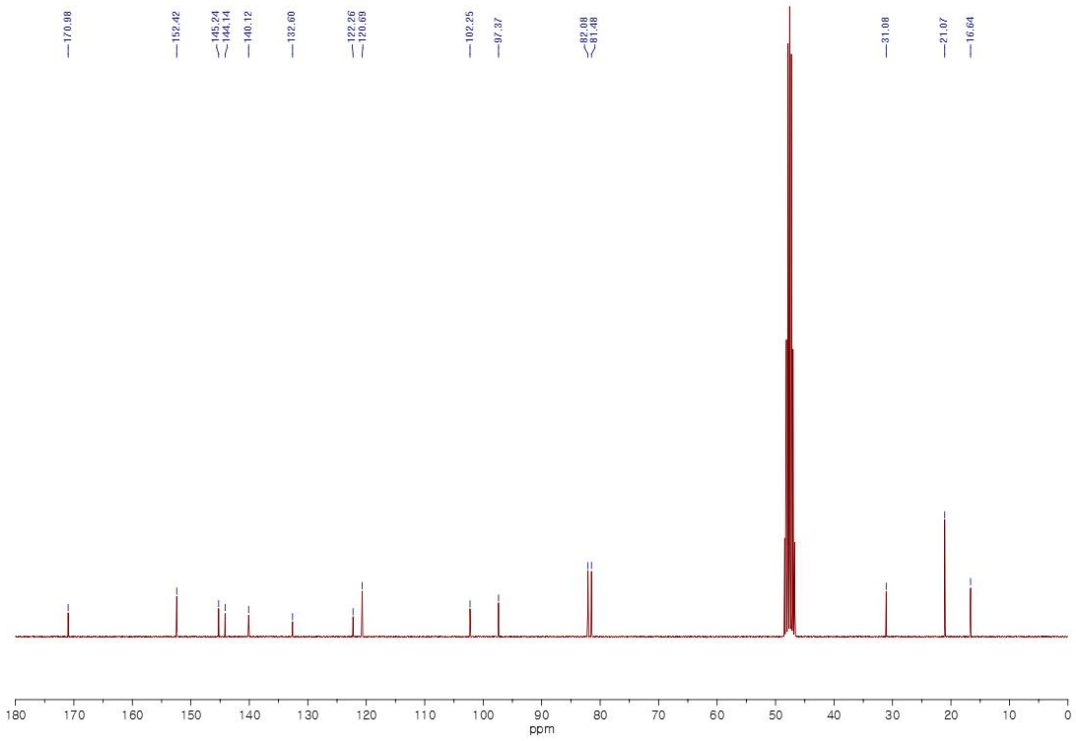

Figure 2.27 ^{13}C NMR spectrum of **3** (CD_3OD [8.0 mM], 75 MHz)

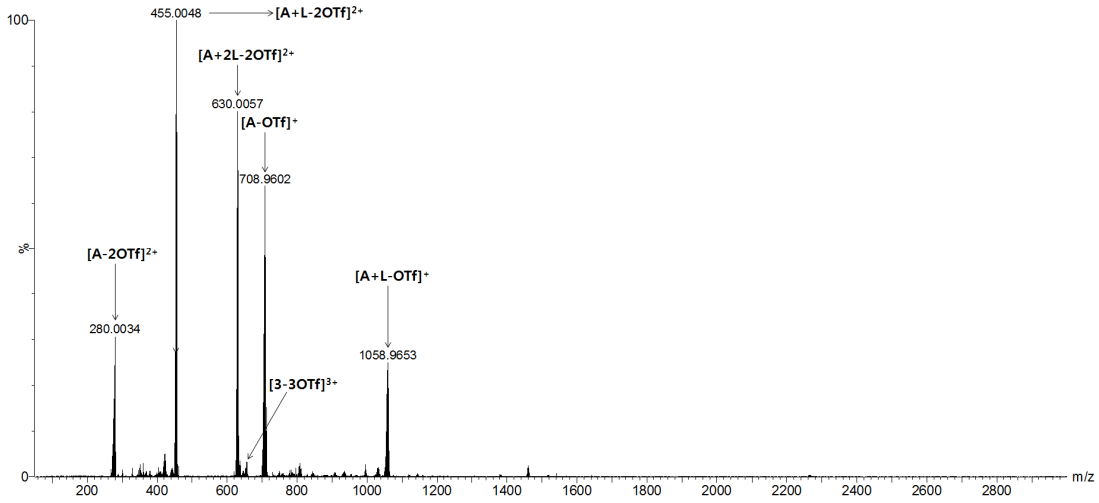

Figure 2.28 full ESI mass spectrums of **3** (Reaction in CD_3OD [8.0 mM])

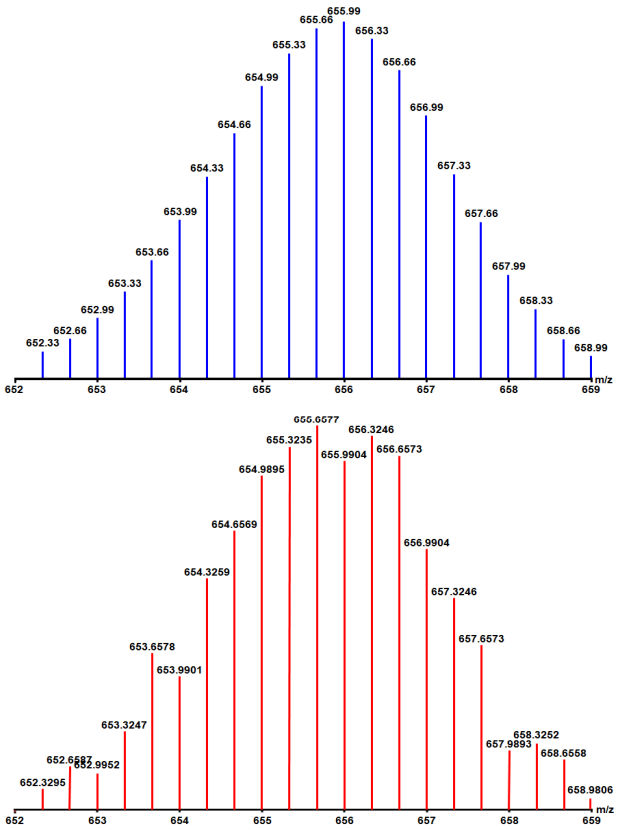

Figure 2.29 Calculated (blue) and experimental (red) ESI mass spectra of [**3**-3OTf]$^{3+}$. (Reaction in CD_3OD [8.0 mM])

2.2.12 Synthesis of self-assembly of [2]catenane 4

The arene-Ru(II) acceptor **A6** (7.25 mg, 8.0 μmol) and donor **L1** (2.80 mg, 8.0 μmol) were stirred in CD_3OD (1.0 mL) at room temperature for 12 h to produce a dark red solution. The products were precipitated and isolated by dropwise addition of diethyl ether into this solution, and washed twice with diethyl ether using centrifugation method. The dark red powder was characterized as **4**. Yield: (7.84 mg, Yield: 78 %), Anal. Calcd for $C_{184}H_{160}F_{24}N_8O_{40}Ru_8S_{20}\cdot 2H_2O$: C 43.63; H 3.26; N 2.21. Found: C 43.49; H 3.27; N 2.21. ^{1}H NMR (300 MHz, CD_3OD) δ 8.34 (d, J = 5.6 Hz, 4H), 8.30 (d, J = 5.6 Hz, 4H), 8.06 (s, 2H), 7.95 (d, J = 5.6 Hz, 4H), 7.79 (dd, J = 12.7, 4.8 Hz, 8H), 7.46 (d, J = 8.6 Hz, 6H), 7.14 (s, 2H), 6.32 (s, 2H), 6.15 (d, J = 6.1 Hz, 4H), 6.12 (t, J = 5.7 Hz, 5H), 6.10 – 6.08 (m, 5H), 6.05 (s, 6H), 6.02 (d, J = 5.8 Hz, 3H), 5.96 (d, J = 5.8 Hz, 3H), 5.95 (d, J = 6.6 Hz, 6H), 5.91 – 5.90 (m, 4H), 5.89 (d, J = 5.7 Hz, 3H), 5.85 (d, J = 5.8 Hz, 4H), 5.81 (d, J = 2.2 Hz, 4H), 5.74 (d, J = 5.7 Hz, 3H), 5.72 (d, J = 5.9 Hz, 2H), 3.01 (dd, J = 14.1, 7.0 Hz, 4H), 2.94 (dd, J = 13.8, 6.9 Hz, 3H), 2.91 – 2.88 (m, 2H), 2.88 – 2.85 (m, 3H), 2.32 (d, J = 12.6 Hz, 12H), 2.24 (s, 8H), 2.20 (s, 8H), 2.10 (s, 8H), 1.47 (dd, J = 9.1, 4.8 Hz, 24H), 1.42 (dd, J = 6.9, 2.2 Hz, 16H), 1.37 (dd, J = 15.6, 6.8 Hz, 24H), 1.34 (d, J = 7.0 Hz, 8H). ^{13}C NMR (75 MHz, CD_3OD) δ 184.64, 184,40, 184.32, 184.28, 184.19, 184.14, 184.10, 184.08, 184.06, 152.80, 152.65, 144.82, 144.41, 144.38, 144.20, 144.10, 143.81, 142.88, 142.75, 141.04, 140.95, 140.35, 139.69, 132.62, 132.39, 132.15, 131.39, 128.47, 125.77, 122.91, 122.21, 121.53, 121.33, 121.23, 121.01, 120.73, 120.43, 119.74, 118.15, 104.25, 103.98, 103.95, 103.92, 103.90, 103.82, 101.88, 101.54, 101.49, 101.41, 98.83, 98.74, 98.70, 98.51, 83.66, 83.51, 83.45, 82.17, 82.13, 81.91, 81.85, 81.77, 81.74, 81.32, 31.24, 31.21, 31.14, 21.38, 21.26, 21.21, 21.20, 21.18, 21.16, 21.15, 21.11, 17.18, 16.93, 16.81, 16.77, 16.69. ESI-HRMS m/z calcd for $[C_{181}H_{160}F_{15}N_8O_{31}Ru_8S_{17}]^{3+}$: 1527.2937; found 1527.6223 [**4**-3OTf]$^{3+}$.

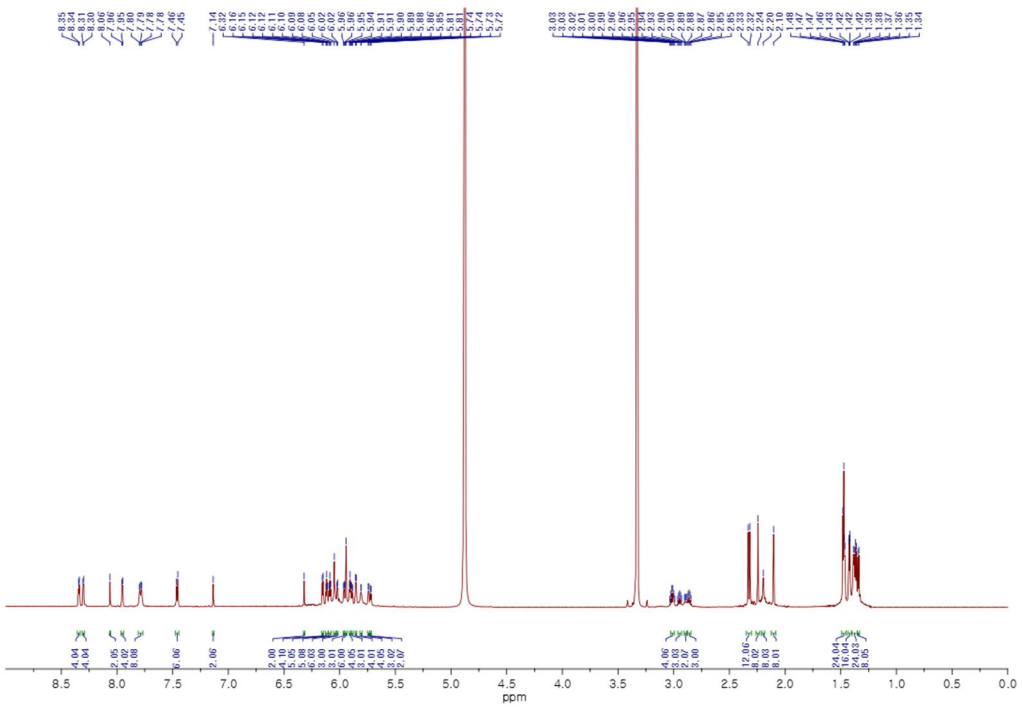

Figure 2.30 ^{1}H NMR spectrum of **4** (CD_3OD [8.0 mM], 300 MHz)

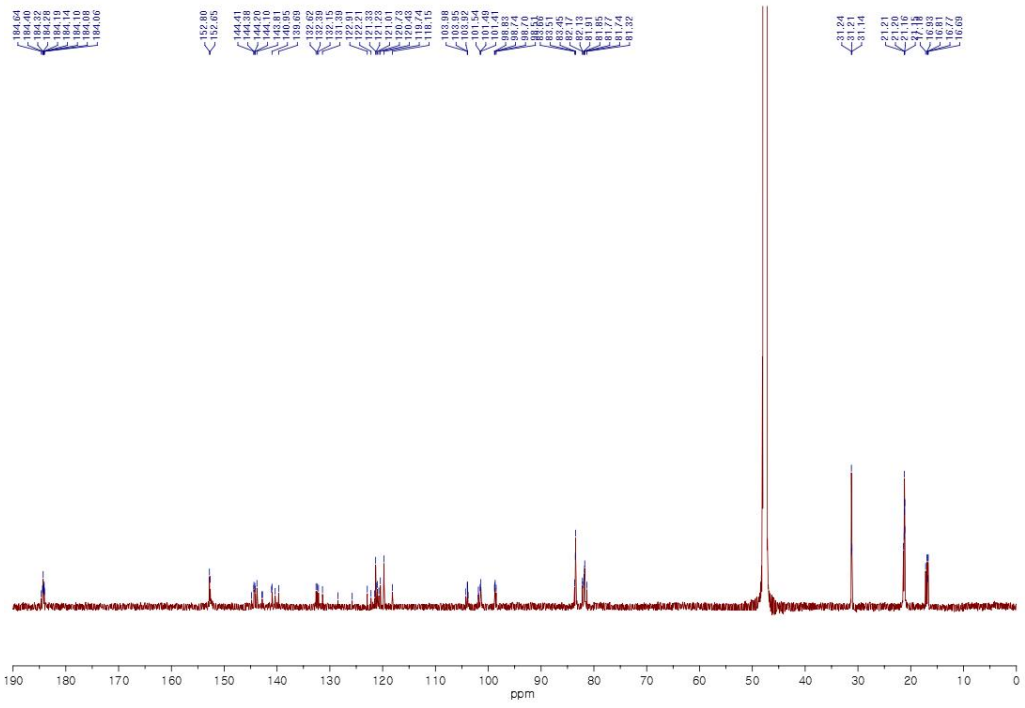

Figure 2.31 ^{13}C NMR spectrum of **4** (CD_3OD [8.0 mM], 75 MHz)

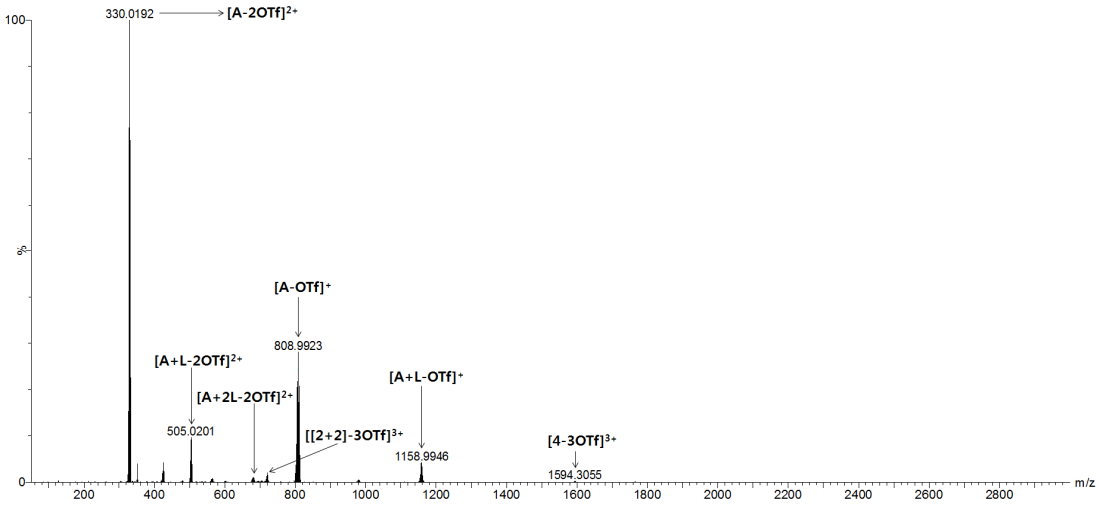

Figure 2.32 full ESI mass spectrums of **4** (Reaction in CD_3OD [8.0 mM])

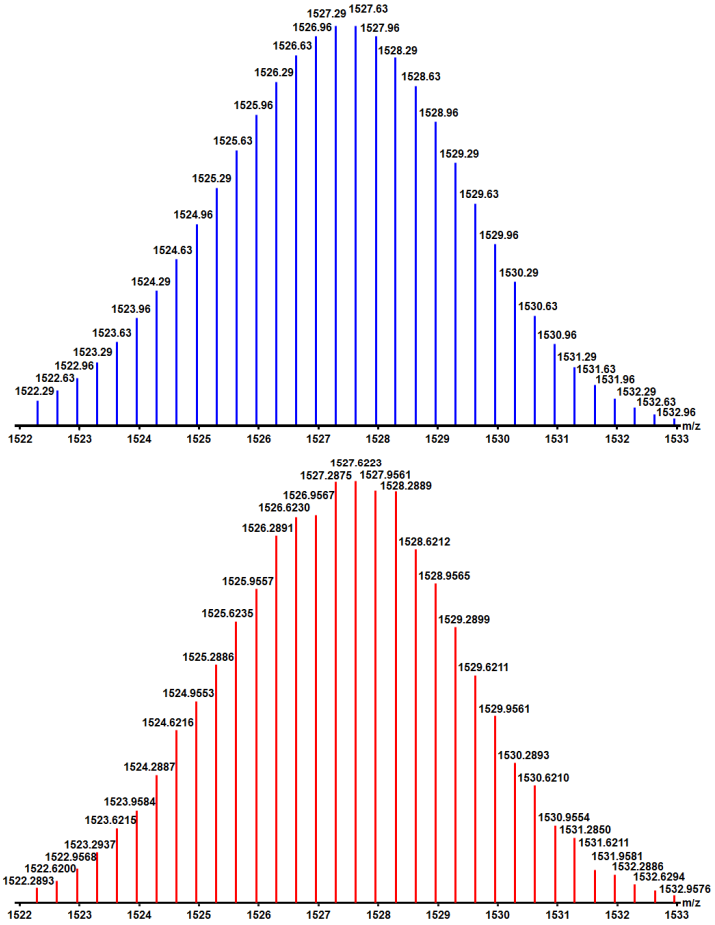

Figure 2.33 Calculated (blue) and experimental (red) ESI mass spectra of [**4**-3OTf]$^{3+}$. (Reaction in CD_3OD [8.0 mM])

2.2.13. Synthesis of self-assembly of [2]catenane 5

The arene-Ru(II) acceptor **A7** (7.65 mg, 8.0 μmol) and donor **L** (2.80 mg, 8.0 μmol) were stirred in CD_3OD (1.0 mL) at room temperature for 12 h to produce a dark brown solution. The products were precipitated and isolated by dropwise addition of diethyl ether into this solution, and washed twice with diethyl ether using centrifugation method. The dark brown powder was characterized as **5**. Yield: (8.88 mg, Yield: 85 %), Anal. Calcd for $C_{200}H_{168}F_{24}N_8O_{40}Ru_8S_{20}\cdot 2H_2O$: C 45.62; H 3.29; N 2.13. Found: C 45.56; H 3.30; N 2.13. ^{1}H NMR (300 MHz, CD_3OD) δ 8.44 (d, J = 6.4 Hz, 4H), 8.38 (d, J = 6.5 Hz, 4H), 8.24 (d, J = 6.3 Hz, 4H), 8.15 (d, J = 6.4 Hz, 4H), 7.83 (s, 2H), 7.62 (d, J = 6.4 Hz, 4H), 7.52 (d, J = 5.8 Hz, 6H), 7.46 (s, 2H), 7.36 (d, J = 5.8 Hz, 14H), 7.18 – 7.08 (m, 6H), 7.00 (d, J = 6.3 Hz, 6H), 5.95 – 5.76 (m, 16H), 5.73 – 5.48 (m, 16H), 2.99 – 2.74 (m, 8H), 2.20 (d, J = 4.6 Hz, 12H), 2.13 (s, 6H), 2.02 (s, 6H), 1.46 – 1.26 (m, 48H). ^{13}C NMR (75 MHz, CD_3OD) δ 170.98, 107.90, 170.71, 151.90, 151.85, 151.75, 151.63, 151.54, 144.21, 143.99, 140.36, 140.21, 139.80, 137.73, 137.73, 137.43, 137.34, 131.85, 131.27, 129.80, 128.47, 126.93, 122.70, 120.65, 120.46, 120.42, 118.47, 111.55, 111.49, 111.38, 111.31, 103.53, 103.47, 99.88, 99.73, 99.64, 84.78, 84.64, 84.54, 84.51, 82.58, 82.48, 30.66, 30.63, 30.56, 21.31, 21.26, 21.21, 21.15, 21.10, 16.32, 16.16, 16.01, 15.94. ESI-HRMS m/z calcd for $[C_{197}H_{168}F_{15}N_8O_{31}Ru_8S_{17}]^{3+}$: 1594.3145; found 1594.3055 [**5**-3OTf]$^{3+}$.

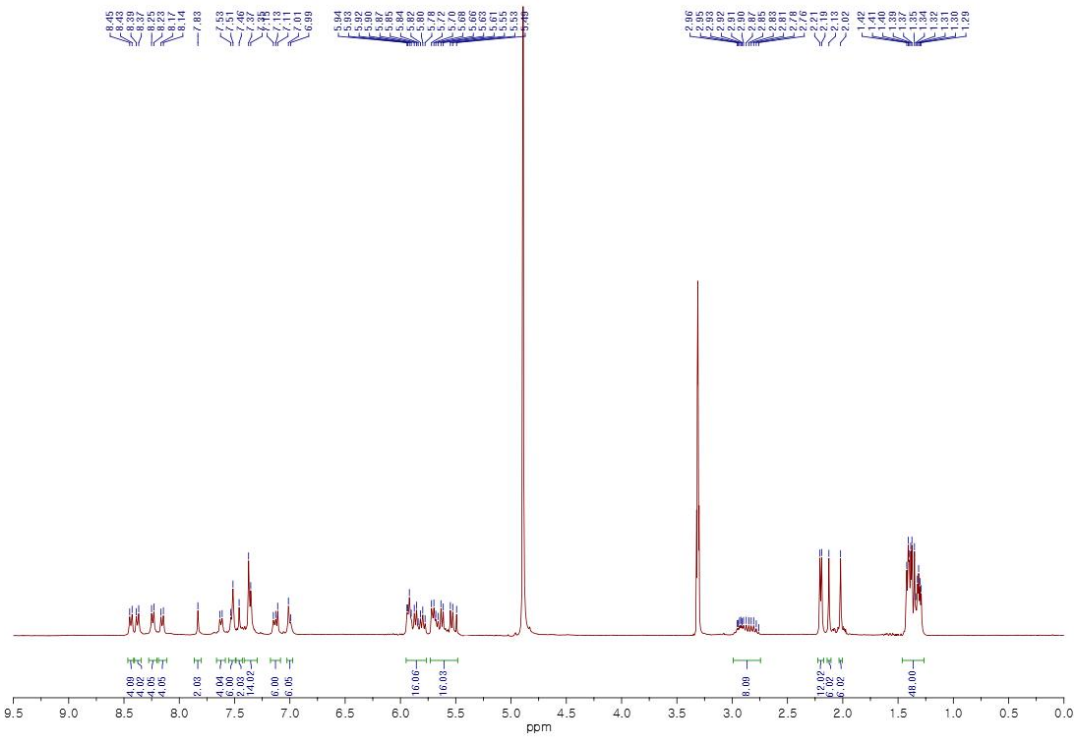

Figure 2.34 ^{1}H NMR spectrum of **5** (CD_3OD [8.0 mM], 300 MHz)

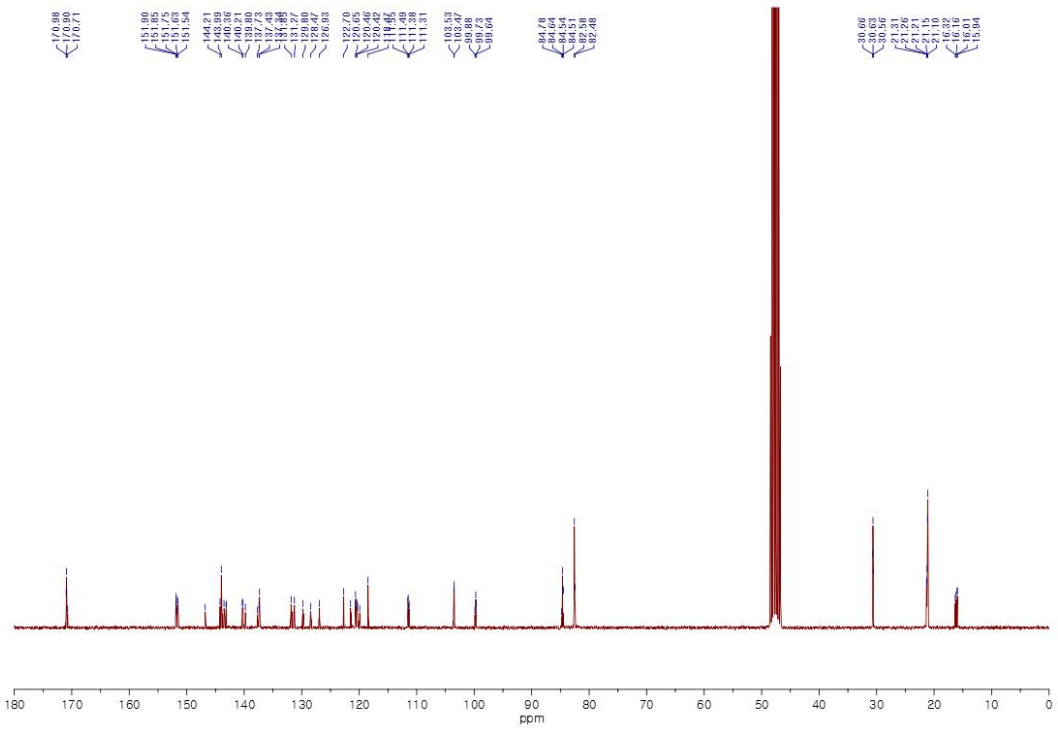

Figure 2.35 ^{13}C NMR spectrum of **5** (CD_3OD [8.0 mM], 75 MHz)

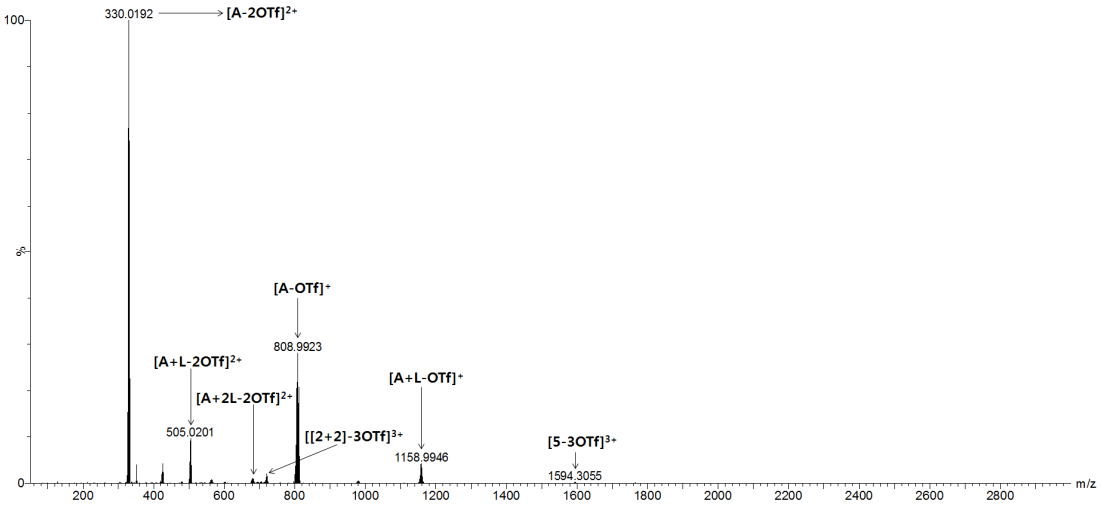

Figure 2.36 full ESI mass spectrums of **5** (Reaction in CD_3OD [8.0 mM])

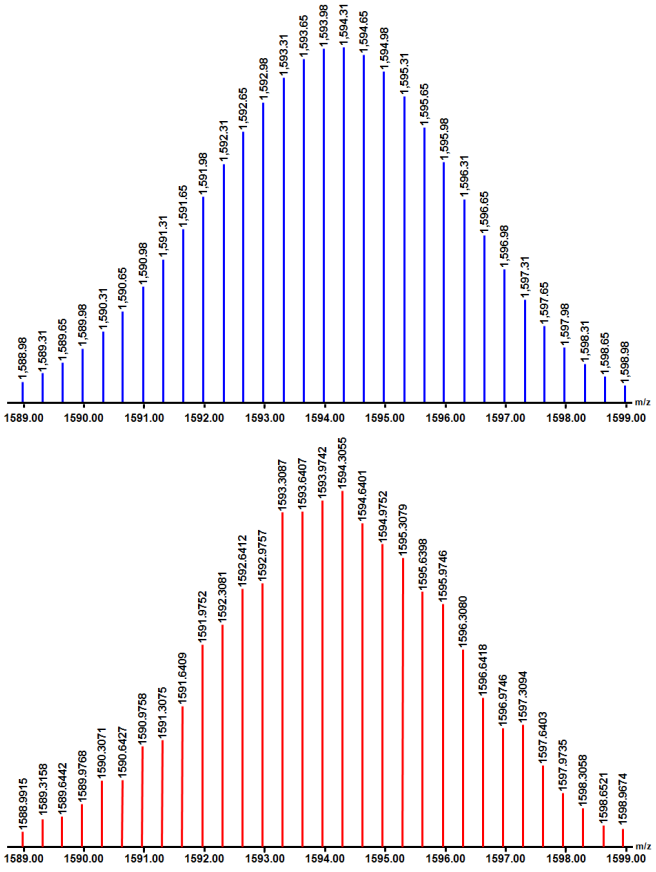

Figure 2.37 Calculated (blue) and experimental (red) ESI mass spectra of [**5**-3OTf]$^{3+}$. (Reaction in CD_3OD [8.0 mM])

2.3. Results and discussion

2.3.1. Synthesis and characterization of Molecular knot 1 and macrocycle 2

An equimolar mixture (8.0 mm) of **A8** and **L** was stirred in CD_3OD for 12 hours at room temperature (Figure 1.38A). The complex ^1H NMR spectrum of the clear greenish solution obtained suggested the formation of a self-assembled product with a complicated molecular structure or a mixture of products as the resonances of almost all equivalent protons in donor **L** and acceptor **A8** were different (see Figures 1.39–1.44 in the Supporting Information). Two different diffusion coefficients at D = 3.5×10^{-10} m^2s^{-1} and 4.2×10^{-10} m^2s^{-1} determined from the diffusion-ordered NMR spectrum (DOSY) indicated the presence of two new compounds in the reaction mixture (Figure 1.38B). Prominent peaks at m/z = 1727.68 $[\mathbf{1}\text{-}6OTf]^{6+}$ and m/z = 789.37 $[\mathbf{2}\text{-}3OTf]^{3+}$ in the ESI-MS spectrum and their perfect agreement with theoretical isotopic distributions confirmed that two products were [8+8] self-assembled compound **1** and the [2+2] self-assembled macrocycle **2** (Figures 1.45, 1.46). The respective proportion of **1** and **2** in CD_3OD at 8.0 mm concentration was found to be 85.2 and 14.8% based on ^1H NMR (Figure 1.41).

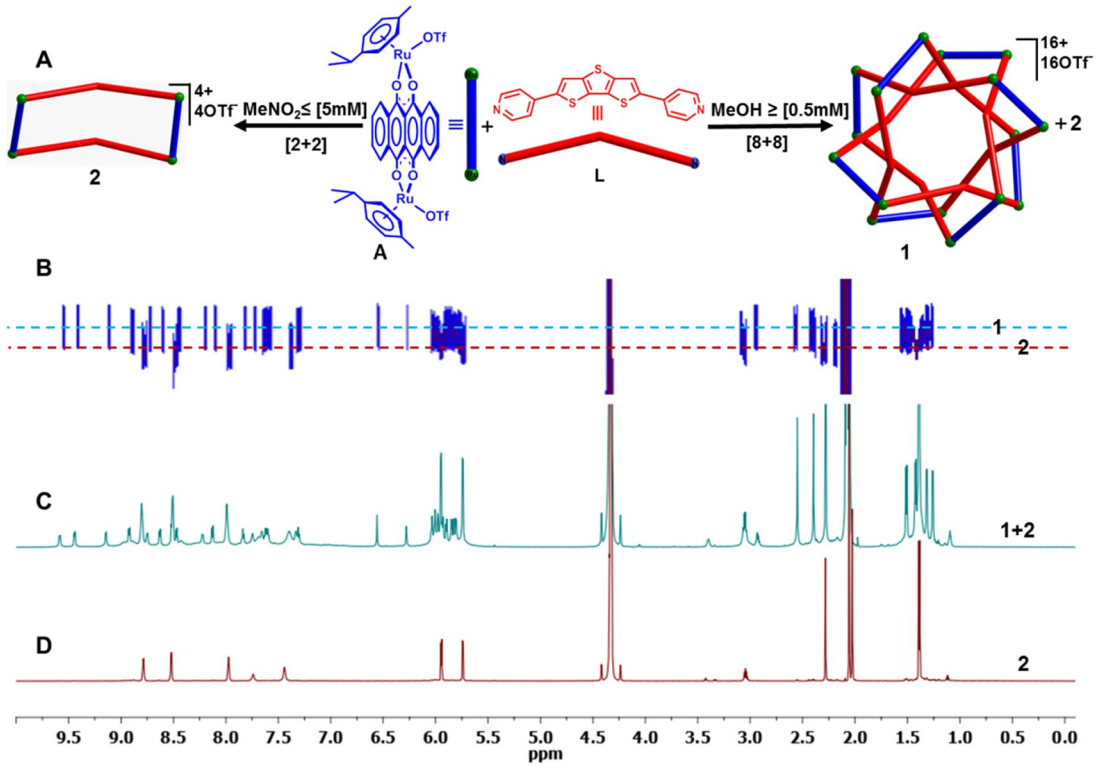

Figure 2.38 Self-assembly and ^{1}H-DOSY NMR of the molecular knot **1** and macrocycle **2**. (A) Coordination driven self-assembly of the molecular knot **1** and macrocycle **2**. DOSY (B) and ^{1}H-NMR (C) of mixture of **1** and **2** (the reaction was carried out in methanol and NMR was then performed in CD_3NO_2 after drying) ([5.0 mm], 800 MHz, 298 K) (D) ^{1}H NMR of **2** (reaction was carried out in CD_3NO_2 and NMR was then performed) ([5.0 mm], 800 MHz, 298 K).

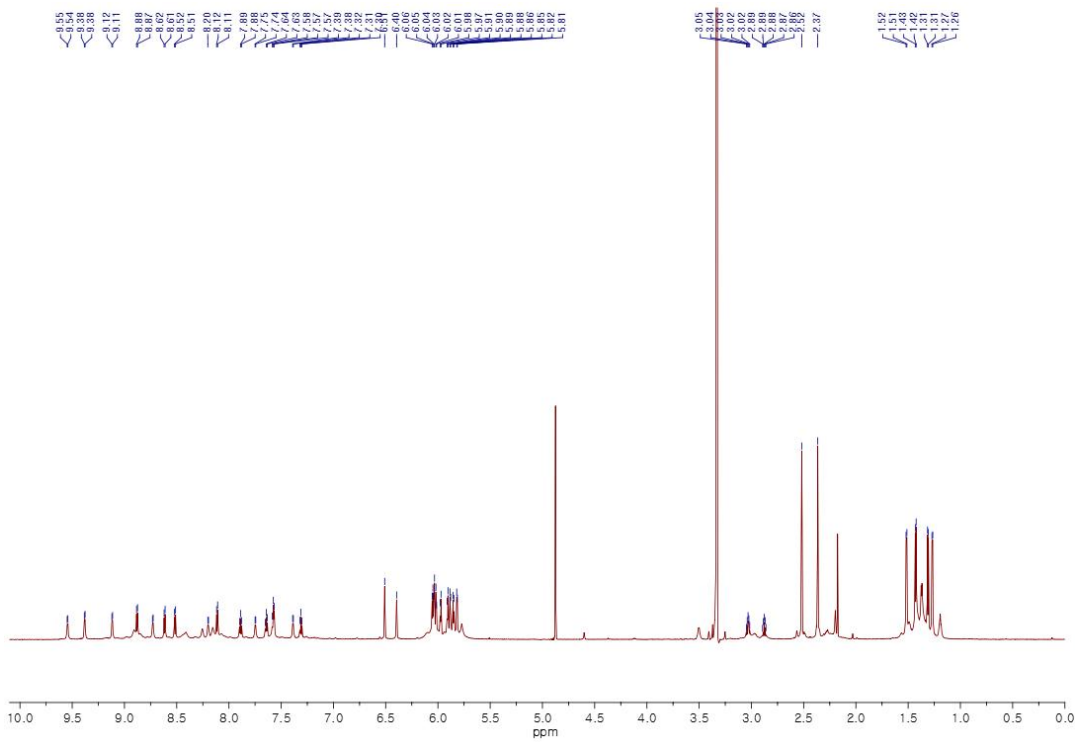

Figure 2.39 ^{1}H NMR spectrum of mixture **1+2** (CD_3OD [8.0 mM], 900 MHz)

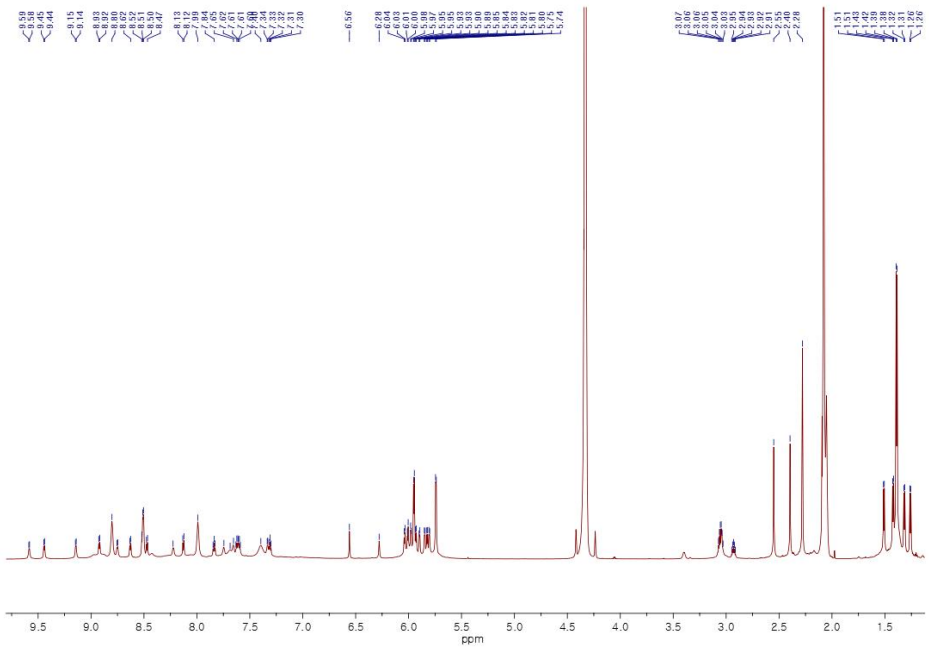

Figure 2.40 ^{1}H NMR spectrum of mixture **1+2** (Prepared in CD_3OD and NMR recorded in CD_3NO_2 after drying) (CD_3NO_2 [5.0 mM], 800 MHz)

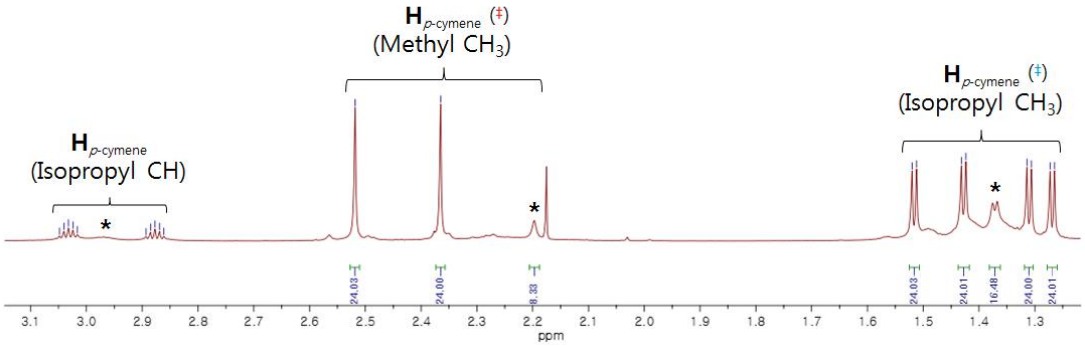

COMPONENT	integral	mol %	MW	mass contrib.	mass %
(2+2) monomeric macrocycle **2**	8.33(‡)	41.0	2814.9	115410.9	14.8
(8+8) molecular knot **1**	48.0(‡)	59.0	11259.6	664316.4	85.2
(total)		100		779727.3	100
(2+2) monomeric macrocycle **2**	16.5(‡)	40.7	2814.9	114681.1	14.7
(8+8) molecular knot **1**	96.0(‡)	49.3	11259.6	667235.6	85.3
(total)		100		781916.7	100

Figure 2.41 Partial ^{1}H NMR spectrum of mixture **1**+**2** (CD_3OD [8.0 mM], 900 MHz)

*[2+2] monomeric macrocycle **2**

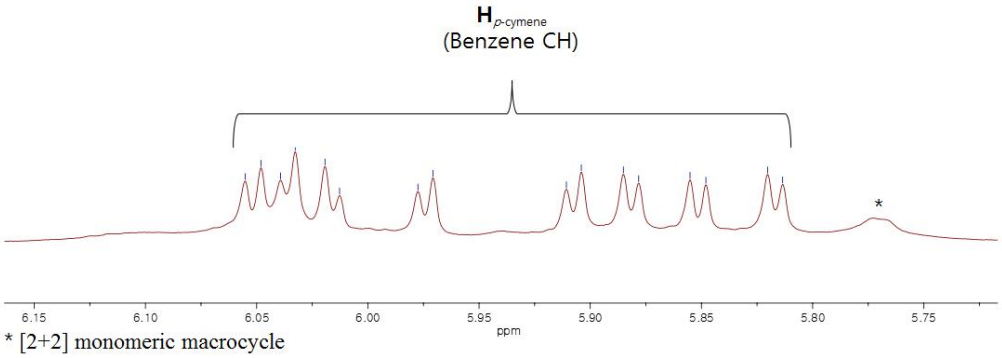

Figure 2.42 ^{1}H NMR expansion spectrum of mixture **1+2** (CD_3OD [8.0 mM], 900 MHz)

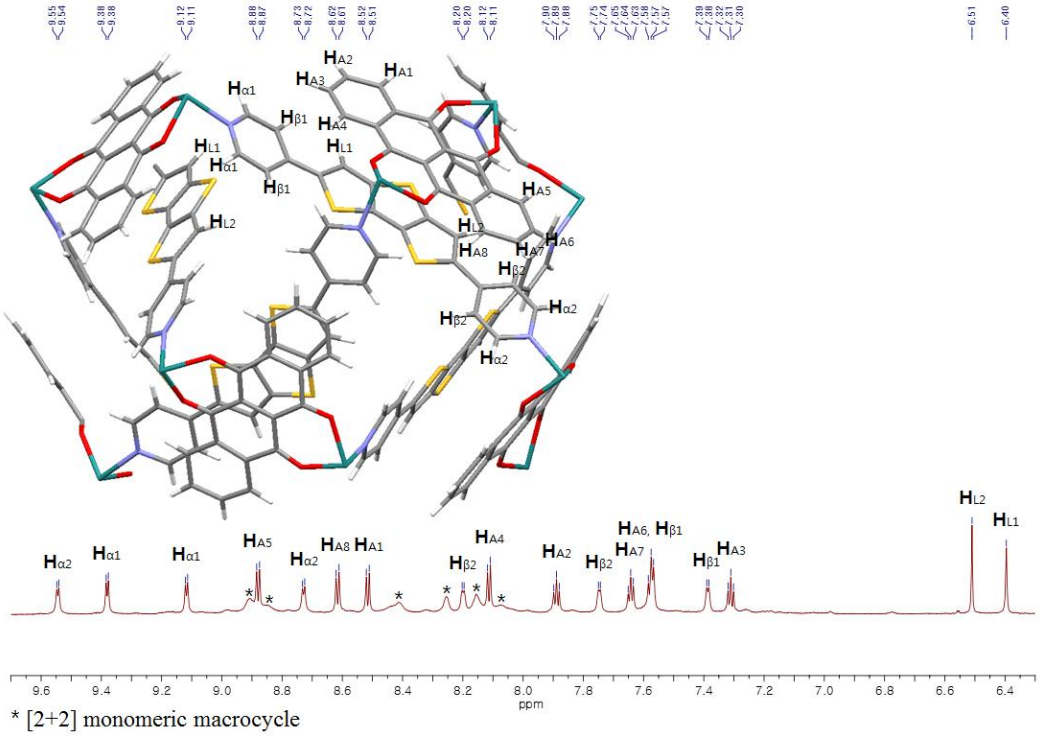

Figure 2.43 ^{1}H NMR expansion spectrum of mixture **1+2** (CD_3OD [8.0 mM], 900 MHz)

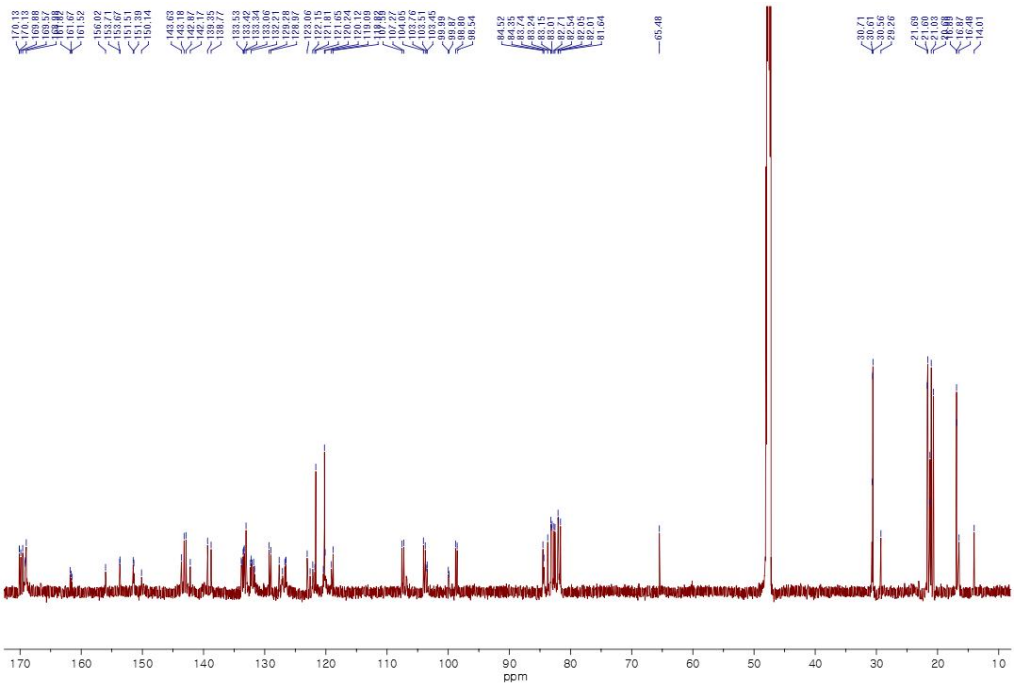

Figure 2.44 ^{13}C NMR spectrum of mixture **1+2** (CD_3OD [8.0 mM], 225 MHz)

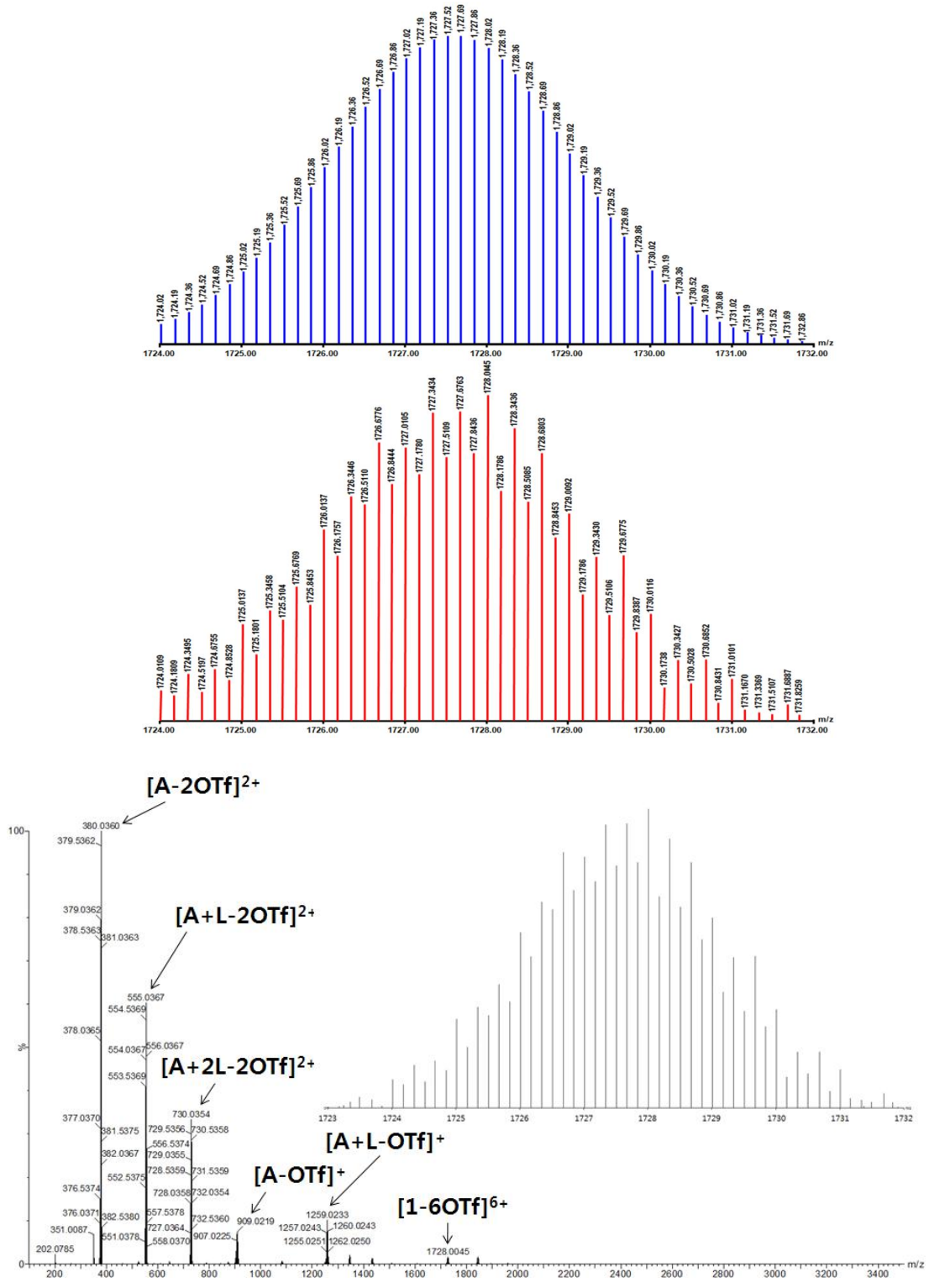

Figure 2.45 Calculated (blue) and experimental (red) ESI mass spectrum of [**1**-6OTf]$^{6+}$ and full spectrum at bottom (Inset figure showing observed peak for [**1**-6OTf]$^{6+}$). (Reaction in CD_3OD).

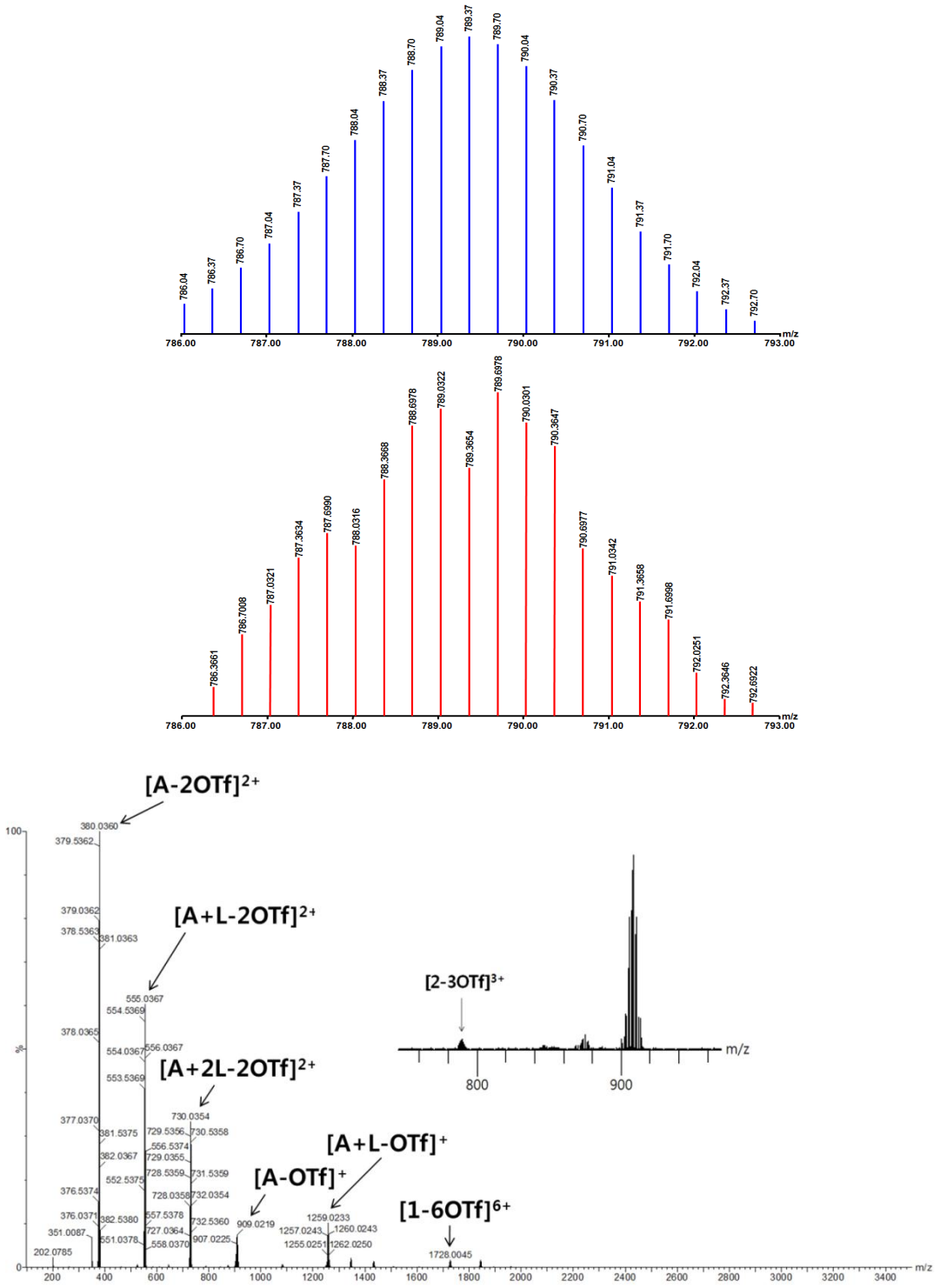

Figure 2.46 Calculated (blue) and experimental (red) ESI mass spectrum of [**2**-3OTf]$^{3+}$ and full spectrum at bottom (Inset figure showing observed peak for [**2**-3OTf]$^{3+}$). (Reaction in CD_3OD).

2.3.2. 2D NMR analysis and titration of Molecular knot 1 and macrocycle 2

Knowing the hydrophobic properties of these macrocycles,[11a] D_2O was added sequentially to the 8.0 mm CD_3OD solution of **1**+**2**, stirred for 2 hours, and NMR spectra were obtained after each addition. ^1H NMR showed a gradual increase in the proportion of **1** upon increasing the amount of D_2O and at a CD_3OD:D_2O ratio of 1:1 the mixture of **1**+**2** fully transformed to **1**. (Figures 1.47 and 1.48). All protons of donor and acceptor moieties in **1** resonated at significantly different chemical shifts, indicating tight packing. A detailed 2D NMR study in combination with ESI-MS analysis strongly supported the symmetrically knotted [8+8] self-assembled structure of **1** in solution (Figures 1.49–1.70). The extreme upfield shift of dithienothiophene protons in the ^1H NMR spectrum confirmed strong π-π stacking of the dithienothiophene moiety of donor **L** and the tetracene moiety of acceptor **A8**. The topology of **1** was unambiguously established by single-crystal X-ray analysis in the solid state. Other similar acceptors[12a] could not produce an analogous topology by self-assembly with donor **L**. Reaction in CD_3NO_2 at concentration lower than 5 mm resulted only in macrocycle **2** and molecular knot started forming upon increasing the concentration beyond 5 mm. The structure of macrocycle **2** was further established by combined ESI-MS (Figures 1.71), ^1H (Figures 1.38 and 1.72), ^{13}C (Figure 1.73), DOSY (Figure 1.51) ROESY (Figure 1.58) and concentration- and template-dependent ^1H NMR analysis (Figures 1.74–1.76). To determine the effect of dilution on the molecular knot **1**, self-assembly was carried out at varying concentrations of donor and acceptor from 0.5 to 8.0 mm. ^1H NMR demonstrated a gradual increase in the proportion of **1** upon increasing concentration from 0.5 to 8.0 mm (Figure 1.74). To investigate the template effect on **1** against a p-electron rich guest, pyrene was added prior and after the reaction. The addition of two equivalents of pyrene during a reaction was enough for preventing formation of the [8+8] knot (Figure 1.75). However, after a reaction in methanol, addition of excess pyrene or solvent change to nitromethane did not fully convert the molecular knot **1** into the monomeric macrocycle **2** even after 24 hour stirring (Figure 1.76).

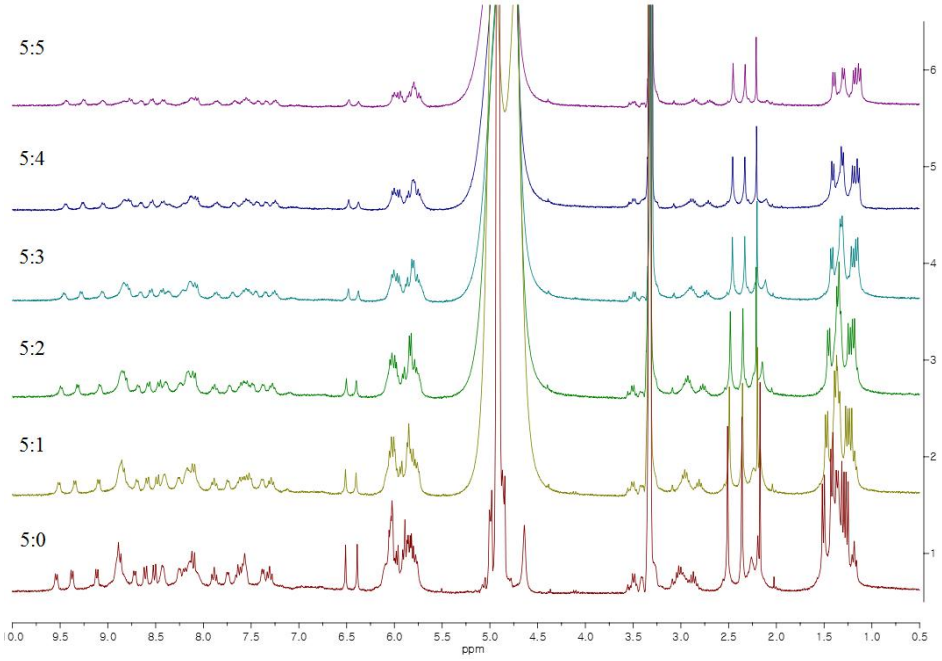

Figure 2.47 ^{1}H NMR spectra showing transformation of mixture of **1+2** into pure molecular knot **1** upon changing solvent ratio (CD_3OD:D_2O) from 5:0 to 5:5 (CD_3OD [8.0 mM]+D_2O, 300 MHz)

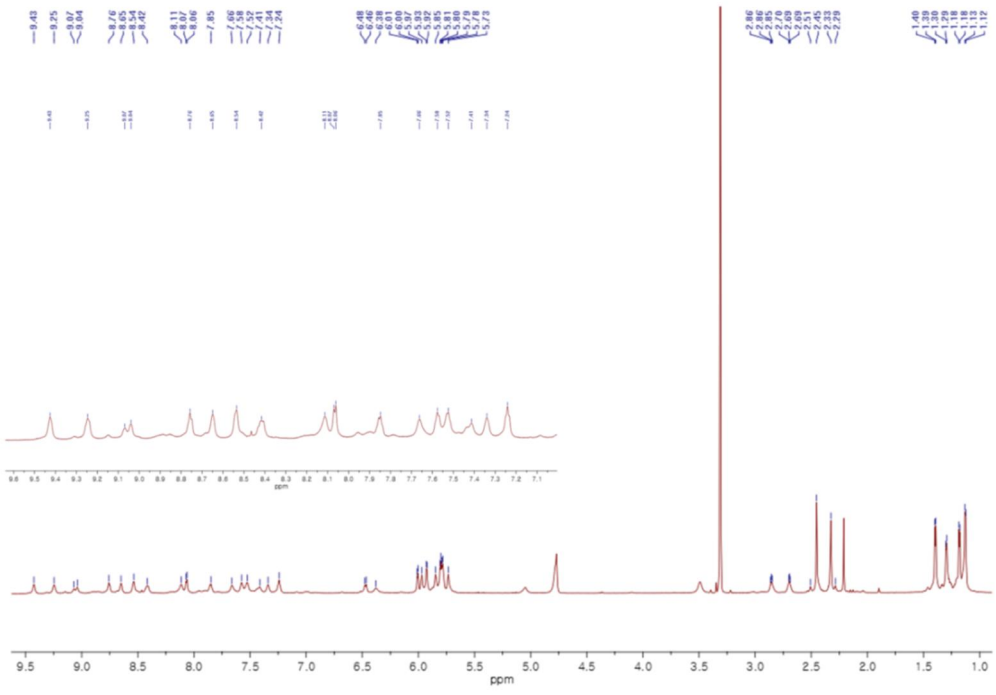

Figure 2.48 ^{1}H NMR spectrum of molecular knot **1** (1:1 CD_3OD [8.0mM]+D_2O, 800 MHz)

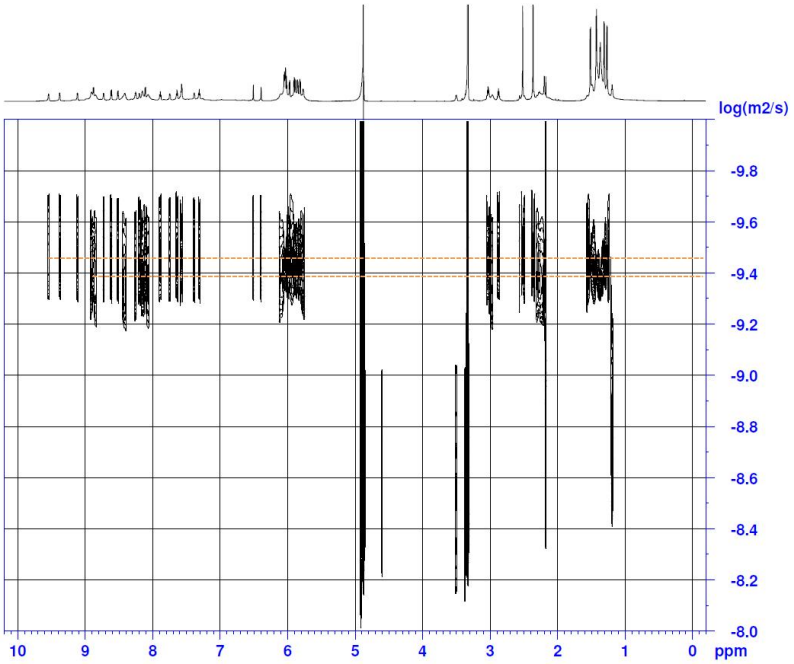

Figure 2.49 ^{1}H-DOSY NMR spectrum of mixture **1+2** (CD_3OD [8.0 mM], 298 K, 800 MHz)

Diffusion coefficient: 3.5×10^{-10} m^2/sec (top), 4.2×10^{-10} m^2/sec(bottom)

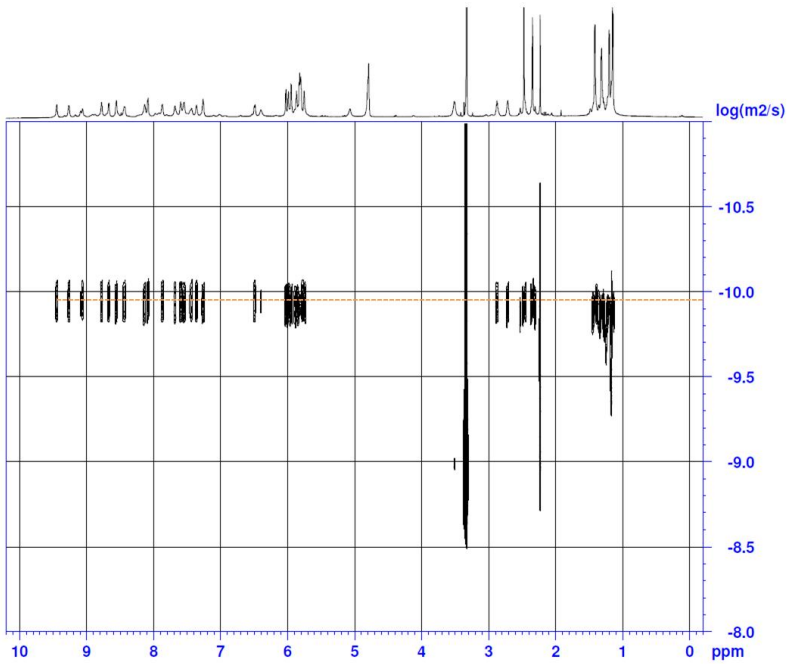

Figure 2.50 ^{1}H-DOSY NMR spectrum of molecular knot **1** (1:1 CD_3OD [8.0 mM]+D_2O, 298 K, 800 MHz). Diffusion coefficient: 1.1×10^{-10} m^2/sec

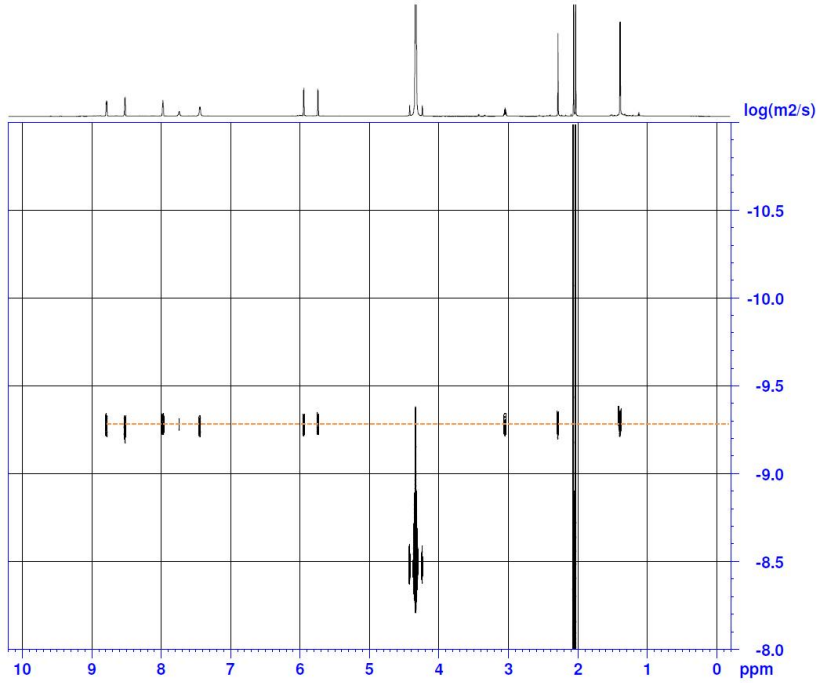

Figure 2.51 ^{1}H-DOSY NMR spectrum of monomeric macrocycle **2** (CD_3NO_2 [5.0 mM], 298 K, 800 MHz) Diffusion coefficient: 5.2×10^{-10} m^2/sec

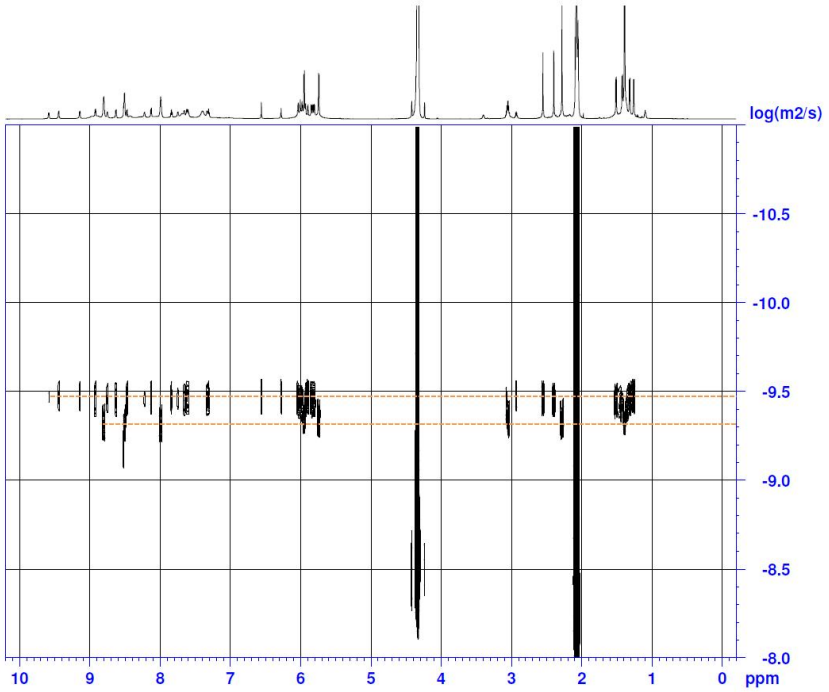

Figure 2.52 ^{1}H-DOSY NMR spectrum of mixture **1+2** (CD_3NO_2 [5.0 mM], 298 K, 800 MHz) Diffusion coefficient: 3.2×10^{-10} m^2/sec (top), 4.9×10^{-10} m^2/sec (bottom). Reaction in CD_3OD.

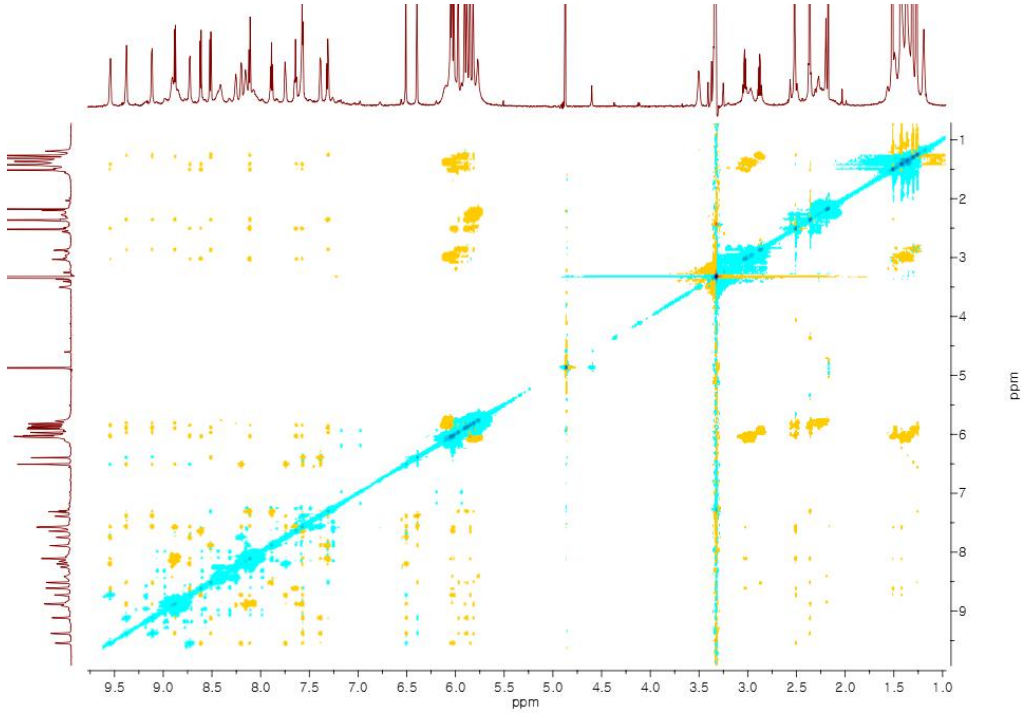

Figure 2.53 ^{1}H-^{1}H ROESY NMR spectrum of mixture **1+2** (CD_3OD [8.0mM], 298K, 900 MHz)

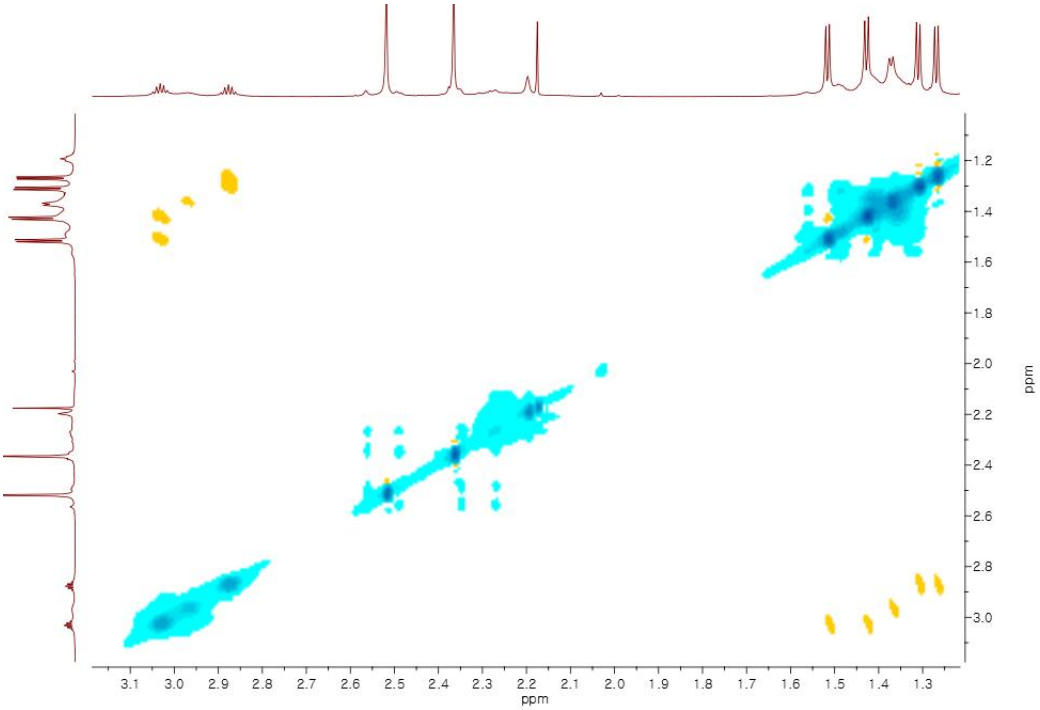

Figure 2.54 ^{1}H-^{1}H ROESY NMR spectrum expansion of mixture **1+2** (CD_3OD [8.0 mM], 298K, 900 MHz)

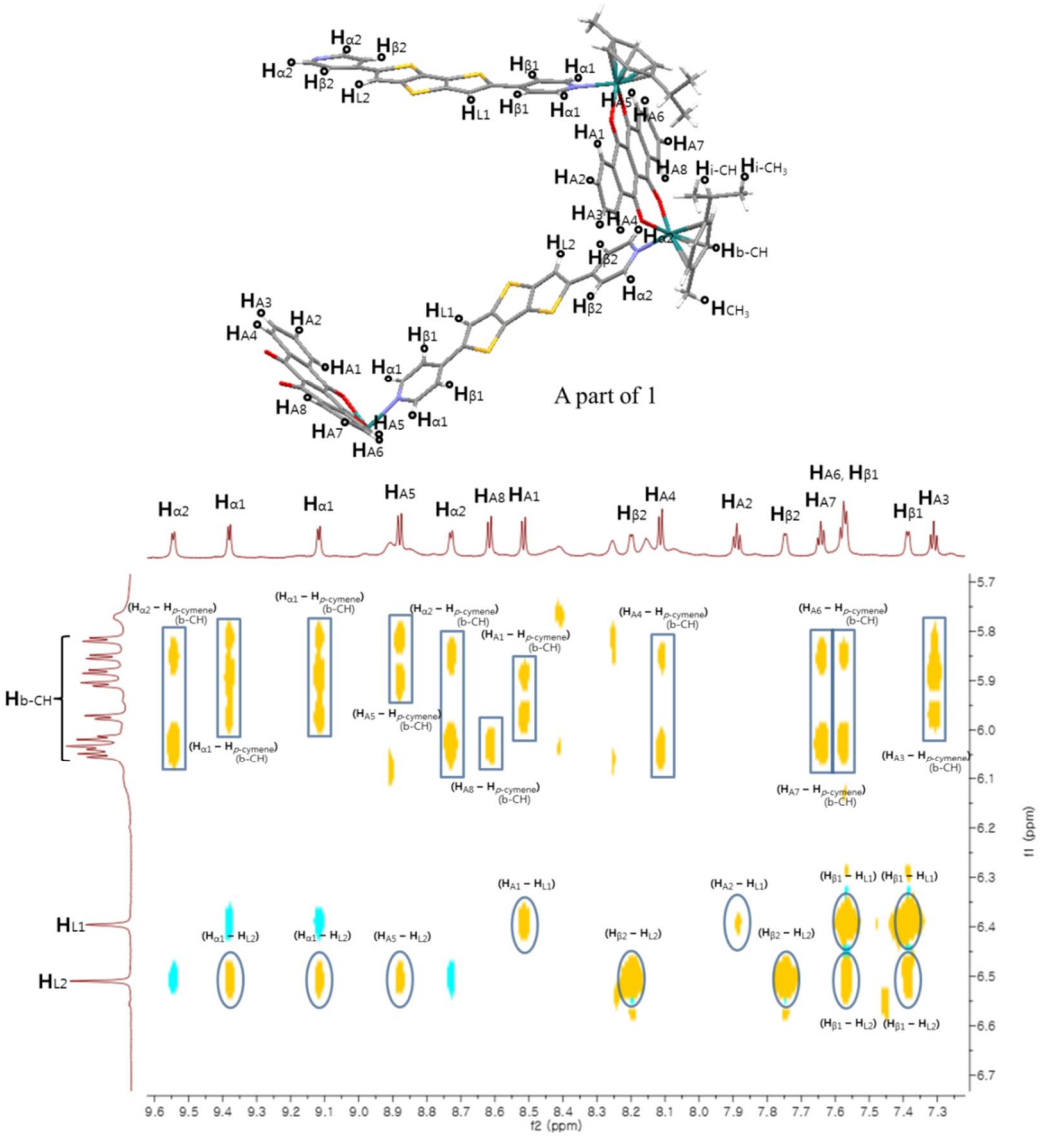

Figure 2.55 ^{1}H-^{1}H ROESY NMR spectrum expansion of mixture **1+2** (CD_3OD [8.0 mM], 298K, 900 MHz)

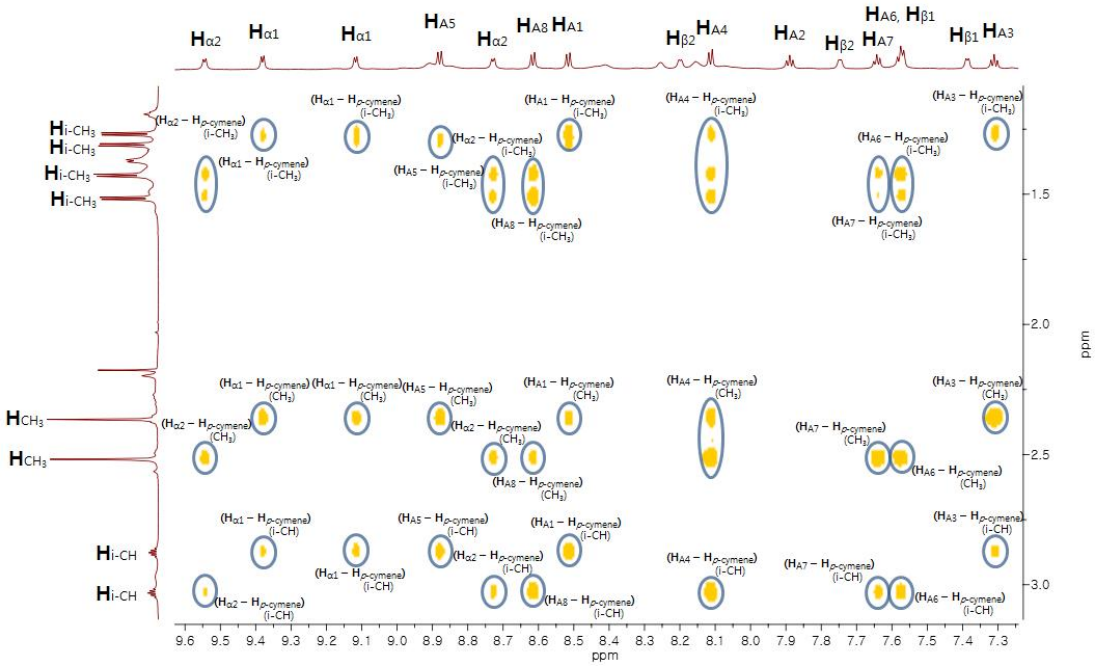

Figure 2.56 ^{1}H-^{1}H ROESY NMR spectrum expansion of mixture **1+2** (CD_3OD [8.0 mM], 298K, 900 MHz)

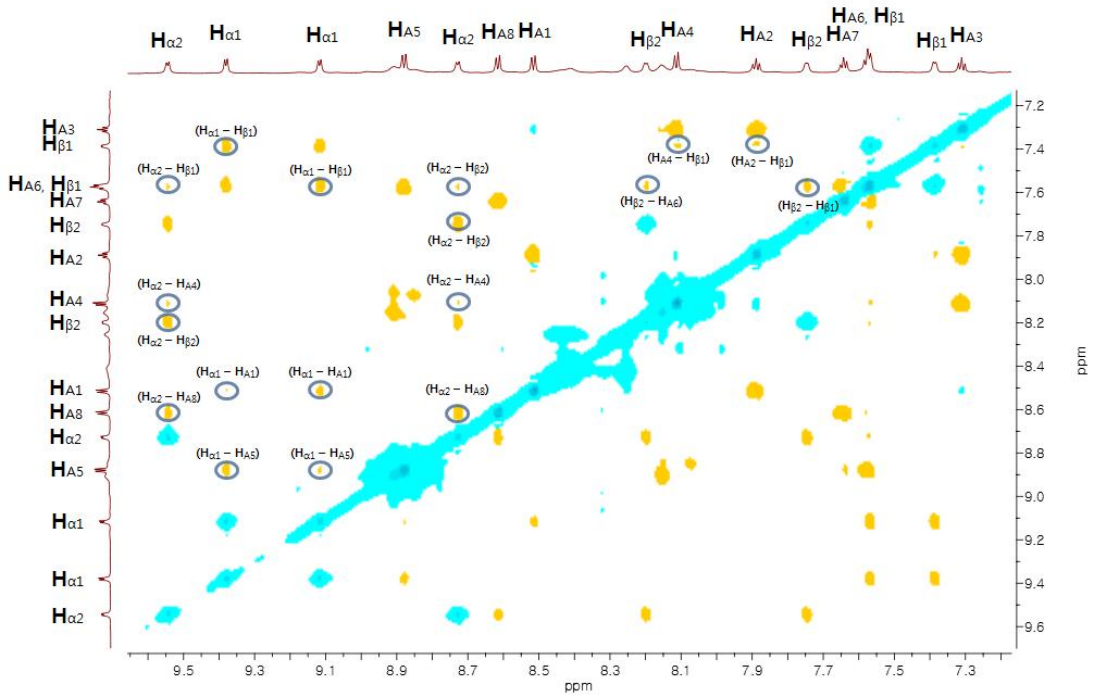

Figure 2.57 ^{1}H-^{1}H ROESY NMR spectrum expansion of mixture **1+2** (CD_3OD [8.0 mM], 298K, 900 MHz)

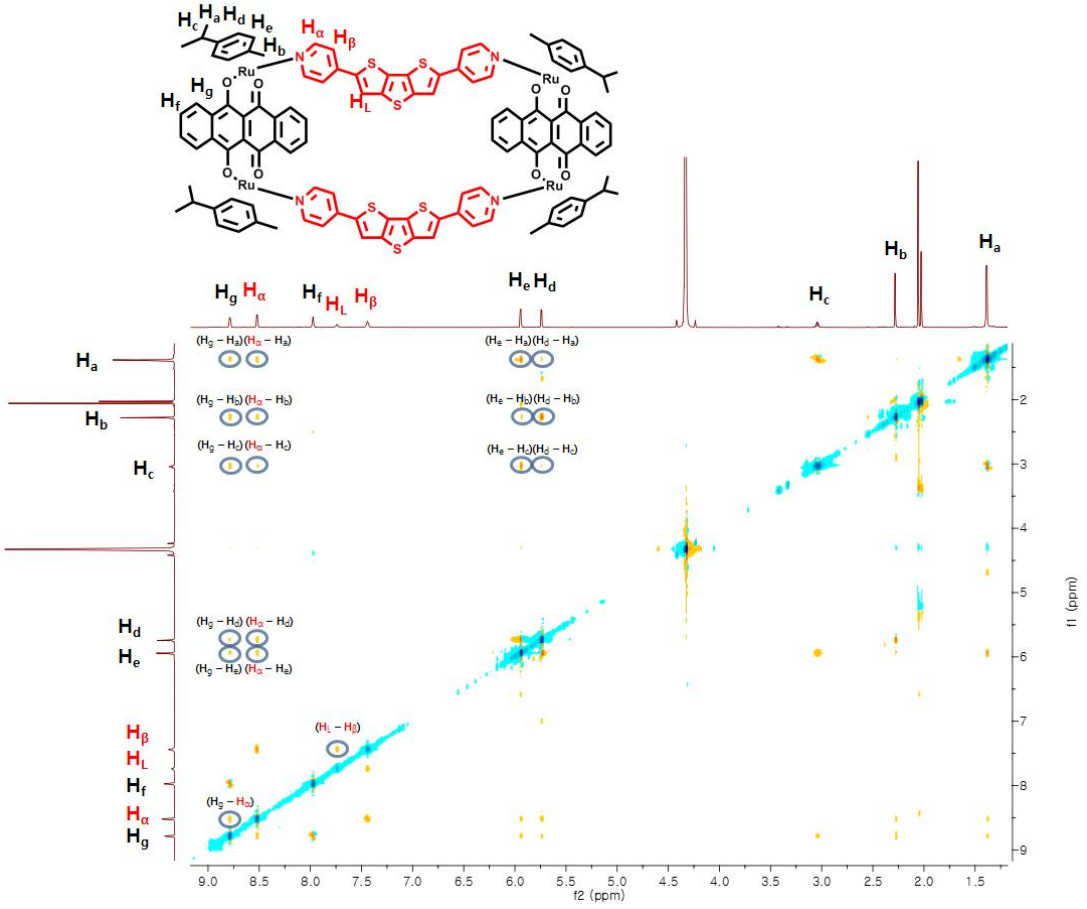

Figure 2.58 ^{1}H-^{1}H ROESY NMR spectrum of monomeric macrocycle **2** (CD_3NO_2 [5.0 mM], 298K, 800 MHz)

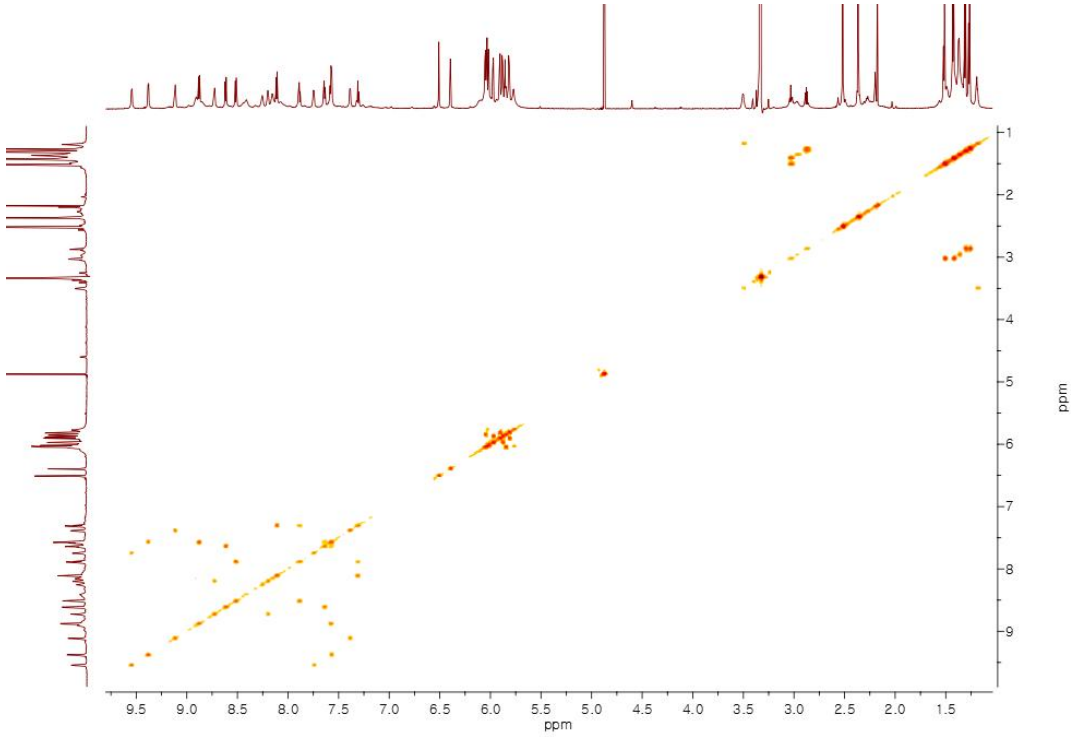

Figure 2.59 ^{1}H-^{1}H COSY NMR spectrum of mixture **1+2** (CD_3OD [8.0 mM], 298 K, 900 MHz)

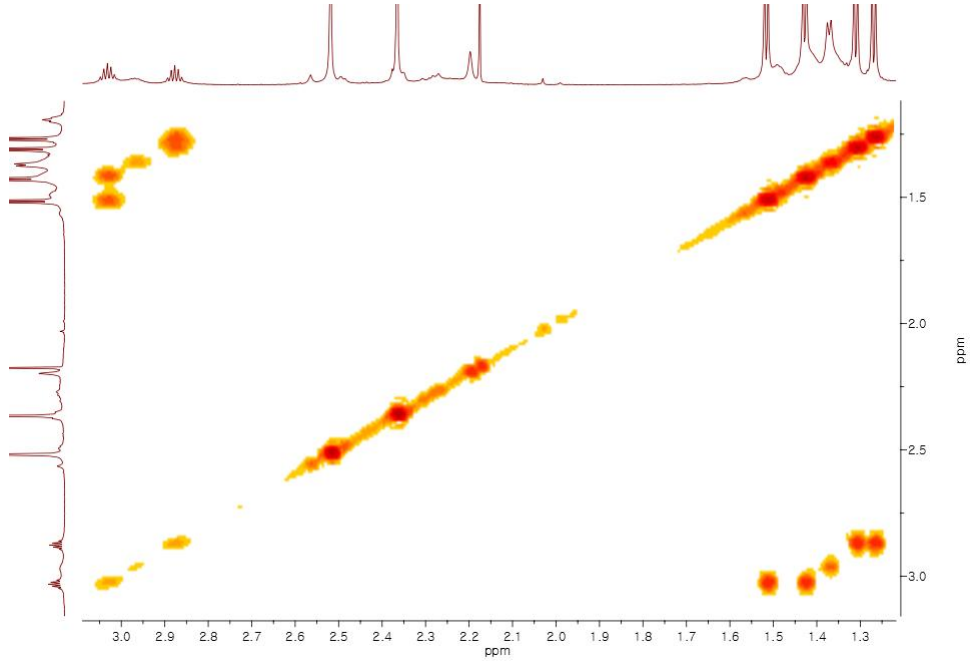

Figure 2.60 ^{1}H-^{1}H COSY NMR spectrum expansion of mixture **1+2** (CD_3OD [8.0 mM], 298 K, 900 MHz)

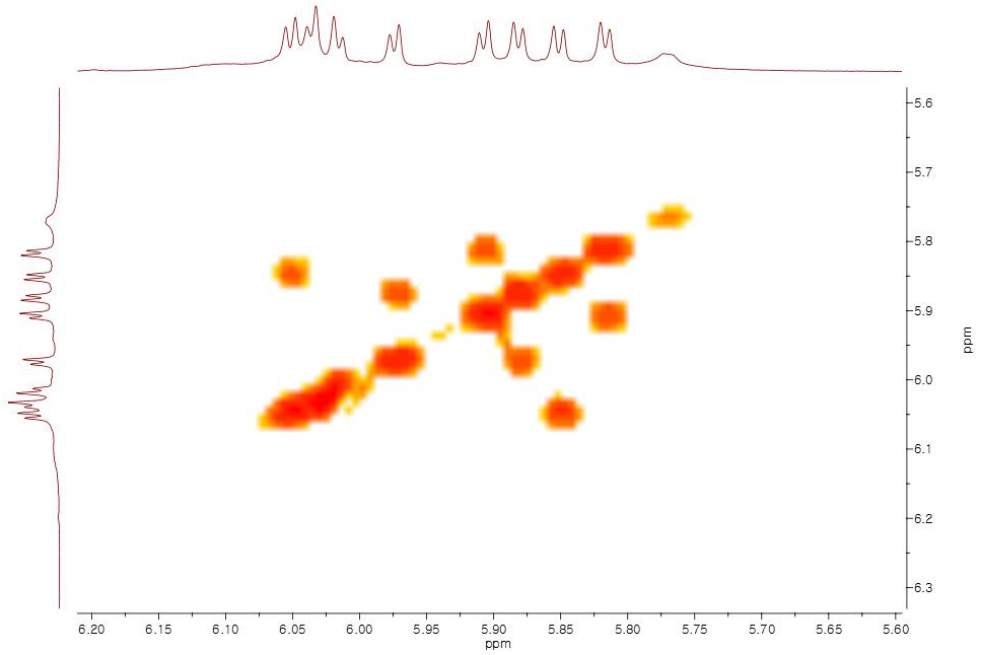

Figure 2.61 ^{1}H-^{1}H COSY NMR spectrum expansion of mixture **1+2** (CD_3OD [8.0 mM], 298K, 900 MHz)

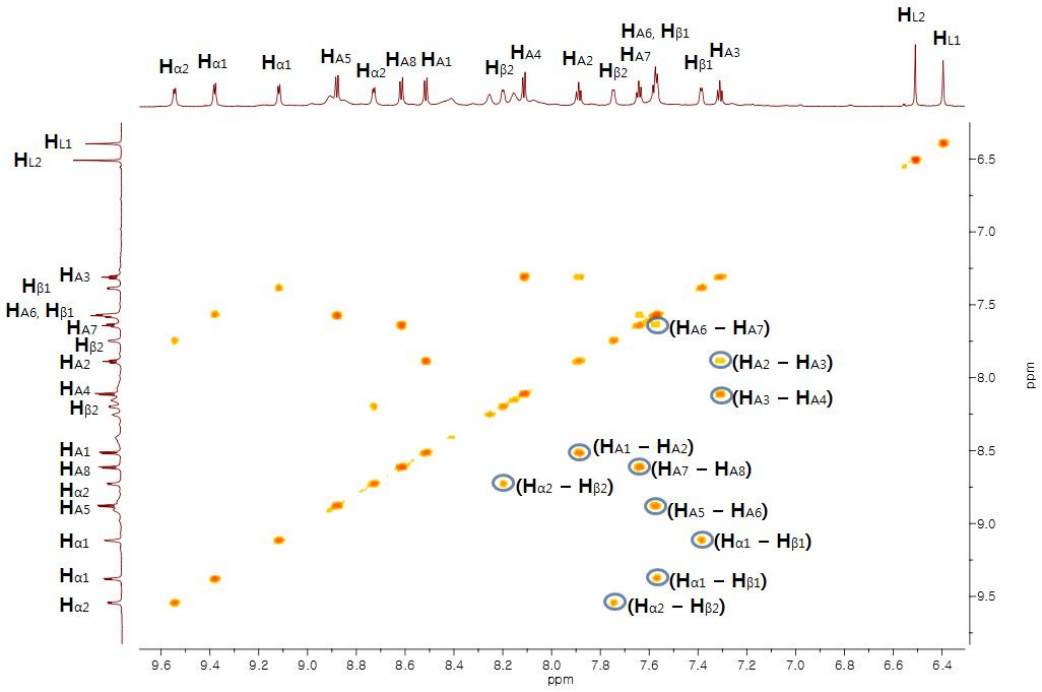

Figure 2.62 ^{1}H-^{1}H COSY NMR spectrum expansion of mixture **1+2** (CD_3OD [8.0 mM], 298K, 900 MHz)

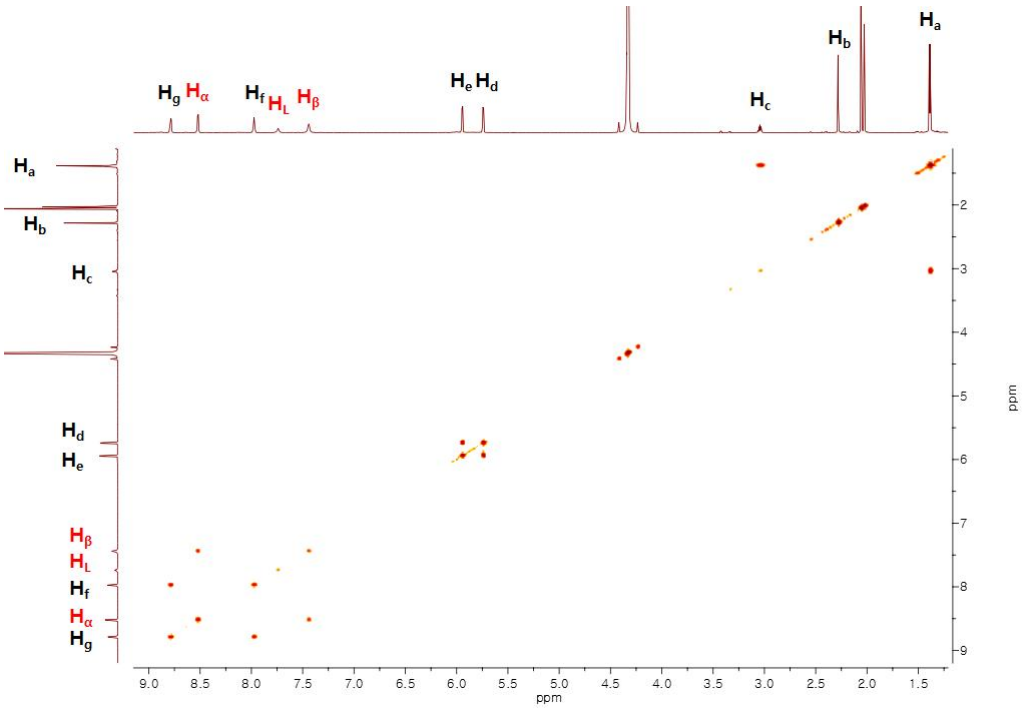

Figure 2.63 ^{1}H-^{1}H COSY NMR spectrum of monomeric macrocycle **2** (CD_3NO_2 [5.0 mM], 298K, 800 MHz)

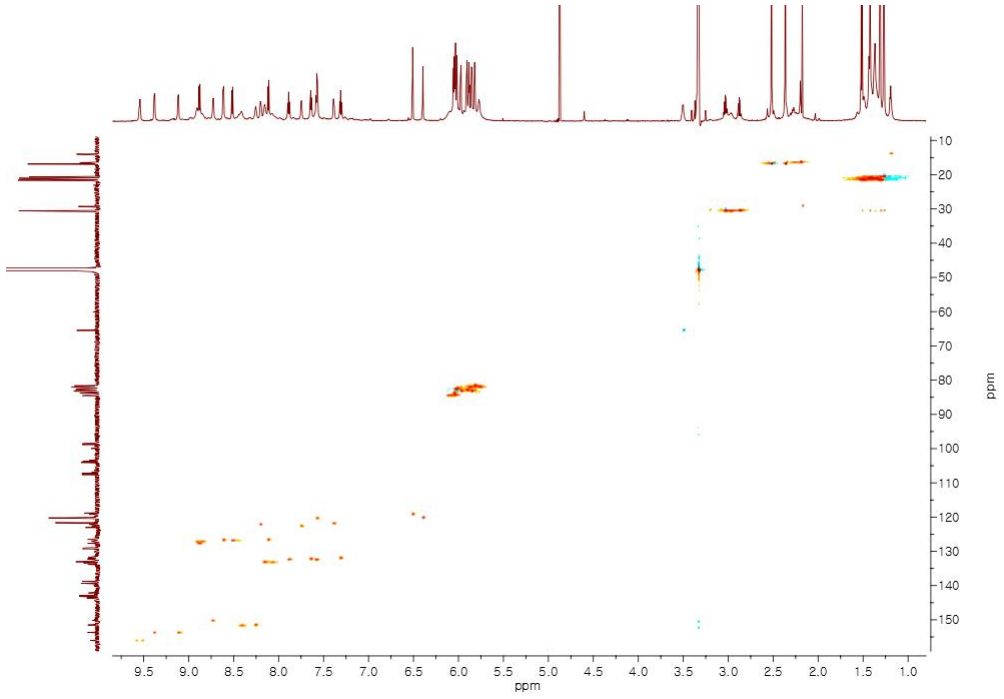

Figure 2.64 ^{1}H-^{13}C HSQC NMR spectrum of mixture **1+2** (CD_3OD [8.0 mM], 298 K, 900 MHz)

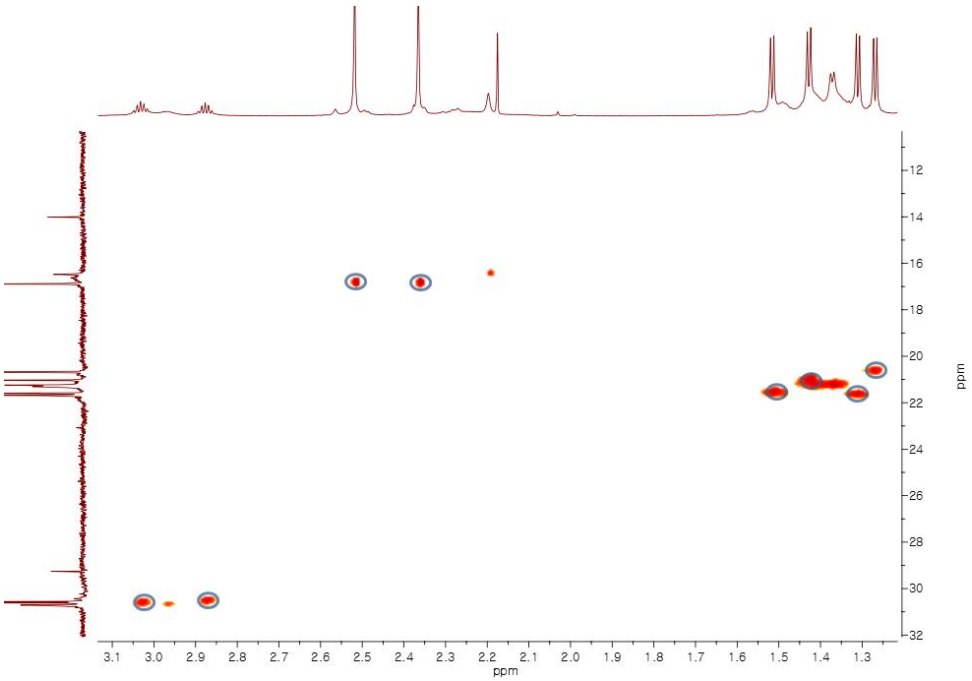

Figure 2.65 ^{1}H-^{13}C HSQC NMR spectrum expansion of mixture **1+2** (CD_3OD [8.0 mM], 298 K, 900 MHz)

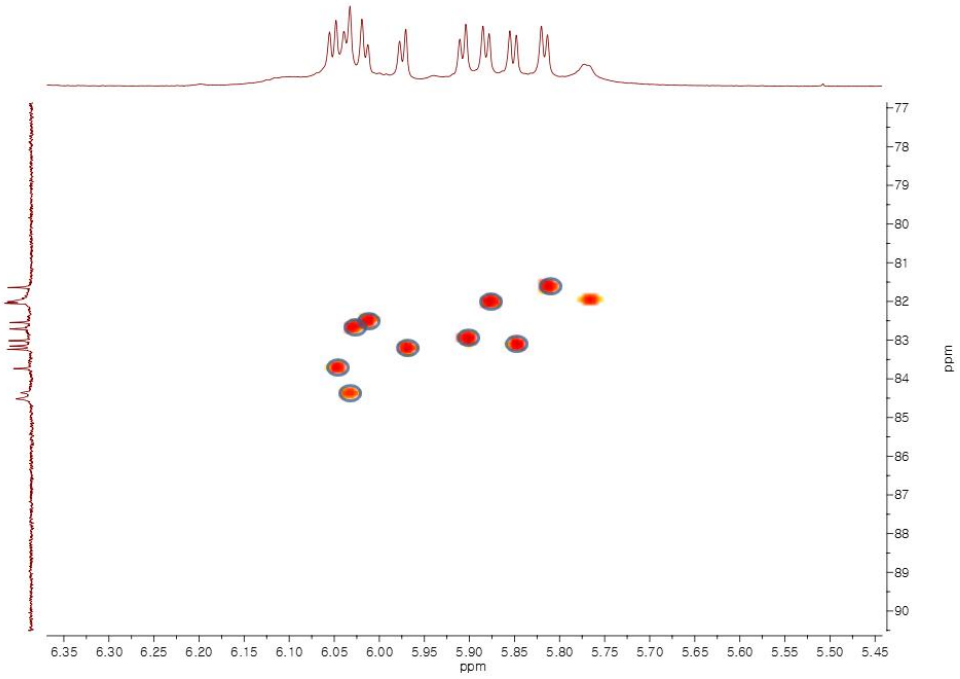

Figure 2.66 ^{1}H-^{13}C HSQC NMR spectrum expansion of mixture **1+2** (CD_3OD [8.0 mM], 298 K, 900 MHz)

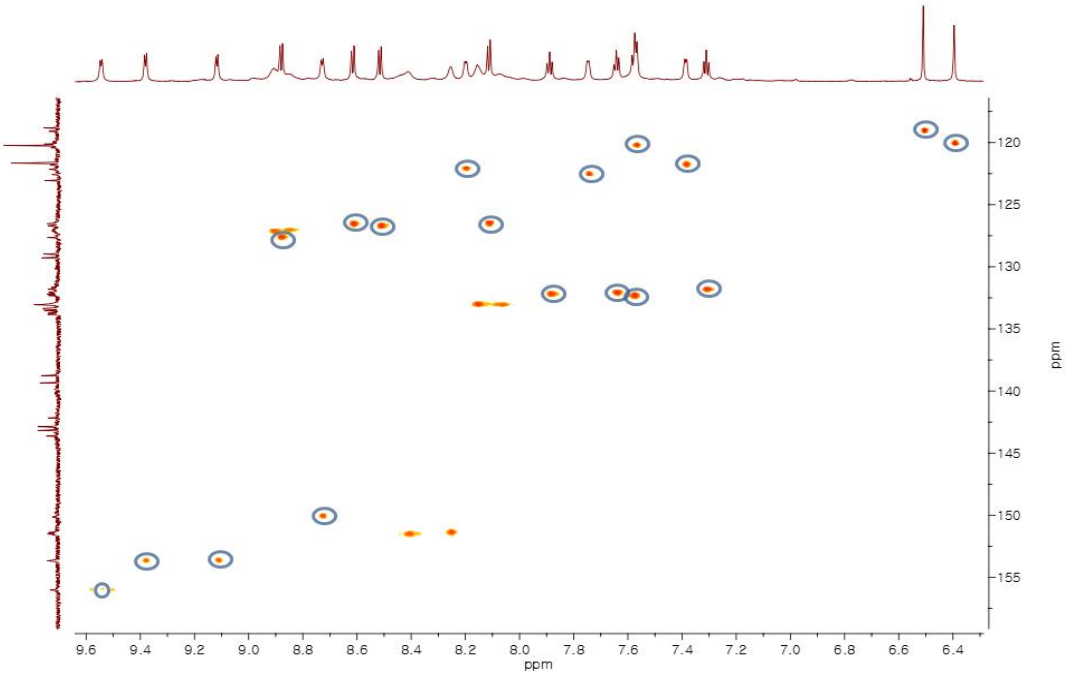

Figure 2.67 ^{1}H-^{13}C HSQC NMR spectrum expansion of mixture **1+2** (CD_3OD [8.0 mM], 298 K, 900 MHz)

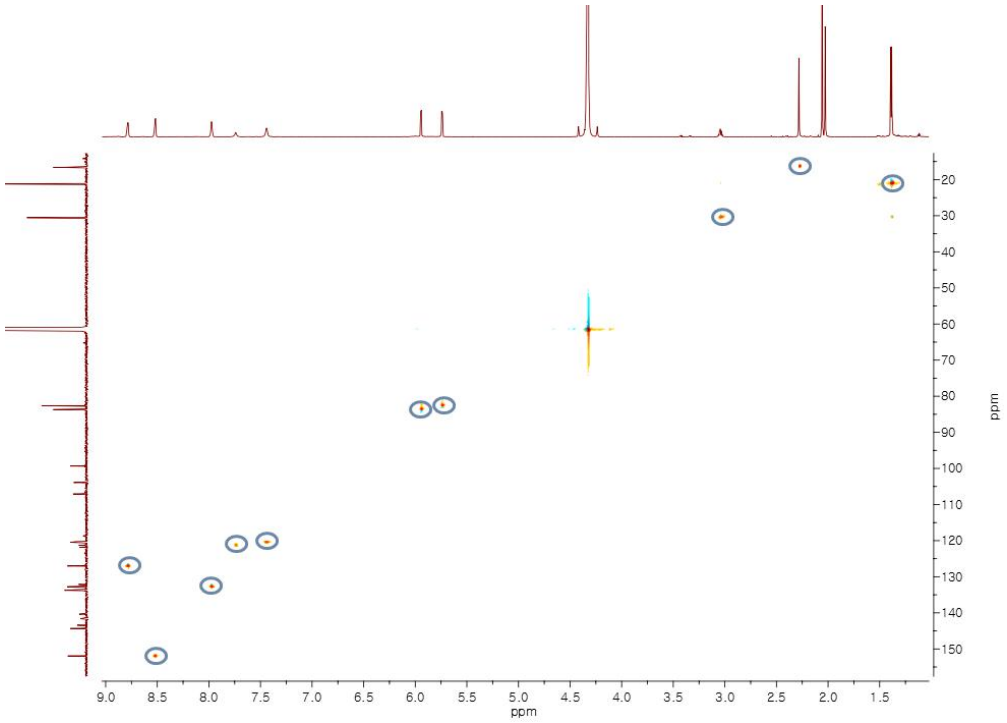

Figure 2.68 ^{1}H-^{13}C HSQC NMR spectrum of monomeric macrocycle **2** (CD_3NO_2 [5.0 mM], 298 K, 800 MHz)

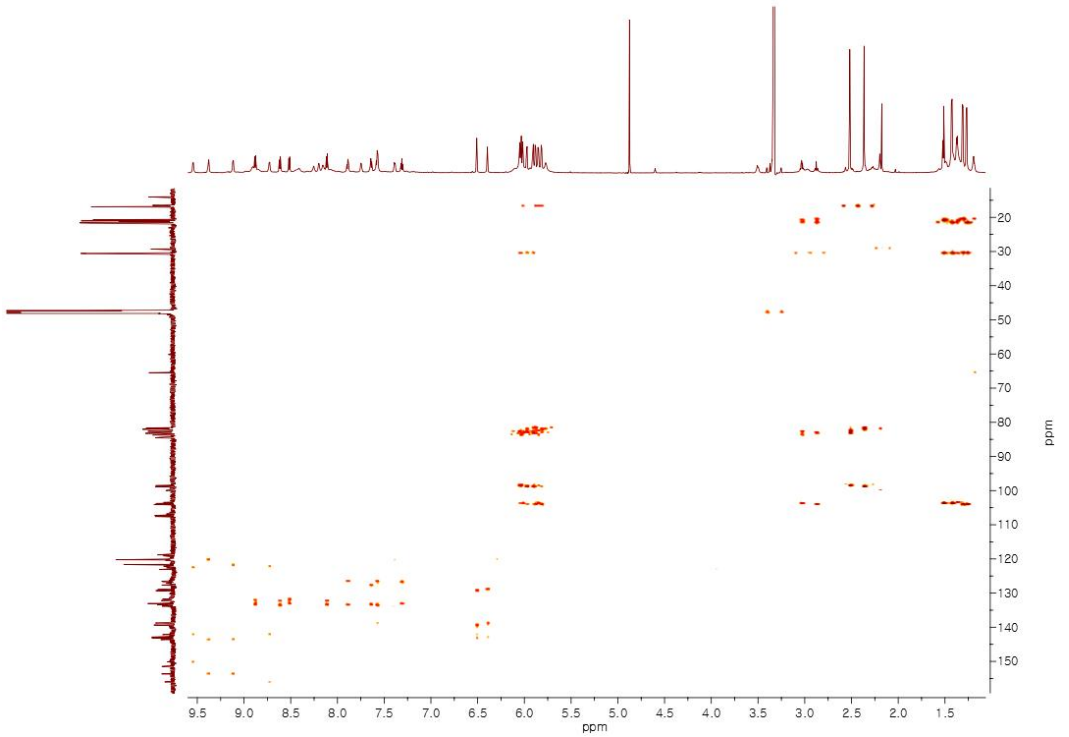

Figure 2.69 ^{1}H-^{13}C HMBC NMR spectrum of mixture **1+2** (CD_3OD [8.0 mM], 298 K, 900 MHz)

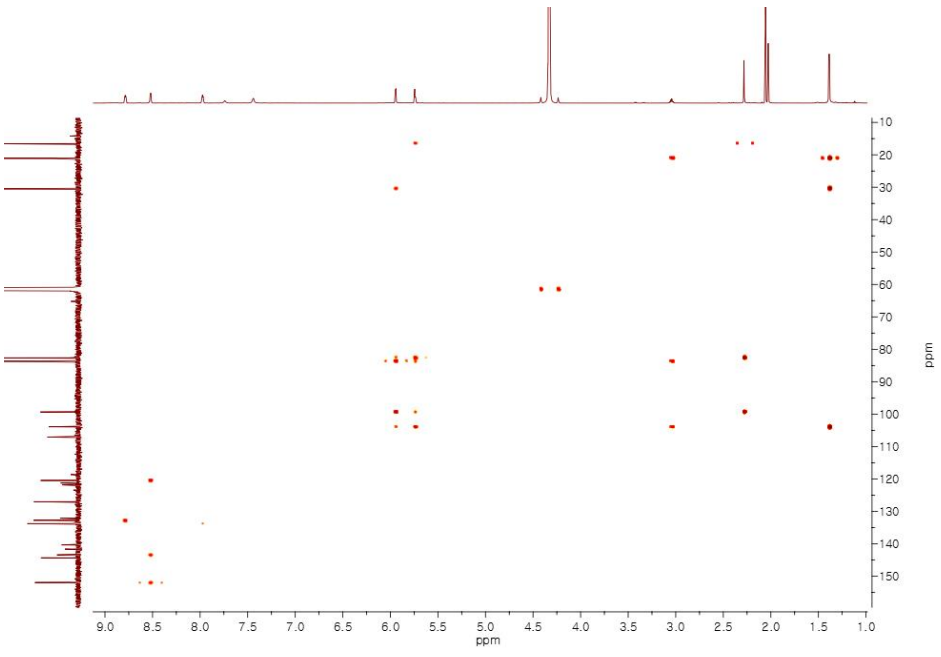

Figure 2.70 ^{1}H-^{13}C HMBC NMR spectrum of monomeric macrocycle **2** (CD_3NO_2 [5.0 mM], 298 K, 800 MHz)

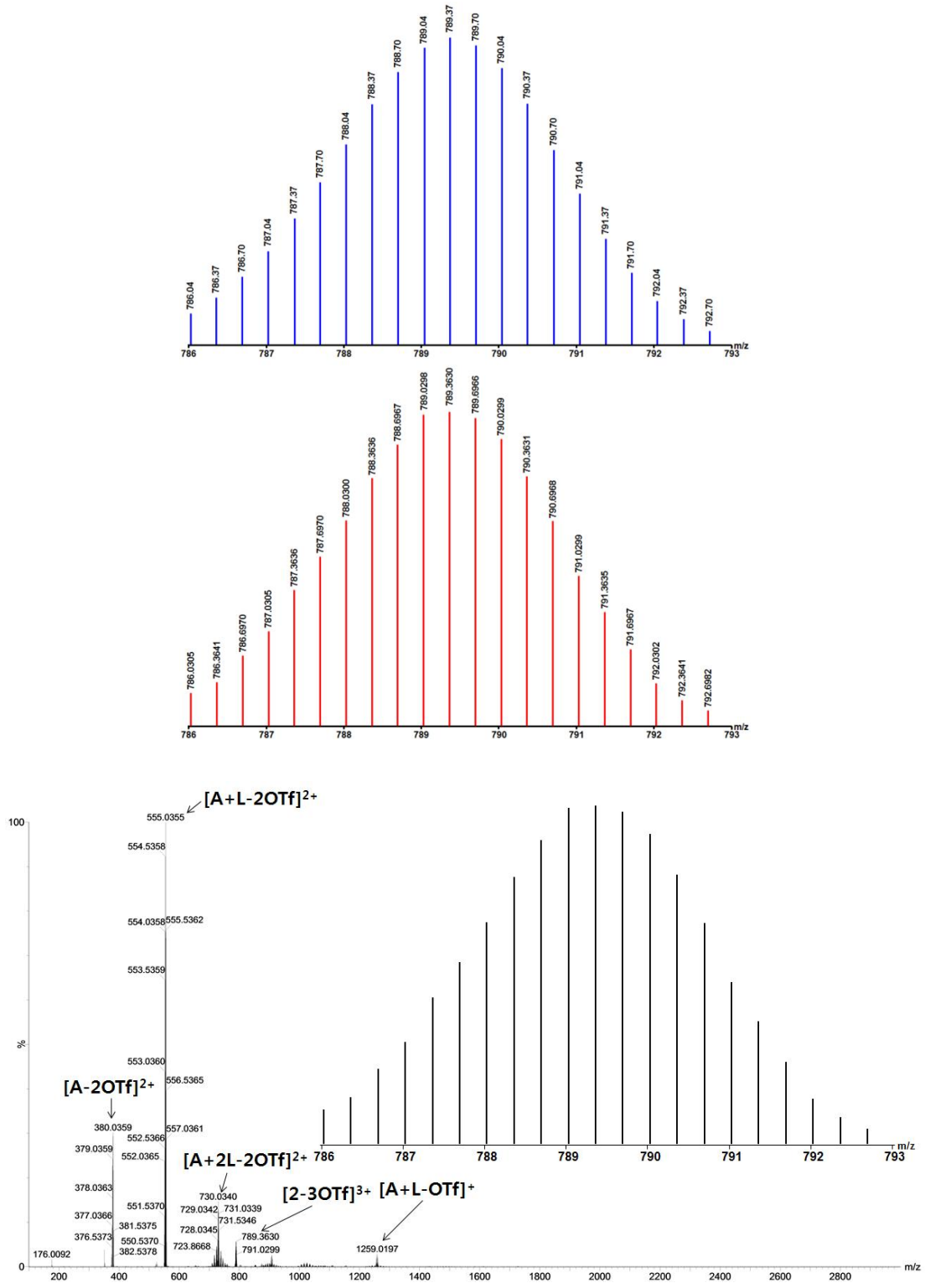

Figure 2.71 Calculated (blue) and experimental (red) ESI mass spectra of [**2**-3OTf]$^{3+}$ and full ESI mass spectrum at bottom (Inset figure showing observed peaks for [**2**-3OTf]$^{3+}$)(top). (Reaction in CD_3NO_2.)

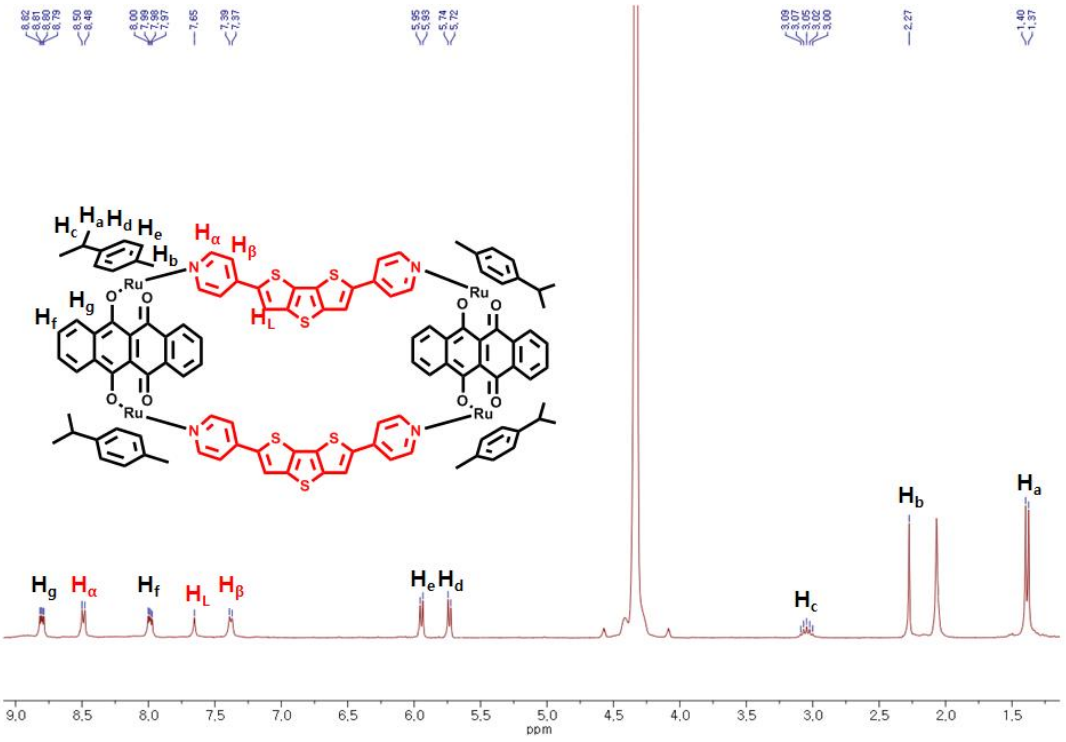

Figure 2.72 ^{1}H NMR spectrum of monomeric macrocycle **2** (CD_3NO_2 [5.0 mM], 300 MHz)

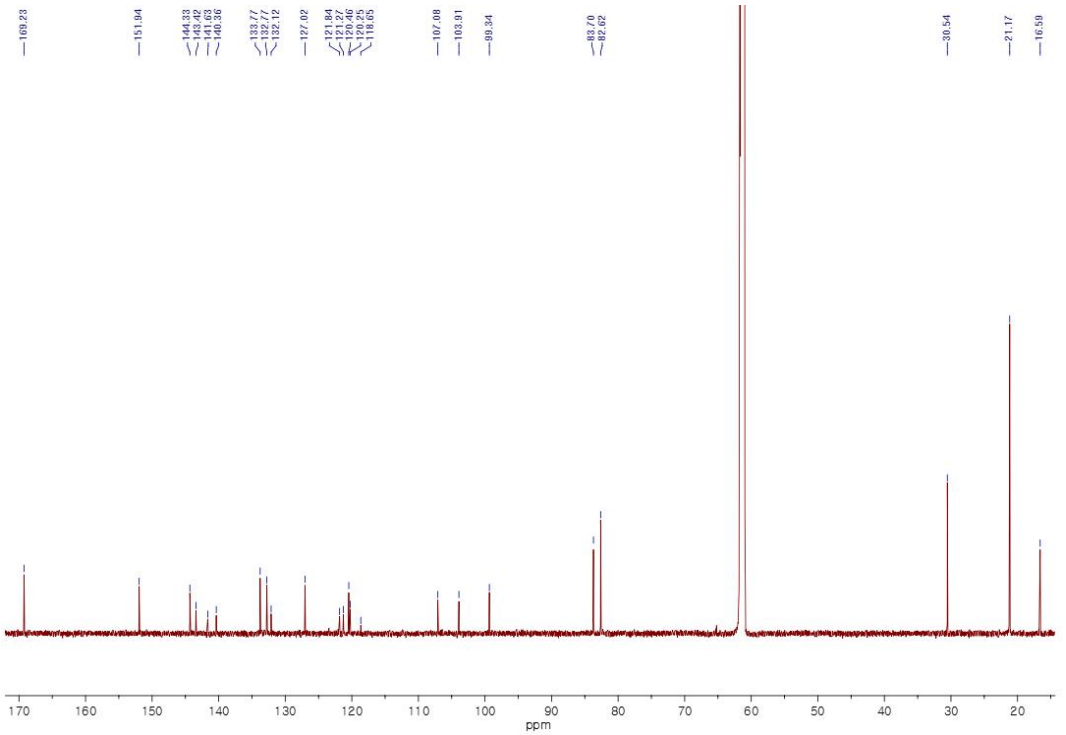

Figure 2.73 ^{13}C NMR spectrum of monomeric macrocycle **2** (CD_3NO_2 [5.0 mM], 200 MHz)

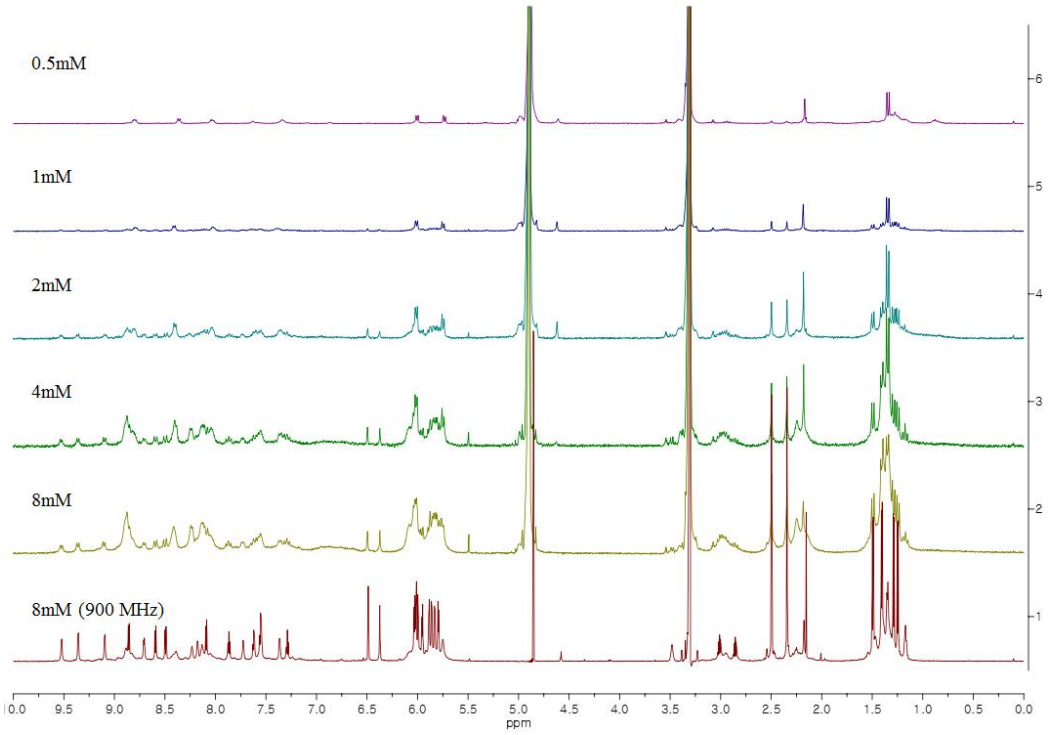

Figure 2.74 ^{1}H NMR spectra showing increasing of proportion of **1** upon sequentially increasing the concentration from 0.5 mM to 8.0 mM (CD_3OD, 300 MHz).

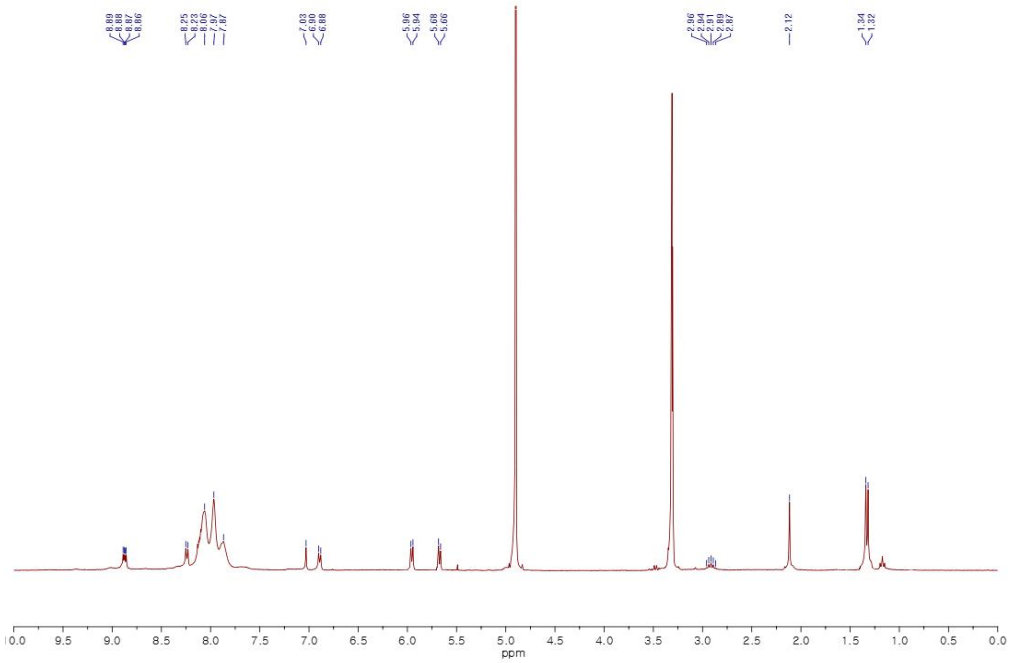

Figure 2.75 ^{1}H NMR spectrum showing formation of only **2** when reaction was carried out in the presence of pyrene (2.5 eq) (CD_3OD [8.0 mM], 300 MHz)

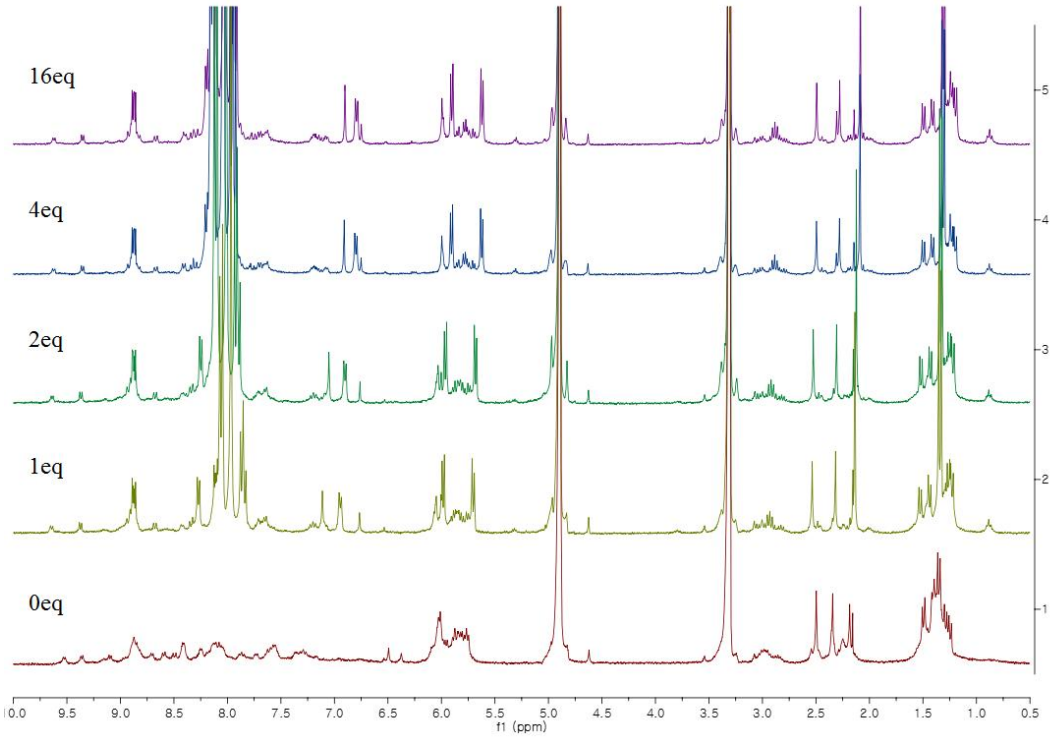

Figure 2.76 ^{1}H NMR spectra of mixture **1+2** showing increasing proportion of monomeric macrocycle **2** upon addition of pyrene from 0 eq to 16.0 eq (CD_3OD [8.0 mM], 300 MHz).

2.3.3 X-ray crystallography

To conclusively confirm the structure and topology of **1**, single crystals suitable for synchrotron X-ray diffraction were obtained by slow vapor diffusion of diethyl ether to methanol/nitromethane solution of mixture of **1**+**2**. The crystal structure of **1** was refined in the $P\bar{4}2_1c$ space group, and this unequivocally showed the knot topology incorporated sixteen crossings (Figure 1.77).[19] Topological feature of the synthesized knot **1** can be described through an artificial geometric folding of carrick knot, 8_{19}, of eight crossings, which results in the sixteen crossings similar to that of the T(3,8) torus knot with a different crossing pattern (Figure 1.2). The main framework of molecular knot **1**, omitting the methyl and isopropyl moieties of acceptor **A8**, is highly symmetric and of point group S_8 (Figure 1.77). Close-contact analysis of the structure reveals a highly complicated knot held together by multiple parallel-displaced π-π interactions (of interlayer distance 3.5 Å) between the dithienothiophene moieties of the donor and the tetracene moieties of the acceptor. Therefore, our results indicate that the non-covalent interactions (NCI), that is, π-π interaction between donor and acceptor moieties, plays a pivotal role in the formation of a higher crossing pattern. The structure looks like a perfect doughnut with average outer and inner diameters of 2.5 and 10 Å, respectively, thus, it contains a well-defined nanoscale cavity.

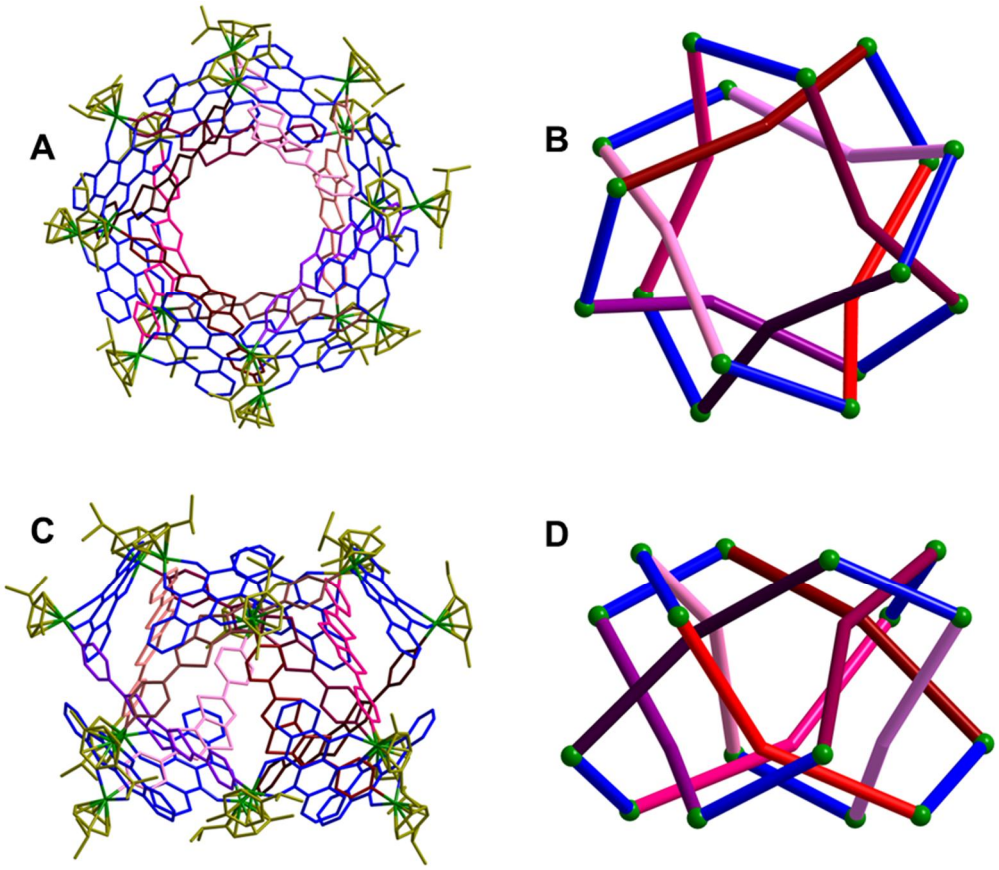

Figure 2.77 X-ray crystal structure of the molecular knot **1**, Top view (A) and side view (C) in Stick model of **1**, and simplified structures in which sticks connect the ruthenium centers: top view (B) and side view (D).

Table 2.1 X-ray crystal structure parameters of molecular knot **1**

Empirical formula	C470.63 H395.43 F48 N16 O87.09 Ru16 S40	
Formula weight	11479.89	
Temperature	100(2) K	
Wavelength	0.700 Å	
Crystal system	Tetragonal	
Space group	$P\bar{4}2_1c$	
Unit cell dimensions	a = 50.707(7) Å	□□= 90°
	b = 50.707(7) Å	□□= 90°
	c = 41.720(8) Å	□ = 90°
Volume	107268 (37) Å^3	
Z	8	
Density (calculated)	1.422 g/cm^3	
Absorption coefficient	0.641 mm^{-1}	
F(000)	46431	
Crystal size	0.200 × 0.200 × 0.100 mm^3	
Theta range for data collection	1.280 to 27.106°	
Index ranges	$-64 \le h \le 64$, $-64 \le k \le 64$, $-54 \le l \le 53$	
Reflections collected	689360	
Independent reflections	108392 [R(int) = 0.1017]	
Completeness to theta = 24.835°	99.5%	
Absorption correction	Semi-empirical from equivalents	
Max. and min. transmission	0.939 and 0.882	
Refinement method	Full-matrix-block least-squares on F^2	
Data / restraints / parameters	108392 / 1926 / 6008	
Goodness-of-fit on F^2	1.161	
Final R indices [I>2sigma(I)]	R_1 = 0.1050, wR_2 = 0.2704	
R indices (all data)	R_1 = 0.1760, wR_2 = 0.3315	
Absolute structure parameter	0.51(3)	
Largest diff. peak and hole	2.484 and -1.439 e.Å^{-3}	

2.3.4 Computational study

To obtain further insight into the formation and stability of molecular knot **1**, a computational study was undertaken using a combined approach based on semi-empirical and DFT methods (see the Supporting Information for computation details), which were used for geometry optimization and electronic energy evaluation, respectively. The spatial distribution of NCI, which was analyzed by plotting the iso-surface of the reduced density gradient[20] (Figure 1.78A), and the optimized distance of 3.4–3.6 Å between dithienothiophene moieties of donor **L** and tetracene moieties of acceptor **A8** revealed the contribution of the π-π stacking to the formation of the molecular knot (Figure 1.78B). The π-π stacking interaction of the thiophene group is widely observed in self-organizing conjugated organic films using polythiophene,[21] of which underlying nature was explained by large dispersive attraction due to the high polarizability of sulfur atoms.[22] The higher stability of [8+8] self-assembly **1** over other possible interlocked $[2+2]_2$ architectures, of which the feasible structures are "molecule in molecule" and catenane structures, was confirmed by comparing their formation energies with respect to that of [2+2] self-assembly **2** (Figures 1.79, 1.80). Their relative formation energies to **2**, which were evaluated using three density functional methods, PBE0, M06-2X, and wB97X-D, also revealed that NCI plays a key role in forming the highly entangled molecular knot **1** (Figures 1.78, 1.81). The energy gap between the highest occupied and lowest unoccupied molecular orbitals (HOMO–LUMO gap) of **1**, obtained using PBE0, M06-2X, and wB97X-D functionals, are 2.14, 3.88, and 5.28 eV, respectively. These values are comparable with those of C_{60}, as a representative large molecule with high stability, of which HOMO–LUMO gaps computed using the same levels of DFT are 3.03, 4.55, and 6.04 eV, respectively. Therefore, the HOMO–LUMO gap of **1** is smaller than that of C_{60} by about 0.7–0.9 eV, which suggests despite its huge molecular size,

knot **1** possesses considerable kinetic stability due to its highly symmetric geometry.[19] DFT computations on the relative stability of **1** to that of **2** upon increasing the dielectric constant of solvent medium also well explain the experimental observation regarding the greater relative stability of **1** than **2** in more polar solvents (Figure 1.82).

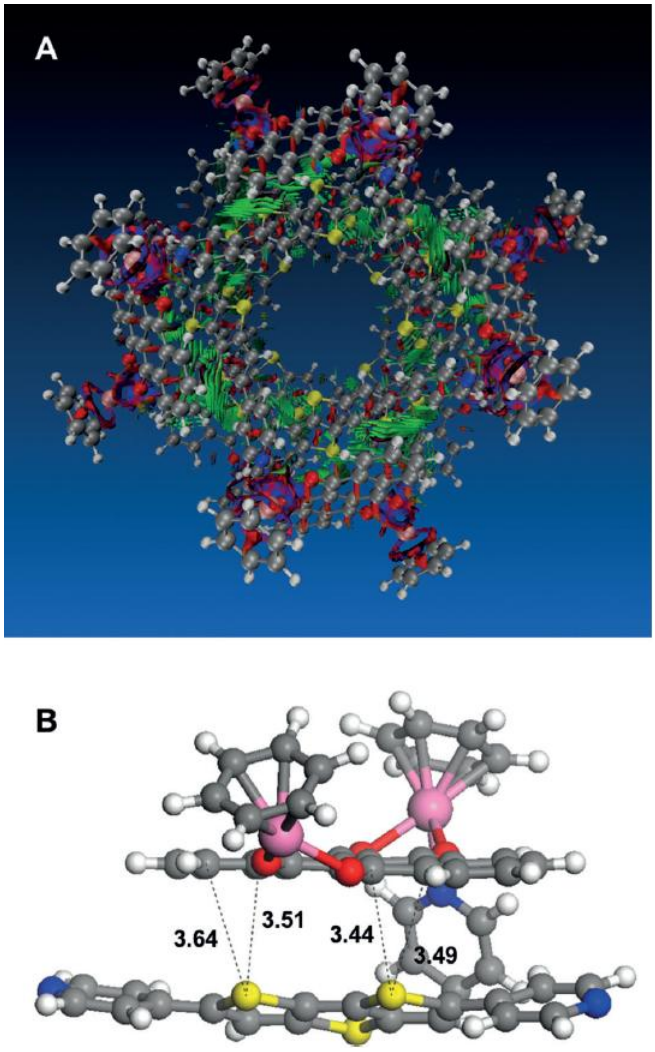

Figure 2.78 Non-covalent interaction of the molecular knot **1**. A) Reduced density gradient iso-surfaces (s = 0.65 au) for **1**. The surfaces are colored on a blue-green-red scale according to the values of sign(λ_2)ρ, ranging from -0.02 to +0.02 au. The

primary intermolecular interactions are the π-π interactions between the dithienothiophene moieties of donor and the tetracene moieties of acceptor, which are indicated by green-colored iso-surfaces. The strong electrostatic interactions indicated by blue- and red-colored iso-surfaces are observed near transition metal cation, Ru^{II}. B) Selective interatomic distance (in Å) between dithienothiophene moieties of the donor and tetracene moieties of the acceptor. (Ru, pink; S, yellow; O, red; C, gray; N, blue; H, white.)

2.4 Conclusion

In conclusion, straightforward coordination-driven selfassembly of a molecular knot with sixteen crossings using only two simple building blocks is unprecedented, and hopefully will lead to the discovery of even higher-generation molecular knots. The rare topology of molecular knot **1** was characterized by single crystal X-ray diffraction in the solid state and results were supported by DFT computation and those of 2D NMR analysis conducted in solution. The driving force behind the stability of **1** and the selectivity of its self-assembly are parallel-displaced π-π interactions between donor and acceptor and their appropriate geometries. It is anticipated that the self-assembly of such a higher-order molecular knot and its structural properties will encourage the synthesis of next-generation topologically complex molecular architectures and take the rational design of biomaterials to new heights.

Publication

Kim, D. H.; Singh, N.; Oh, J.; Kim, E.-H.; Jung, J.; Kim, H.; Chi, K.-W.

Angew. Chemie Int. Ed. **2018**, *57*, 5669–5673.

2.5 Reference

1. a) Fielden, S. D. P.; Leigh, D. A.; Woltering, S. L. *Angewandte Chemie International Edition* **2017**, *56,* 11166-11194; b) Forgan, R. S.; Sauvage, J.-P.; Stoddart, J. F. *Chemical Reviews* **2011**, *111*, 5434-5464; c) Castelvecchi, D; *Nature* **2017**, *547*, 272; d) Lim, N. C. H.; Jackson, S. E; Journal of Physics Condensed Matter **2015**, *27*, 354101.

2. Wasserman, S.; Cozzarelli, N; *Science* **1986**, *232*, 951-960.

3. a) Pieters, B. J. G. E.; van Eldijk, M. B.; Nolte, R. J. M.; Mecinović, J. *Chemical Society Reviews* **2016**, *45*, 24-39; b) Sulkowska, J. I.; Rawdon, E. J.; Millett, K. C.; Onuchic, J. N.; Stasiak, A. *Proceedings of the National Academy of Sciences* **2012**, *109*, E1715-E1723.

4. Marenduzzo, D.; Orlandini, E.; Stasiak, A.; Sumners, D. W.; Tubiana, L.; Micheletti, C. *Proceedings of the National Academy of Sciences* **2009**, *106*, 22269-22274.

5. a) Tkalec, U.; Ravnik, M.; Copar, S.; Zumer, S.; Musevic, I. *Science* **2011**, *333*, 62-65; b) Hashemi, S. M.; Jagodič, U.; Mozaffari, M. R.; Ejtehadi, M. R.; Muševič, I.; Ravnik, M. *Nature Communications* **2017**, *8*, 14026.

6. Sloane, N. J. A. *Annales Mathematicae et Informaticae* **2013**, A002863

7. a) Adams, C.C. *American Mathematical Society* **1994**; b) Hoste, J.; Thistlethwaite, M.; Weeks, J. *The Mathematical Intelligencer* **1998**, *20*, 33-48

8. a) Dietrich-Buchecker, C. O.; Sauvage, J.-P. *Angewandte Chemie International Edition in English* **1989**, *28*, 192-194; b) Ponnuswamy, N.; Cougnon, F. B. L.; Clough, J. M.; Pantos, G. D.; Sanders, J. K. M. *Science* **2012**, *338*, 783-785; c) Ponnuswamy, N.; Cougnon, F. B. L.; Pantoş, G. D.;

Sanders, J. K. M. *Journal of the American Chemical Society* **2014**, *136*, 8284-8251; d) Ayme, J.-F.; Beves, J. E.; Leigh, D. A.; McBurney, R. T.; Rissanen, K.; Schultz, D. A *Nature chemisty* **2012**, *4*, 15-20; e) Danon, J. J.; Krüger, A.; Leigh, D. A.; Lemonnier, J.-F.; Stephens, A. J.; Vitorica-Yrezabal, I. J.; Woltering, S. L. *Science* **2017**, *355*, 159-162.

9. a) Stang, P. J.; Olenyuk, B. *Accounts of Chemical Research* **1997**, *30*, 502-518; b) Chakrabarty, R.; Mukherjee, P. S.; Stang, P. J. *Chemical Reviews* **2011**, *111*, 6810-6918; c) Cook, T. R.; Stang, P. J. *Chemical Reviews* **2015**, *115*, 7001-7045; d) Wang, W.; Wang, Y.-X.; Yang, H.-B. *Chemical Society Reviews* **2016**, *45*, 2656-2693; e) Fujita, M. *Chemical Society Reviews* **1998**, *27*, 417-425; f) Fujita, M.; Tominaga, M.; Hori, A.; Therrien, B. *Accounts of Chemical Research* **2005**, *38*, 369-378; g) Hori, A.; Sawada, T.; Yamashita, K.; Fujita, M. *Angewandte Chemie International Edition* **2005**, *44*, 4974-4977; h) Black, S. P.; Stefankiewicz, A. R.; Smulders, M. M. J.; Sattler, D.; Schalley, C. A.; Nitschke, J. R.; Sanders, J. K. M. *Angewandte Chemie International Edition* **2013**, *52*, 5749-5752; i) Beves, J. E.; Blight, B. A.; Campbell, C. J.; Leigh, D. A.; McBurney, R. T. *Angewandte Chemie International Edition* **2011**, *50*, 9260-9327; j) Browne, C.; Ronson, T. K.; Nitschke, J. R. *Angewandte Chemie International Edition* **2014**, *53*, 10701-10705; k) Jansze, S. M.; Cecot, G.; Wise, M. D.; Zhurov, K. O.; Ronson, T. K.; Castilla, A. M.; Finelli, A.; Pattison, P.; Solari, E.; Scopelliti, R.; Zelinskii, G. E.; Vologzhanina, A. V.; Voloshin, Y. Z.; Nitschke, J. R.; Severin, K. *Journal of the American Chemical Society* **2016**, *138*, 2046-2054.

10. Fujita, D.; Ueda, Y.; Sato, S.; Mizuno, N.; Kumasaka, T.; Fujita, M. *Nature* **2016**, *540*, 563-566.

11. a) Kim, T.; Singh, N.; Oh, J.; Kim, E.-H.; Jung, J.; Kim, H.; Chi, K.-W. *Journal of the American Chemical Society* **2016**, *138*, 8368-8371; b) Lu, Y.; Zhang, H.-N.; Jin, G.-X. *Accounts of Chemical Research* **2018**, *51*, 110-121; c)

Zhang, L.; Lin, L.; Liu, D.; Lin, Y.-J.; Li, Z.-H.; Jin, G.-X. *Journal of the American Chemical Society* **2017**, *139*, 1653-1660; d) Huang, S.-L.; Lin, Y.-J.; Li, Z.-H.; Jin, G.-X. *Journal of the American Chemical Society* **2014**, *53*, 11400-11404.

12. a) Song, Y. H.; Singh, N.; Jung, J.; Kim, H.; Kim, E.-H.; Cheong, H.-K.; Kim, Y.; Chi, K.-W. *Angewandte Chemie International Edition* **2016**, *55*, 2007-2011; b) Schouwey, C.; Holstein, J. J.; Scopelliti, R.; Zhurov, K. O.; Nagornov, K. O.; Tsybin, Y. O.; Smart, O. S.; Bricogne, G.; Severin, K. *Angewandte Chemie International Edition* **2014**, *53*, 11261-11265; c) Pentecost, C. D.; Chichak, K. S.; Peters, A. J.; Cave, G. W. V.; Cantrill, S. J.; Stoddart, J. F. *Journal of the American Chemical Society* **2007**, *46*, 11443-11447; d) Ibukuro, F.; Fujita, M.; Yamaguchi, K.; Sauvage, J.-P. *Journal of the American Chemical Society* **1999**, *121*, 11014-11015; e) Beves, J. E.; Danon, J. J.; Leigh, D. A.; Lemonnier, J.-F.; Vitorica-Yrezabal, I. J. *Angewandte Chemie International Edition* **2015**, *54*, 7665-7669.

13. a) Lee, H.; Elumalai, P.; Singh, N.; Kim, H.; Lee, S. U.; Chi, K.-W. *Journal of the American Chemical Society* **2015**, *137*, 4674-4677; b) Yamashita, K.; Kawano, M.; Fujita, M. *Journal of the American Chemical Society* **2007**, *129*, 1850-1851.

14. Wood, C. S.; Ronson, T. K.; Belenguer, A. M.; Holstein, J. J.; Nitschke, J. R. *Nature chemisty* **2015**, *7*, 354-358.

15. Hoste, J.; Thistlethwaite, M.; Weeks, J. *The Mathematical Intelligencer* **1998**, *20*, 33-48.

16. a) Yan, H.; Süss-Fink, G.; Neels, A.; Stoeckli-Evans, H. *Journal of the Chemical Society, Dalton Transactions* **1997**, No. 22, 4345-4350; b) Therrien, B.; Süss-Fink, G.; Govindaswamy, P.; Renfrew, A. K.; Dyson, P. J.

Angewandte Chemie International Edition **2008**, *47*, 3773-3776; c) Barry, N. P. E.; Therrien, B. *European Journal of Inorganic Chemistry* **2009**, *2009*, 4695-4700; d) Barry, N. P. E.; Furrer, J.; Therrien, B. *Helvetica Chimica Acta* **2010**, *93*, 1313-1328.

17. Sheldrick, G. M. *Acta Crystallographica Section A Foundations of Crystallography* **2008**, *64*, 112-122.

18. a) Spek, A. L. *Acta Crystallographica Section D Biological Crystallography* **2009**, *65*, 148-155; b) van der Sluis, P.; Spek, A. L. *Acta Crystallographica Section A Foundations of Crystallography* **1990**, *46*, 194-201.

19. Ruiz-Morales, Y. *The Journal of Physical Chemistry A* **2002**, *106*, 11283–11308.

20. Johnson, E. R.; Keinan, S.; Mori-Sánchez, P.; Contreras-García, J.; Cohen, A. J.; Yang, W. *Journal of the American Chemical Society* **2010**, *132*, 6498–6506.

21. Nielsen, C. B.; McCulloch, I. *Progress in Polymer Science* **2013**, *38*, 2053–2069.

22. Tsuzuki, S.; Honda, K.; Azumi, R. *Journal of the American Chemical Society* **2002**, *124*, 12200–12209.

23. Stewart, J. J. P. *Journal of Molecular Modeling* **2013**, *19* , 1–32.

24. Stewart, J. J. P. MOPAC2012 (Stewart Computational Chemistry, Colorado Springs, CO, USA, **2012**).

25. Adamo, C.; Barone, V. *The Journal of Chemical Physics* **1999**, *110*, 6158–6170.

26. Zhao, Y.; Truhlar, D. G. *Theoretical Chemistry Accounts* **2008**, *120* , 215–241.

27. Chai, J.-D.; Head-Gordon, M. *Physical Chemistry Chemical Physics* **2008**, *10*, 6615-6620.

28. Scalmani, G.; Frisch, M. J. *The Journal of Chemical Physics* **2010**, *132*, 114110.

29. Frisch, M. J. et al. Gaussian 09, Revision E. 01 (Gaussian, Inc., Wallingford CT, **2013**).

30. Hay, P. J.; Wadt, W. R. *The Journal of Chemical Physics* **1985**, *82*, 299–310.

31. Lu, T.; Chen, F. *Journal of Computational Chemistry* **2012**, *33*, 580–592.

32. Lu, R.; Han, Y.; Zhang, W.; Zhu, X.; Fei, Z.; Hodsden, T.; Anthopoulos, T. D.; Heeney, M. *Journal of Materials Chemistry C* **2018**, *6*, 2004–2009.

33. Parr, R. G.; Zhou, Z. *Accounts of Chemical Research* **1993**, *26*, 256–258.

Chapter 3. Selective and quantitative synthesis of a linear [3] catenane by two component coordination-driven self-assembly

3.1. Introduction

The syntheses of interlocked or intertwined compounds, such as catenanes, rotaxanes, and knots, present some of the more promising advances in supramolecular chemistry.[1] The production of these non-trivial topological structures, which are found in peptides[2], proteins[3], long chain polymers[4] and DNA,[5] has been driven by the utilization of nanoscale devices[6] and smart materials[7] and was the subject of the 2016 Nobel Prize for Chemistry[8]. Linear [n]catenanes, consist of two or more linearly interlocked rings and have captured widespread interest because of their intriguing structures, topological importance, and ability to show intercycler movements, i.e., quasi-mechanical movements.[9] Although a plethora of examples of the synthesis of [2] catenane or Hopf's link have been reported[10], linear [n] catenanes (n≥3) represents a major challenge. Despite extensive research in this area, relatively few examples linear [3]catenane formation have been described since they were first reported by Schill et al.[11] in 1969. Notable examples include Savauge's metal-ion template[12], Stoddart's electron deficient/electron-rich π—π template[13], and Stang's self-assembly using an external loop[14]. Unfortunately, the use of multiple components and several low yielding steps remain important obstacles to the widespread application of [n] catenanes (n≥3).[15] Selective synthesis of linear [3]catenanes from three rings is not straightforward because topologies such as Borromean rings, cyclic [3]catenane, and others are possible (Figure 3.1).[16] Furthermore, devised procedures also result in the formation of [2] catenanes and non-interlocked structures, thus, more efficient, selective strategies are required.[17] The use of coordination-driven self-assembly over the past three decades has simplified the synthesis of various 2D and 3D supramolecules.[18] This approach takes advantage of the well-defined coordination geometries of transition metalbased acceptors and suitable pyridyl donors to transform simple components into structurally exquisite and complex supramolecular

architectures.[19] The potential impact of this approach is immense because it allows researchers to prepare desired supramolecular complexes easily and use them for applications as varied as catalysis, encapsulation, and host-guest reactions.[20] Our group synergistically used weak secondary but pivotal inter/intra cycler interactions (π—π and CH—π) for the production of complex and diverse supramolecular topologies such as Solomon link[21a], Borromean rings[21b], Hopf's link[21c], and a non-catenane "rectangle in a rectangle"[21d] by two component self-assmbly. The outstanding usefulness of this concept was recently eloquently demonstrated by the synthesis of a complex molecular knot 8_{18} using secondary weak intracycler interactions.[22] As a result of our ongoing efforts to understand and develop topologically non-trivial compounds, we report the synthesis of a linear [3]catenane by coordination-driven self-assembly, which was achieved by introducing the 1,2,3-triazole moiety into a dipyridyl donor. The described method provides efficient access for the external template-free selective formation of linear [3]catenane.

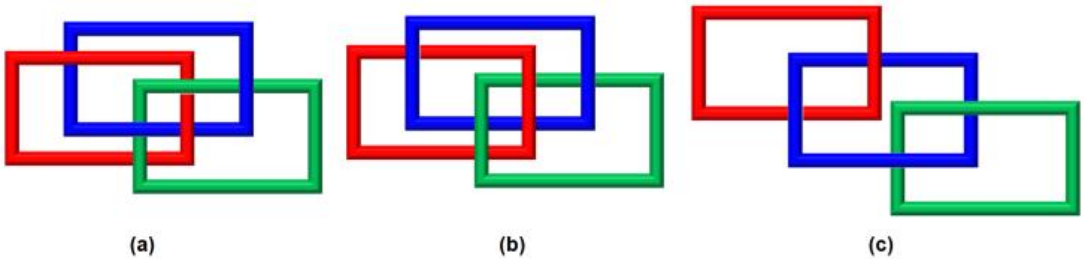

Figure 3.1 Representative topologies with three interlocked rings (a) Borromean rings $[6_2^3]$ in Alexander-Briggs notation (b) cyclic [3]catenane $[6_3^3]$ (c) linear [3] catenane $[4_1^3]$

3.2. Material and methods

Arene-ruthenium acceptors **A7** and **A5** were prepared according to the reported methods.[23] Deuterated NMR solvents were purchased from Cambridge Isotope Laboratory (Andover, MA, USA). NMR spectra were recorded on Bruker 300, 400, 800 and 900 MHz spectrometers (University of Ulsan and Korea Basic Science Institute, Ochang). ^{1}H NMR chemical shifts are reported relative to the residual protons of deuterated CD_3OD (3.31 ppm) and deuterated CD_3NO_2 (4.33 ppm). ESI-MS data of all compounds were recorded on Synapt G2 quadrupole time-of flight (TOF) mass spectrometer equipped with an electrospray ion source (Waters, Milford, MA, USA) and analyzed with the MassLynx software suite system at the Korea Basic Science Institute, Ochang).

3.2.1. Crystallographic data collection and structure refinement

Diffraction data of **7** was collected at 100 K on an ADSC Quantum 210 CCD diffractometer with synchrotron radiation (λ = 0.70000 Å) at the Supramolecular Crystallography Beamline 2D, Pohang Accelerator Laboratory (PAL), Pohang, Korea. The raw data were processed and scaled using the program HKL3000. The structure was solved by direct methods, and the refinements were carried out with full-matrix least-squares on F^2 with appropriate software implemented in the SHELXTL program package.[24] All the non-hydrogen atoms were refined anisotropically, and hydrogen atoms were added to their geometrically ideal positions. The contributions of the most disordered solvent molecules were removed from the diffraction data using the SQUEEZE routine of PLATON software,[25] and then final refinements were carried out. X-ray crystallographic data is provided in Table 3.1.

3.2.2. Synthesis of dipyridyl triazole donor L2 [1,4-bis(1-(pyridin-4-yl)-1H-1,2,3-triazol-4-yl)benzene]

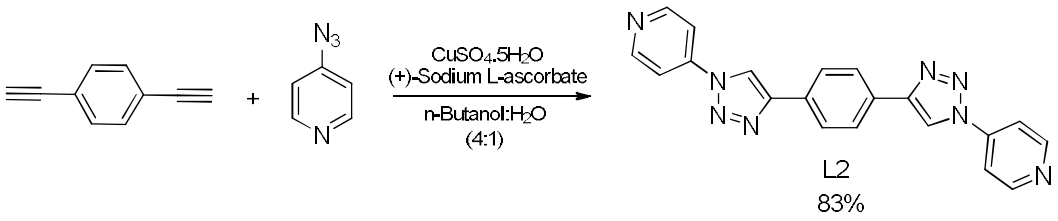

4-Azidopyridine (10.56 mg, 0.088 mmol), 1,4-bis(ethynyl)benzene (50.0 mg, 0.040 mmol), $CuSO_4 \cdot 5H_2O$ (0.53 mg, 0.002 mmol) and (+)-sodium L-ascorbate (0.85 mg, 0.004 mmol) were added to a 4:1 (v/v) solution of n-butanol and water and stirred at 50°C for 24 h. The precipitated product was filtered and washed several times with methanol and water. The pale yellow powder obtained was characterized as ligand **L2**. Yield: (41.5 mg, Yield: 83 %), Mp: > 300 ℃. Anal. Calcd for $C_{20}H_{14}N_8$: C, 65.56; H, 3.85; N, 30.58. Found: C, 65.44; H, 3.86; N, 30.47. ^{1}H NMR (400 MHz, CF_3COOD) δ 8.63 (dd, J = 4.6, 1.6 Hz, 2H), 7.73 (s, 1H), 7.50 (dd, J = 4.6, 1.6 Hz, 2H); ^{13}C NMR (100 MHz, CF_3COOD) δ 150.55, 142.97, 142.48, 141.31, 131.55, 119.51, 118.93; ESI-HRMS calcd for $C_{20}H_{15}N_8$ (**L2**+H^+): 367.1420; found 367.1420.

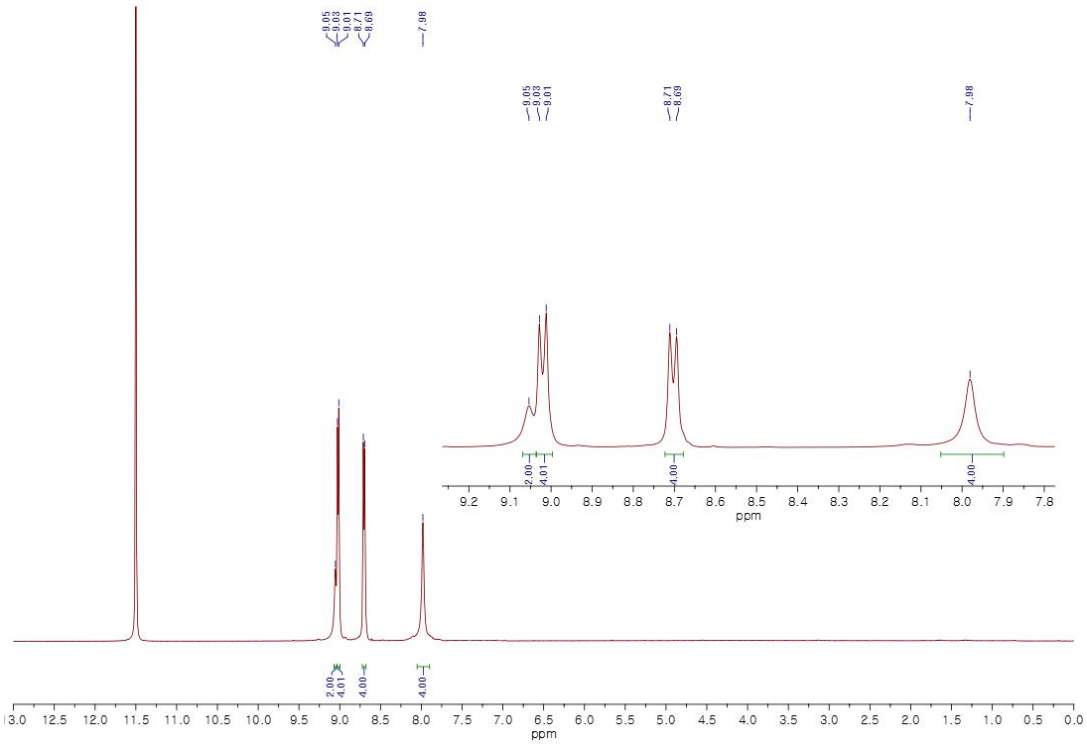

Figure 3.2 ^{1}H NMR spectrum of **L2** (CF_3COOD, 400 MHz)

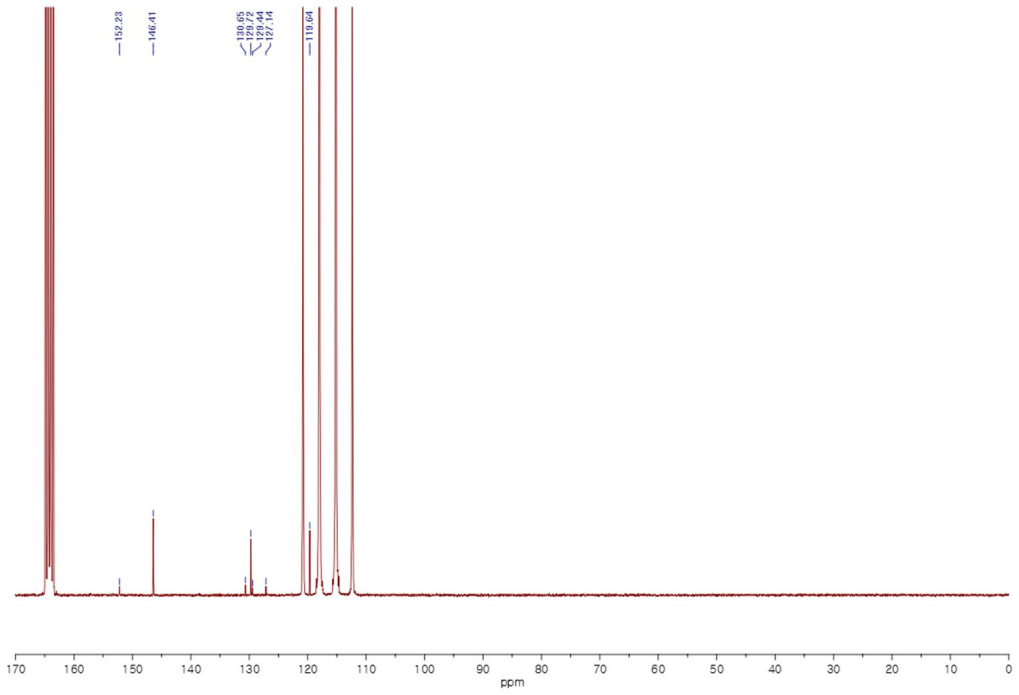

Figure 3.3 ^{13}C NMR spectrum of **L2** (CF_3COOD, 100 MHz)

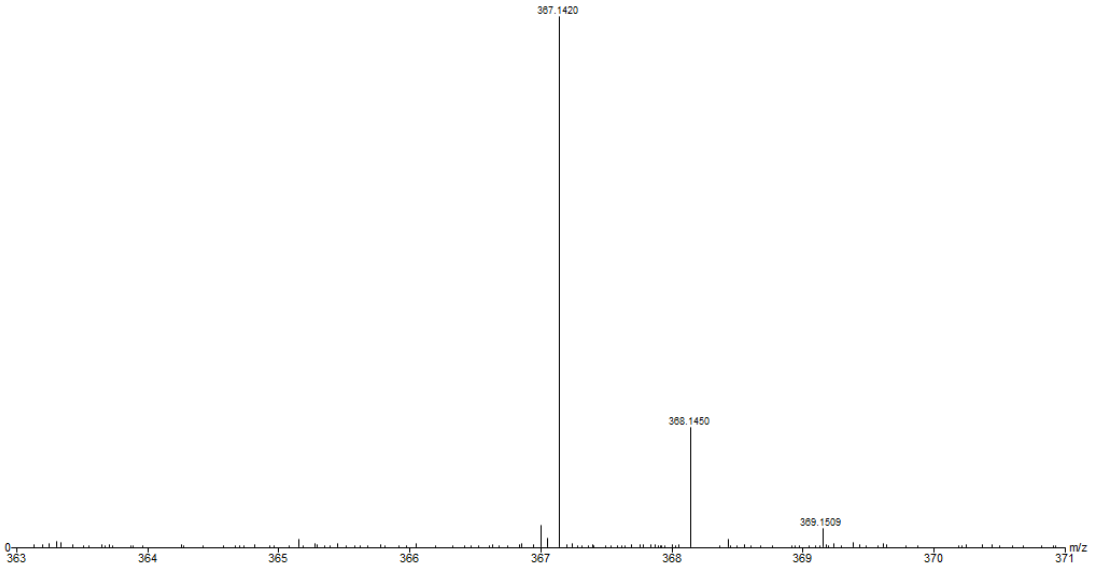

Figure 3.4 ESI-HRMS spectrum of **L2** ($C_{20}H_{15}N_8$ ($L+H^+$))

3.2.3. Synthesis of dipyridyl triazole donor L3 [1,4-bis(1-(3,5-dimethylpyridin-4-yl)-1H-1,2,3-triazol-4-yl)benzene]

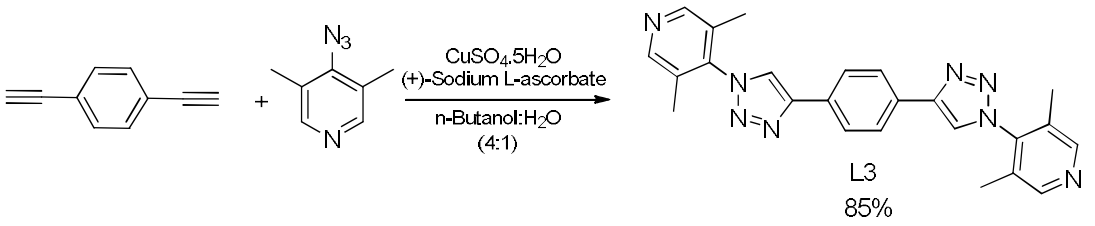

4-Azido-3,5-dimethylpyridine (12.84 mg, 0.088 mmol), 1,4-bis(ethynyl)benzene (50.0 mg, 0.040 mmol), $CuSO_4 \cdot 5H_2O$ (0.53 mg, 0.002 mmol) and (+)-sodium L-ascorbate (0.85 mg, 0.004 mmol) were added to a 4:1 (v/v) solution of n-butanol and water and stirred at 50°C for 24 h. The precipitated product was filtered and washed several times with methanol and water. The pale yellow powder obtained was characterized as ligand **L3**. Yield: (42.3 mg, Yield: 85 %), Mp: 286 ℃ (dec.) Anal. Calcd for $C_{24}H_{22}N_8$: C, 68.23; H, 5.25; N, 26.52. Found: C, 68.01; H, 5.26; N, 26.42. ^{1}H NMR (400 MHz, CD_3OD+$CDCl_3$ (1:1)) δ 8.54 (s, 2H), 8.46 (s, 2H), 8.07 (s, 4H), 2.20 (s, 12H); ^{13}C NMR (100 MHz, CD_3OD+$CDCl_3$ (1:1)) δ 150.12, 148.35, 144.02, 131.08, 130.60, 127.05, 122.65, 14.62; ESI-HRMS calcd for $C_{24}H_{23}N_8$ (**L3**+H^+): 423.2046; found 423.2040.

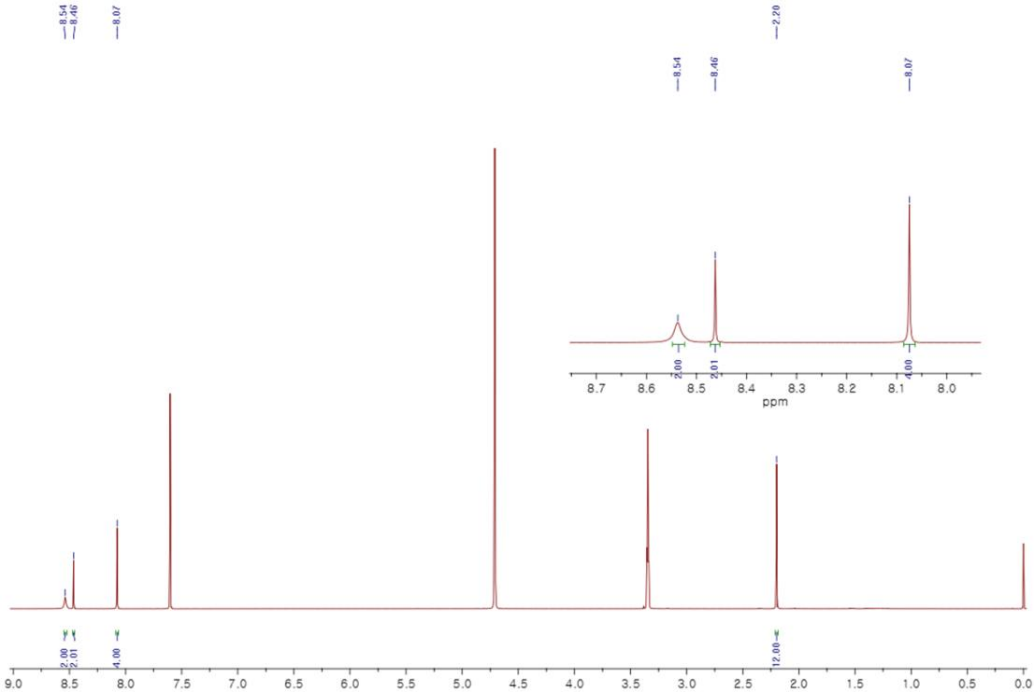

Figure 3.5 ^{1}H NMR spectrum of **L3** (CD_3OD+$CDCl_3$ (1:1), 400 MHz)

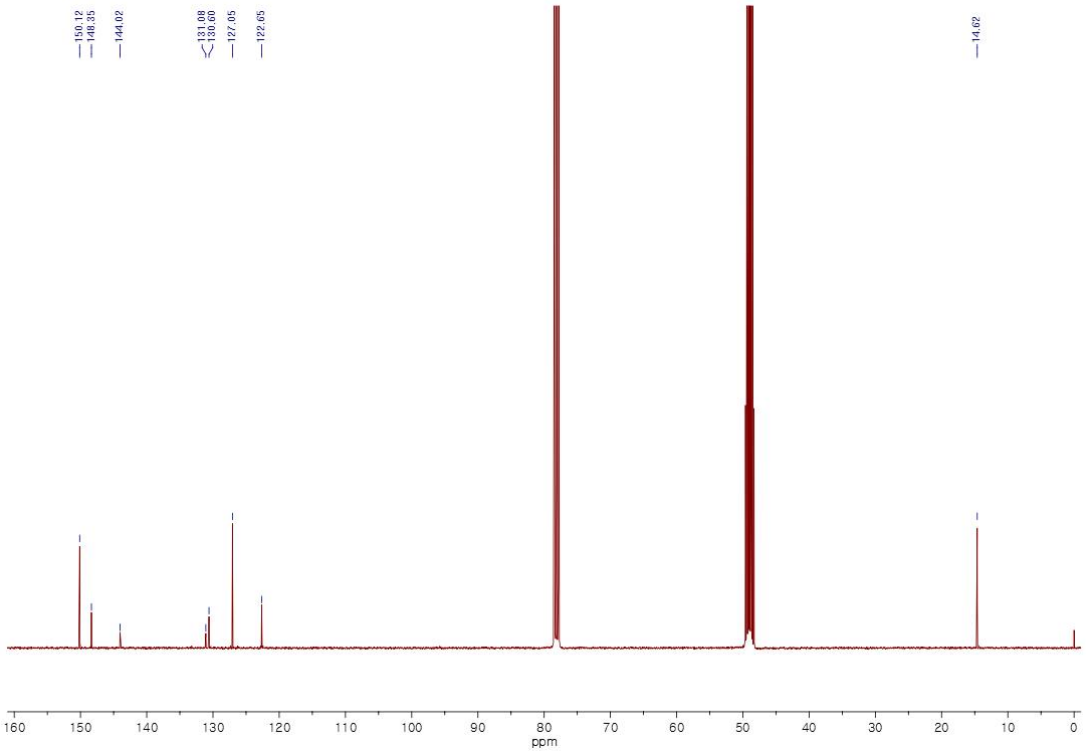

Figure 3.6 ^{13}C NMR spectrum of **L3** (CD_3OD+$CDCl_3$ (1:1), 100 MHz)

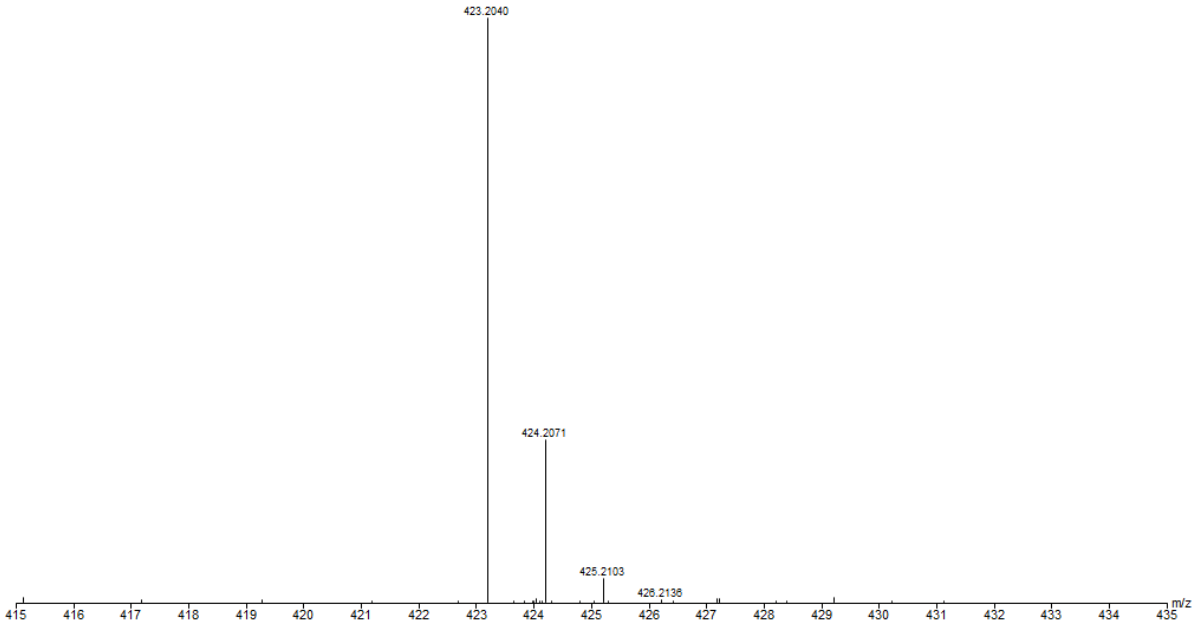

Figure 3.7 ESI-HRMS spectrum of **L3** ($C_{24}H_{23}N_8$ (**L3**+H^+))

3.2.4 Synthesis of dipyridyl triazole donor L4 [9,10-bis(1-(pyridin-4-yl)-1H-1,2,3-triazol-4-yl)anthracene]

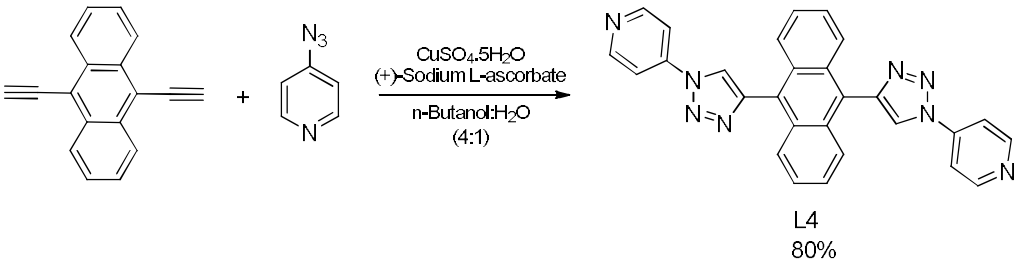

4-Azidopyridine (11.35 mg, 0.094 mmol), 1,4-bis(ethynyl)anthracene (20.0 mg, 0.043 mmol), $CuSO_4 \cdot 5H_2O$ (0.53 mg, 0.002 mmol) and (+)-sodium L-ascorbate (0.85 mg, 0.004 mmol) were added to a 4:1 (v/v) solution of n-butanol and water and stirred at 50°C for 24 h. The precipitated product was filtered and washed several times with methanol and water. The light brown powder obtained was characterized as ligand **L4**. Yield: (16 mg, Yield: 80 %), Mp: > 300 ℃. Anal. Calcd for $C_{28}H_{18}N_8$: C, 72.09; H, 3.89; N, 24.02. Found: C, 71.81; H, 3.90; N, 23.95. ^{1}H NMR (400 MHz, CD_3OD+$CDCl_3$ (1:1)) δ 9.01 (s, 2H), 8.85 (d, *J* = 6.3 Hz, 4H), 8.18 (dd, *J* = 4.7, 1.6 Hz, 4H), 7.90 (dd, *J* = 6.8, 3.2 Hz, 4H), 7.52 (dd, *J* = 6.8, 3.2 Hz, 4H); ^{13}C NMR (100 MHz, CD_3OD+$CDCl_3$ (1:1)) δ 151.87, 145.80, 140.24, 134.39, 131.60, 127.40, 126.53, 126.22, 114.88; ESI-HRMS calcd for $C_{28}H_{19}N_8$ (**L4**+H^+): 467.1733; found 467.1727.

3.2.5 Coordination-driven self-assembly of monoreactangle 6

The arene-Ru(II) acceptor **A7** (1.91 mg, 2.0 μmol) and donor **L2** (0.73 mg, 2.0 μmol) were stirred in CD_3OD (4.0 mL) at room temperature for 12 h to produce a green solution. ^1H NMR (900 MHz, CD_3OD) δ 8.93 (s, 4H), 8.60 (d, *J* = 6.3 Hz, 8H), 7.96 (d, *J* = 5.4 Hz, 8H), 7.82 (s, 8H), 7.33 (s, 8H), 5.90 (d, *J* = 6.0 Hz, 8H), 5.67 (d, *J* = 6.0 Hz, 8H), 2.87 (dt, *J* = 14.0, 7.0 Hz, 4H), 2.15 (s, 12H), 1.37 (d, *J* = 7.0 Hz, 24H); ^{13}C NMR (225 MHz, CD_3OD) δ 170.95, 153.46, 148.17, 145.06, 137.32, 129.47, 125.81, 118.26, 115.09, 111.32, 103.67, 99.79, 84.40, 82.59, 30.64, 21.08, 15.99; ESI-MS for **6** ($C_{104}H_{92}F_{12}N_{16}O_{20}Ru_4S_4$): m/z = 733.4337 [**6**-3OTf]$^{3+}$.

3.2.6 Coordination-driven self-assembly of linear [3]catenane 7

The arene-Ru(II) acceptor **A7** (16.9 mg, 20 μmol) and donor **L2** (7.33 mg, 20 μmol) were stirred in CD_3OD (1.0 mL) at room temperature for 12 h to produce a dark green solution. The products were precipitated and isolated by dropwise addition of diethyl ether into this solution, and washed twice with diethyl ether using centrifugation method. The dark-green powder was characterized as **7**. Yield: (22.6 mg, Yield: 93 %), Anal. Calcd for $C_{312}H_{276}F_{36}N_{48}O_{60}Ru_{12}S_{12}\cdot 2H_2O$: C 46.99; H 3.54; N 8.58. Found: C 46.82; H 3.55; N 8.55. ^{1}H NMR (900 MHz, CD_3OD) δ 9.24 (s, 2H), 9.13 (s, 2H), 8.77 (s, 2H), 8.75 (s, 6H), 8.69 (s, 12H), 8.43 (s, 8H), 8.24 (s, 4H), 8.20 (s, 2H), 8.17 (s, 5H), 8.14 (s, 3H), 8.07 (s, 4H), 7.94 (s, 10H), 7.76 (s, 8H), 7.72 (s, 4H), 7.64 (s, 4H), 7.59 (d, *J* = 13.0 Hz, 2H), 7.52 (s, 6H), 7.49 (d, *J* = 12.4 Hz, 2H), 7.43 (d, *J* = 12.9 Hz, 8H), 7.40 (d, *J* = 9.9 Hz, 6H), 7.17 (s, 8H), 6.11 (s, 4H), 6.05 (d, *J* = 5.3 Hz, 2H), 6.01 (s, 3H), 5.97 (d, *J* = 10.2 Hz, 7H), 5.93 (s, 4H), 5.90 (s, 3H), 5.86 (s, 5H), 5.81 (s, 3H), 5.76 (d, *J* = 13.9 Hz, 5H), 5.70 (s, 4H), 5.67 (s, 3H), 5.59 (s, 5H), 3.26 – 3.20 (m, 2H), 3.09 (dt, *J* = 13.4, 6.5 Hz, 2H), 2.96 (s, 2H), 2.91 (s, 2H), 2.89 – 2.83 (m, 4H), 2.51 (s, 4H), 2.45 (d, *J* = 12.7 Hz, 3H), 2.39 (d, *J* = 11.5 Hz, 8H), 2.28 (d, *J* = 18.0 Hz, 4H), 2.23 (d, *J* = 12.9 Hz, 6H), 2.22 – 2.19 (m, 3H), 2.18 (s, 4H), 2.15 (s, 3H), 2.12 (s, 5H), 2.05 (s, 8H), 1.62 (s, 2H), 1.60 (s, 3H), 1.56 (s, 8H), 1.53 (s, 3H), 1.51 (d, *J* = 5.6 Hz, 6H), 1.48 (d, *J* = 5.2 Hz, 6H), 1.43 (s, 16H), 1.39 (s, 15H), 1.35 (s, 18H), 1.31 (d, *J* = 9.3 Hz, 10H), 1.25 (s, 5H), 1.13 (s, 4H); ^{13}C NMR (225 MHz, CD_3OD) δ 171.63, 171.38, 171.14, 170.96, 170.76, 153.56, 153.34, 147.97, 147.63, 147.49, 147.16, 147.05, 146.64, 146.15, 145.26, 145.12, 144.89, 144.13, 143.86, 143.57, 138.90, 138.68, 138.48, 137.56, 137.37, 134.72, 129.48, 129.39, 128.95, 128.87, 128.83, 128.67, 128.46, 125.93, 125.76, 125.59, 125.23, 125.07, 124.72, 124.25, 122.58, 121.17, 119.76, 118.35, 117.14, 115.52, 115.34, 114.19, 113.27, 111.33, 111.31, 111.23, 111.20, 111.13, 111.11, 104.50, 104.05, 103.68, 103.58, 103.46, 99.89, 99.55, 99.45, 98.64, 84.61, 84.51, 84.36, 83.30, 82.64, 82.43, 35.13, 34.40, 33.54, 31.65, 30.87, 30.71, 30.62, 30.55, 30.25, 29.42, 29.19, 29.04, 28.91, 28.83, 26.72, 25.51, 23.15, 22.33, 21.88, 21.50, 21.44,

21.24, 21.18, 21.10, 21.06, 20.62, 19.61, 18.61, 17.90, 16.70, 16.35, 16.03, 15.93; ESI-MS for **7** ($C_{312}H_{276}F_{36}N_{48}O_{60}Ru_{12}S_{12}$): m/z = 1835.9700 [**7**-4OTf]$^{4+}$, 1438.9819 [**7**-5OTf]$^{5+}$.

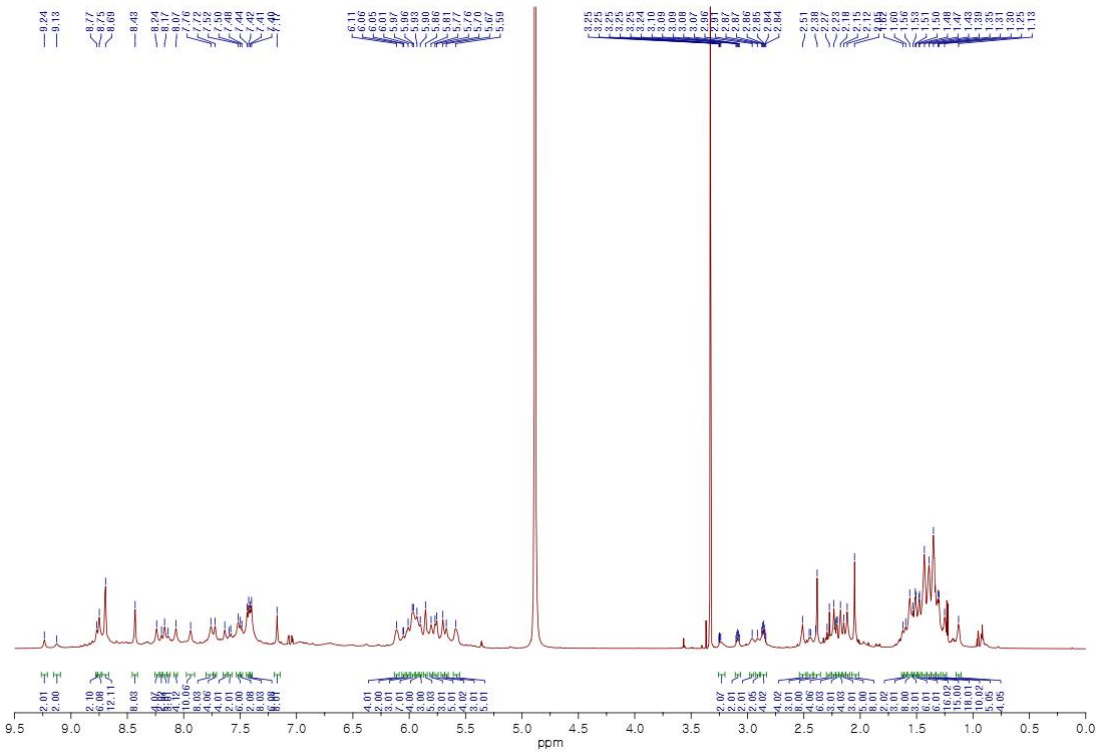

Figure 3.8 ^{1}H NMR spectrum of **7** (CD_3OD [20 mM], 900 MHz)

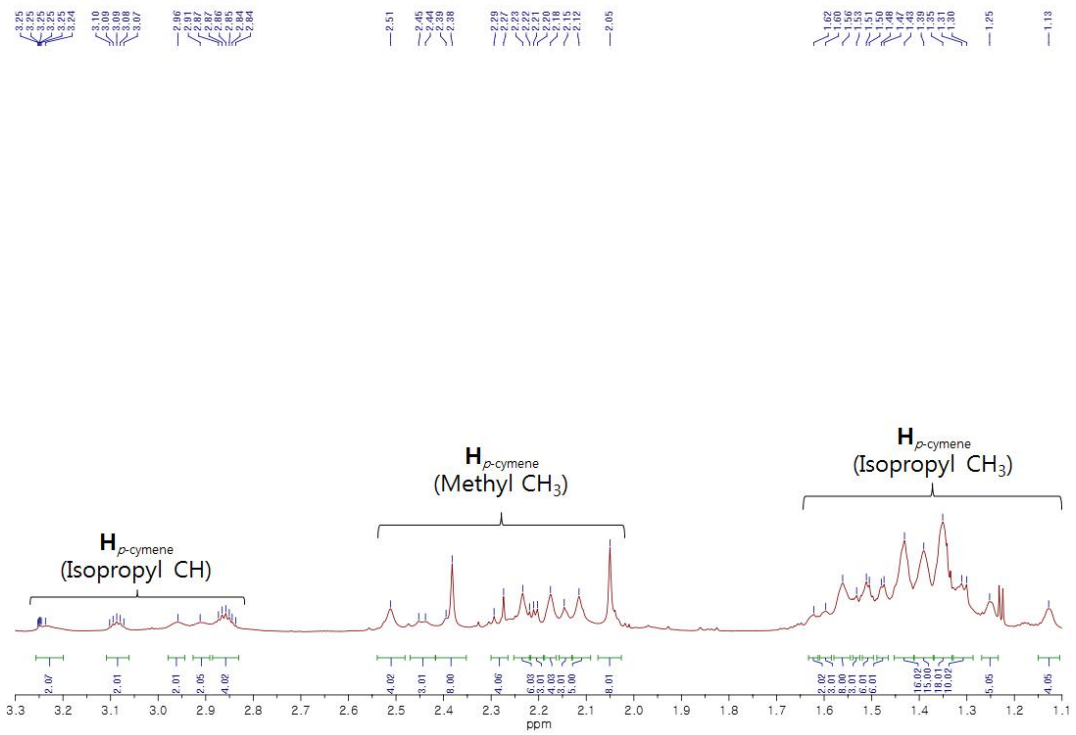

Figure 3.9 Expanded ^{1}H NMR spectrum of **7** (CD_3OD [20 mM], 900 MHz)

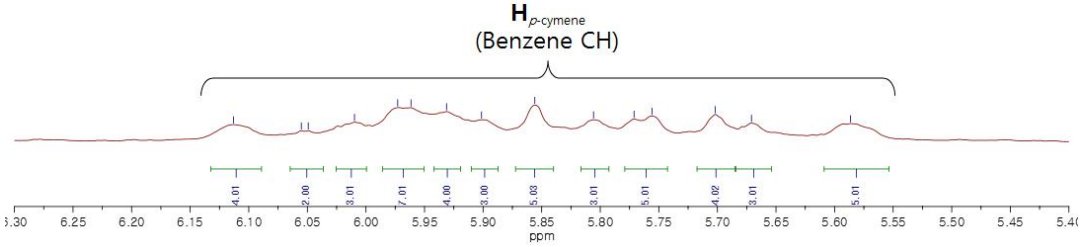

Figure 3.10 Expanded ^{1}H NMR spectrum of **7** (CD_3OD [20 mM], 900 MHz)

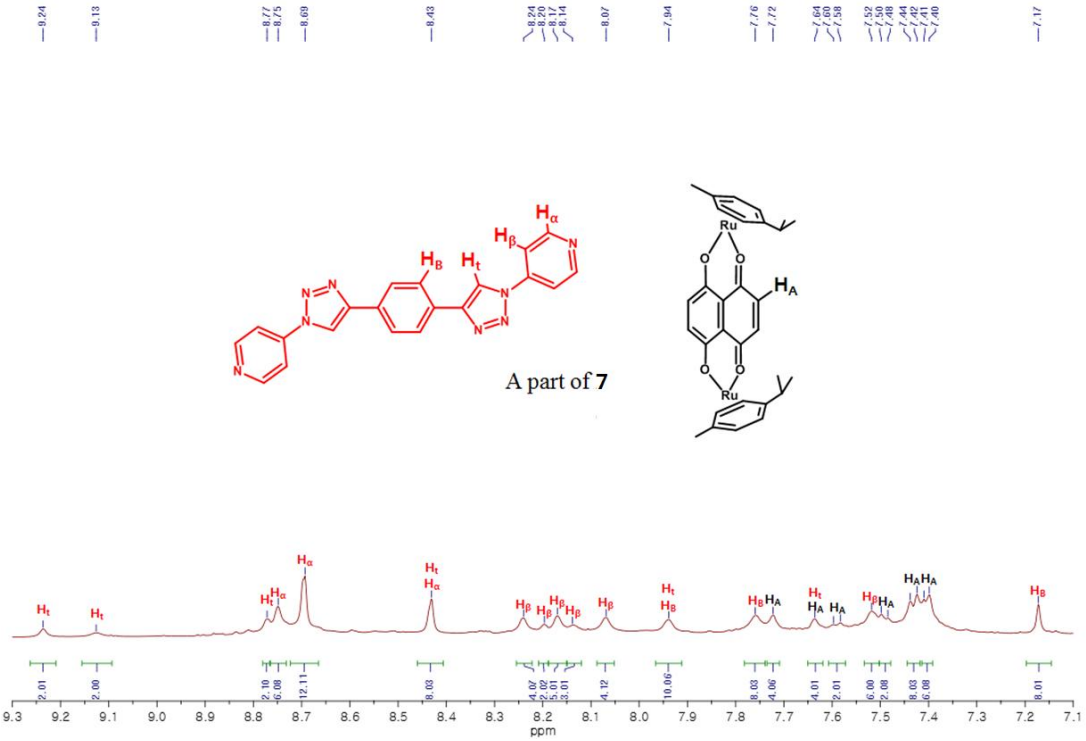

Figure 3.11 Expanded ^{1}H NMR spectrum of **7** (CD_3OD [20 mM], 900 MHz)

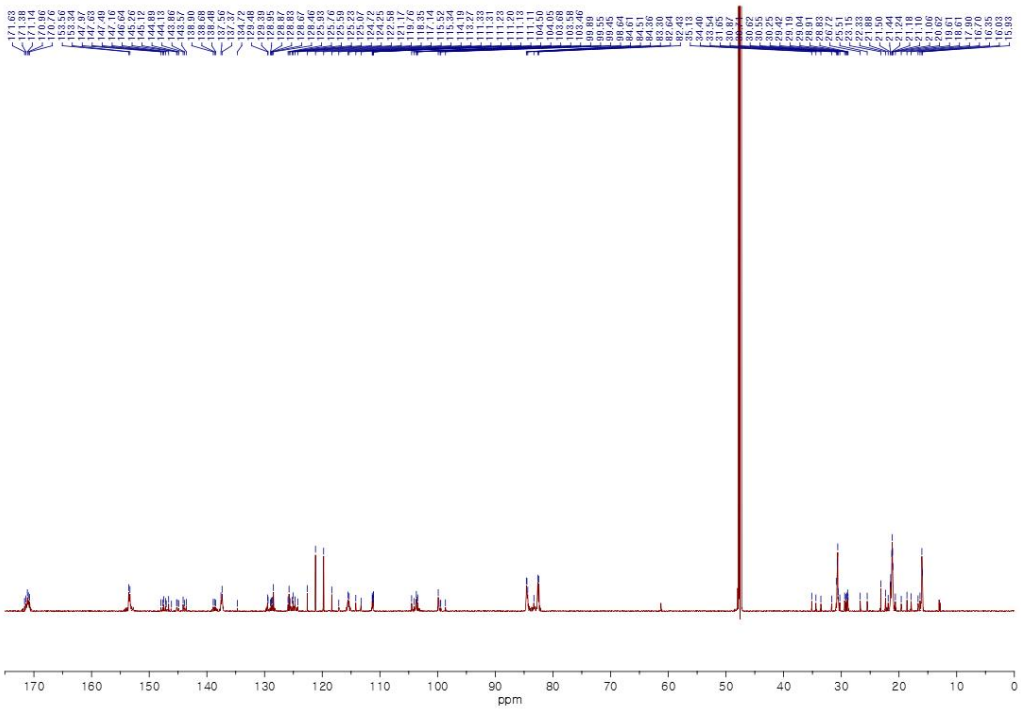

Figure 3.12 ^{13}C NMR spectrum of **7** (CD_3OD [20 mM], 225 MHz)

3.2.7 Coordination-driven self-assembly of 9

The arene-Ru(II) acceptor **A7** (7.65 mg, 8.0 μmol) and donor **L3** (3.38 mg, 8.0 μmol) were stirred in CD_3OD (1.0 mL) at room temperature for 12 h to produce a dark brown solution. The products were precipitated and isolated by dropwise addition of diethyl ether into this solution, and washed twice with diethyl ether using centrifugation method. The dark-green powder was characterized as **9**. Yield: (9.9 mg, Yield: 90%), Anal. Calcd for $C_{112}H_{108}F_{12}N_{16}O_{20}Ru_4S_4 \cdot 2H_2O$: C, 48.13; H, 4.04; N, 8.02. Found: C, 48.07; H, 4.05; N, 8.02. ^{1}H NMR (400 MHz, CD_3OD) δ 8.63 (s, 4H), 8.48 (s, 8H), 8.15 (s, 8H), 7.31 (s, 8H), 5.93 (d, *J* = 6.4 Hz, 8H), 5.70 (d, *J* = 6.3 Hz, 8H), 2.88 (dt, *J* = 13.6, 6.9 Hz, 4H), 2.15 (s, 12H), 2.09 (s, 24H), 1.35 (d, *J* = 6.9 Hz, 24H); ^{13}C NMR (100 MHz, CD_3OD) δ 172.53 (s), 153.38 (s), 149.41 (s), 148.37 (s), 139.01 (s), 135.07 (s), 131.56 (s), 127.92 (s), 127.12 (s), 112.93 (s), 105.34 (s), 101.82 (s), 86.31 (s), 84.24 (s), 32.35 (s), 22.81 (s), 17.77 (s), 15.07 (s). ESI-MS for **9** ($C_{112}H_{108}F_{12}N_{16}O_{20}Ru_4S_4$): m/z = 770.8080 [**9**-3OTf]$^{3+}$.

3.2.8 Coordination-driven self-assembly of 10

The arene-Ru(II) acceptor **A7** (7.65 mg, 8.0 μmol) and donor **L4** (3.73 mg, 8.0 μmol) were stirred in CD_3OD (1.0 mL) at room temperature for 12 h to produce a dark green solution. The products were precipitated and isolated by dropwise addition of diethyl ether into this solution, and washed twice with diethyl ether using centrifugation method. The dark-green powder was characterized as **10**. Yield: (10.4 mg, Yield: 91%), Anal. Calcd for $C_{120}H_{100}F_{12}N_{16}O_{20}Ru_4S_4 \cdot 2H_2O$: C, 50.00; H, 7.91; N, 7.77. Found: C, 49.89; H, 7.91; N, 7.76. ^{1}H NMR (300 MHz, CD_3OD) δ 9.06 (s, 4H), 8.67 (d, *J* = 6.8 Hz, 8H), 8.11 (d, *J* = 6.8 Hz, 8H), 7.59 (dd, *J* = 6.9, 3.2 Hz, 8H), 7.29 (s, 8H), 6.95 (dd, *J* = 6.9, 3.2 Hz, 8H), 5.93 (d, *J* = 6.3 Hz, 8H), 5.70 (d, *J* = 6.3 Hz, 8H), 2.88 (dt, *J* = 13.7, 6.7 Hz, 4H), 2.14 (s, 12H), 1.36 (d, *J* = 6.9 Hz, 24H); ^{13}C NMR (75 MHz, CD_3NO_2) δ 172.62 (s), 155.24 (s), 146.65 (s), 146.37 (s), 138.71 (s), 131.97 (s), 127.67 (s), 127.10 (s), 125.03 (s), 117.06 (s), 112.94 (s), 105.14 (s),

101.09 (s), 85.62 (s), 84.25 (s), 32.05 (s), 22.49 (s), 17.58 (s). ESI-MS for **10** ($C_{120}H_{100}F_{12}N_{16}O_{20}Ru_4S_4$): m/z = 800.1315 [**10**-3OTf]$^{3+}$.

3.2.9 Coordination-driven self-assembly of 11

The arene-Ru(II) acceptor **A7** (7.65 mg, 8.0 μmol) and donor **L5** (2.24 mg, 8.0 μmol) were stirred in CD_3OD (1.0 mL) at room temperature for 12 h to produce a dark brown solution. The products were precipitated and isolated by dropwise addition of diethyl ether into this solution, and washed twice with diethyl ether using centrifugation method. The dark-green powder was characterized as **11**. Yield: (9.2 mg, Yield: 93%), ^{1}H NMR (300 MHz, CD_3OD) δ 8.42 (d, *J* = 6.7 Hz, 8H), 7.48 (s, 8H), 7.46 (d, J = 6.7 Hz, 8H), 7.24 (s, 8H), 5.85 (d, *J* = 6.3 Hz, 8H), 5.61 (d, *J* = 6.3 Hz, 8H), 2.82 (dt, *J* = 13.8, 6.9 Hz, 4H), 2.09 (s, 12H), 1.32 (d, *J* = 6.9 Hz, 24H); ^{13}C NMR (75 MHz, CD_3OD) δ 170.95 (s), 138.40 (s), 137.24 (s), 134.98 (s), 128.00 (s), 122.46 (s), 119.76 (s), 118.23 (s), 112.26 (s), 107.17 (s), 103.69 (s), 99.99 (s), 84.52 (s), 78.82 (s), 30.61 (s), 21.21 (s), 16.02 (s). ESI-MS for **11** ($C_{112}H_{108}F_{12}N_{16}O_{20}Ru_4S_4$): m/z = 676.0780 [**11**-3OTf]$^{3+}$.

3.2.10 Coordination-driven self-assembly of 12

The arene-Ru(II) acceptor **A5** (6.85 mg, 8.0 μmol) and donor **L2** (3.38 mg, 8.0 μmol) were stirred in CD_3OD (1.0 mL) at room temperature for 12 h to produce a yellow solution. The products were precipitated and isolated by dropwise addition of diethyl ether into this solution, and washed twice with diethyl ether using centrifugation method. The dark-green powder was characterized as **12**. Yield: (8.4 mg, Yield: 83 %), Anal. Calcd for $C_{88}H_{84}F_{12}N_{16}O_{20}Ru_4S_4 \cdot 2H_2O$: C, 42.58; H, 3.57; N,9.03. Found: C, 42.75; H, 3.59; N, 9.06. ^{1}H NMR (300 MHz, CD_3OD) δ 8.85 (s, 1H), 8.26 (d, *J* = 6.0 Hz, 2H), 7.96 (d, *J* = 6.0 Hz, 2H), 7.69 (s, 2H), 5.98 (d, *J* = 6.0 Hz, 2H), 5.81 (d, *J* = 5.9 Hz, 2H), 2.87 (dt, *J* = 13.6, 7.0 Hz, 1H), 2.26 (s, 3H), 1.39

(d, J = 6.8 Hz, 6H); ^{13}C NMR (75 MHz, CD_3OD) δ 154.35 (s), 148.55 (s), 147.32 (s), 125.89 (s), 114.89 (s), 103.20 (s), 102.53 (s), 99.99 (s), 97.61 (s), 82.06 (s), 81.52 (s), 31.10 (s), 21.07 (s), 16.65 (s); ESI-MS for **12** ($C_{88}H_{84}F_{12}N_{16}O_{20}Ru_4S_4$): m/z = 666.4131 [**12**-3OTf]$^{3+}$.

3.3. Results and discussion

3.3.1. Synthesis and characterization of monorectangle 6 and linear [3]catenane 7

Self-assembly reaction of a 1:1 mixture of acceptor **A7** {(p-cymene)$_2$Ru$_2$(5,8-dihydroxy-1,4-naphthoquinone)(OTf)$_2$} and donor **L2** {1,4-bis(1-(pyridin-4-yl)-1H-1,2,3-triazol-4-yl)benzene} (8.0mM) in CD_3OD for 12 hours at room temperature resulted in the formation of new self-assembled product with a highly complex ^{1}H NMR spectrum. The new self-assembled product was quantitatively produced upon increasing concentration to 20mM (Scheme 1). At 20mM, only one diffusion coefficient at D = 3.4 × 10^{-10} m^2 s^{-1} was observed in the DOSY NMR spectrum (Figures 3.13a and 3.14), and prominent peaks were observed at m/z = 1438.9819 (**7**-5OTf)$^{5+}$ and at 1835.9700 (**7**-4OTf)$^{4+}$ in its ESI-MS data. Perfect agreement with the theoretical isotopic distributions indicated the selective formation of a [6+6] self-assembled product (Figures 3.15-3.17).

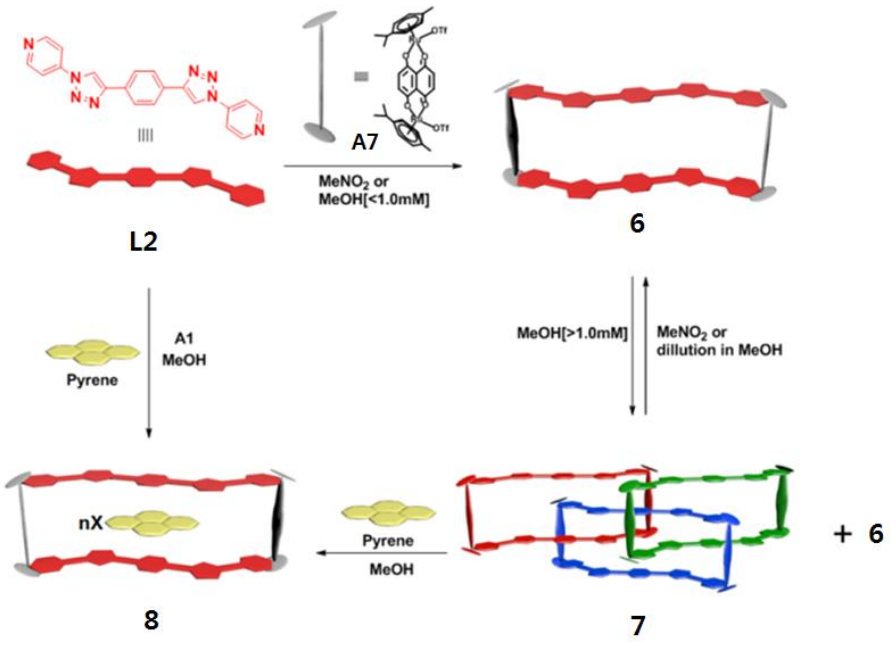

Scheme 3.1 Self-assembly and interconversion of linear [3]catenane and monorectangles

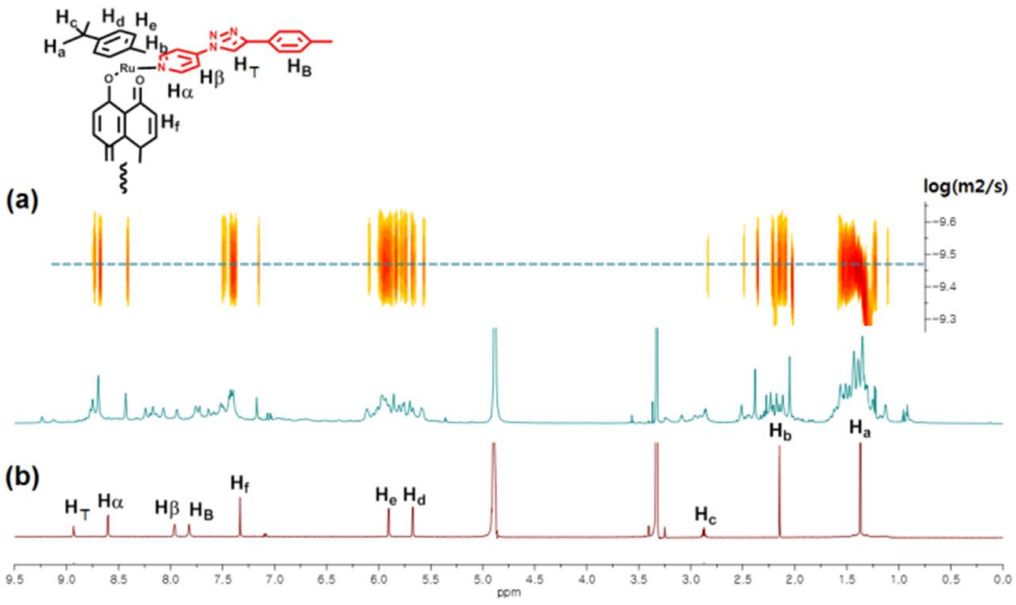

Figure 3.13 ^{1}H NMR spectra of monorectangle **6** and of linear [3]catenane **7**, (a) ^{1}H and DOSY NMR spectra of **7** at 20mM (b) ^{1}H-NMR spectrum of monorectangle **6** at 0.5mM (the reaction was conducted in CD_3OD and spectra were recorded at 900 MHz)

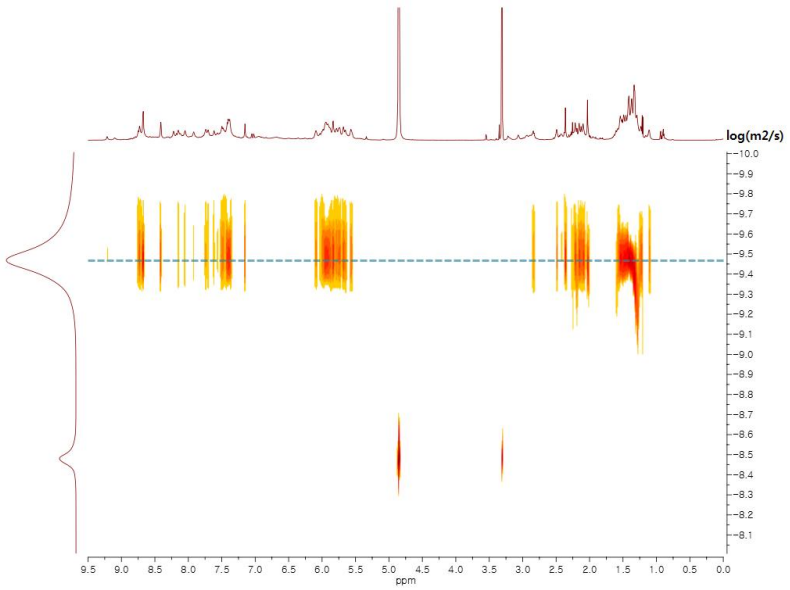

Figure 3.14 ^{1}H-DOSY NMR spectrum of **7** (CD_3OD [20 mM], 298 K, 800 MHz)

Diffusion coefficient: 3.4×10^{-10} m^2/sec

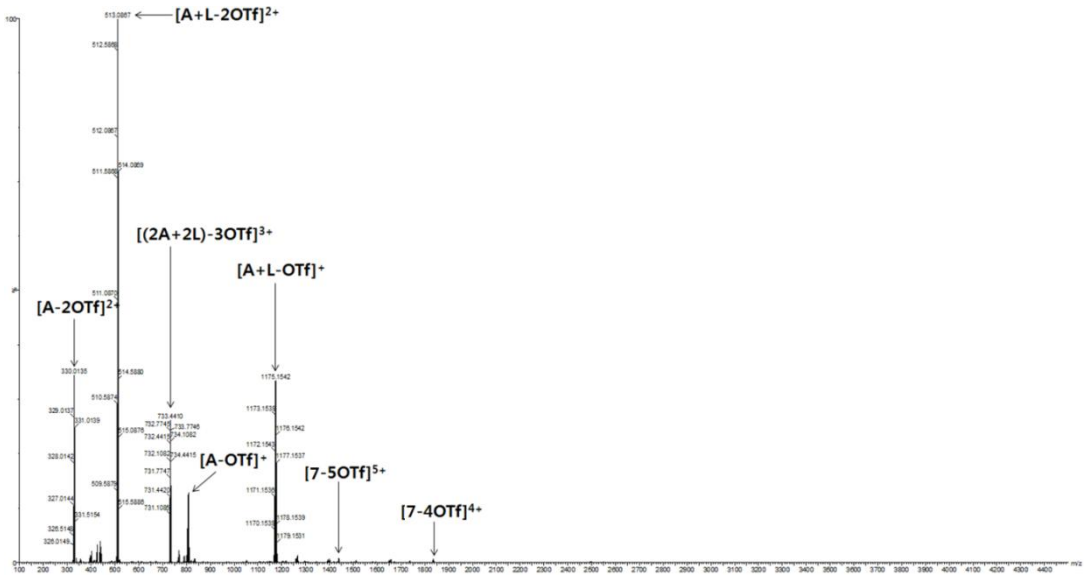

Figure 3.15 Full ESI mass spectrum of **7**. (Reaction in CD_3OD [20 mM])

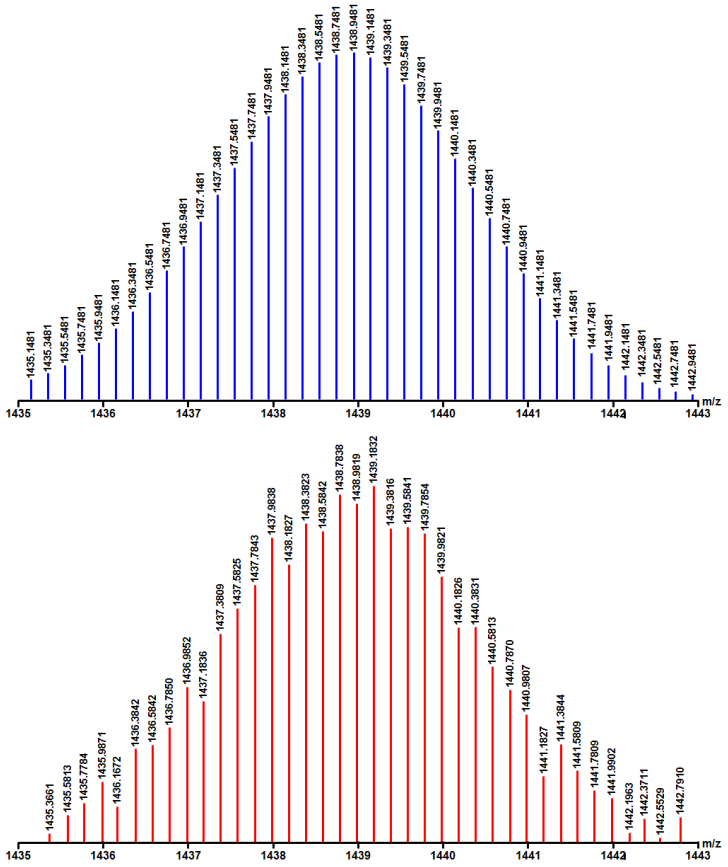

Figure 3.16 Calculated (blue) and experimental (red) ESI mass spectra of [**7**-5OTf]$^{5+}$.

(Reaction in CD_3OD [20 mM])

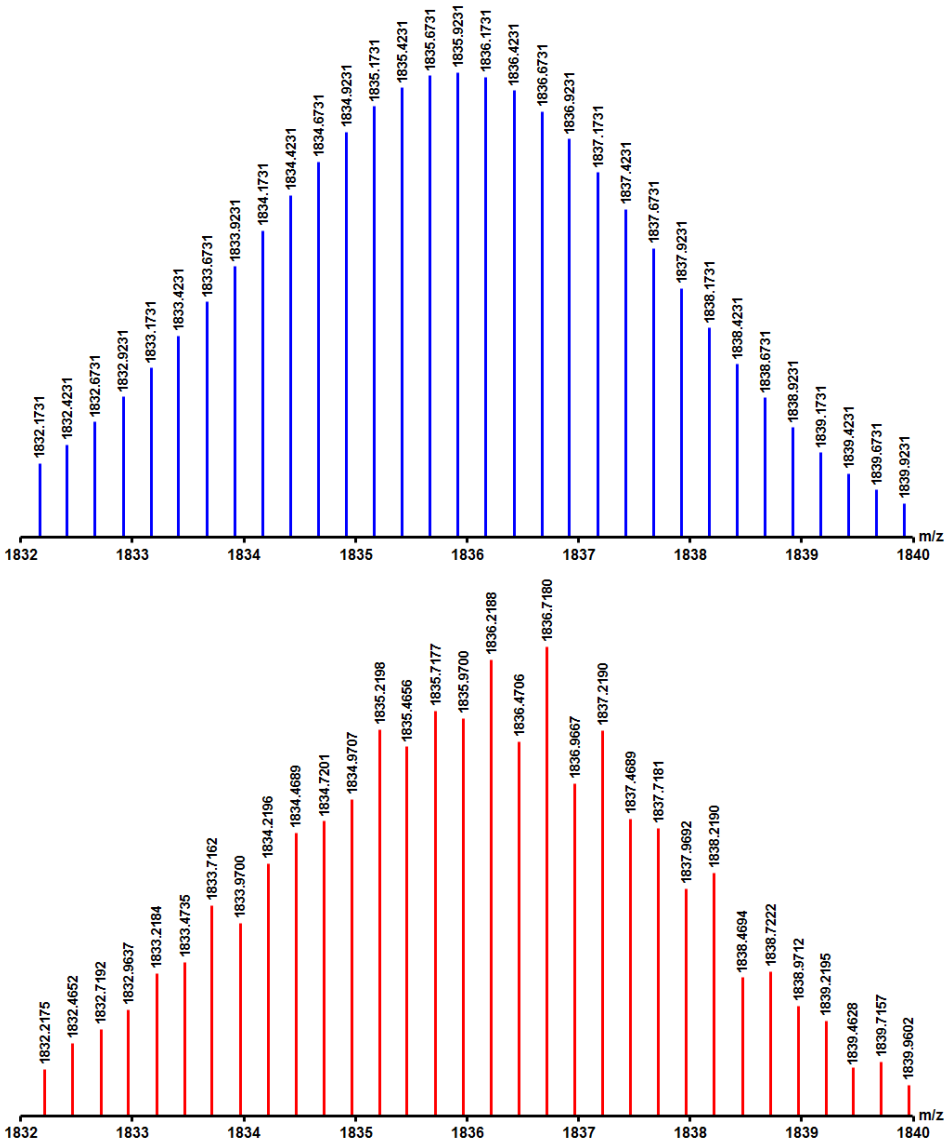

Figure 3.17 Calculated (blue) and experimental (red) ESI mass spectra of [**7**-4OTf]$^{4+}$.

(Reaction in CD_3OD [20 mM])

Upon decreasing the concentration, [2+2] monorectangle **6** started to appear, and fully formed at 0.5 mM (Figures 3.13b, 3.18) with only one diffusion coefficient at D = 6.1 × 10^{-10} m^2 s^{-1} (Figure 3.21). Similar reactions in CD_3NO_2 at concentration between 0.5 to 20 mM provided **6** only. (Scheme 3.1 and Figures 3.22-3.24) Combined NMR studies and a prominent ESI-MS peak at m/z = 733.4337 (**6**-3OTf)$^{3+}$ further confirmed the formation of monorectangle **6**. (Figures 3.19-3.28 and 3.31-3.36)

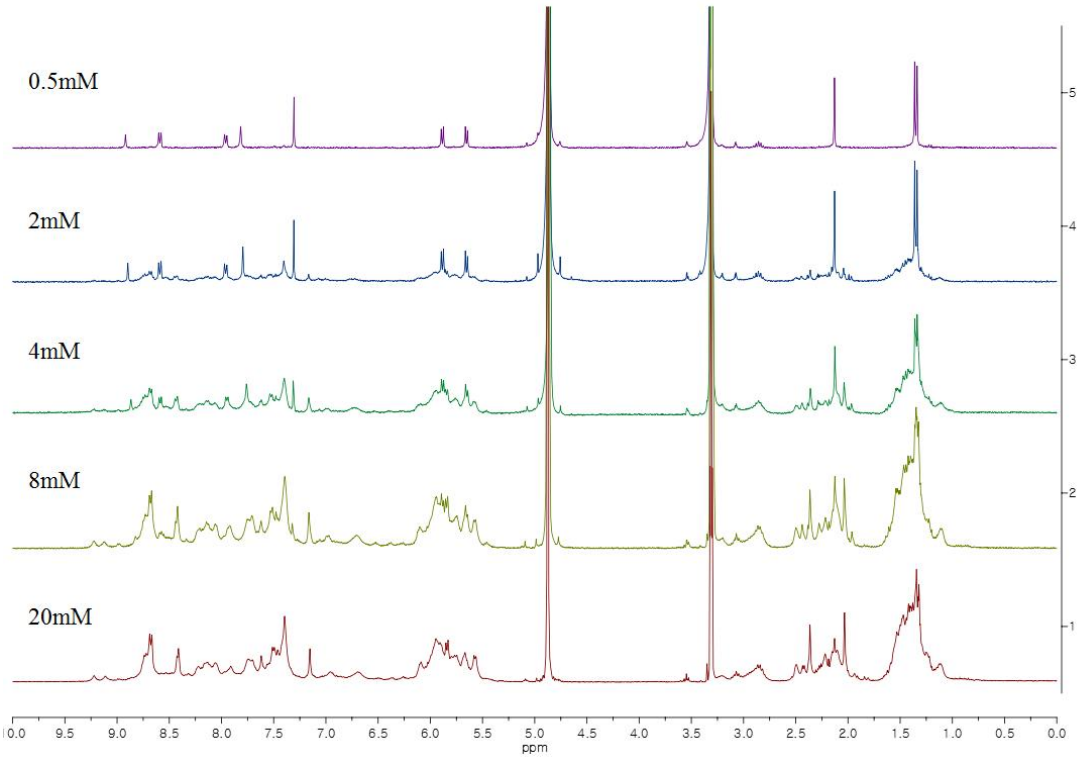

Figure 3.18 ^{1}H NMR spectra showing increasing of proportion of **7** upon sequentially increasing the concentration from 0.5 mM to 20 mM (CD_3OD, 300 MHz).

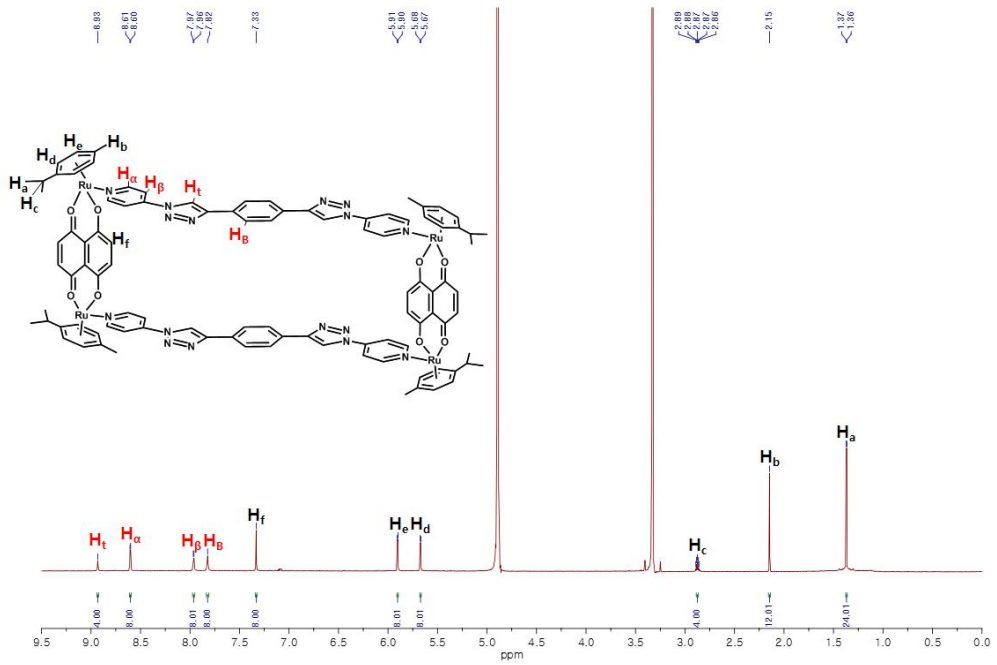

Figure 3.19 ^{1}H NMR spectrum of **6** (CD_3OD [0.5 mM], 900 MHz)

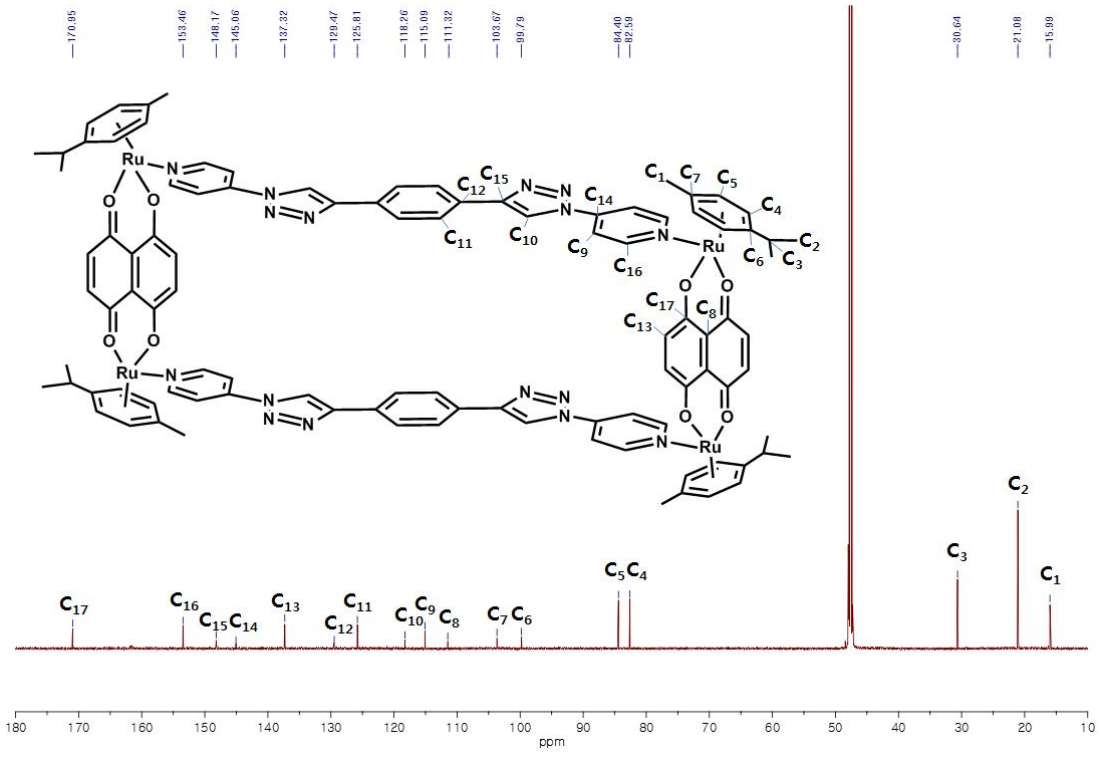

Figure 3.20 ^{13}C NMR spectrum of **6** (CD_3OD [0.5 mM], 225 MHz)

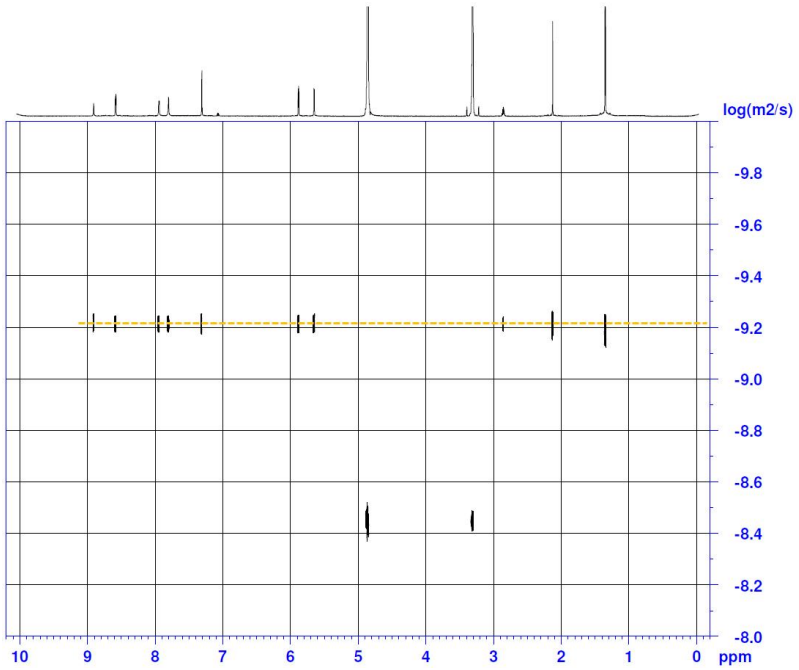

Figure 3.21 ^{1}H-DOSY NMR spectrum of **6** (CD_3OD [0.5 mM], 298 K, 800 MHz)

Diffusion coefficient: 6.1×10^{-10} m^2/sec

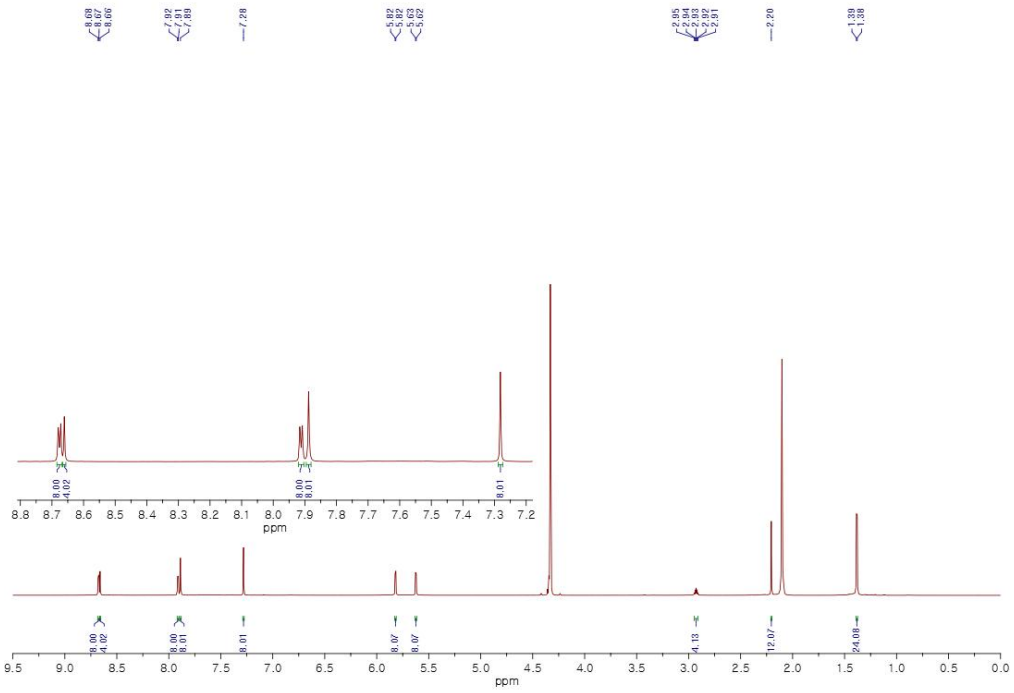

Figure 3.22 ^{1}H NMR spectrum of **6** (CD_3NO_2 [8.0 mM], 900 MHz)

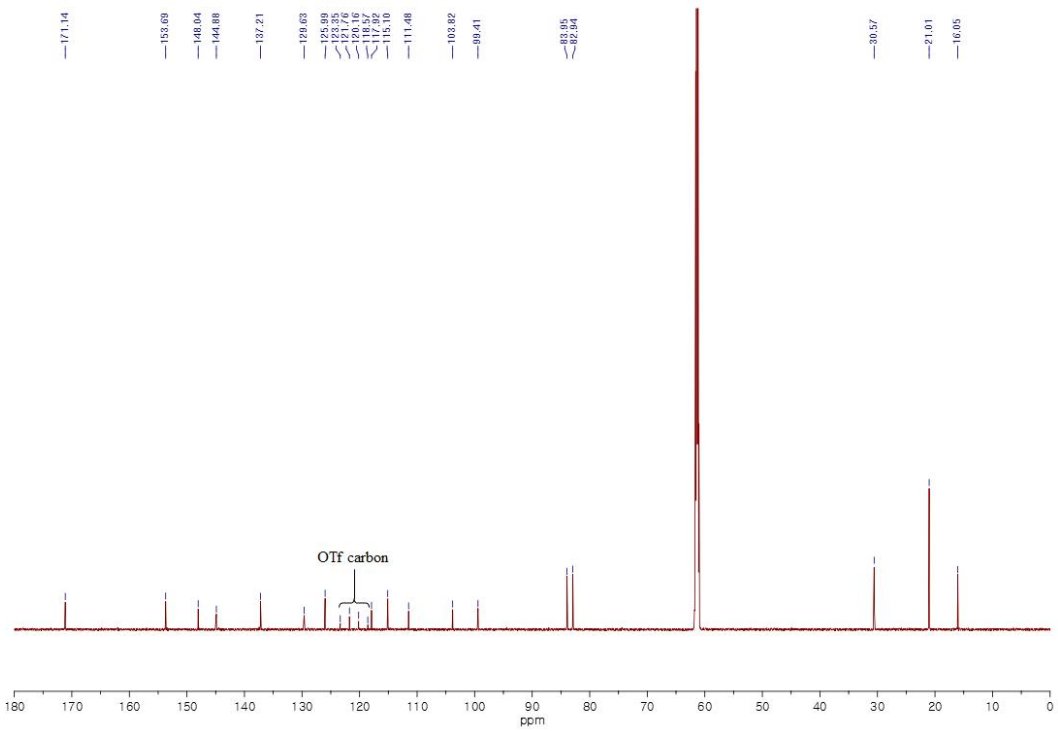

Figure 3.23 ^{13}C NMR spectrum of **6** (CD_3NO_2 [8.0 mM], 225 MHz)

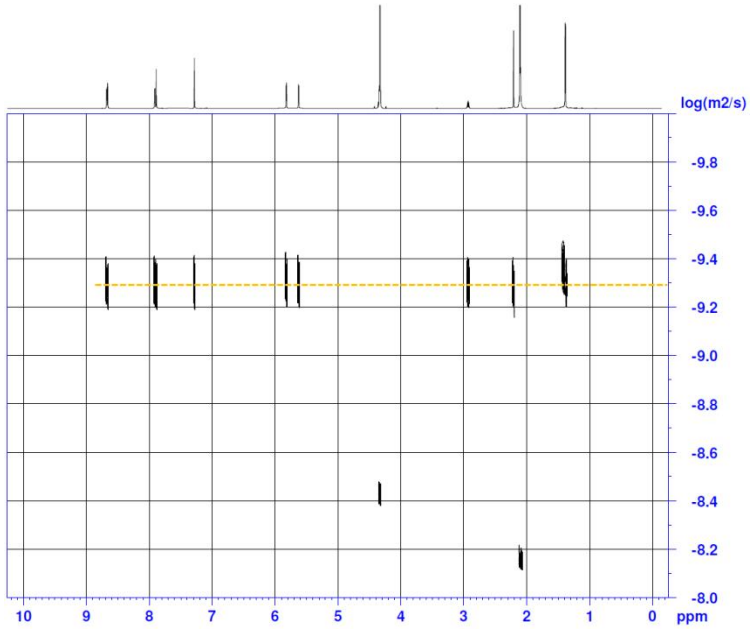

Figure 3.24 ^{1}H-DOSY NMR spectrum of **6** (CD_3NO_2 [8.0 mM], 298 K, 800 MHz)

Diffusion coefficient: 5.1×10^{-10} m^2/sec

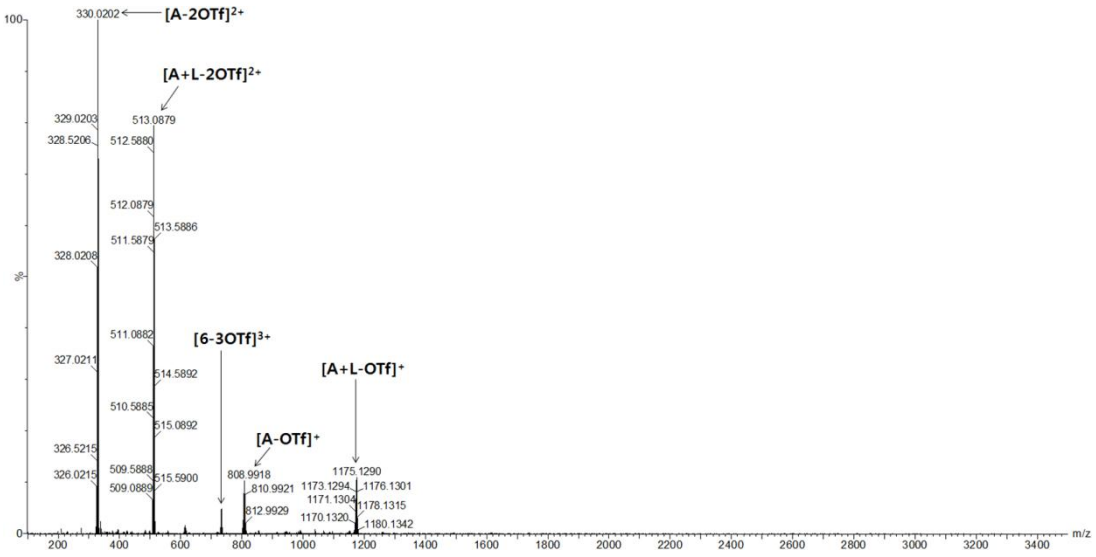

Figure 3.25 Full ESI mass spectrum of **6**. (Reaction in CD_3OD [0.5 mM])

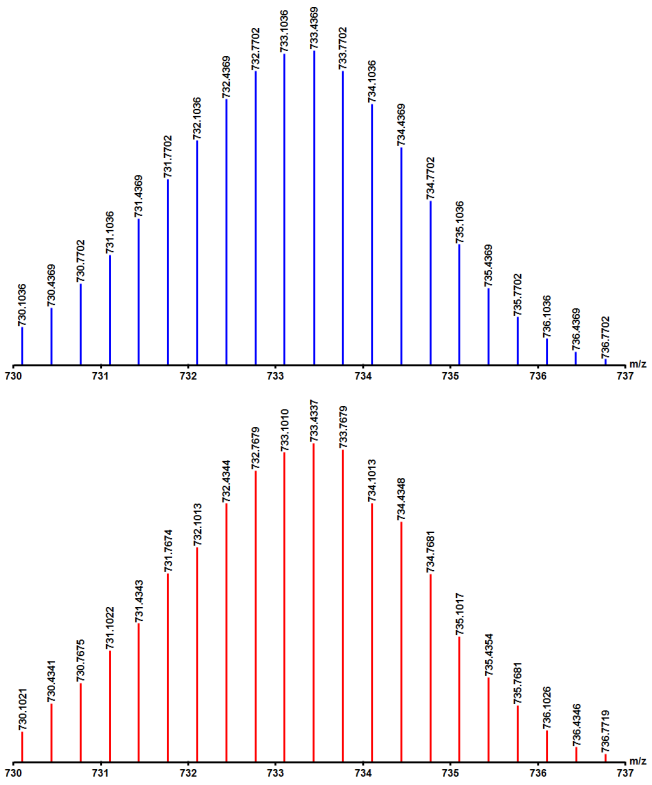

Figure 3.26 Calculated (blue) and experimental (red) ESI mass spectra of [**6**-3OTf]$^{3+}$.

(Reaction in CD_3OD [0.5 mM])

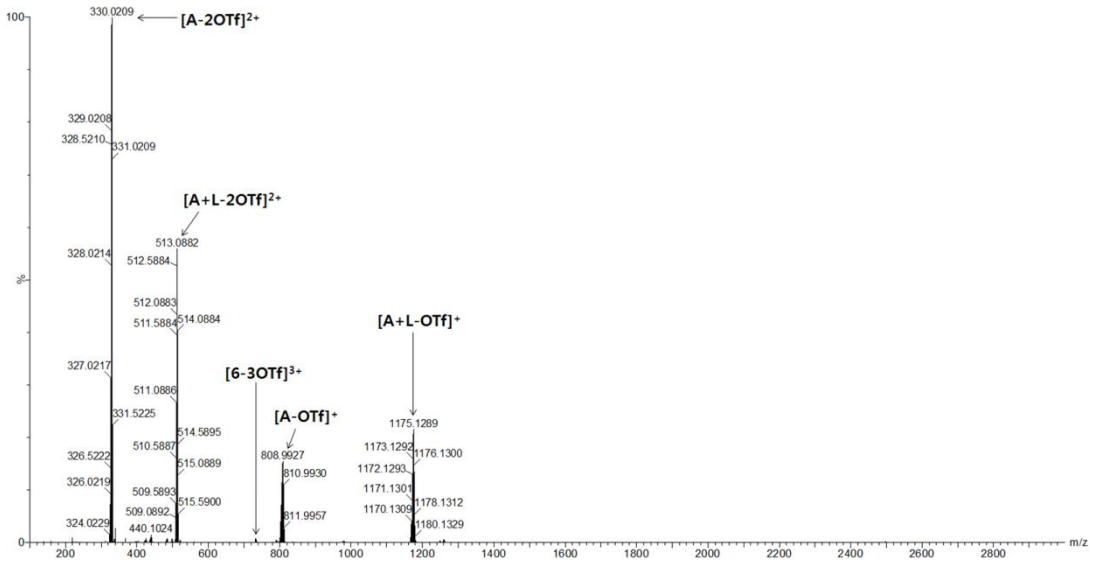

Figure 3.27 Full ESI mass spectrum of **6**. (Reaction in CD_3NO_2 [8.0 mM])

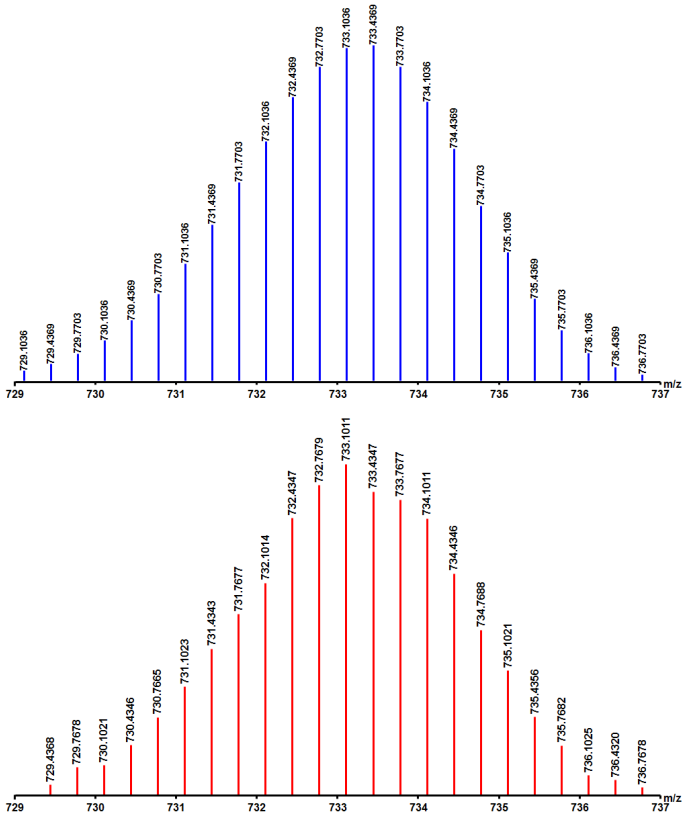

Figure 3.28 Calculated (blue) and experimental (red) ESI mass spectra of [**6**-3OTf]$^{3+}$

(Reaction in CD_3NO_2 [8.0 mM])

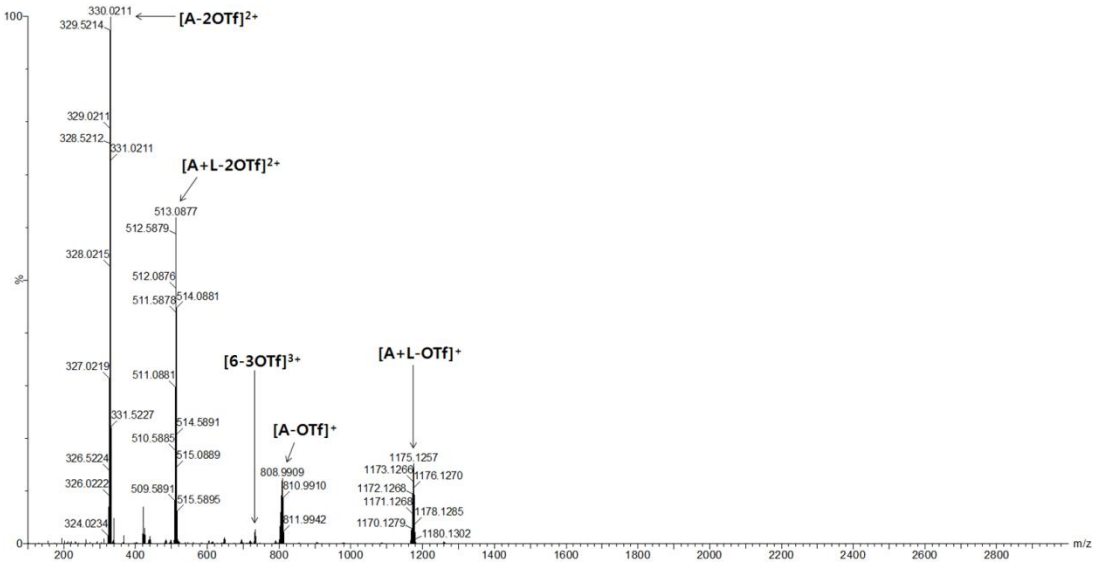

Figure 3.29 Full ESI mass spectrum of **6** (Reaction was carried out in the presence of pyrene [2.0 eq] in CD_3OD [8.0 mM])

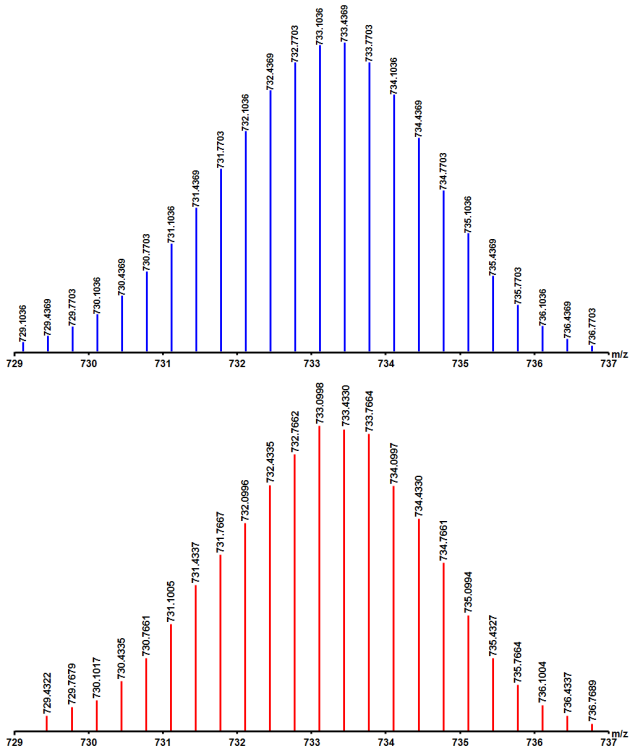

Figure 3.30 Calculated (blue) and experimental (red) ESI mass spectra of [**6**-3OTf]$^{3+}$

(Reaction was carried out in the presence of pyrene [2.0 eq] in CD_3OD [8.0 mM]

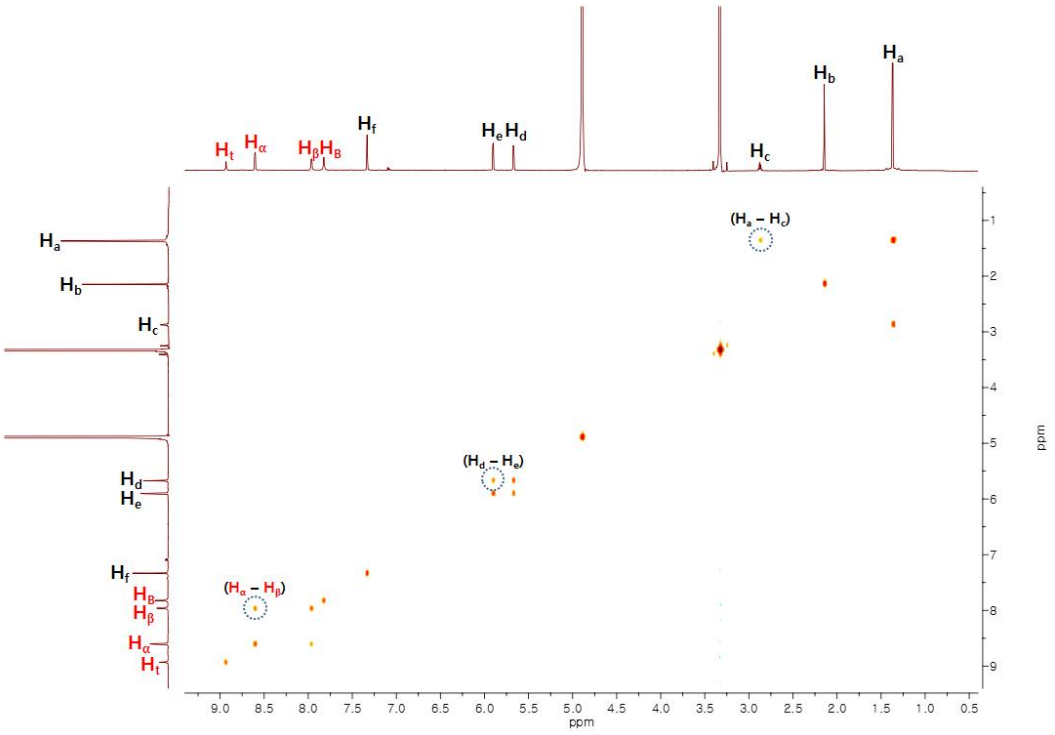

Figure 3.31 ^{1}H-^{1}H COSY NMR spectrum of **6** (CD_3OD [0.5 mM], 298 K, 900 MHz)

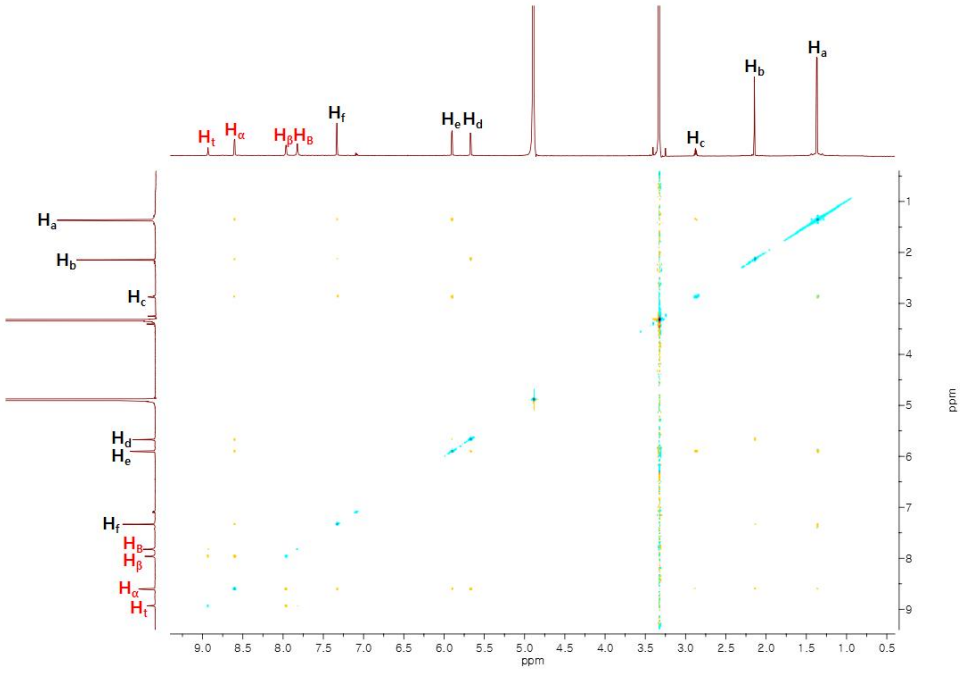

Figure 3.32 ^{1}H-^{1}H ROESY NMR spectrum of **6** (CD_3OD [0.5 mM], 298 K, 900 MHz)

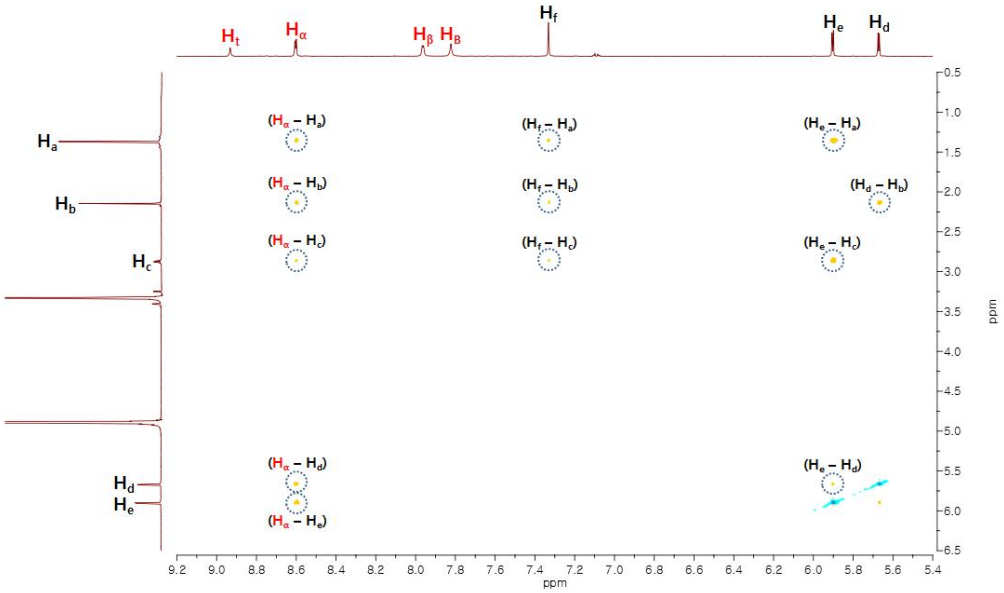

Figure 3.33 Expanded ^{1}H-^{1}H ROESY NMR spectrum of **6** (CD_3OD [0.5 mM], 298 K, 900 MHz)

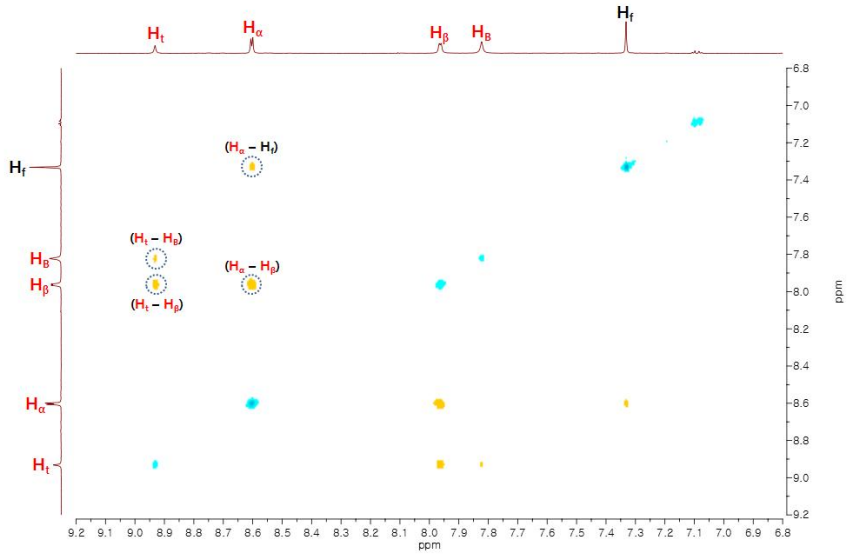

Figure 3.34 Expanded ^{1}H-^{1}H ROESY NMR spectrum of **6** (CD_3OD [0.5 mM], 298 K, 900 MHz)

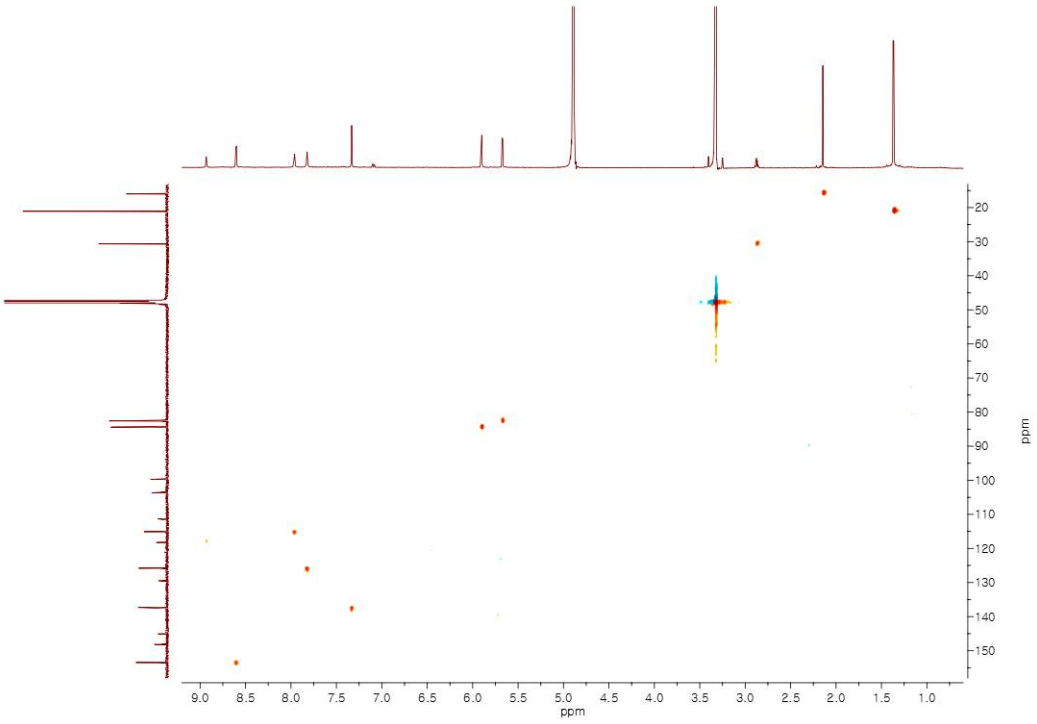

Figure 3.35 ^{1}H-^{13}C HSQC NMR spectrum of **6** (CD_3OD [0.5 mM], 298 K, 900 MHz)

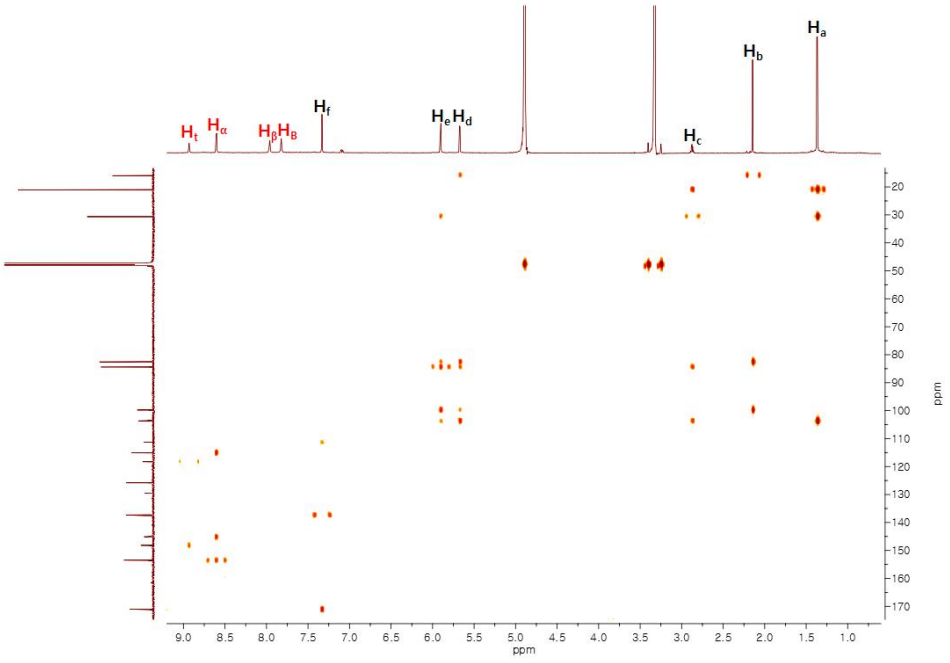

Figure 3.36 ^{1}H-^{13}C HMBC NMR spectrum of **6** (CD_3OD [0.5 mM], 298 K, 900 MHz)

In contrast to the ^{1}H NMR spectrum of monorectangle **6** at 0.5mM, all protons of donor and acceptor moieties of **7** at 20mM resonated at significantly different chemical shifts, and the spectrum by itself proved too complicated to interpret. (Figures 3.13a and 3.13b) Therefore, single-crystal X-ray diffraction analysis was used to elucidate the topology of **7**. (Figure 3.37) A single crystal of **7** suitable for X-ray analysis was obtained by slow vapor diffusion of diethyl ether into a solution of **7** in methanol at room temperature. The crystal structure of **7** was refined in the Cc space group, and the interlocking of one ring in other two parallel rings (*C*2-symmetry) was observed to form a linear [3]catenane. (Figure 3.37b) Detail structural analysis highlighted the presence of multiple π—π interactions between donors (triazole and phenyl) and CH—π interactions between donor and acceptor (phenyl and naphthalene) moieties. Strong sandwich-type π—π interactions between triazole-triazole and triazole-phenyl moieties lead to the preorganization of rings and stacking distances ranging from 3.3 to 3.9 Å. (Figure 3.38a) As was expected for CH—π interactions, distances between acceptor naphthalene and donor phenyl moieties were observed in the range 3.6 to 4.2 Å. (Figure 3.38b)

Surprisingly, two π-stacked rings (red and green, Figure 3.38c) were also engaged in CH—N interactions; distances between these parallel rings ranged from 2.1 to 2.7 Å. (Figure 3.38c) These serendipitous CH—N interactions provided framework stability by locking the two rings parallel to each other.

Based on results obtained by detailed 2D NMR analysis (DOSY, COSY, ROSEY, HSQC and HMBC) in methanol, all peaks in ^{1}H NMR spectrum of **7** at 20mM were successfully assigned. (Figures 3.39-3.46) To understand the role of the π—π interaction in the formation of the topology of **7**, two equivalents of π-electron rich pyrene were added before and after the self-assembly reactions (4.0mM) in methanol. This addition of pyrene prevented the formation of linear [3]catenane **7**. (Scheme 3.1, Figure 3.47) Similarly, ^{1}H NMR titration clearly showed the gradual transformation of linear [3]catenane **7** into monorectangle **8** upon increasing the equivalence of pyrene. (Figure 3.48)

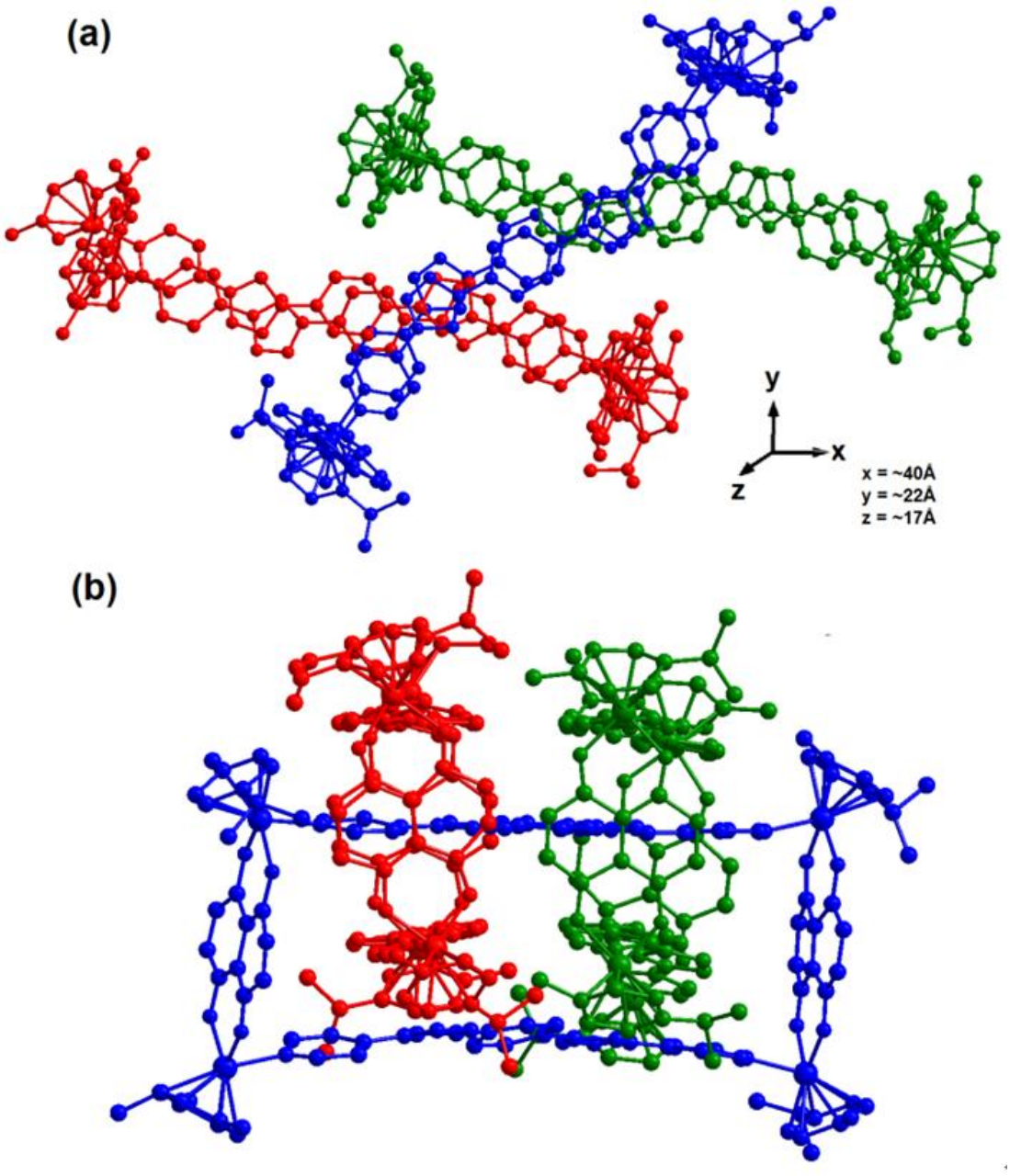

Figure 3.37 Crystal structure of linear [3]catenane **7** (a) top view (b) side view

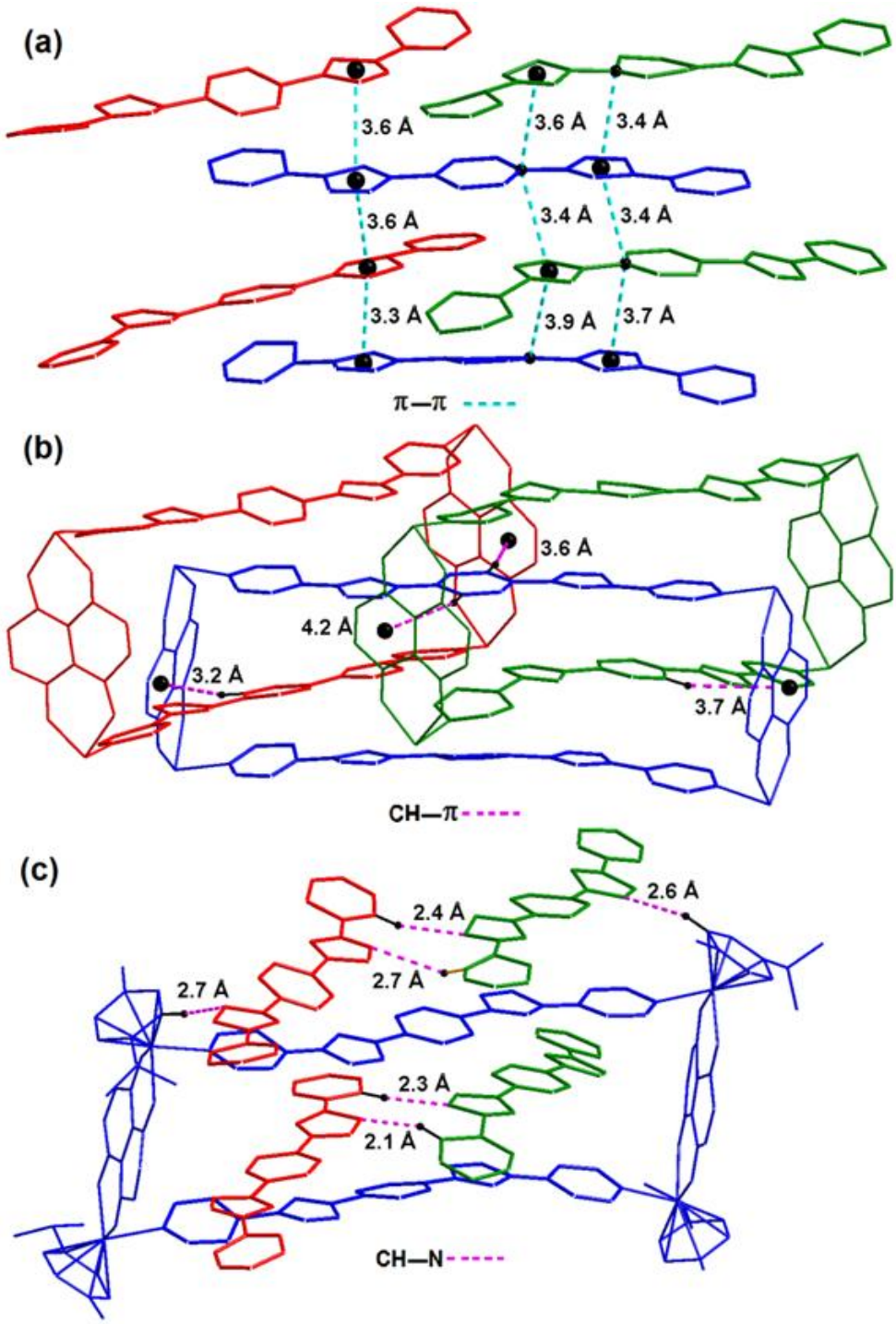

Figure 3.38 Diagram showing important intercycler interactions of **7**. (a) π—π stacking (b) CH—π interactions and (c) CH—N interactions (Figures are generated from the crystal structure of **7**).

Table 3.1 X-ray crystal structure parameters of **7**

Empirical formula	C104 H120.33 F8 N16 O20.50 Ru4 S2.67	
Formula weight	2564.26	
Temperature	100(2) K	
Wavelength	0.700 Å	
Crystal system	Monoclinic	
Space group	Cc	
Unit cell dimensions	a = 28.000(6) Å	□ = 90°
	b = 48.956(10) Å	□ = 105.96(3)°
	c = 30.810(6) Å	□ = 90°
Volume	40605 (15) $Å^3$	
Z	12	
Density (calculated)	1.258 g/cm^3	
Absorption coefficient	0.522 mm^{-1}	
F(000)	15732	
Crystal size	0.200 × 0.200 × 0.100 mm^3	
Theta range for data collection	1.354 to 32.637°	
Index ranges	$-35 \le h \le 37$, $-62 \le k \le 65$, $-38 \le l \le 34$	
Reflections collected	107465	
Independent reflections	58400 [R(int) = 0.0296]	
Completeness to theta = 25.000°	80.0%	
Absorption correction	Empirical	
Max. and min. transmission	1.000 and 0.880	
Refinement method	Full-matrix-block least-squares on F^2	
Data / restraints / parameters	58400 / 2505 / 4116	
Goodness-of-fit on F^2	1.082	
Final R indices [I>2sigma(I)]	R_1 = 0.1086, wR_2 = 0.2818	
R indices (all data)	R_1 = 0.1521, wR_2 = 0.3209	
Absolute structure parameter	0.80(4)	
Largest diff. peak and hole	0.875 and -0.512 $e.Å^{-3}$	

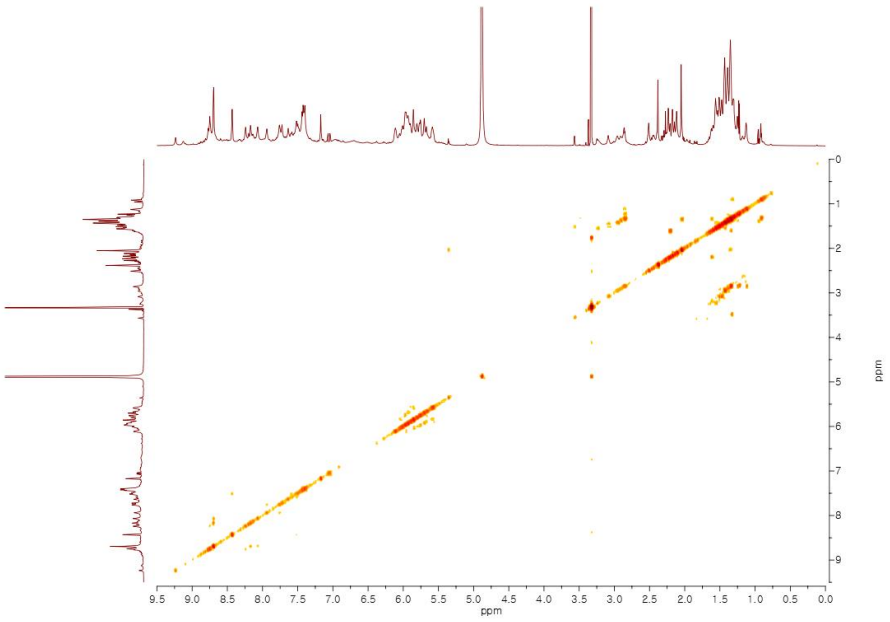

Figure 3.39 ^{1}H-^{1}H COSY NMR spectrum of **7** (CD_3OD [20 mM], 298 K, 900 MHz)

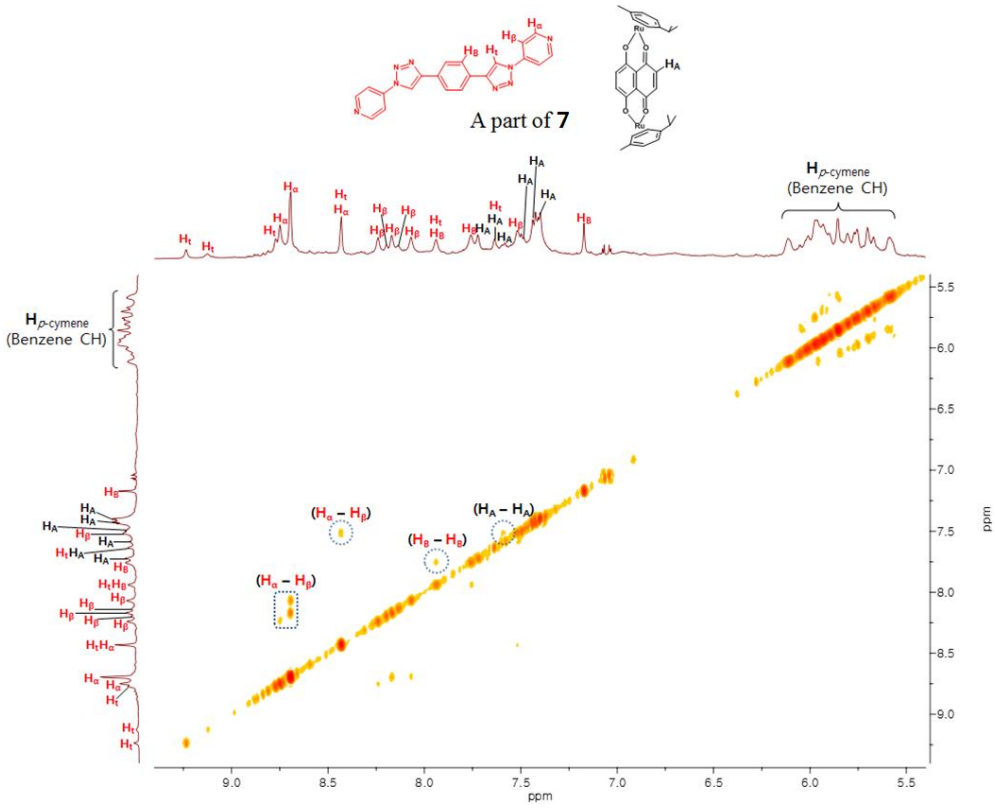

Figure 3.40 Expanded ^{1}H-^{1}H COSY NMR spectrum of **7** (CD_3OD [20 mM], 298 K, 900 MHz)

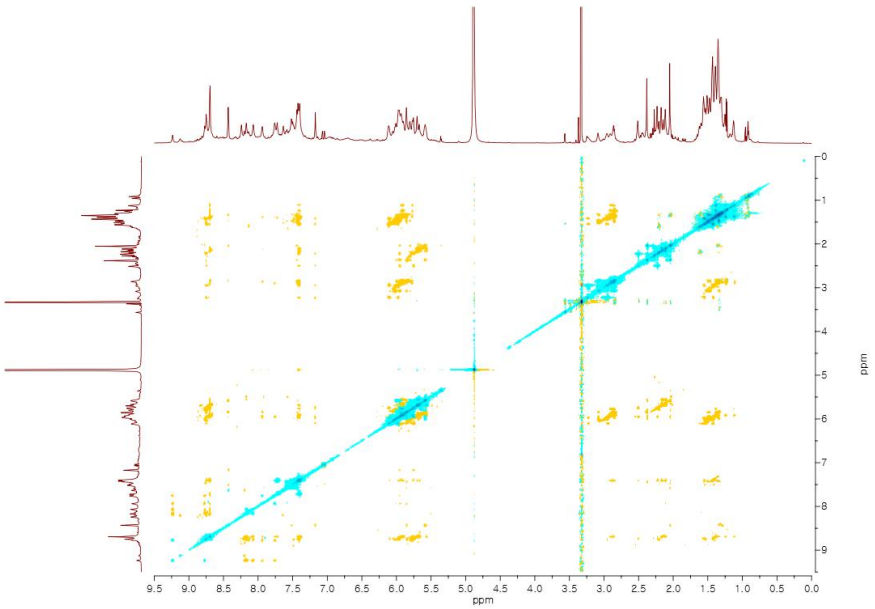

Figure 3.41 ^{1}H-^{1}H ROESY NMR spectrum of **7** (CD_3OD [20 mM], 298 K, 900 MHz)

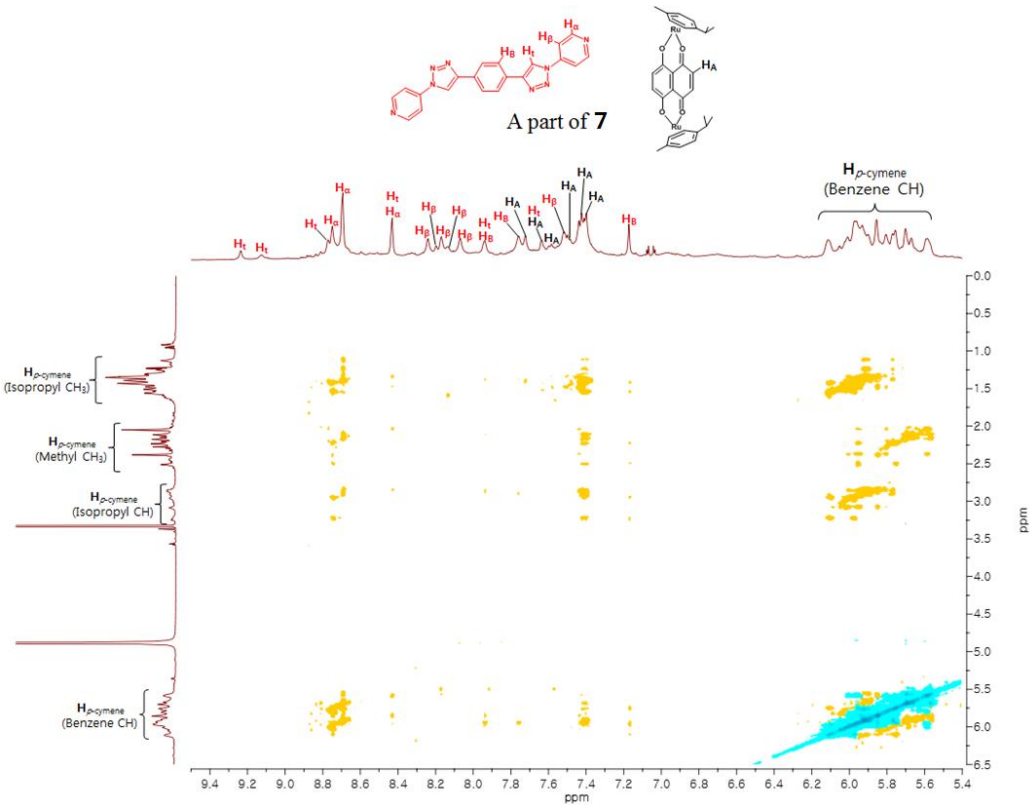

Figure 3.42 Expanded ^{1}H-^{1}H ROESY NMR spectrum of **7** (CD_3OD [20 mM], 298 K, 900 MHz)

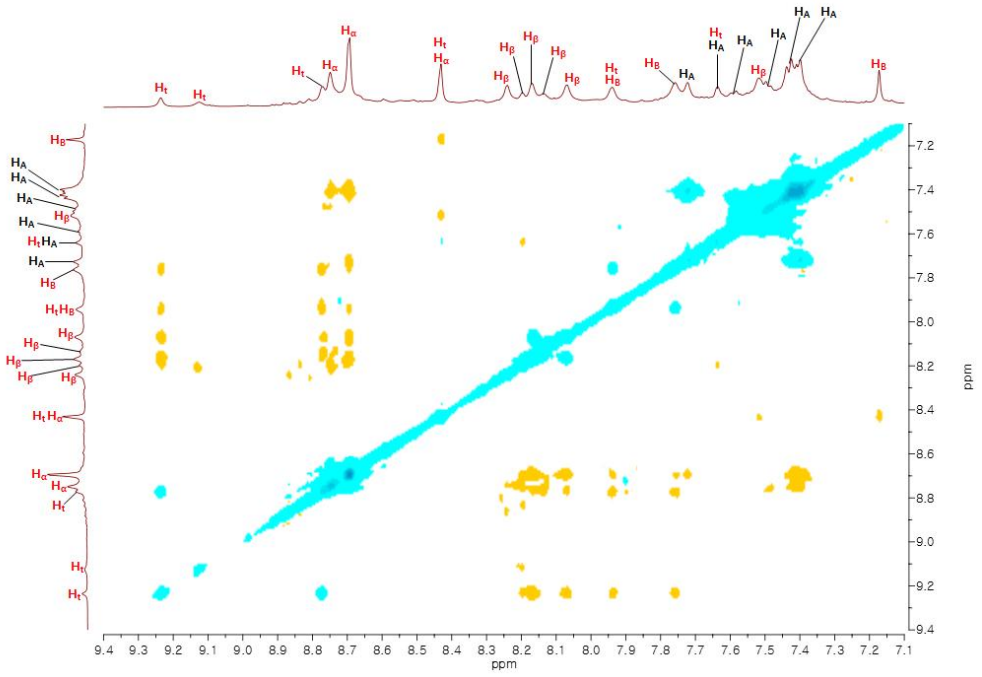

Figure 3.43 Expanded ^{1}H-^{1}H ROESY NMR spectrum of **7** (CD_3OD [20 mM], 298 K, 900 MHz)

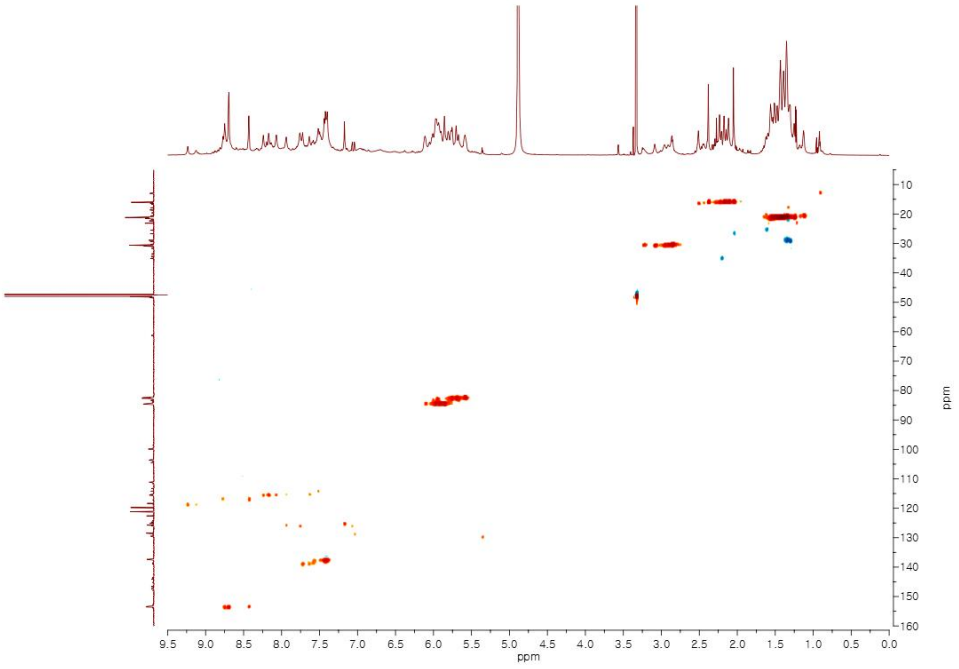

Figure 3.44 ^{1}H-^{13}C HSQC NMR spectrum of **7** (CD_3OD [20 mM], 298 K, 900 MHz)

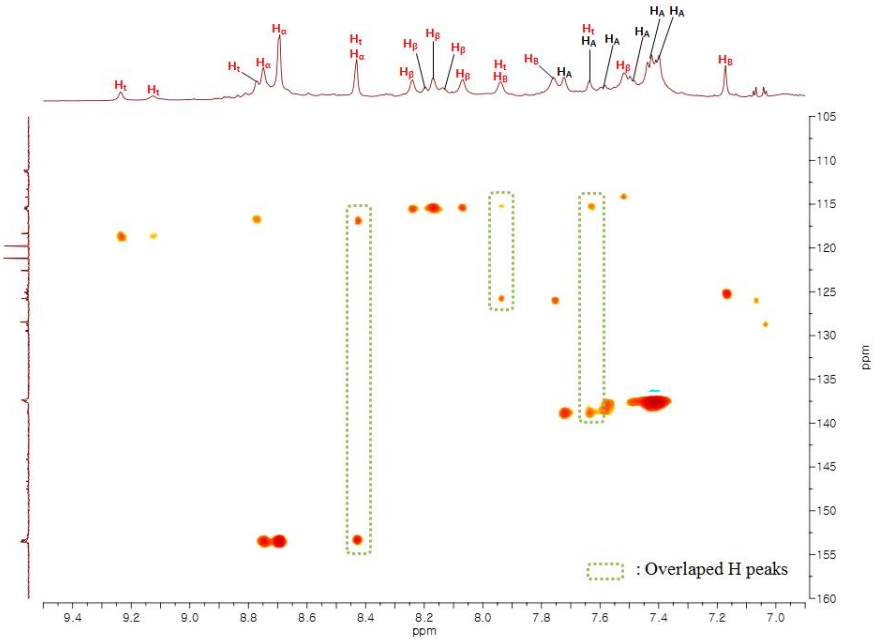

Figure 3.45 Expanded ^{1}H-^{13}C HSQC NMR spectrum of **7** (CD_3OD [20 mM], 298 K, 900 MHz)

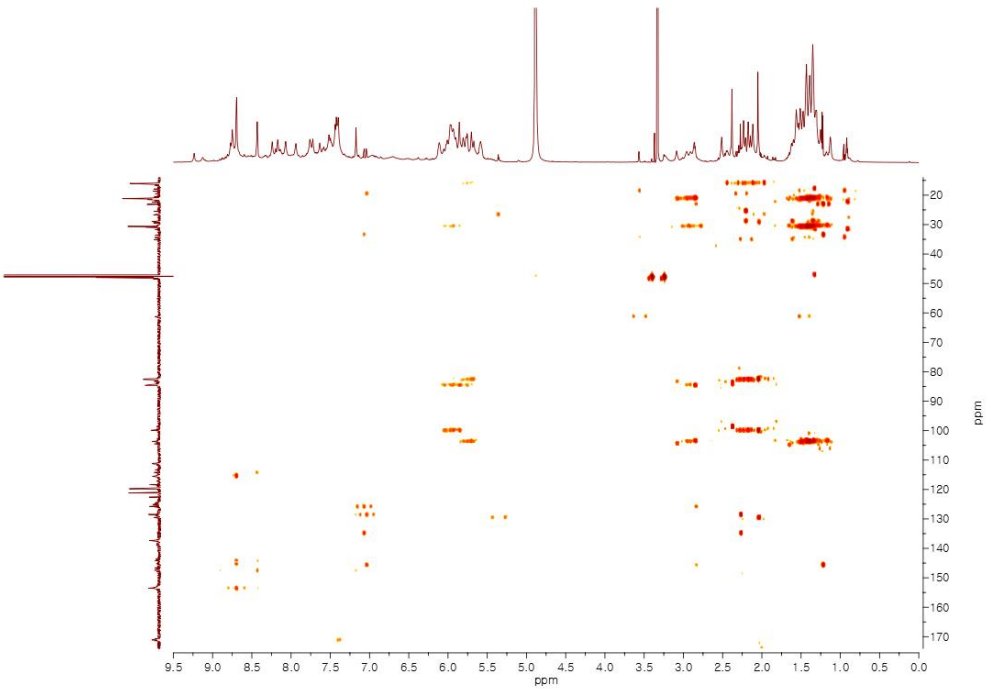

Figure 3.46 ^{1}H-^{13}C HMBC NMR spectrum of **7** (CD_3OD [20 mM], 298 K, 900 MHz)

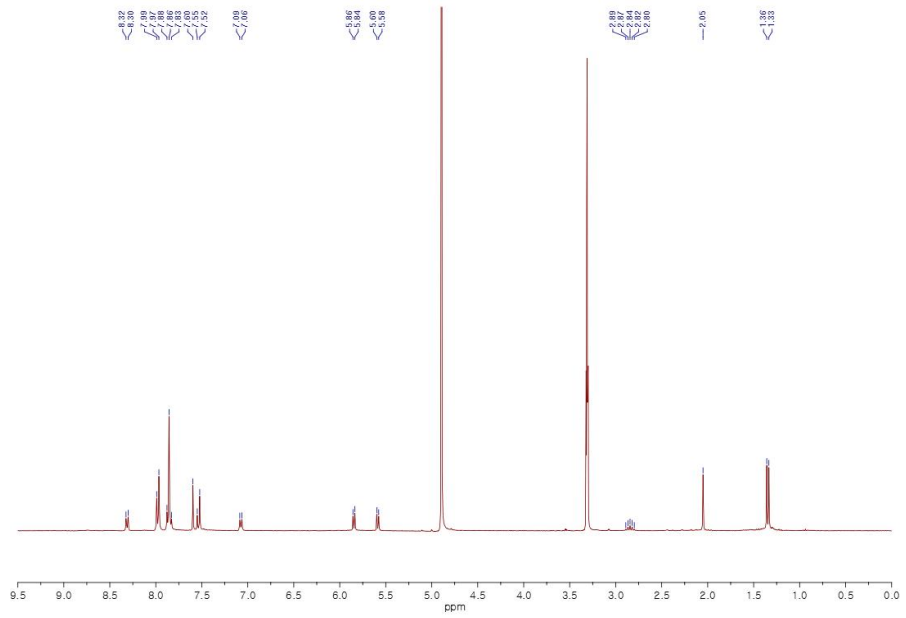

Figure 3.47 ^{1}H NMR spectrum showing formation of only **6** when reaction was carried out in the presence of pyrene (2.0 eq) (CD_3OD [4.0 mM], 300 MHz)

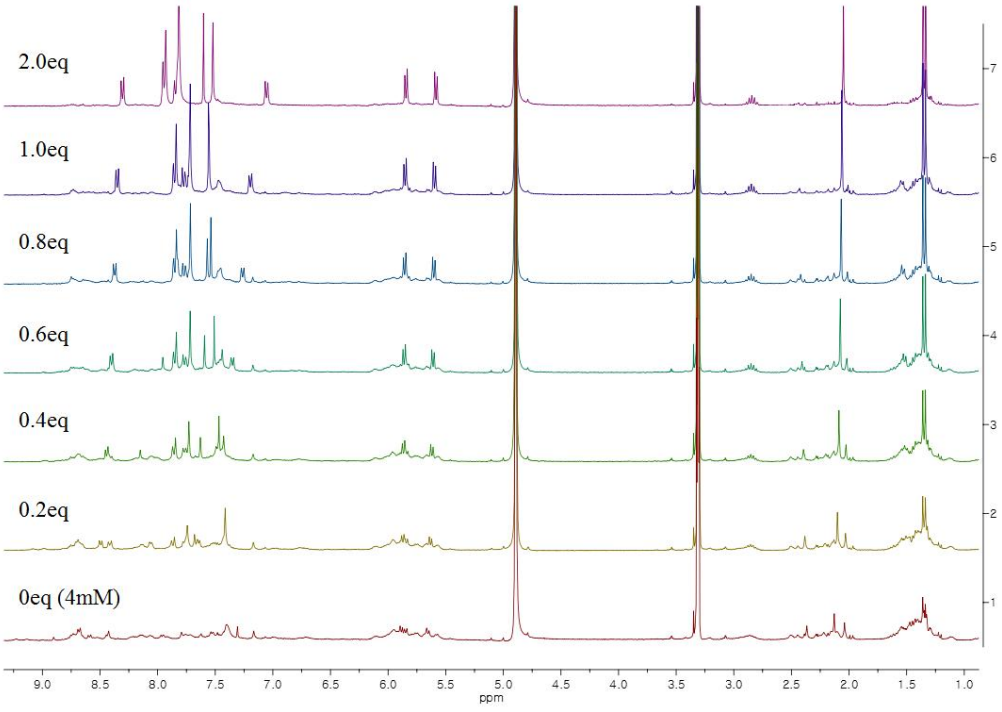

Figure 3.48 ^{1}H NMR spectra of mixture **6+7** showing increasing proportion of monomeric macrocycle **6** upon addition of pyrene from 0 eq to 2.0 eq (CD_3OD [4.0 mM], 300 MHz)

3.3.2. Synthesis and characterization of monorectangle 9, 10, 11 and 12

In order to further understand the role of intercycler interactions on the formation of [3]catenane, we attempted the self-assemblies of **A7** with **L3** or **L4** (both analogues of **L2**). (Scheme 3.2) These reactions resulted in the exclusive formations of [2+2] monorectangles **9** and **10**. The presence of steric hindrance around the triazole ring due to tetramethyl (**L3**) and anthracene (**L4**) moieties prevented ring interlocking. In addition, we also attempted the self-assembly of **A7** with alkyne-based (1,4-bis(4-pyridinylethynyl) benzene) donor **L5**, that is, a more linear dipyridyl donor without a triazole moiety, and this exclusively yielded [2+2] monorectangle **11**. NMR data and prominent ESI-MS peaks at m/z = 770.8080 [**9**-3OTf]$^{3+}$, 800.1202 [**10**-3OTf]$^{3+}$ and 676.0780 [**11**-3OTf]$^{3+}$, which agreed well with theoretical isotopic distributions, confirmed the formations of monorectangles **9**, **10** and **11**. (Figure 3.49-3.60) These results demonstrate that the presence of an appropriate functional group in ligands is important and the **L2** containing triazole group is optimal for the selective formation of a linear [3]catenane.

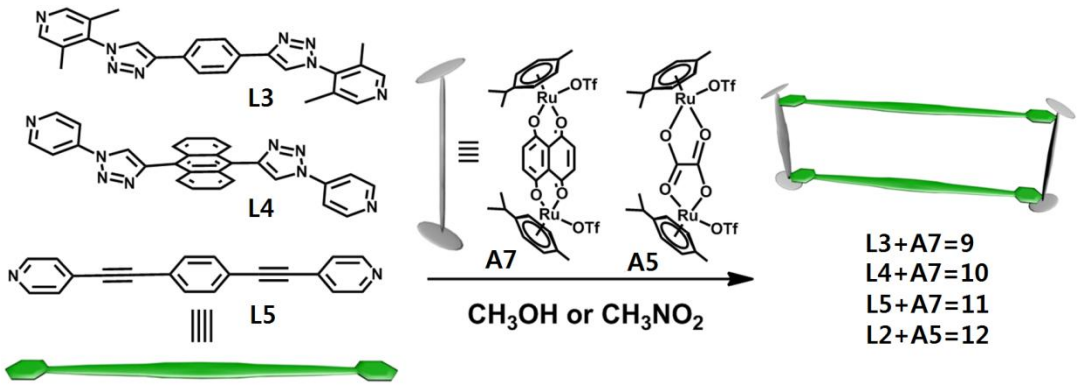

Scheme 3.2 Self-assemblies of donors **L2**-**L5** and acceptors **A7** and **A5**.

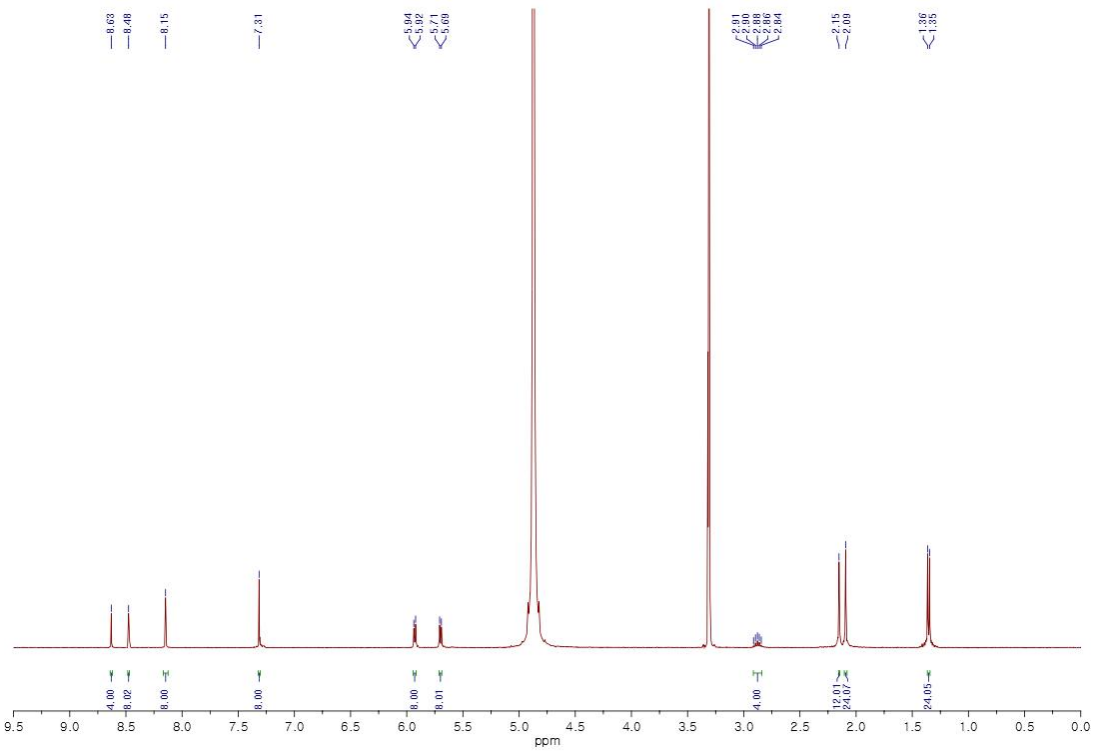

Figure 3.49 ^{1}H NMR spectrum of **9** (CD_3OD [8.0 mM], 400 MHz)

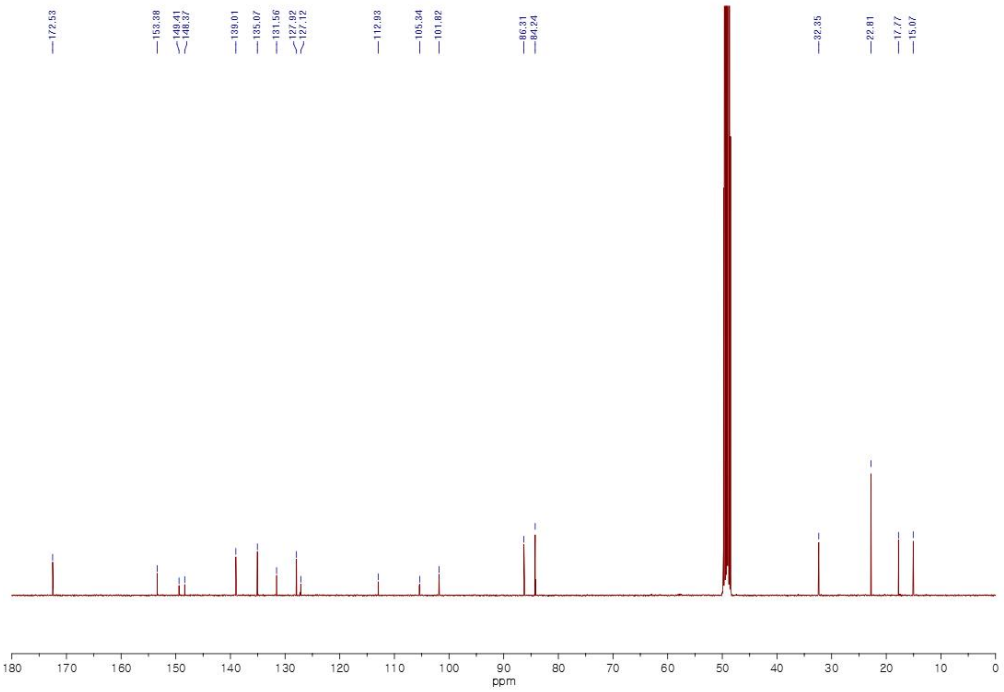

Figure 3.50 ^{13}C NMR spectrum of **9** (CD_3OD [8.0 mM], 100 MHz)

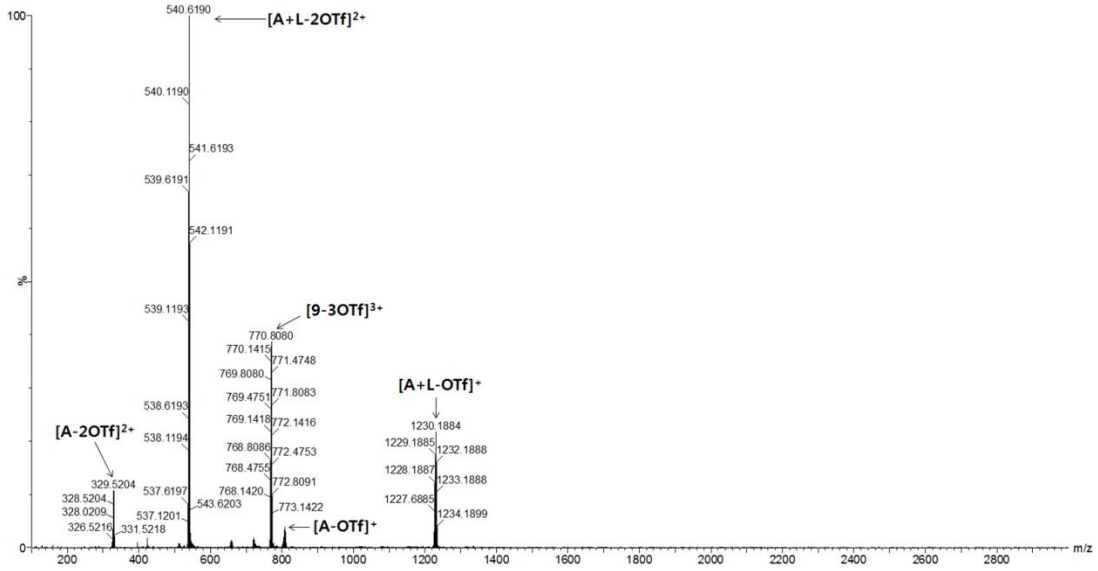

Figure 3.51 Full ESI mass spectrum of **9**

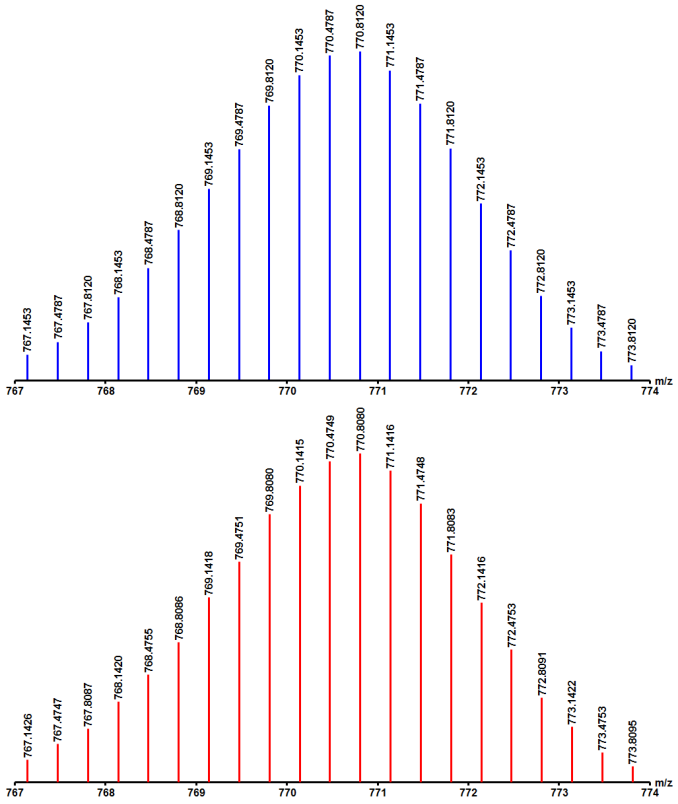

Figure 3.52 Calculated (blue) and experimental (red) ESI mass spectra of [**9**-3OTf]$^{3+}$ (Reaction in CD_3OD [8.0 mM])

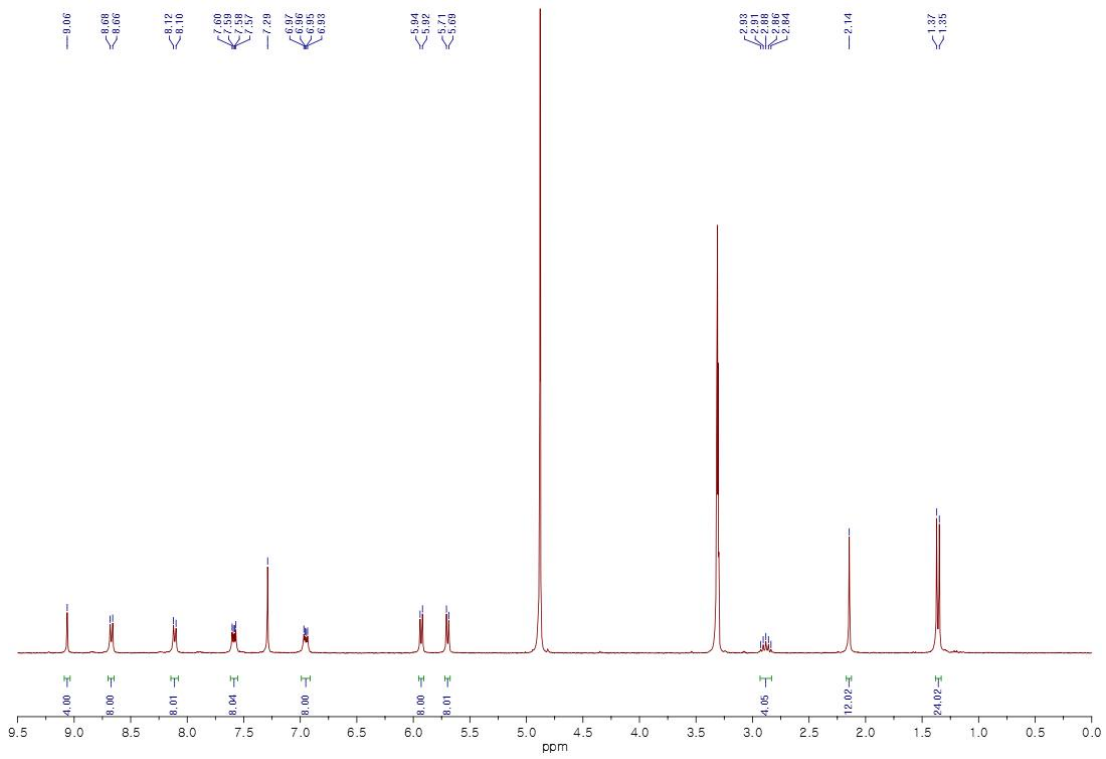

Figure 3.53 ^{1}H NMR spectrum of **10** (CD_3OD [8.0 mM], 300 MHz)

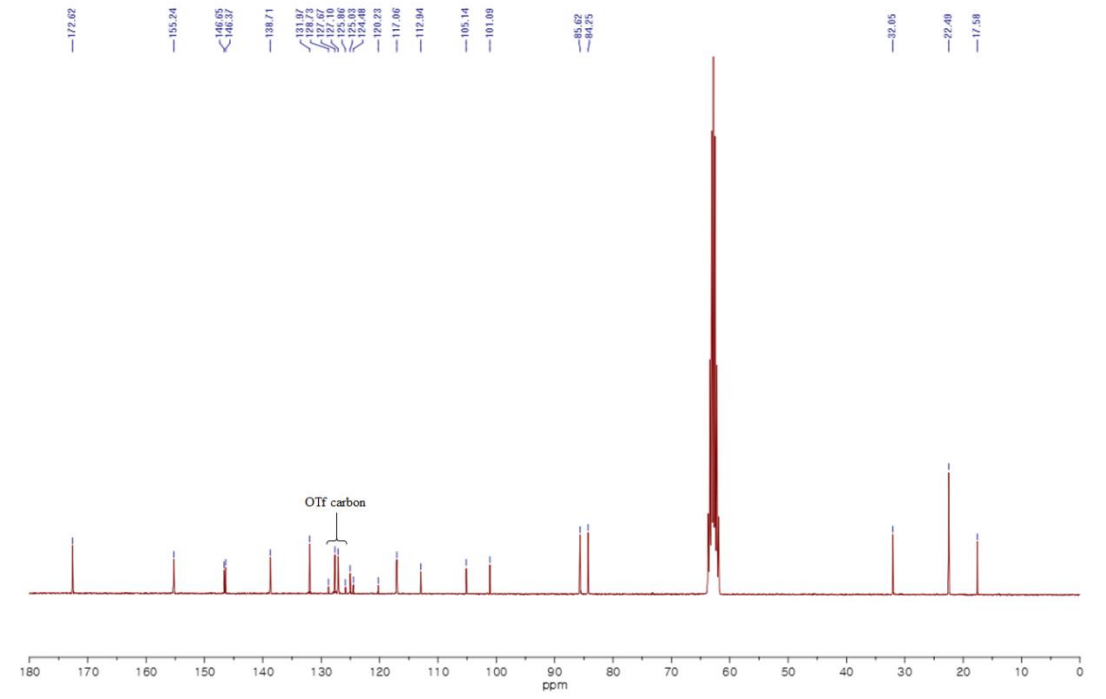

Figure 3.54 ^{13}C NMR spectrum of **10** (CD_3NO_2 [8.0 mM], 75 MHz)

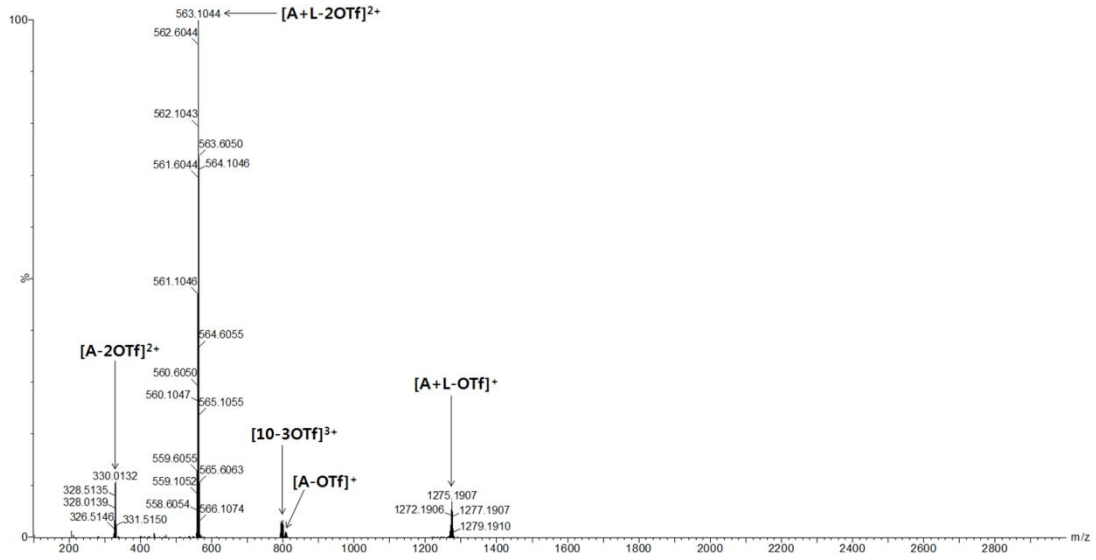

Figure 3.54 Full ESI mass spectrum of **10**

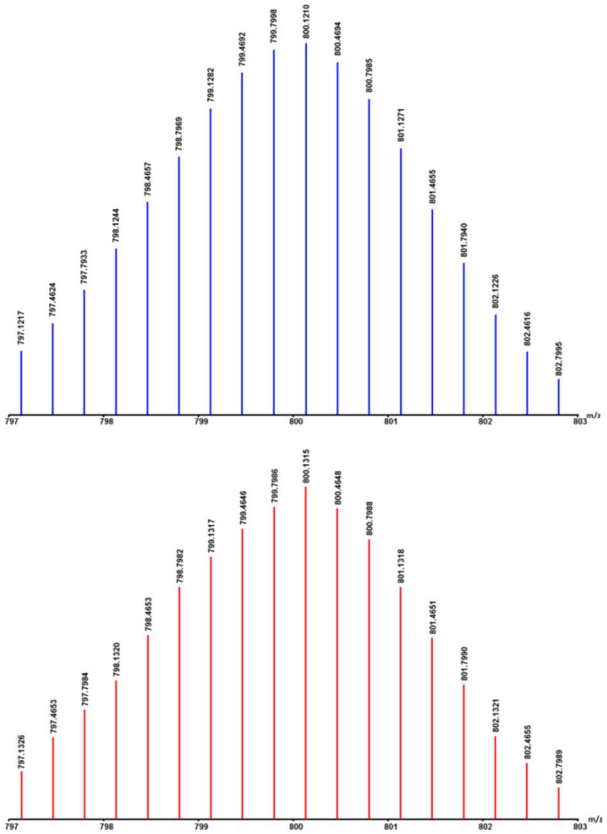

Figure 3.56 Calculated (blue) and experimental (red) ESI mass spectra of [**10**-3OTf]$^{3+}$. (Reaction in CD_3OD [8.0 mM])

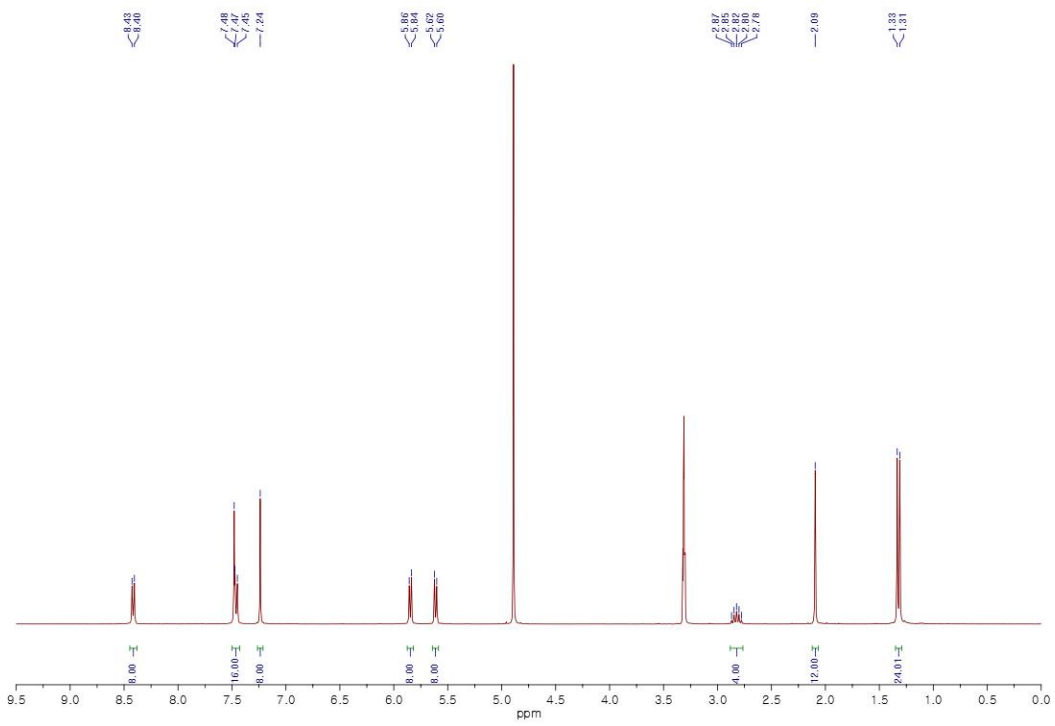

Figure 3.57 ^{1}H NMR spectrum of **11** (CD_3OD [8.0 mM], 400 MHz)

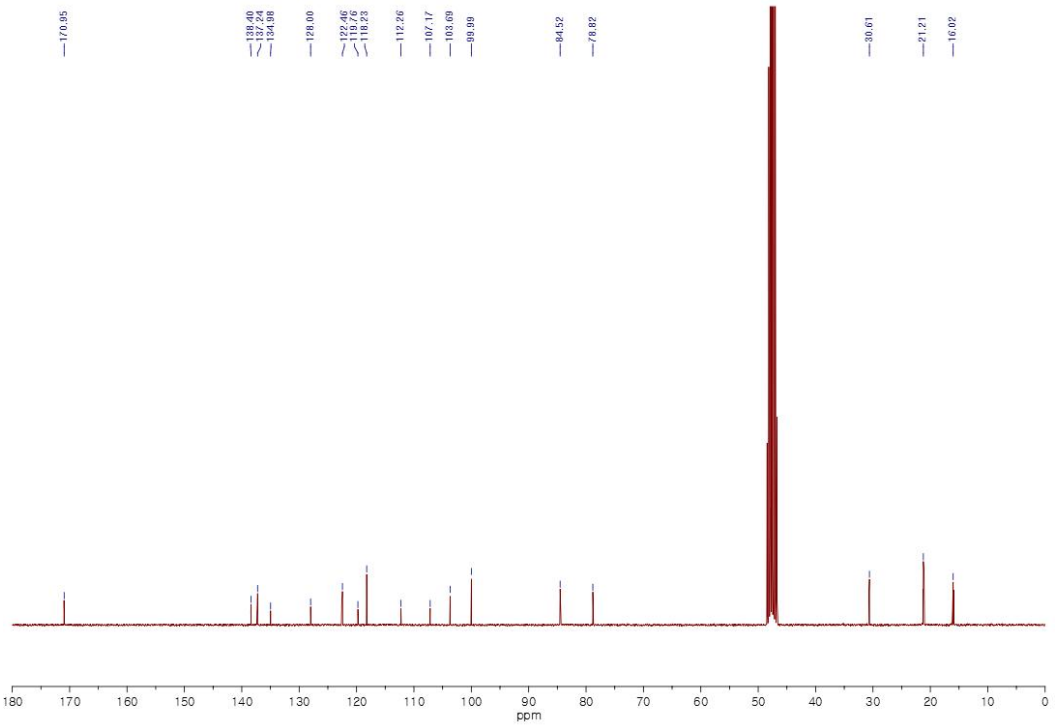

Figure 3.58 ^{13}C NMR spectrum of **11** (CD_3OD [8.0 mM], 100 MHz)

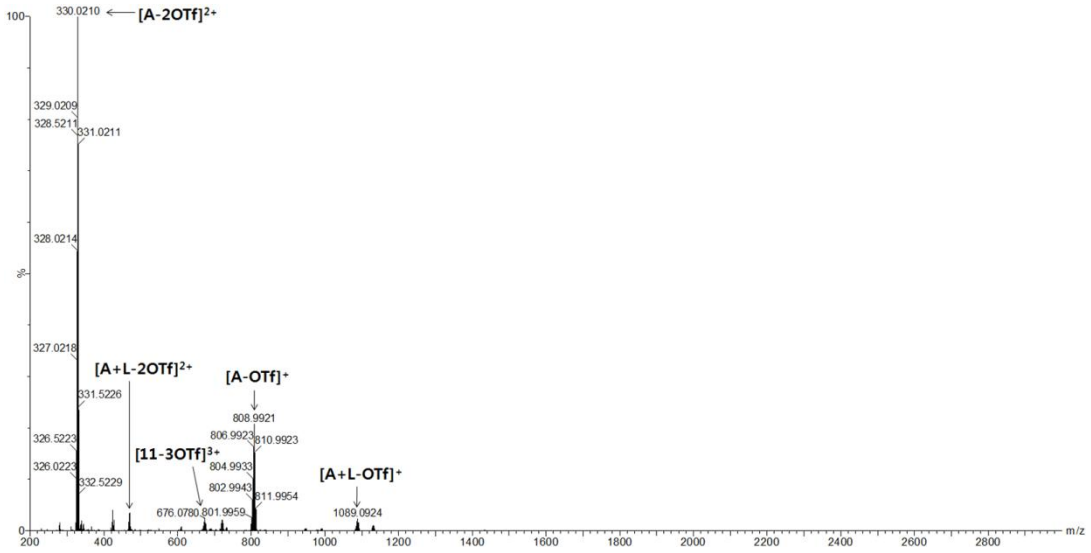

Figure 3.59 Full ESI mass spectrum of **11**

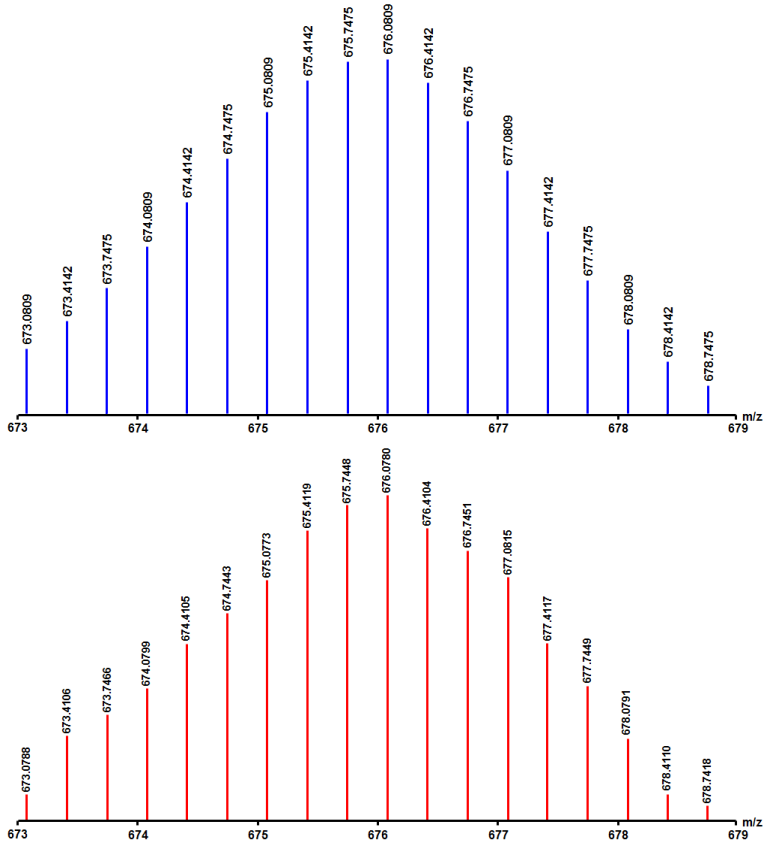

Figure 3.60 Calculated (blue) and experimental (red) ESI mass spectra of [**11**-3OTf]$^{3+}$. (Reaction in CD_3OD [8.0 mM])

We also carried out self-assembly reactions between donor **L2** and other Ru(II) acceptors [(p-cymene)$_2$Ru$_2$(OO∩OO)(OTf)$_2$ [OO∩OO = oxalate, 2,5-Dihydroxy-1,4-benzoquinone (benzene), and 6,11-Dihydroxy-5,12-naphtha-cenedione (tetracene)]. As was expected, self-assembly of **L2** with the shorter oxalate acceptor **A5** produced only [2+2] monorectangle **12**. (Scheme 3.2 and Figures 3.61-3.64) On the other hand, self-assembly reactions between **L2** and benzene and tetracene acceptors did not produce any specific topology as evidenced by ESI-MS, which showed the presence of multiple products.

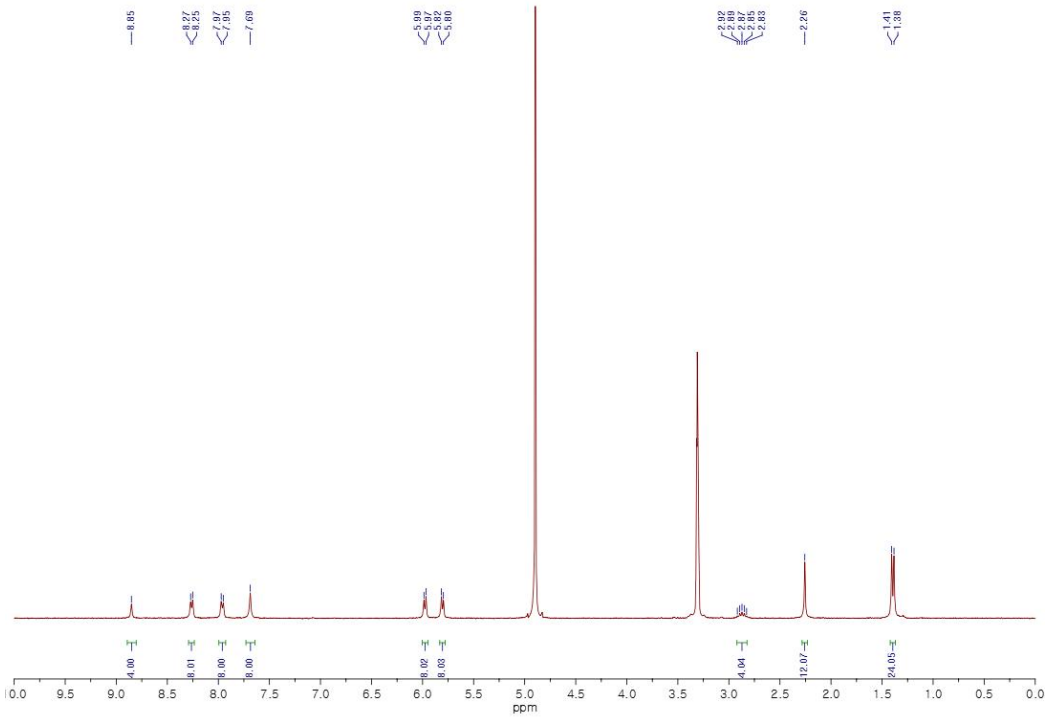

Figure 3.61 ^{1}H NMR spectra of **12** (CD_3OD [8.0 mM], 300 MHz)

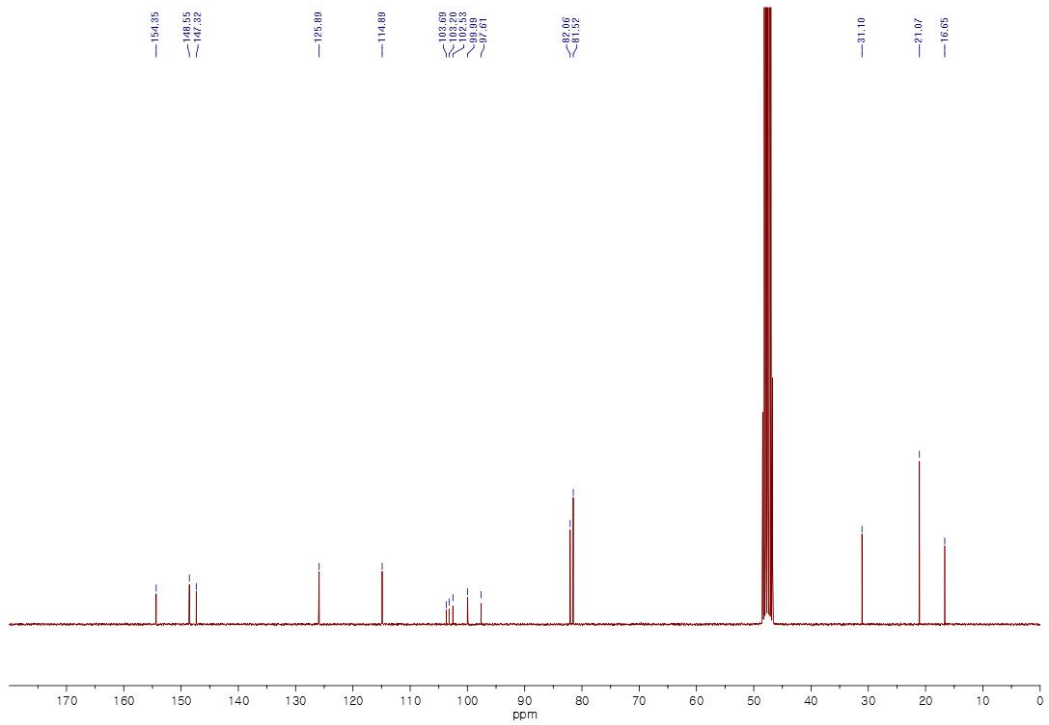

Figure 3.62 ^{13}C NMR spectra of **12** (CD_3OD [8.0 mM], 75 MHz)

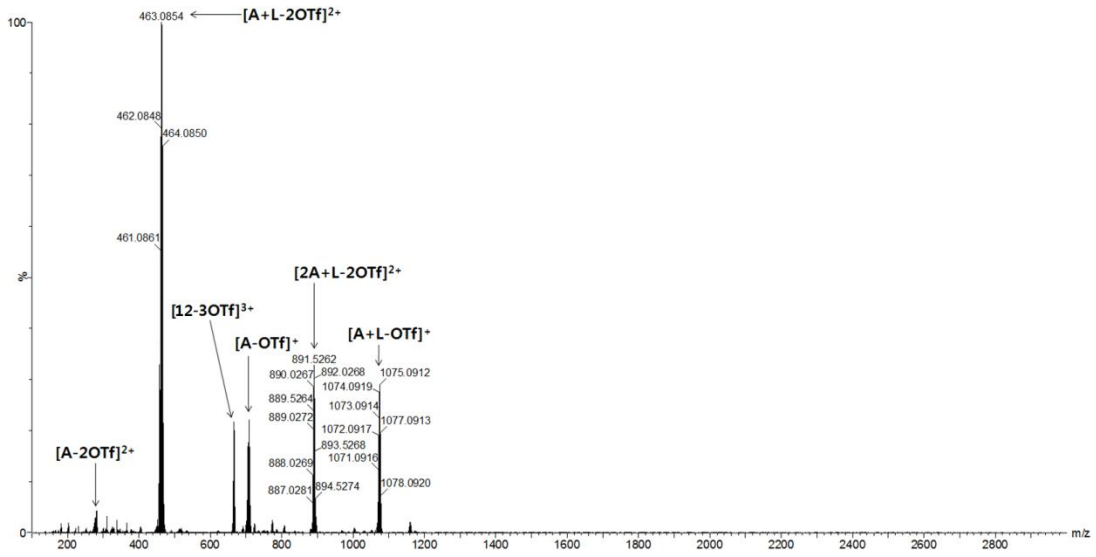

Figure 3.63 Full ESI mass spectrum of **12**

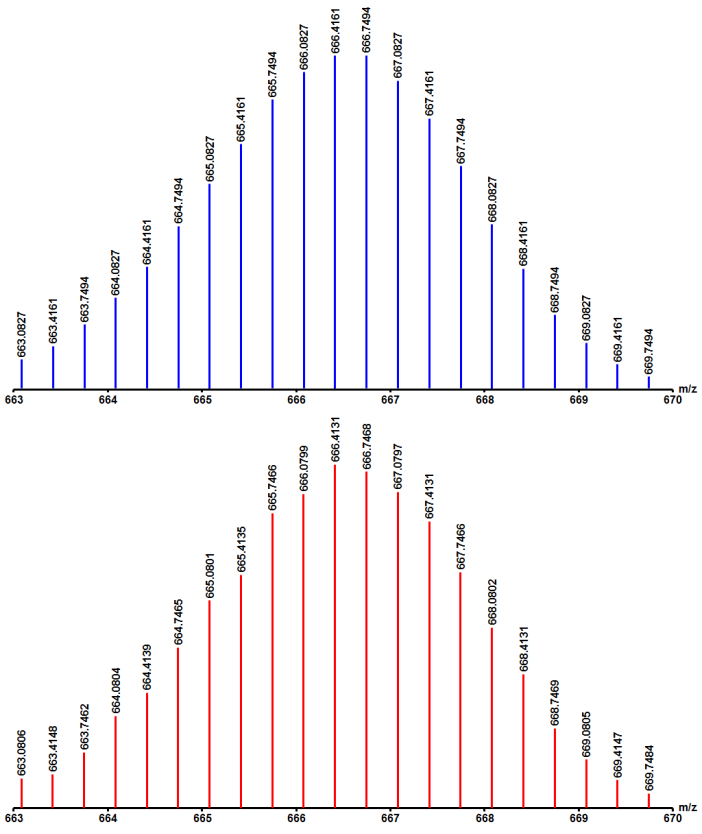

Figure 3.64 Calculated (blue) and experimental (red) ESI mass spectra of [**12**-3OTf]$^{3+}$. (Reaction in CD_3OD [8.0 mM])

3.4. Conclusion

In conclusion, selective, quantitative and template-free synthesis of a linear [3] catenane was achieved via the coordination-driven self-assembly of two components. Experimental observations and theoretical computations showed synergistic, non-covalent, intercycler interactions (π—π, CH—π and CH—N) play crucial roles in the formation of the linear [3]catenane topology. The size and angularity of the di-pyridyl donor **L2** were also found to be critical features of the selective synthesis of this topology. Self-assembly of naphthalene-based acceptor **A7** with triazole-based bulky donors (**L3** or **L4**) or an alkyne-based donor (**L5**) resulted in the formation of [2+2] monorectangles, which further highlighted the importance of steric effects and of the triazole moiety. Of the various donors, acceptors and solvents examined, the triazole-derived donor **L2** and the naphthalene-based acceptor **A7** in methanol provided the best reaction conditions to produce the linear [3]catenane topology. This result demonstrates the right combination of functional groups in donor and acceptor facilitating non-covalent inter- and/or intra- cycler interactions is a key requirement for the effective synthesis of supramolecules with complex and high-ordered topologies via coordination-driven self-assembly.

Publication

Singh, J.; Kim, D. H.; Kim, E.-H.; Singh, N.; Kim, H.; Hadiputra, R.; Jung, J.; Chi, K.-W. *Chem. Commun.* **2019**, *55*, 6866–6869.

3.5. Reference

1. a) Sauvage, J. P.; Dietrich-Buchecker, Eds.; Wiley-VCH Verlag GmbH: Weinheim, Germany, **1999**; b) Raymo, M.; Stoddart, J. F. *Chemical Reviews* **1999**, *99*, 1643−1663; c) Forgan, R. S.; Sauvage, J.-P.; Stoddart, J. F. *Chemical Reviews* **2011**, *111*, 5434–5464.

2. a) Sawada, T.; Yamagami, M.; Ohara, K.; Yamaguchi, K.; Fujita, M. *Angewandte Chemie International Edition* **2016**, *55*, 4519–4522; b) Allen, C. D.; Link, A. J. *Journal of the American Chemical Society* **2016**, *138*, 14214–14217; c) Sawada, T.; Inomata, Y.; Yamagami, M.; Fujita, M. *Chemistry Letters* **2017**, *46*, 1119–1121.

3. a) Wang, X.-W.; Zhang, W.-B. *Angewandte Chemie International Edition* **2016**, *55*, 3442–3446; b) Liu, D.; Wu, W.-H.; Liu, Y.-J.; Wu, X.-L.; Cao, Y.; Song, B.; Li, X.; Zhang, W.-B. *ACS Central Science* **2017**, *3*, 473–481; c) Pieters, B. J. G. E.; van Eldijk, M. B.; Nolte, R. J. M.; Mecinović, J. *Chemical Society Reviews* **2016**, *45*, 24–39; d) Sulkowska, J. I.; Rawdon, E. J.; Millett, K. C.; Onuchic, J. N.; Stasiak, A. *Proceedings of National Academy of Sciences* **2012**, *109*, 1715–1723.

4. a) Wu, Q.; Rauscher, P. M.; Lang, X.; Wojtecki, R. J.; de Pablo, J. J.; Hore, M. J. A.; Rowan, S. J. *Science* **2017**, *358*, 1434–1439; b) Scarff, C. A.; Snelling, J. R.; Knust, M. M.; Wilkins, C. L.; Scrivens, J. H. *Journal of the American Chemical Society* **2012**, *134*, 9193–9198; c) Takata, T.; Kihara, N.; Furusho, Y. *Advances in Polymer Science*; **2004**, 1–75.

5. a) Wasserman, S.; Cozzarelli, N. *Science* **1986**, *232*, 951–960; b) Champoux, J. J. *Annual Review of Biochemistry* **2001**, *70*, 369–413; c) Valero, J.; Lohmann, F.; Famulok, M. *Current Opinion in Biotechnology* **2017**, *48*, 159–167.

6. a) van Dongen, S. F. M.; Cantekin, S.; Elemans, J. A. A. W.; Rowan, A. E.; Nolte, R. J. M. *Chemical Society Reviews* **2014**, *43*, 99–122; b) Jester, S.-S.; Famulok, M. *Accounts of Chemical Research* **2014**, *47*, 1700–1709; c) List, J.; Falgenhauer, E.; Kopperger, E.; Pardatscher, G.; Simmel, F. C. *Nature Communications* **2016**, *7*, 12414.

7. Qu, D.-H.; Wang, Q.-C.; Zhang, Q.-W.; Ma, X.; Tian, H. *Chemical reviews* **2015**, *115*, 7543–7588.

8. Sauvage, J.-P. *Angewandte Chemie International Edition* **2017**, *56*, 11080–11093.

9. a) Erbas-Cakmak, S.; Leigh, D. A.; McTernan, C. T.; Nussbaumer, A. L. *Chemical Reviews* **2015**, *115*, 10081–10206; b) Neal, E. A.; Goldup, S. M. *Chemical Communications* **2014**, *50*, 5128–5142.

10. Gil-Ramírez, G.; Leigh, D. A.; Stephens, A. J. *Angewandte Chemie International Edition* **2015**, *54*, 6110–6150.

11. a) Schill, G.; Zürcher, C. *Angewandte Chemie International Edition* **1969**, *8*, 988–988. (b) Schill, G.; Zürcher, C. *Chemische Berichte* **1977**, *110*, 2046–2066.

12. Dietrich-Buchecker, C. O.; Sauvage, J. P.; Kintzinger, J. P. *Tetrahedron Lett.* **1983**.

13. Ashton, P. R.; Brown, C. L.; Chrystal, E. J. T.; Goodnow, T. T.; Kaifer, A. E.; Parry, K. P.; Slawin, A. M. Z.; Spencer, N.; Stoddart, J. F.; Williams, D. J. *Angewandte Chemie International Edition* **1991**, *30*, 1039–1042.

14. a) Li, S.; Huang, J.; Cook, T. R.; Pollock, J. B.; Kim, H.; Chi, K.-W.; Stang, P. J. *Journal of the American Chemical Society* **2013**, *135*, 2084–2087; b) Ye, Y.;

Wang, S.-P.; Zhu, B.; Cook, T. R.; Wu, J.; Li, S.; Stang, P. J. *Organic. Letters* **2015**, *17*, 2804–2807.

15. a) Iwamoto, H.; Itoh, K.; Nagamiya, H.; Fukazawa, Y. *Tetrahedron Letters* **2003**, *44*, 5773–5776; b) Wang, K.; Yee, C.-C.; Au-Yeung, H. Y. *Chemical Science* **2016**, *7*, 2787–2792.

16. a) Chichak, K. S.; Cantrill, S. J.; Pease, A. R.; Chiu, S. H.; Cave, G. W. V.; Atwood, J. L.; Stoddart, J. F. *Science* **2004**, *304*, 1308-1312; b) Zhang, L.; Stephens, A. J.; Nussbaumer, A. L.; Lemonnier, J.-F.; Jurček, P.; Vitorica-Yrezabal, I. J.; Leigh, D. A. *Nature Chemistry* **2018**, *10*, 1083–1088.

17. a) Cougnon, F. B. L.; Jenkins, N. A.; Pantoş, G. D.; Sanders, J. K. M. *Angewandte Chemie International Edition* **2012**, *51*, 1443-1447; b) Iwamoto, H.; Takizawa, W.; Itoh, K.; Hagiwara, T.; Tayama, E.; Hasegawa, E.; Haino, T. *The Journal of Organic Chemistry* **2013**, *78*, 5205–5217; c) Hori, A.; Kumazawa, K.; Kusukawa, T.; Chand, D. K.; Fujita, M.; Sakamoto, S.; Yamaguchi, K. *Chemistry - A European Journal* **2001**, *7*, 4142–4149.

18. a) Jansze, S. M.; Cecot, G.; Wise, M. D.; Zhurov, K. O.; Ronson, T. K.; Castilla, A. M.; Finelli, A.; Pattison, P.; Solari, E.; Scopelliti, R.; Zelinskii, G. E.; Vologzhanina, A. V.; Voloshin, Y. Z.; Nitschke, J. R.; Severin, K. *Journal of the American Chemical Society* **2016**, *138*, 2046–2054; b) Cook, T. R.; Stang, P. J. *Chemical Reviews* **2015**, *115*, 7001–7045; c) Fujita, D.; Ueda, Y.; Sato, S.; Mizuno, N.; Kumasaka, T.; Fujita, M. *Nature* **2016**, *540*, 563–566; d) Chen, L.; Chen, Q.; Wu, M.; Jiang, F.; Hong, M. *Accounts of Chemical Research* **2015**, *48*, 201–210; e) Wood, C. S.; Ronson, T. K.; Belenguer, A. M.; Holstein, J. J.; Nitschke, J. R. *Nature Chemistry* **2015**, *7*, 354–358.

19. a) Stang, P. J. *Journal of the American Chemical Society* **2012**, *134*, 11829–11830; b) Chakrabarty, R.; Mukherjee, P. S.; Stang, P. J. *Chemical Reviews*

2011, *111*, 6810–6918; c) Fujita, M. *Chemical Society Reviews* **1998**, *27*, 417–425.

20. a) Mondal, B.; Mukherjee, P. S. *J. Am. Chem. Soc.* **2018**, *140*, 12592–12601; b) Howlader, P.; Mondal, B.; Purba, P. C.; Zangrando, E.; Mukherjee, P. S. *Journal of the American Chemical Society* **2018**, *140*, 7952–7960; c) Howlader, P.; Das, P.; Zangrando, E.; Mukherjee, P. S. *Journal of the American Chemical Society* **2016**, *138*, 1668–1676; d) Singh, N.; Jo, J.-H.; Song, Y. H.; Kim, H.; Kim, D.; Lah, M. S.; Chi, K.-W. *Chemical Communications* **2015**, *51*, 4492–4495; d) Lu, C.; Zhang, M.; Tang, D.; Yan, X.; Zhang, Z.; Zhou, Z.; Song, B.; Wang, H.; Li, X.; Yin, S.; Sepehrpour, H.; Stang, P. J. *Journal of the American Chemical Society* **2018**, *140*, 7674–7680.

21. a) Song, Y. H.; Singh, N.; Jung, J.; Kim, H.; Kim, E.-H.; Cheong, H.-K.; Kim, Y.; Chi, K.-W. *Angewandte Chemie International Edition* **2016**, *55*, 6, 2007-2011; b) Kim, T.; Singh, N.; Oh, J.; Kim, E.-H.; Jung, J.; Kim, H.; Chi, K.-W. *Journal of the American Chemical Society* **2016**, *138*, 8368-8371; c) Lee, H.; Elumalai, P.; Singh, N.; Kim, H.; Lee, S. U.; Chi, K.-W. *Journal of the American Chemical Society* **2015**, *137*, 4674-4677; (d) Vajpayee, V.; Song, Y. H.; Cook, T. R.; Kim, H.; Lee, Y.; Stang, P. J.; Chi, K.-W. *Journal of the American Chemical Society* **2011**, *133*, 19646–19649.

22. Kim, D. H.; Singh, N.; Oh, J.; Kim, E.-H.; Jung, J.; Kim, H.; Chi, K.-W. *Angewandte Chemie International Edition* **2018**, *57*, 5669–5673.

23. Barry, N. P. E.; Furrer, J.; Therrien, B. *Helvetica Chimica Acta* **2010**, *93*, 1313-1328.

24. Sheldrick, G. M. *Acta Crystallographica Section A Foundations of Crystallography* **2008**, *64*, 112-122.

25. a) Speck, A. L. *Acta Crystallographica Section A Foundations of Crystallography* **2009**, D53, 148-155; b) Speck, A. L. *Acta Crystallographica Section A Foundations of Crystallography* **2008**, A46, 194-201;

Chapter 4. The first quantitative synthesis of a closed three–link chain (6_1^3) using coordination and non–covalent interactions–driven self–assembly

4.1 Introduction

Interlocked or intertwined compounds are a novel family of structurally diverse supramolecules used in various disciplines such as chemistry, mathematics and biology.[1] Recent advances in the synthesis of these supramolecules have enabled a range of applications in smart materials, molecular machines, and nano devices that were previously inaccessible through traditional cyclic or acyclic compounds.[2] Generally, the synthesis of singly interlocked rings[3] (i.e. [2] catenane) and highly ordered interlocked structures[4] involves the preorganization of acyclic and cyclic units by metal ion template[5], electron deficient/electron–rich π–π template[6] and active–metal template.[7] However, achieving selective and quantitative synthesis in order to harvest the materials for real–world applicability is a challenge. Despite recent spurting interest, there have been few reports of higher order interlocked molecules (where number of rings > 2). Besides the synthesis of a linear [3]catenane [8] and Borromean rings[9], examples of other topological isomers from three rings remains scarce. (Figure 4.1) For example, Nitschke et al., were among the first to synthesize the topology of cyclic [3]catenane via metal–templated self–assembly.[10] Furthermore, among the typical topological isomers of mechanically interlocked three rings, only one study reported the formation of a closed three–link chain (Liang et al.,), where three oligonucleotides were utilized for its synthesis.[11]

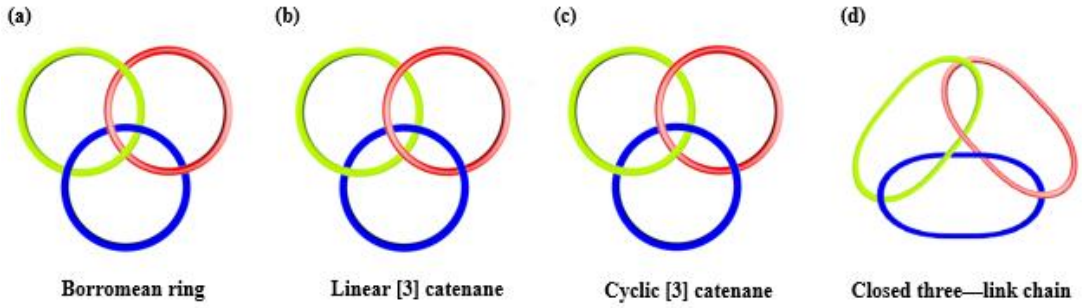

Figure 4.1. Typical topological isomers of mechanically interlocked three rings (a) Borromean rings (6_2^3) in Alexander–Briggs notation (b) linear [3]catenane (4_1^3) (c) cyclic [3]catenane (6_3^3) (d) closed three–link chain (6_1^3).

The bottom–up coordination–driven self–assembly[12],[13] along with NCIs[14] is an efficient and selective methodology of producing complex supramolecular topologies. [15] The modularity of coordination–driven self–assembly process offers the ability to incorporate and decorate components with π–electron containing functionalities, facilitating inter– or intra−cycler interaction to produce non−trivial supramolecular topologies. Using this strategy, various complex supramolecular topologies such as

Borromean rings, Solomon links, [n] catanenes (n=2,3), trefoil knot, "rectangle in rectangle", molecular figure–eight knot and 8_{18} molecular knot have been realized so far.[16] NCIs play a fundamental role in various naturally occurring and artificial chemical transformations. Despite the weak magnitude in comparison to covalent or coordination bonding between atoms, summation and synergistic effect of NCIs give characteristic to these interactions. A fundamental understanding of the interactions involved in the formation of complicated non−trivial supramolecules is essential for controlling the final structure and topology that holds the key to optimizing its function. The developments of synthetic models to predict the product topology based on NCIs is challenging, therefore, further experimental results are needed to form its foundation.

A complementary approach of achieving complexity and selectivity requires maximizing NCIs through strategic design of self–assembling components. Although various studies have taken advantage of π–stacking and CH–π arising from the self–assembling units of fixed length and geometry, their scope to yield complex supramolecular topologies remains limited. In our previous study, we reported the application of the concept of coordination–driven self–assembly with intercycler NCIs for the production of various supramolecules. We also reported the efficient synthesis of a linear [3]catenane using coordination–driven self–assembly and synergic NCIs from a triazole based flexible dipyridyl donor and a naphthalene–based Ru(II) acceptor.[17] Since the sandwich type interactions between π–rich donors have been successful in our previous synthesis of [2] catenane and a linear [3]catenane, similar complex and high−ordered molecular topologies can be constructed by fine tuning of flexible dipyridyl donors incorporated with NCIs. Our research group has made significant efforts toward constructing interlocked or intertwined compounds and as a part of our ongoing efforts for the synthesis and utilization of interlocked compounds, this current study proposed a selective and quantitative synthesis and the X–ray characterization of a closed three–link chain via two component coordination–driven self–assembly of a naphthalene–based acceptor **A7** and flexible benzimidazole–based donor **L6**. The donor used in this study provides distinctive angularity along with intercycler interactions to produce this rare topology.

4.2 Materials and methods

Donor **L6** and ruthenium acceptors **A5** and **A7** were prepared according to the

reported methods.[18],[19] Deuterated NMR solvents were purchased from Cambridge Isotope Laboratory (Andover, MA, USA). NMR spectra were recorded on Bruker 300, 800 and 900 MHz spectrometers (University of Ulsan and Korea Basic Science Institute, Ochang). ^{1}H–NMR chemical shifts were reported relative to the residual protons of deuterated CD_3OD (3.31 ppm), deuterated CD_3NO_2 (4.33 ppm), deuterated CD_3CN (1.94 ppm) and deuterated DMF–d_7 (8.03 ppm). ESI–MS data of all compounds were recorded on Synapt G2 quadrupole time–of flight (TOF) mass spectrometer equipped with an electrospray ion source (Waters, Milford, MA, USA) and analyzed with the MassLynx software suite system at the Korea Basic Science Institute, Ochang).

4.2.1 Crystallographic data collection and structure refinement

Diffraction data of **14** was collected at 100 K on an ADSC Quantum 210 CCD diffractometer with synchrotron radiation (λ = 0.70000 Å) at the Supramolecular Crystallography Beamline 2D, Pohang Accelerator Laboratory (PAL), Pohang, Korea. The raw data were processed and scaled using program HKL3000. The structure was solved by direct methods, and the refinements done with full–matrix least–squares on F^2 with appropriate software implemented in the SHELXTL program package.[20]All the non–hydrogen atoms were refined anisotropically, and hydrogen atoms were added to their geometrically ideal positions. The contributions of the most disordered solvent molecules were removed from the diffraction data using the SQUEEZE routine of PLATON software,[21] and then final refinements were carried out. X–ray crystallographic data was as provided in Table 4.1.

4.2.2 Coordination-driven self-assembly of 13, 14 and 15

Coordination-driven self-assembly of monorectangle 13

The arene-Ru(II) acceptor **A7** (1.9 mg, 2.0 μmol) and donor **L6** (0.78 mg, 2.0 μmol) were stirred in CD_3OD (4.0 mL) at room temperature for 12 h to produce a green solution. ^{1}H NMR (800 MHz, MeOD) δ 8.55 (s, 8H), 7.91 (s, 8H), 7.70 (s, 4H), 7.55 (s, 4H), 7.43 (s, 2H), 7.35 (s, 2H), 7.28 (s, 8H), 5.88 (d, J = 5.9 Hz, 8H), 5.65 (d, J = 5.9 Hz, 8H), 2.87 – 2.85 (m, 4H), 2.13 (s, 12H), 1.35 (d, J = 6.9 Hz, 24H). ^{13}C NMR (200 MHz, CD_3OD) δ 170.82, 161.67, 161.49, 152.48, 137.29, 124.86, 122.09,

121.21, 119.63, 116.86, 111.23, 109.77, 105.13, 103.67, 99.79, 84.50, 82.65, 30.66, 21.09, 15.99; ESI-MS for **13** ($C_{112}H_{96}F_{12}N_{12}O_{20}Ru_4S_4$): m/z = 748.1082 [**13**-3OTf]$^{3+}$.

Coordination-driven self-assembly of close three-link chain 14

The arene-Ru(II) acceptor **A7** (19.1 mg, 20 μmol) and donor **L6** (7.77 mg, 20 μmol) were stirred in CD_3OD (1.0 mL) at room temperature for 12 h to produce a dark green solution. The products were precipitated and isolated through dropwise addition of diethyl ether into this solution, and washed twice with diethyl ether using centrifugation method. The dark-green powder was characterized as **14**. Yield: (24.5 mg, Yield: 91 %), Anal. Calcd for $C_{336}H_{288}F_{36}N_{36}O_{36}Ru_{12}S_{12}\cdot 2H_2O$: C 49.77; H 3.63; N 6.22. Found: C 49.83; H 3.64; N 6.23. ^{1}H NMR (900 MHz, CD_3OD) δ 8.83-8.29 (m, 17H), 8.17-6.93 (m, 67H), 5.75 (m, 48H), 3.17 (m, 12H), 2.46-1.80 (m, 36H), 1.66-1.07 (m, 72H); ^{13}C NMR (225 MHz, CD_3OD) δ 171.59, 170.98, 170.77, 170.01, 153.27, 152.46, 152.02, 151.16, 137.70, 137.37, 128.48, 125.77, 122.63, 121.88, 121.22, 119.81, 118.40, 111.73, 111.48, 111.21, 103.69, 103.37, 100.18, 99.82, 85.08, 84.53, 84.20, 82.66, 82.18, 30.65, 30.45, 21.35, 21.13, 21.04, 16.49, 16.13, 16.00, 15.97, 15.88, 15.77; ESI-MS for **14** ($C_{336}H_{288}F_{36}N_{36}O_{36}Ru_{12}S_{12}$): m/z = 2541.5706 [**14**-3-OTf] $^{3+}$, 1835.9700 [**14**-4OTf]$^{4+}$, 1438.9819 [**14**-5OTf]$^{5+}$.

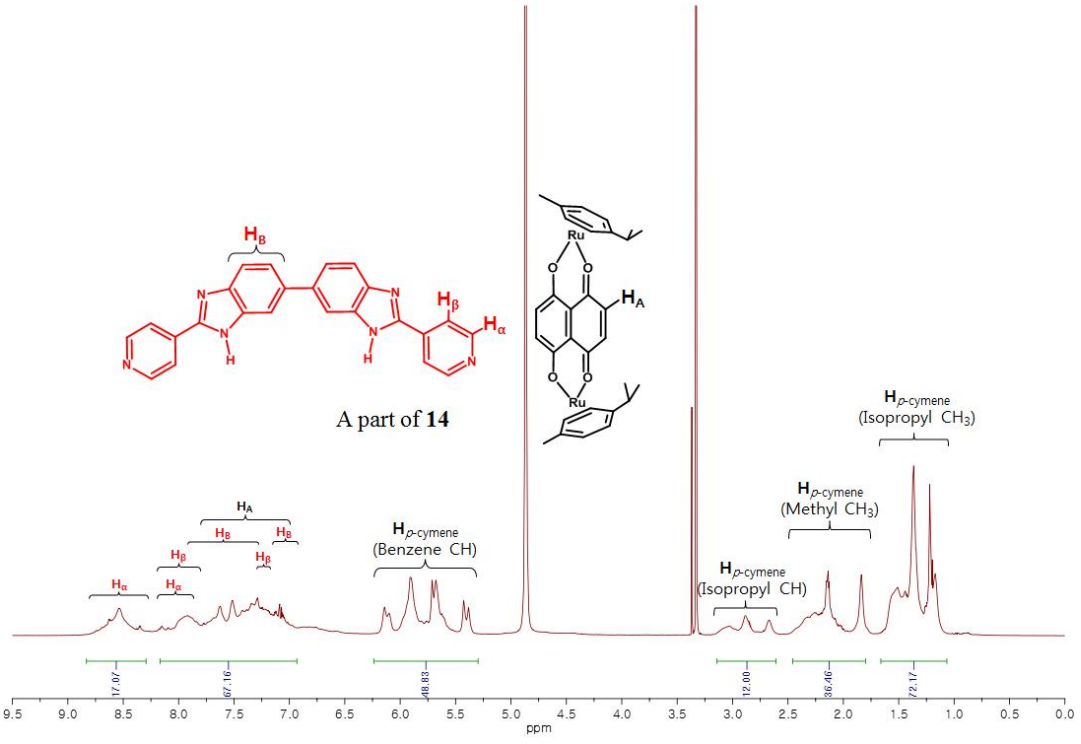

Figure 4.2 ^{1}H NMR spectrum of **14** (CD_3OD [20 mM], 900 MHz)

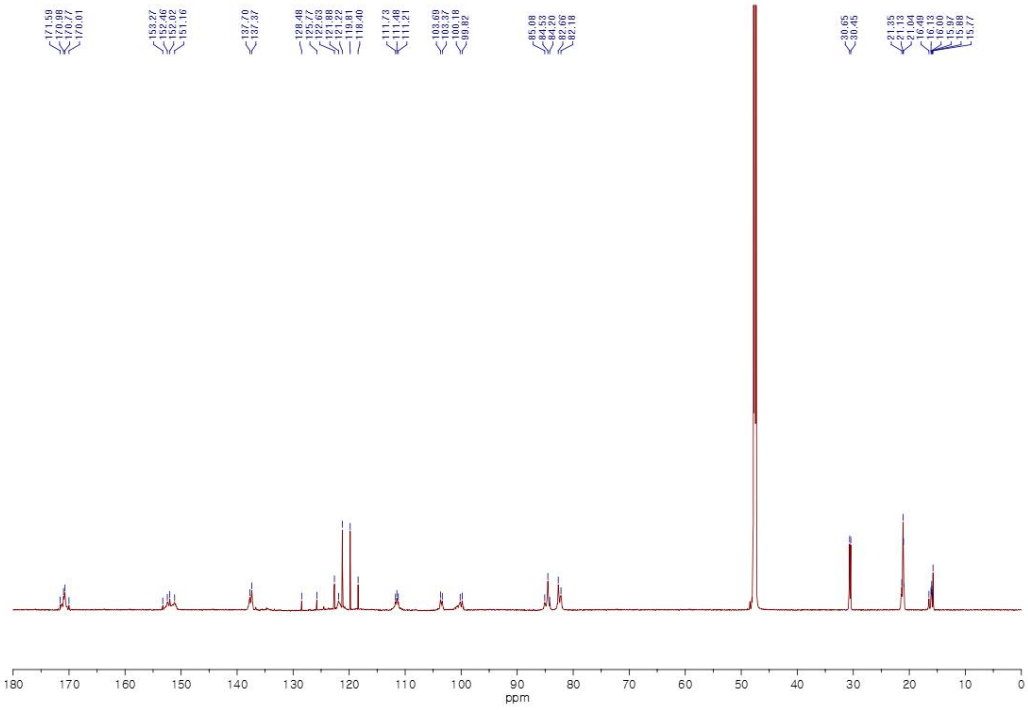

Figure 4.3 ^{13}C NMR spectrum of **14** (CD_3OD [20 mM], 225 MHz)

Coordination-driven self-assembly of 15

The arene-Ru(II) acceptor **A5** (6.9 mg, 8.0 μmol) and donor **L6** (3.1 mg, 8.0 μmol) were stirred in CD_3OD (1.0 mL) at room temperature for 12 h to produce an orange solution. The products were precipitated and isolated by dropwise addition of diethyl ether into this solution, and washed twice with diethyl ether using centrifugation method. The dark-green powder was characterized as **15**. Yield: (8.7 mg, Yield: 87 %), Anal. Calcd for $C_{96}H_{88}F_{12}N_{12}O_{20}Ru_4S_4 \cdot 2H_2O$: C 45.64; H 3.67; N 6.65. Found: C 45.55; H 3.68; N 6.63. ^{1}H NMR (300 MHz, CD_3OD) δ 8.22 (d, J = 6.7 Hz, 8H), 7.92 (d, J = 6.7 Hz, 8H), 7.44 (s, 4H), 7.35 (s, 8H), 5.98 (d, J = 6.4 Hz, 8H), 5.81 (d, J = 6.4 Hz, 8H), 2.89 (dt, J = 13.8, 6.9 Hz, 4H), 2.26 (s, 12H), 1.41 (d, J = 6.9 Hz, 24H); ^{13}C NMR (75 MHz, CD_3OD) δ 171.07, 153.10, 148.24, 145.91, 139.32, 137.56, 124.95, 124.20, 122.55, 121.80, 118.33, 102.46, 97.53, 82.10, 81.60, 31.08, 21.10, 16.65; ESI-MS for **15** ($C_{96}H_{88}F_{12}N_{12}O_{20}Ru_4S_4$): m/z = 681.4213 [**15**-3OTf] $^{3+}$.

4.3. Results and discussion

4.3.1. Synthesis and characterization of monorectangle 13 and close three-link chain 14

As shown in scheme 4.1, coordination–driven self–assembly of acceptor **A7** (8.0 mM) and donor **L6** (8.0 mM) performed in CD_3OD for 12h gave the self–assembled product **14** along with [2+2] macrocycle **13** as a clear green solution. The latter can also be obtained from a similar reaction of **A7** and **L6** at ≤1.0 mM concentration in methanol (Scheme 1). Upon increasing the concentration to 20 mM, only one diffusion coefficient at $D = 4.8 \times 10^{-10}$ m^2 s^{-1} was observed in the ^{1}H–DOSY NMR spectrum–result in the quantitative synthesis of product **14** (Figure 4.4). ^{1}H–NMR spectrum of this solution was found to be very complex, indicating the formation of a non-trivial supramolecular structure. Prominent peaks at m/z = 1868.9348 (**14**–4OTf)$^{4+}$ and at 2541.5706 (**14**–3OTf)$^{3+}$ and their perfect agreement with the theoretical isotopic distributions' values indicated the selective formation of a $[2+2]_3$ self–assembled product (Figures 4.5–4.8). Upon decreasing the concentration macrocycle **13** starts to appear from 16 mM, and forms quantitatively at 1.0 mM concentration. The combined 2D NMR analysis and a prominent ESI–MS peak at m/z = 748.1082 (**13**–3OTf)$^{3+}$ further confirmed the identity of macrocycle **13** (Figures 4.18–4.22).

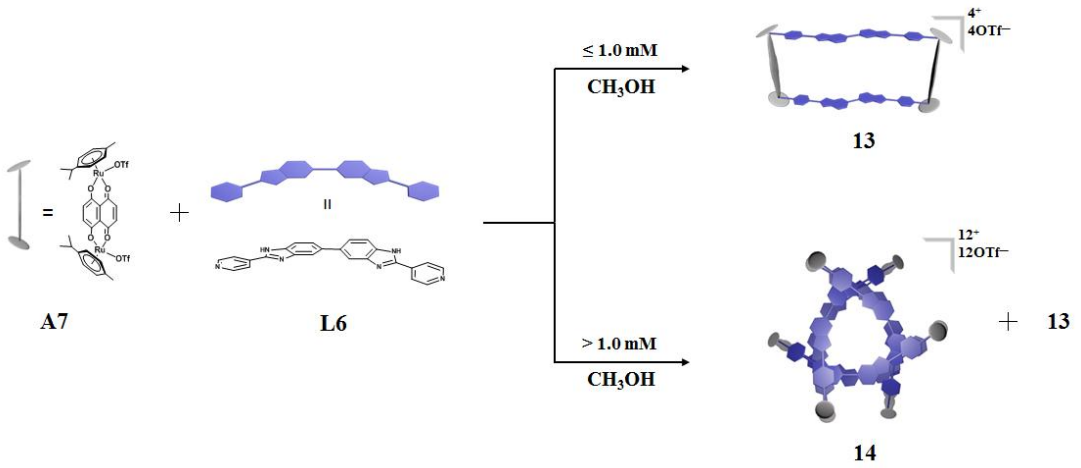

Scheme 4.1 Coordination−driven self−assembly of macrocycle **13** and closed three−link chain **14**.

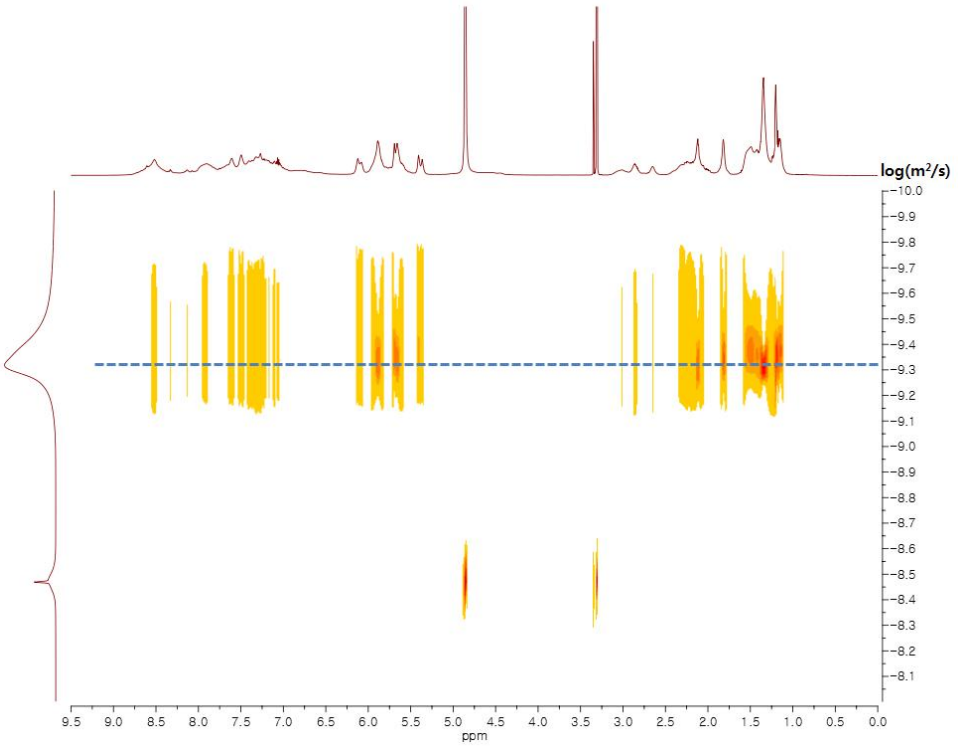

Figure 4.4 ^{1}H-DOSY NMR spectrum of **14** (CD_3OD [20 mM], 298 K, 800 MHz)

Diffusion coefficient: 4.8×10^{-10} m^2/sec

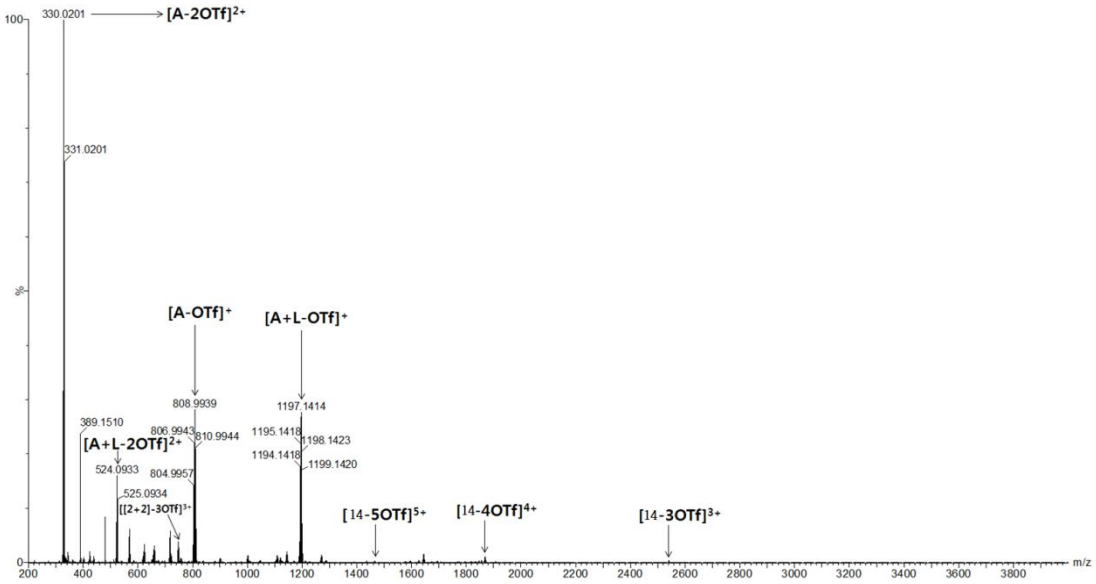

Figure 4.5 Full ESI mass spectrum of **14** (Reaction in CD_3OD [20 mM])

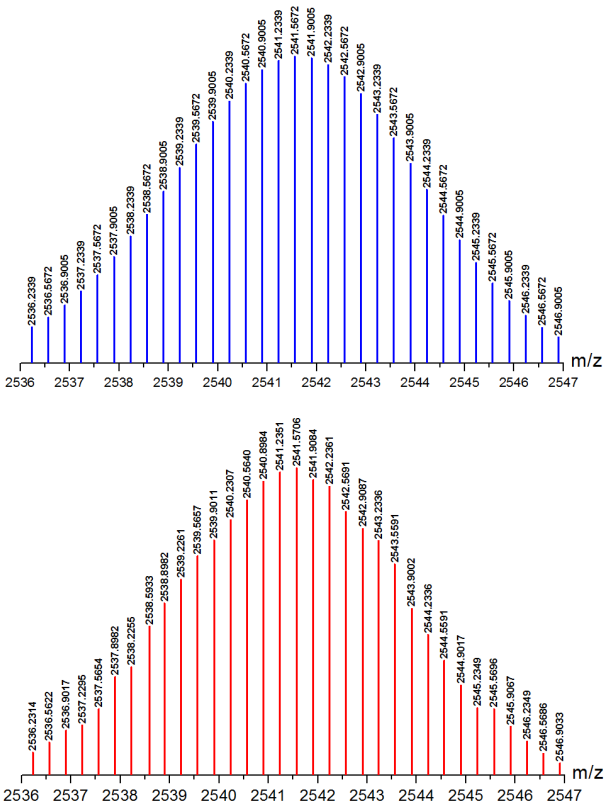

Figure 4.6 Calculated (blue) and experimental (red) ESI mass spectra of [**14**-3OTf]$^{3+}$.

(Reaction in CD_3OD [20 mM])

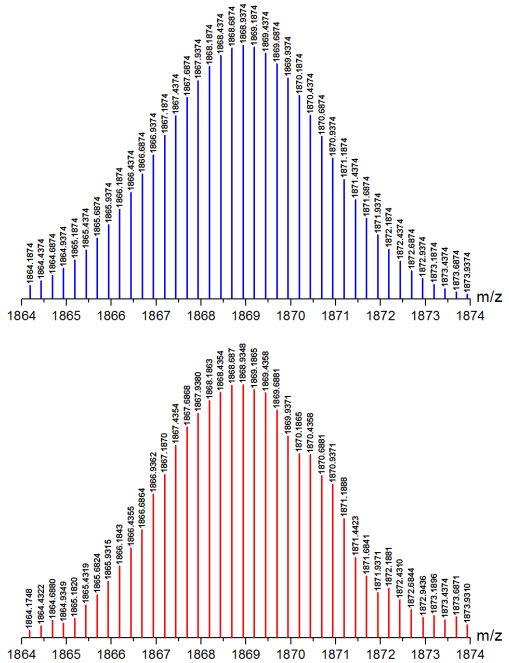

Figure 4.7 Calculated (blue) and experimental (red) ESI mass spectra of [**14**-4OTf]$^{4+}$.

(Reaction in CD_3OD [20 mM])

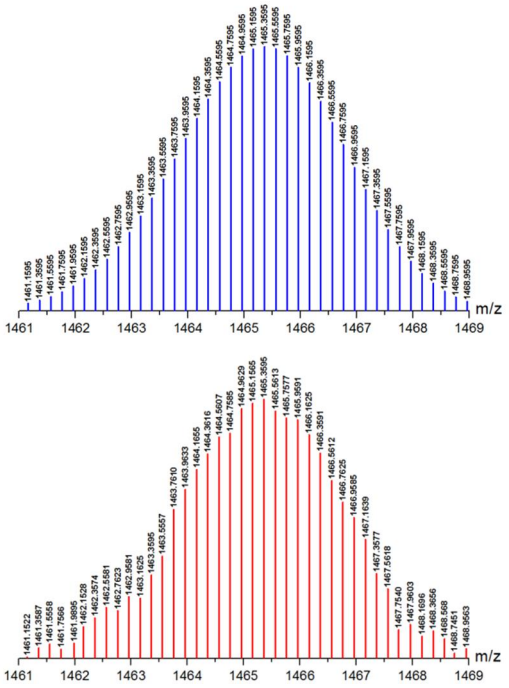

Figure 4.8 Calculated (blue) and experimental (red) ESI mass spectra of [**14**-5OTf]$^{5+}$.

(Reaction in CD_3OD [20 mM])

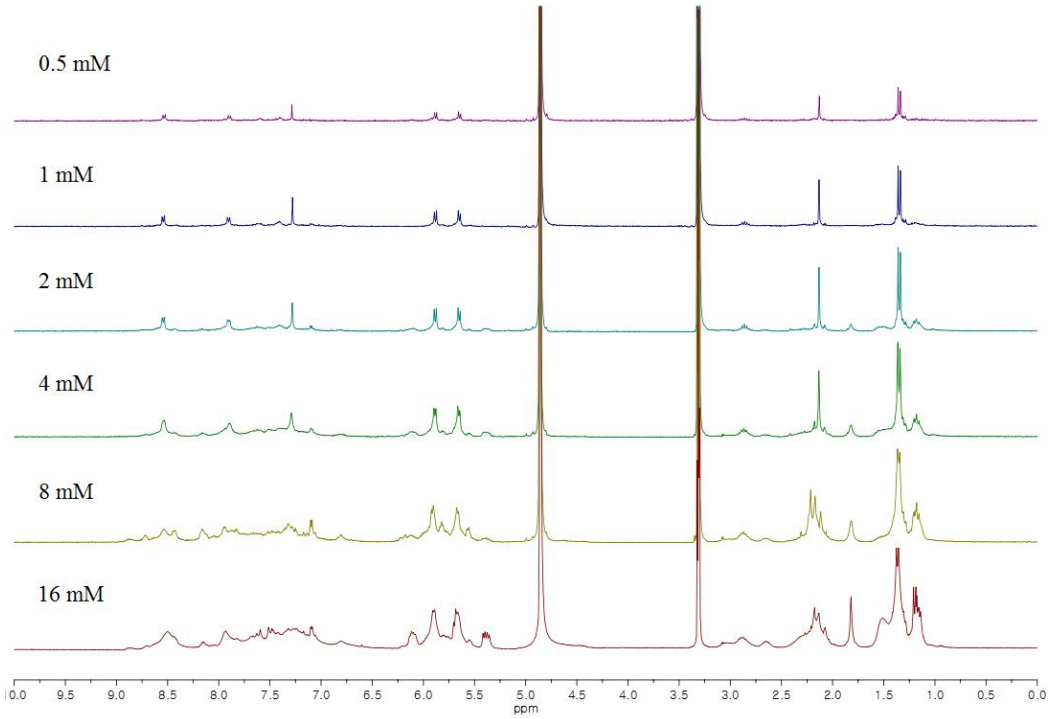

Figure 4.9 ^{1}H NMR spectra showing increasing of proportion of **14** upon sequentially increasing the concentration from 0.5 mM to 16 mM (CD_3OD, 300 MHz).

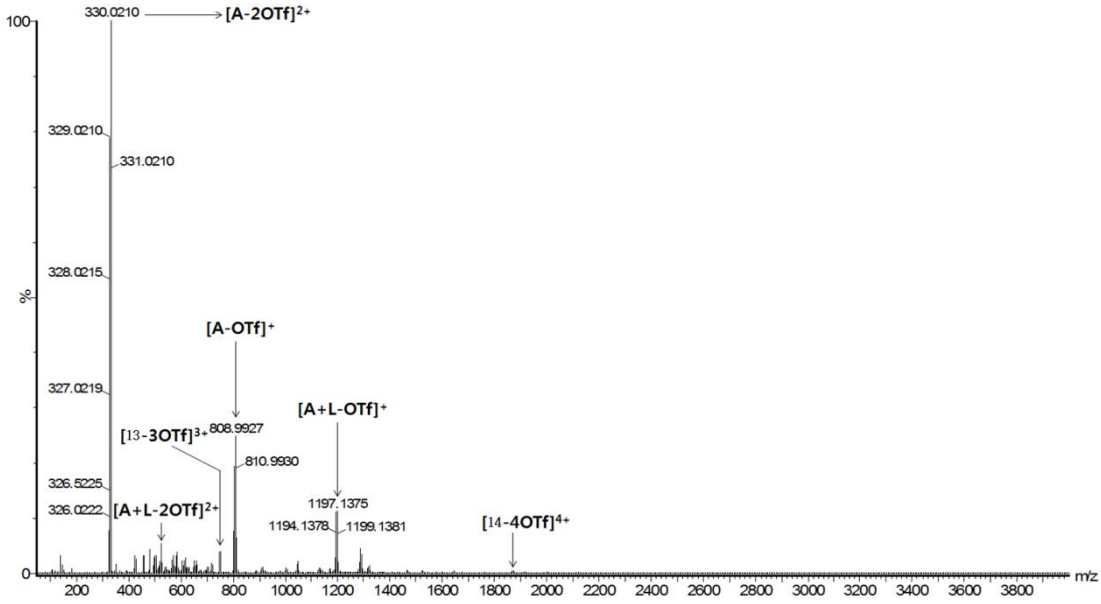

Figure 4.10 Full ESI mass spectrum of mixture **13+14** (Reaction in DMF [8.0 mM])

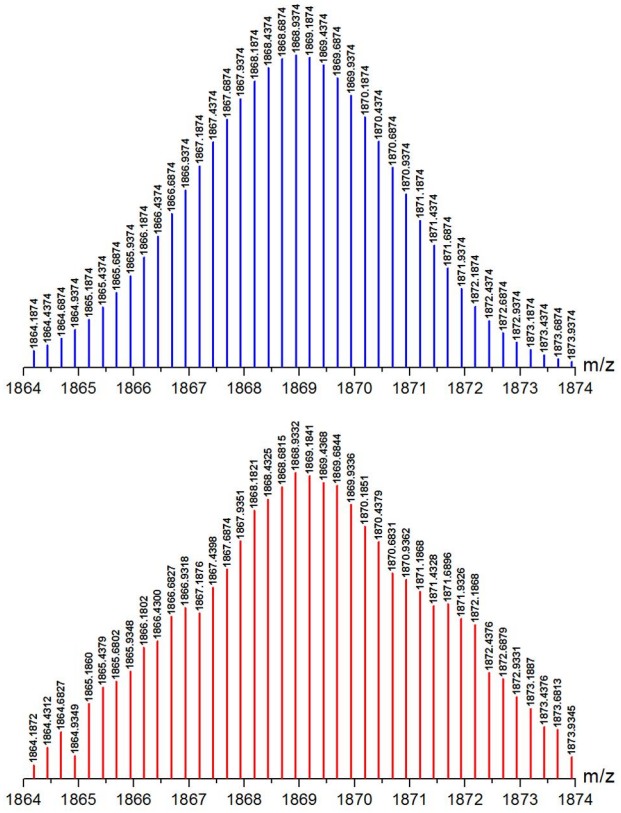

Figure 4.11 Calculated (blue) and experimental (red) ESI mass spectra of [**14**-4OTf]$^{4+}$.

(Reaction in DMF [8.0 mM])

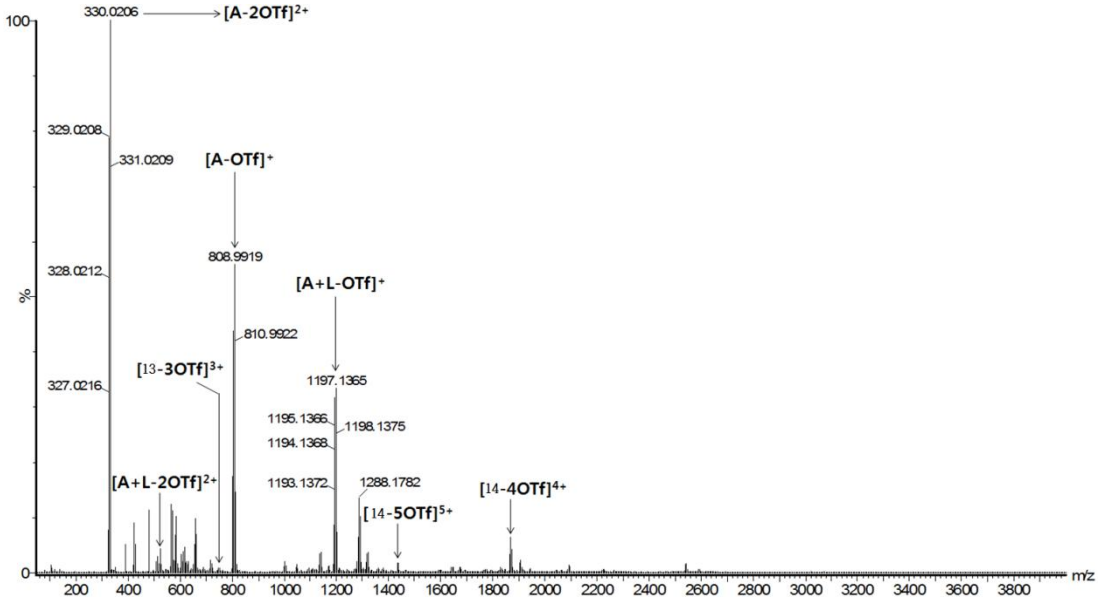

Figure 4.12 Full ESI mass spectrum of mixture **13+14** (Reaction in CD_3NO_2 [8.0 mM])

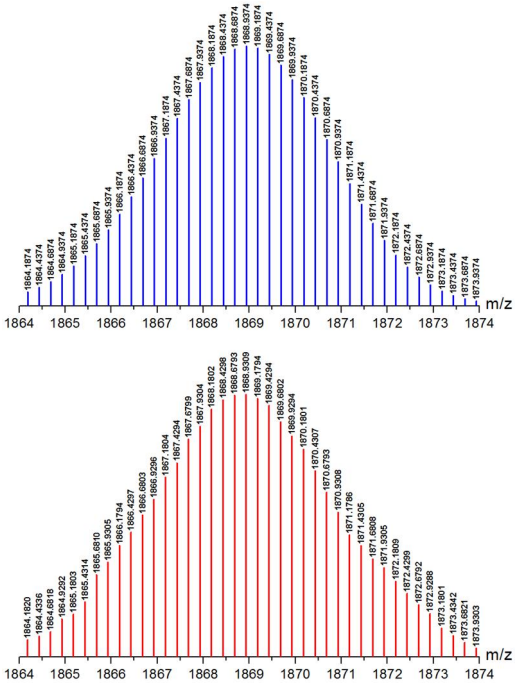

Figure 4.13 Calculated (blue) and experimental (red) ESI mass spectra of [**14**-4OTf]$^{4+}$.

(Reaction in CD_3NO_2 [8.0 mM])

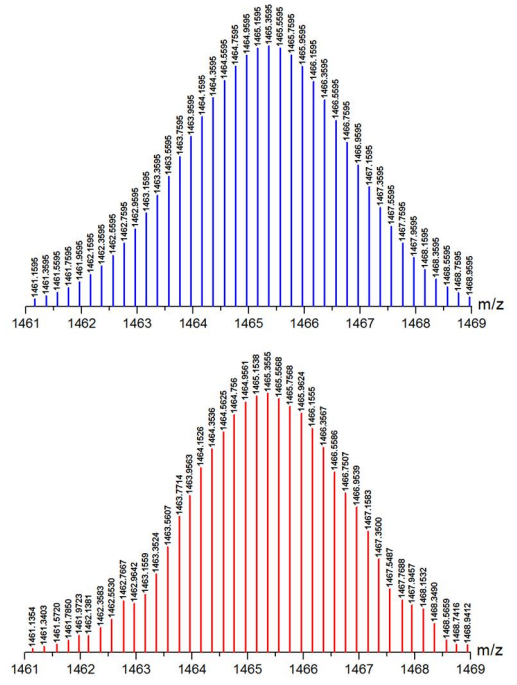

Figure 4.14 Calculated (blue) and experimental (red) ESI mass spectra of [**14**-5OTf]$^{5+}$.

(Reaction in CD_3NO_2 [8.0 mM])

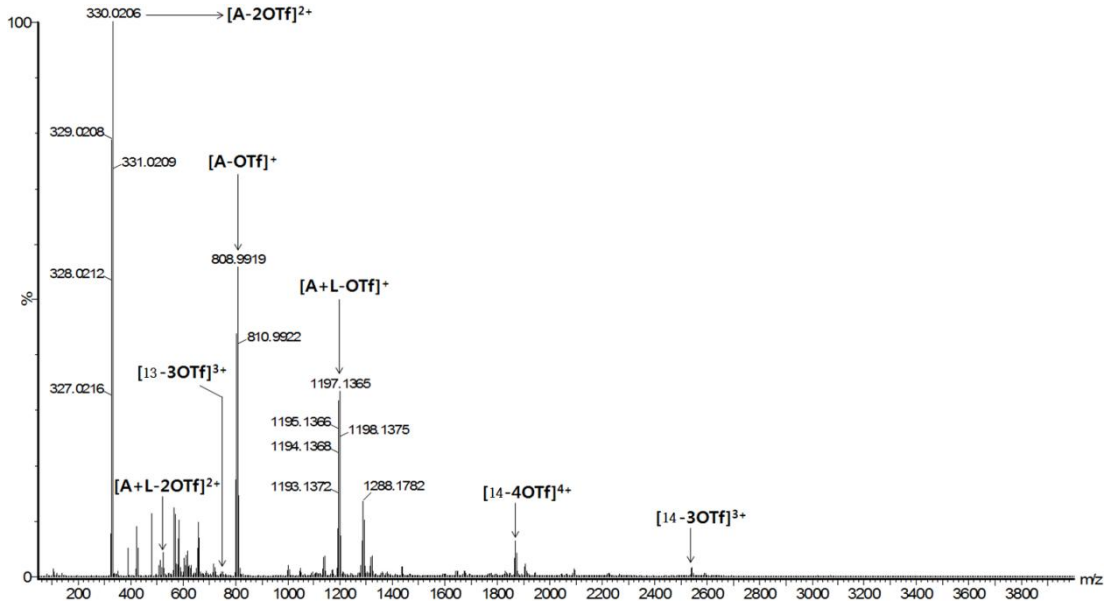

Figure 4.15 Full ESI mass spectrum of mixture **13+14** (Reaction in CD_3CN [8.0 mM])

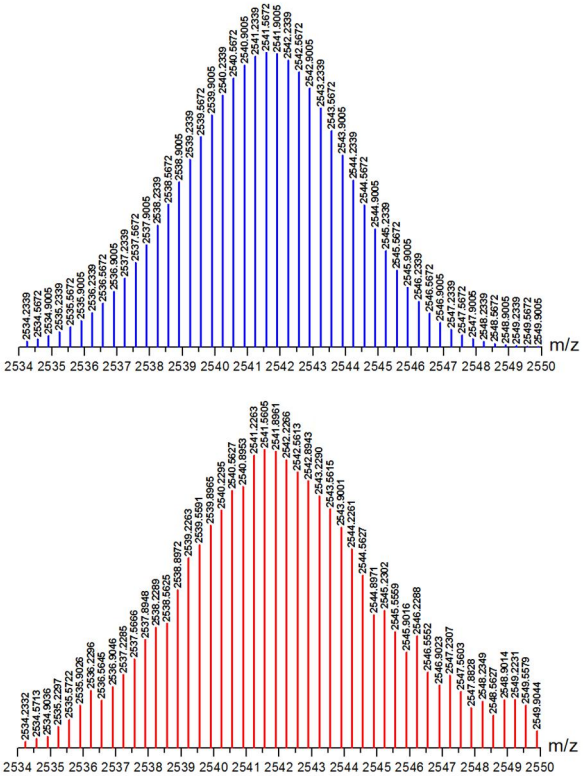

Figure 4.16 Calculated (blue) and experimental (red) ESI mass spectra of [**14**-3OTf]$^{3+}$.

(Reaction in CD_3CN [8.0 mM])

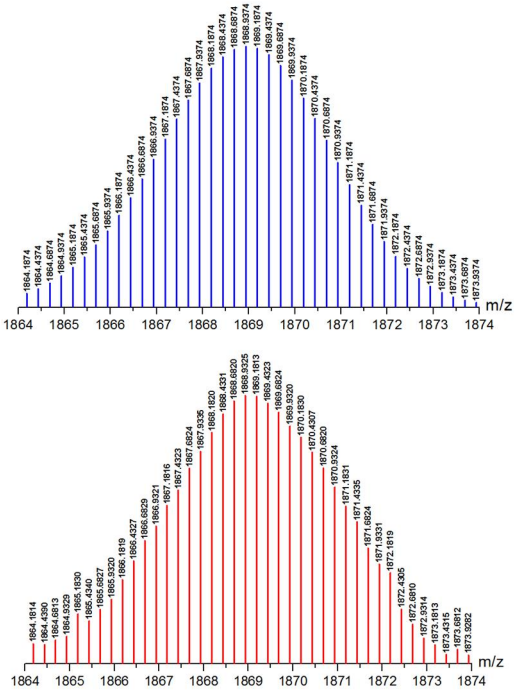

Figure 4.17 Calculated (blue) and experimental (red) ESI mass spectra of [**14**-4OTf]$^{4+}$.

(Reaction in CD_3CN [8.0 mM])

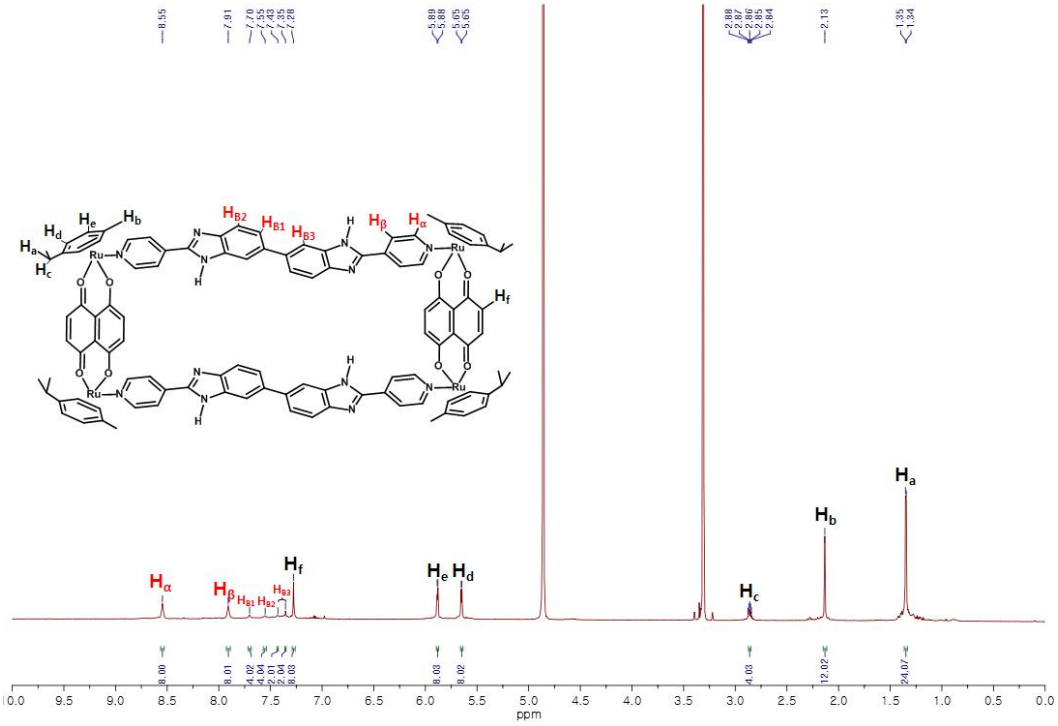

Figure 4.18 ^{1}H NMR spectrum of **13** (CD_3OD [1.0 mM], 800 MHz)

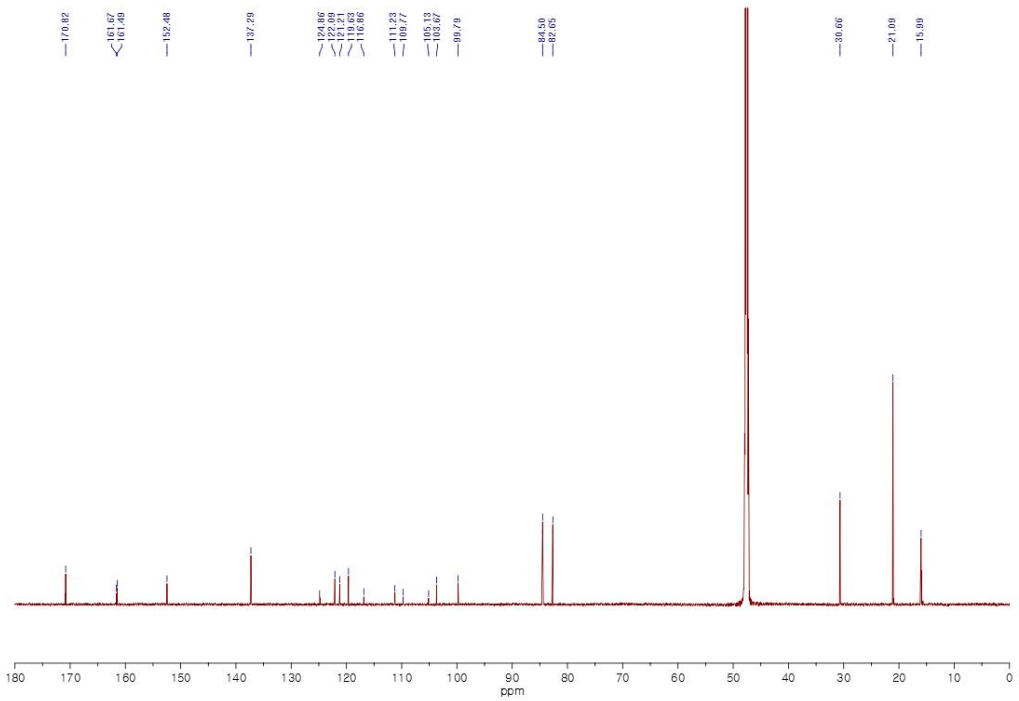

Figure 4.19 ^{13}C NMR spectrum of **13** (CD_3OD [1.0 mM], 200 MHz)

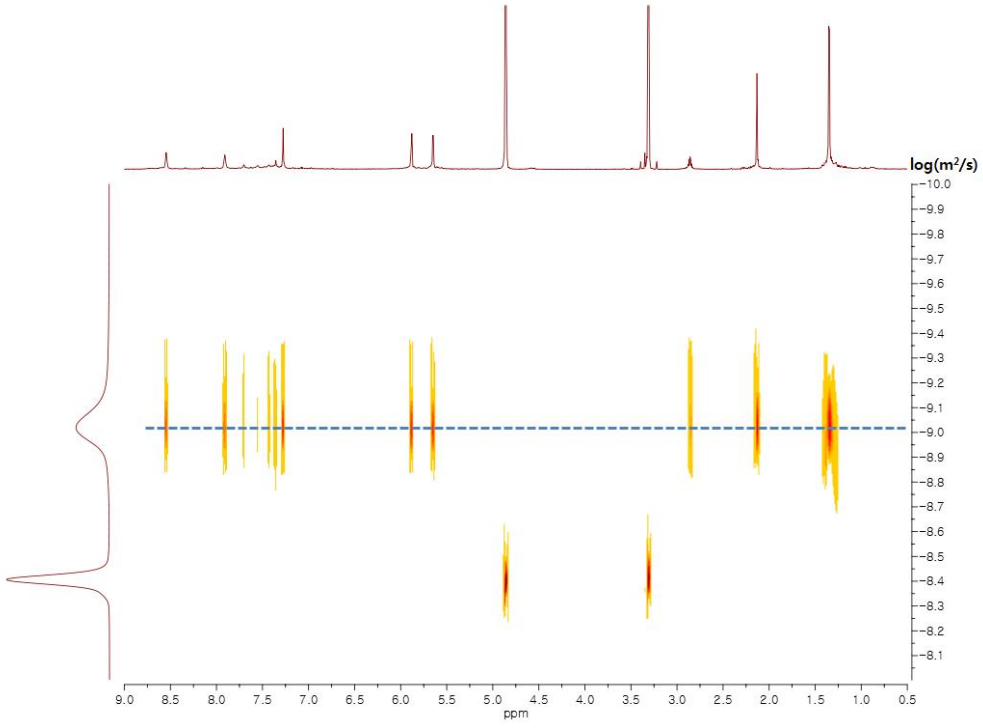

Figure 4.20 ^{1}H-DOSY NMR spectrum of **13** (CD_3OD [1.0 mM], 298 K, 800 MHz)

Diffusion coefficient: 9.7×10^{-10} m^2/sec

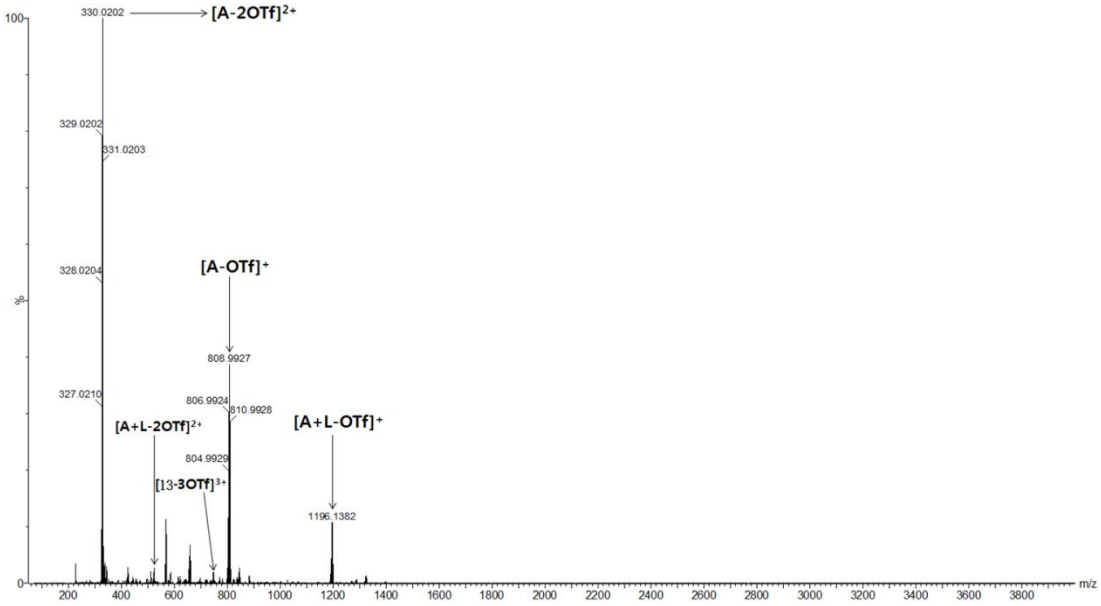

Figure 4.21 Full ESI mass spectrum of **13** (Reaction in CD_3OD [1.0 mM])

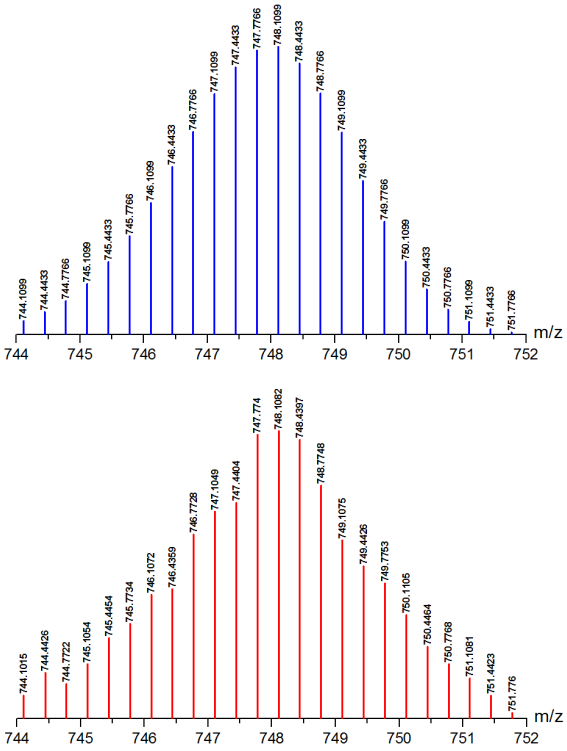

Figure 4.22 Calculated (blue) and experimental (red) ESI mass spectra of [**13**-3OTf]$^{3+}$.

(Reaction in CD_3OD [1.0 mM])

The single–crystal X–ray diffraction (SCXRD) analysis using synchrotron radiation not only confirmed the interlocking of three [2+2] rings but also revealed that the rings form a closed three–link chain (6_1^3) (Figure 4.23). Single crystals suitable for SCXRD analysis were obtained through slow vapor diffusion of diethyl ether into a solution of **14** in methanol at room temperature. The structure is best defined by the space group *R*3 with trigonal lattice (Table 4.1).

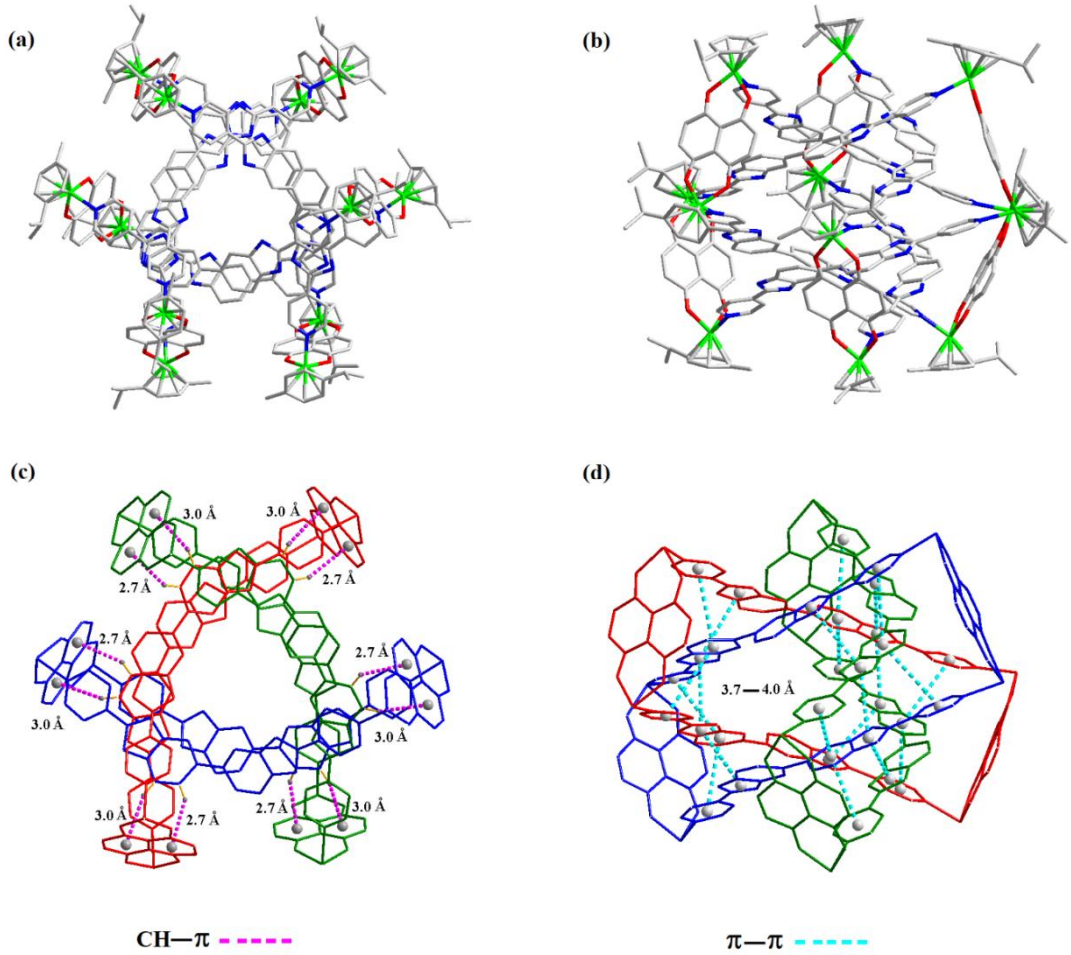

Figure 4.23 Crystal structure of closed–three link chain **14**: (a) top view and (b) side view (c) diagram showing important intercycler CH–π interactions and (d) π–π stacking interactions. (*p*–cymene rings were removed for clarity)

Table 4.1 X-ray crystal structure parameters of **14**

Empirical formula	C115.01 H107.40 F12 N12.64 O23.65 Ru4 S4	
Formula weight	2805.53	
Temperature	100 K	
Wavelength	0.700 Å	
Crystal system	Trigonal	
Space group	R3	
Unit cell dimensions	a = 42.315(6) Å	□□□□ α = 90°
	b = 42.315(6) Å	□□□□ β = 90°
	c = 19.337(4) Å	□ □ γ = 90°
Volume	29986 (10) Å^3	
Z	9	
Density (calculated)	1.398 g/cm^3	
Absorption coefficient	0.561 mm^{-1}	
F(000)	12808	
Crystal size	0.100 × 0.100 × 0.100 mm^3	
Theta range for data collection	1.508 to 22.882°	
Index ranges	-46≤h≤46, -46≤k≤46, -20≤l≤20	
Reflections collected	39534	
Independent reflections	16752 [R(int) = 0.0688]	
Completeness to theta = 22.882°	91.1%	
Absorption correction	Semi-empirical from equivalents	
Max. and min. transmission	0.946 and 0.946	
Refinement method	Full-matrix least-squares on F^2	
Data / restraints / parameters	16752 / 184 / 1571	
Goodness-of-fit on F^2	1.037	
Final R indices [I>2sigma(I)]	R_1 = 0.0846, wR_2 = 0.2272	
R indices (all data)	R_1 = 0.0875, wR_2 = 0.2367	
Absolute structure parameter	0.59(5)	
Largest diff. peak and hole	0.598 and -0.305 e.Å^{-3}	

The cyclic structure of **14** represents a rare form of ring interlocking, in which each ring is interlocked with both the neighboring rings. This interlocking of rings in a closed three–link chain is similar to that in a cyclic [3]catenane – topological isomer of [3]catenane such that if any one ring is broken, the remaining two rings remain interlocked. Along with the intercycler NCIs arising from acceptor and donor moieties, the three rings are arranged such that the interlocking gives a closed–three link chain. Figure 4.23c and 4.23d shows the important intercycler NCIs responsible for the formation of thermodynamic stable product **14**. The framework is held together by multiple sandwich type π–π interactions between stacked rings, and CH–π interactions between donor's phenyl and acceptors naphthalene moieties. CH–π interactions in closed three–link chain were shorter (2.7–3.0 Å) as compared to π–π stacking of rings (3.7–4.0 Å). The π–stacking of rings was also observed by the ^{1}H–NMR spectra of **2** with upfield shifts of pyridyl protons as compared to donor **L6**. In addition, comparison between the ^{1}H NMR spectrum of **14** and macrocycle **13** (both recorded in CD_3OD) shows the upfield shifts for the pyridyl protons, which further highlights the occurrence of π–π stacking interactions. Although donor **L6** can adopt two extreme (*syn* and *anti*) conformations due to the rotation along the phenyl rings, it adopted a syn conformation with respect to pyridyl rings (Figure 4.23). *Syn* (136^{0}) conformation of **L6** in **14** maximizes intercycler NCIs between rings so that the closed three–link chain **14** is more stable than three monocycles with anti-conformation.

4.3.2. 2D NMR analysis and titration of monorectangle 1 and close three-link chain 14

The ^{1}H–NMR spectrum of **14** was found to be very complicated based on the orientation and geometry of the rings. In contrast to a 1D ^{1}H NMR, 2D NMR spectrum provides more detail about the structure. Therefore, 2D NMR analysis (DOSY, COSY, ROESY and HSQC) in methanol was carried out to identify the peaks corresponding to acceptors and donor moieties (Figures 4.24–4.27). Particularly, ^{1}H–^{13}C HSQC experiment plays an important role in the identification of the ^{1}H and the ^{13}C nuclei connected through direct C−H covalent bonds. Due to the large chemical shift range of ^{13}C nuclei the spectral overlap greatly reduces, and thus helps to identify the proton–bearing carbons and their relation with corresponding protons. In this light, ^{13}C peaks in compound **14** were identified using ^{1}H–^{13}C HSQC NMR, and thus peaks in ^{1}H–NMR spectra were labeled. As illustrated in figure 4.28, the ^{1}H–NMR, ^{1}H–DOSY and ^{1}H–^{13}C HSQC NMR spectra of **14** perfectly overlap, confirming its selective and quantitative synthesis.

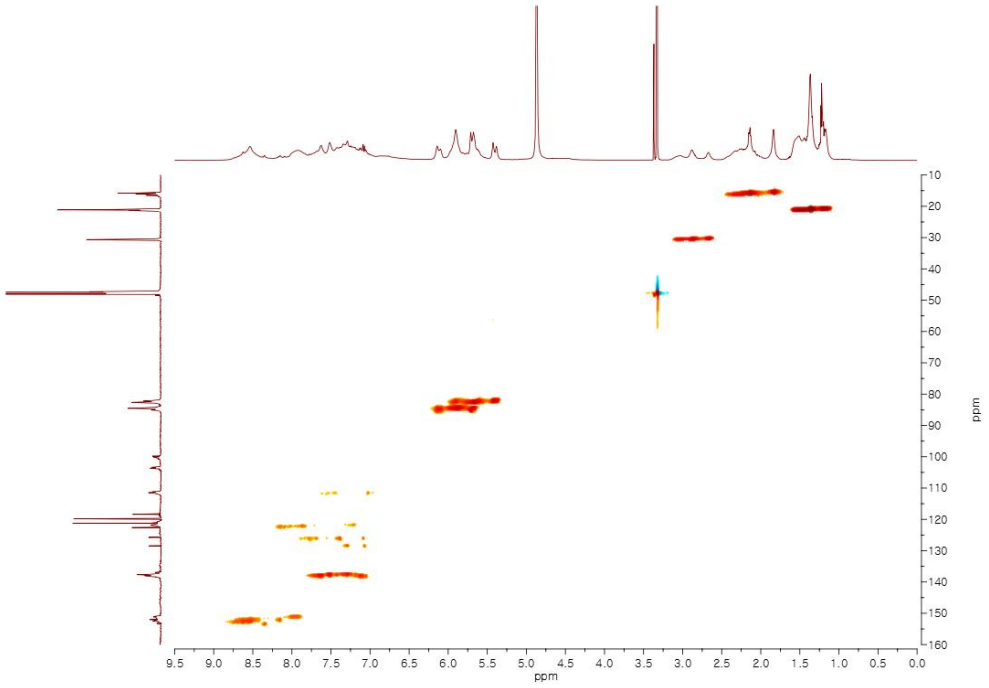

Figure 4.24 ^{1}H-^{13}C HSQC NMR spectrum of **14** (CD_3OD [20 mM], 298 K, 900 MHz)

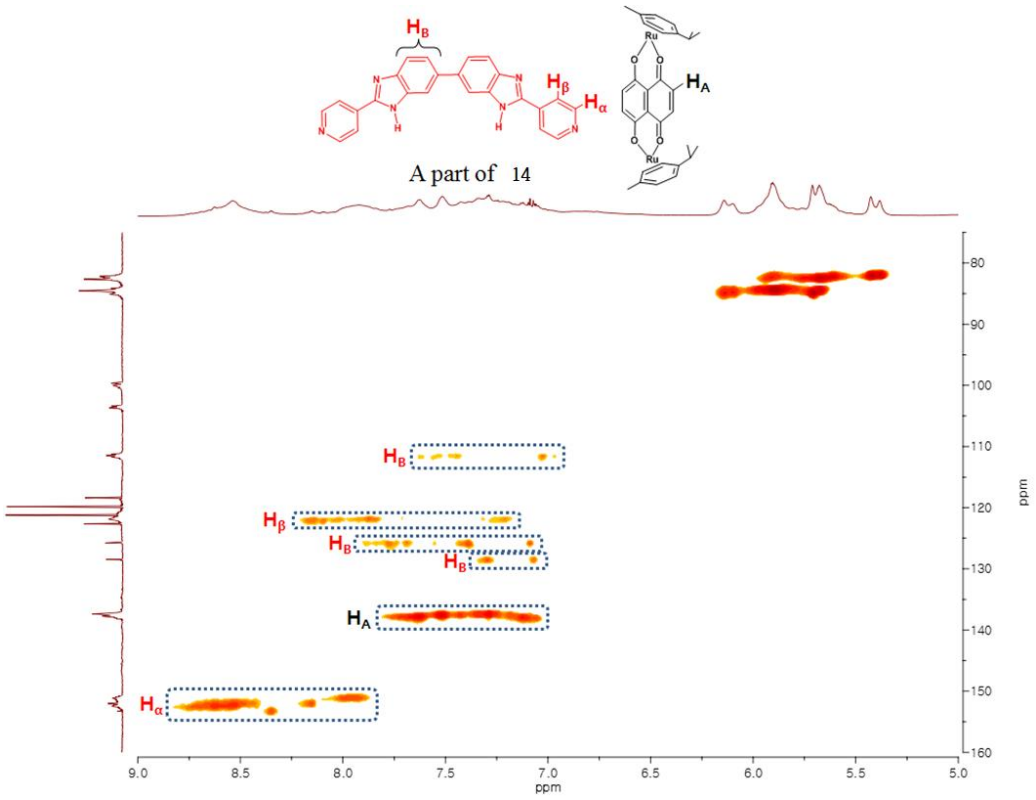

Figure 4.25 Expanded ^{1}H-^{13}C HSQC NMR spectrum of **14** (CD_3OD [20 mM], 298 K, 900 MHz)

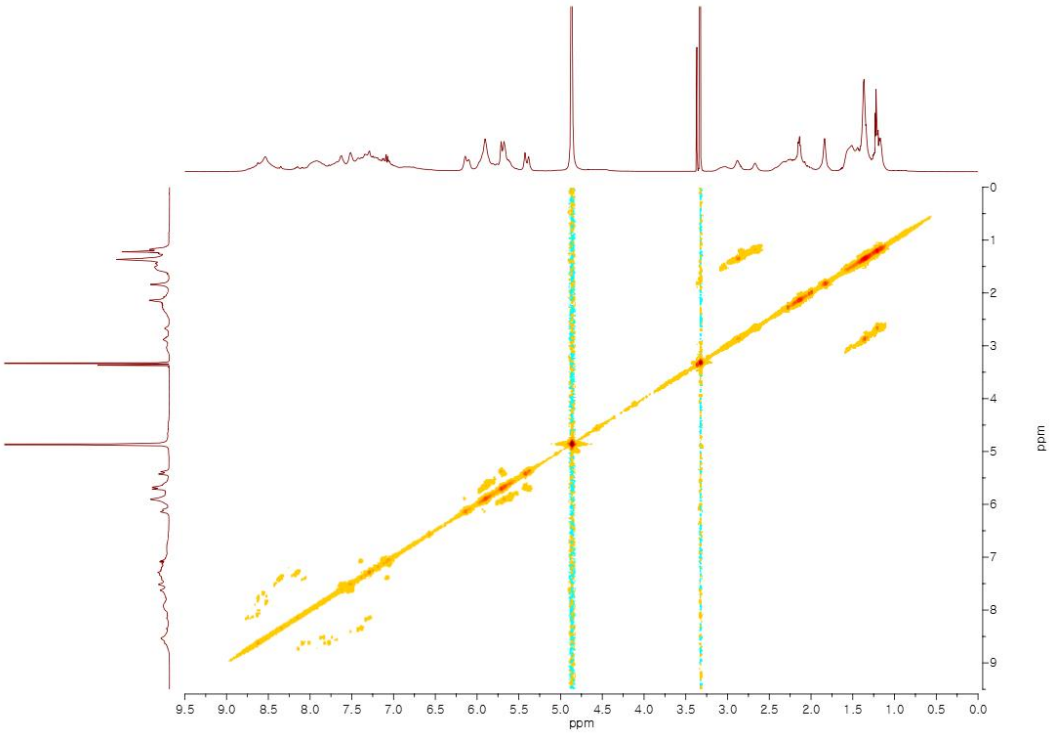

Figure 4.26 ^{1}H-^{1}H COSY NMR spectrum of **14** (CD_3OD [20 mM], 298 K, 900 MHz)

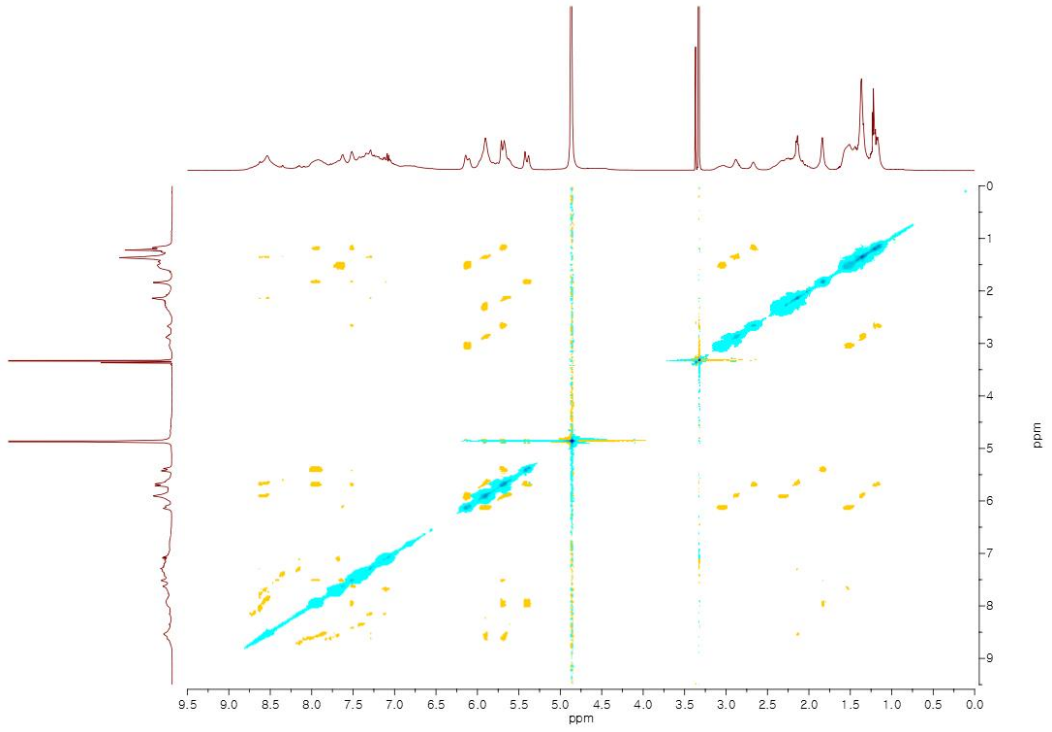

Figure 4.27 ^{1}H-^{1}H ROESY NMR spectrum of **14** (CD_3OD [20 mM], 298 K, 900 MHz)

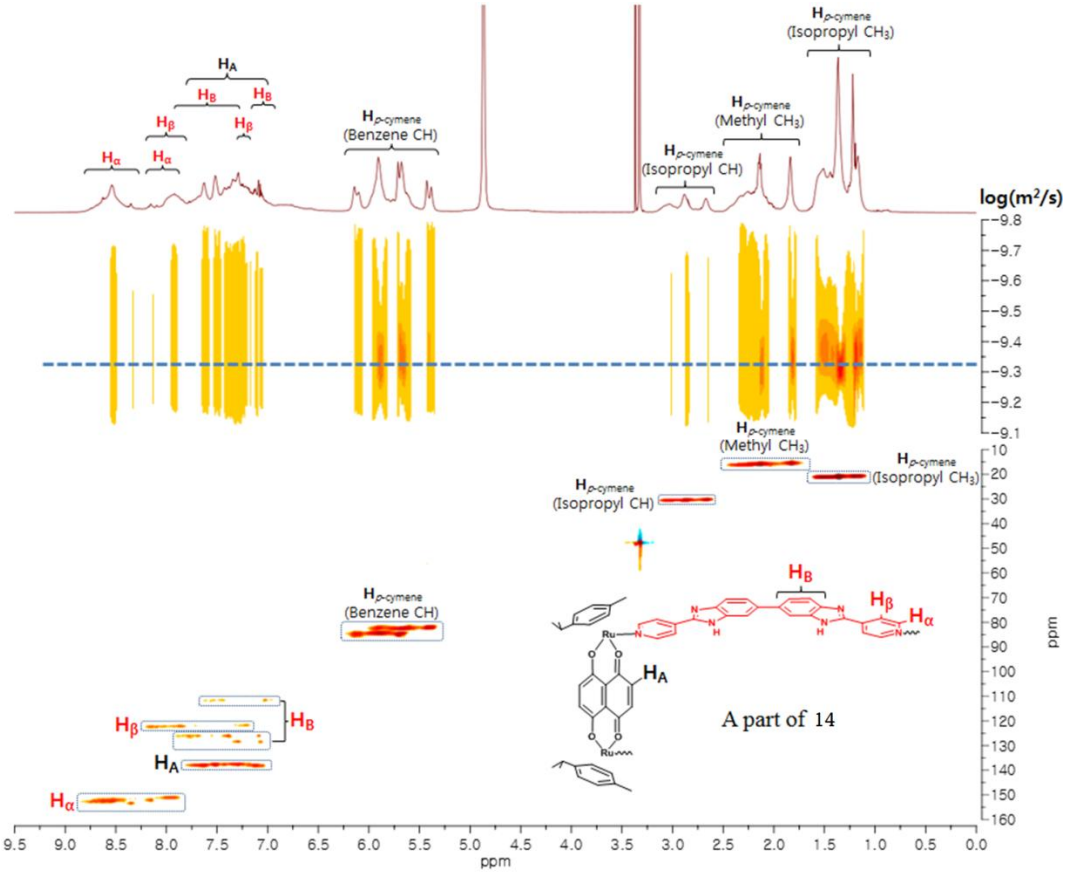

Figure 4.28 ^{1}H NMR, ^{1}H–DOSY and ^{1}H–^{13}C HSQC NMR spectra of **14** (CD_3OD [20 mM], 298 K, 900 MHz

Furthermore, 2D NMR analysis helped in establishing the solution-state structure of macrocycle **13**. In case of [2+2] macrocycle **13**, donor **L6** can adopt two extreme (*syn* and *anti*) conformations due to the rotation along the phenyl rings. In contrast, *anti*-conformation of donors in macrocycle **13** is more stable as revealed by ^{1}H-ROESY NMR analysis. (Figure 4.33 and 4.45)

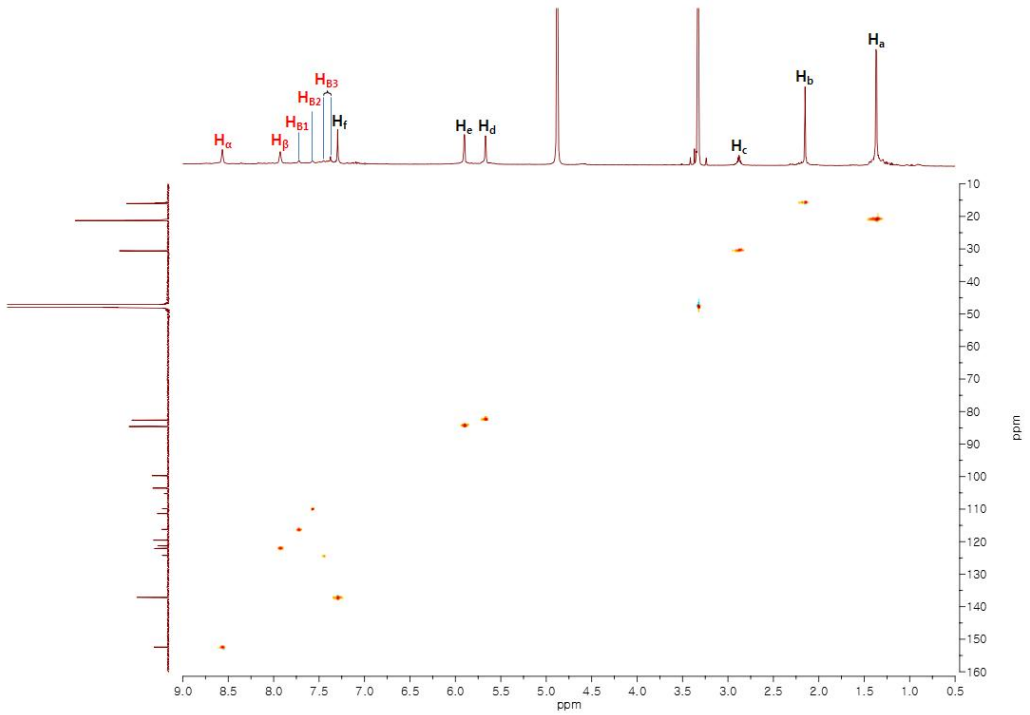

Figure 4.29 ^{1}H-^{13}C HSQC NMR spectrum of **13** (CD_3OD [1.0 mM], 298 K, 800 MHz)

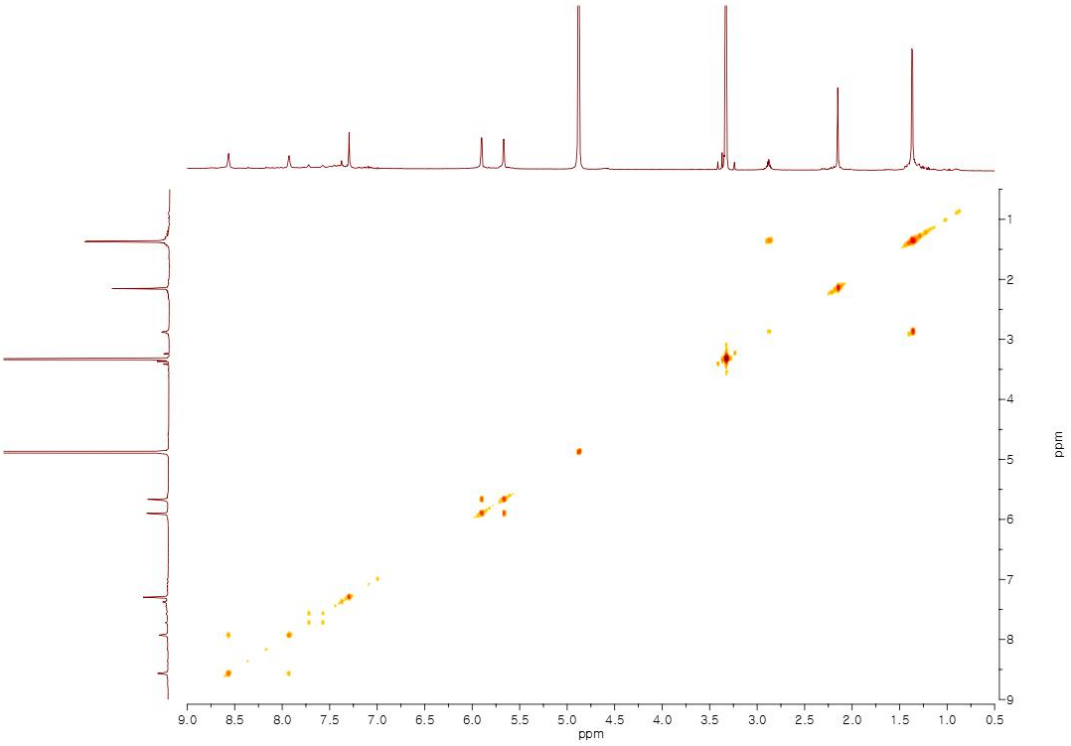

Figure 4.30 ^{1}H-^{1}H COSY NMR spectrum of **13** (CD_3OD [1.0 mM], 298 K, 800 MHz)

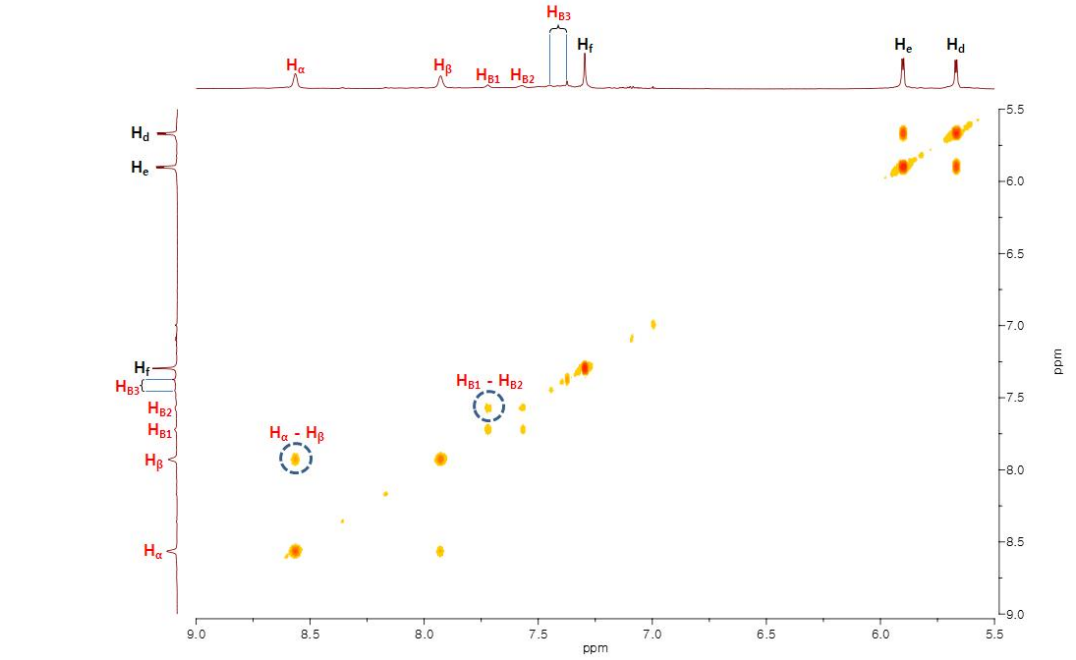

Figure 4.31 Expanded ^{1}H-^{1}H COSY NMR spectrum of **13** (CD_3OD [1.0 mM], 298 K, 800 MHz)

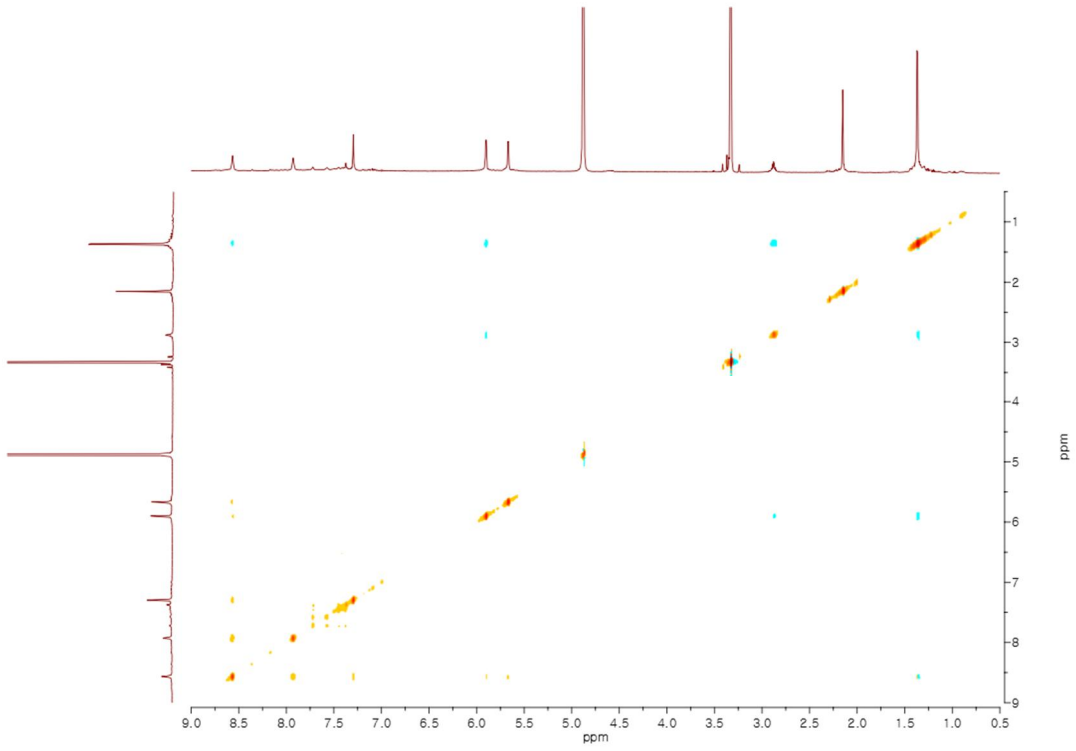

Figure 4.32 ^{1}H-^{1}H NOESY NMR spectrum of **13** (CD_3OD [1.0 mM], 298 K, 800 MHz)

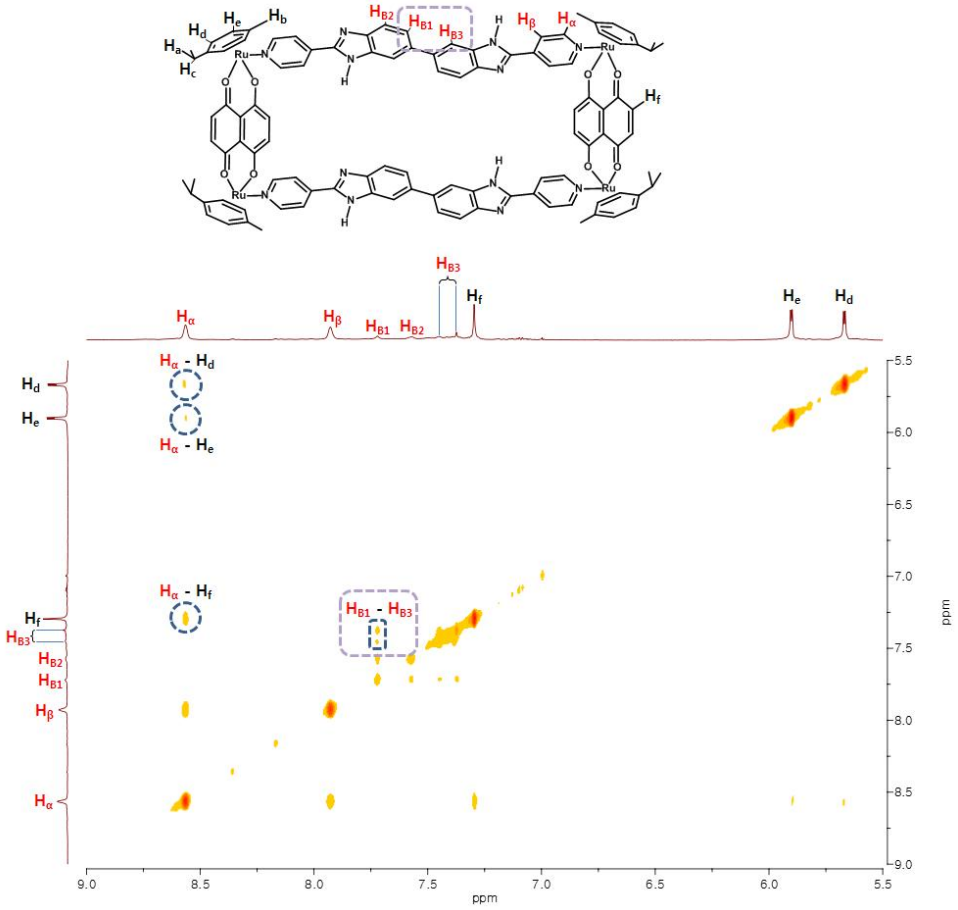

Figure 4.33 Expanded ^{1}H-^{1}H NOESY NMR spectrum of **13** (CD_3OD [1.0 mM], 298 K, 800 MHz)

Along with coordination–driven self–assembly and NCIs, solvent also plays a significant role in the thermodynamic stabilization of supramolecular topologies. According to our previous study, methanol is a better solvent than nitromethane for the formation of more complex topologies; however, the closed three–link chain **14** can be synthesized as a major product even in nitromethane (8.0 mM). Additionally, self-assembly reaction (8mM) in acetonitrile also resulted in the formation of $[2+2]_3$ product, as revealed by the ESI-MS analysis. Macrocycle **13** was formed prefer to **14** (mass ratio 66:39) only in *N*,*N*–dimethylforamide (8.0 mM) (Figures 4.34–4.35).

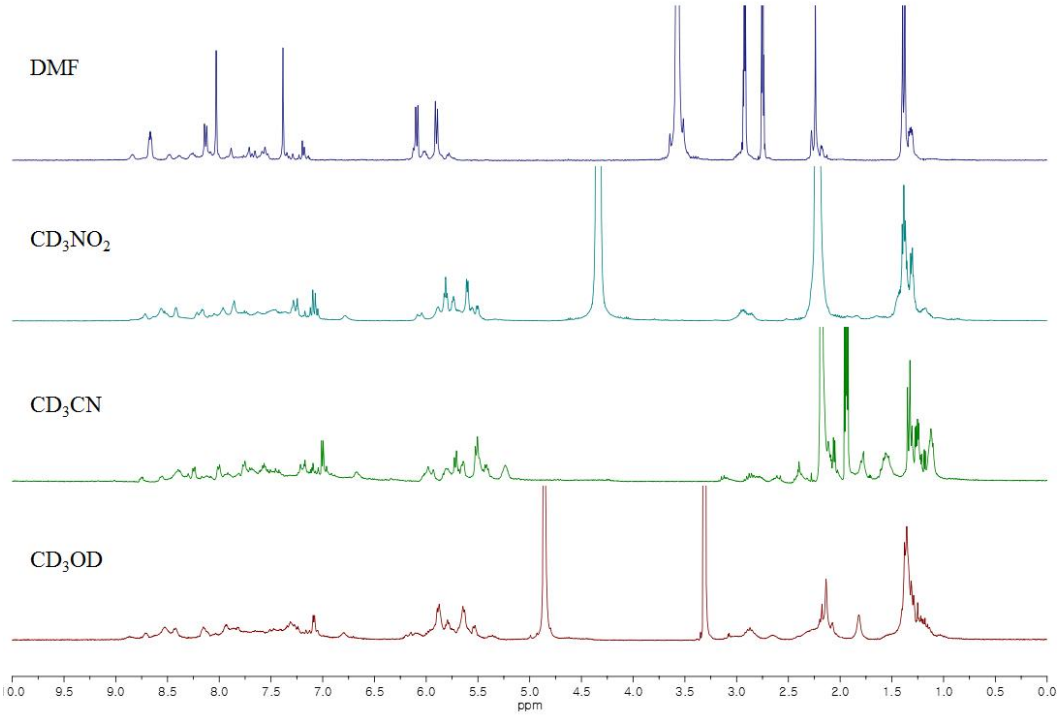

Figure 4.34 ^{1}H NMR spectra of mixture **13+14** ([8.0 mM], 300 MHz)

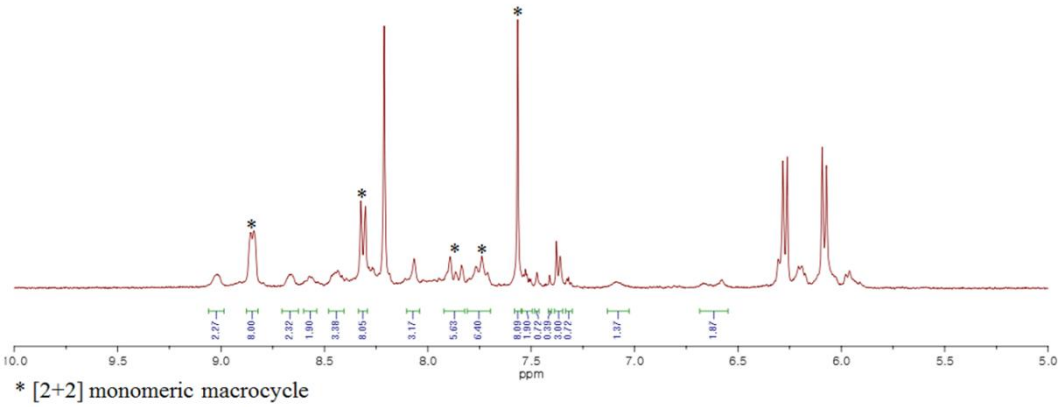

Figure 4.35 Expanded ^{1}H NMR spectra of mixture **13+14** (DMF-d_7 [8.0 mM], 300 MHz)

4.3.3. Other Ru(II) self-assemblies and titration of monorectangle 13 and close three-link chain 14

To further understand the role of intercycler NCIs, pyrene was added before and after the self–assembly reactions (8.0 mM) in methanol. Addition of two equivalents of π–electron rich pyrene prevented the formation of $[2+2]_3$ structure (Figures 4.36–4.39). As can be seen from Figure 4.37, increasing the equivalents of pyrene (0.5eq to 6.0 eq) gradually transformed of closed three–link chain **14** to rectangle **13**. Pyrene addition experiment highlights the importance of intercycler NCIs as it is stack between the two rings of [2+2] macrocycle and thus pyrene prevents the interlocking of rings (Figures 4.36–4.45). To probe the effect of functionalities present in **A7**, we turned our attention to the other Ru(II) acceptors [(*p*–cymene)$_2$Ru$_2$(OO∩OO)(OTf)$_2$] [OO∩OO = oxalate **A5**, 2,5–dihydroxy–1,4–benzoquinone **A6** and 6,11–dihydroxy–5,12–naphthacenedione **A8**]. Reaction of oxalate acceptor **A5** with **L6** result only in the isolation of [2+2] macrocycle (Figure 4.46-4.48), while acceptors **A6** and **A8** did not result in the isolation of any selective topology as reveled by ESI–MS.

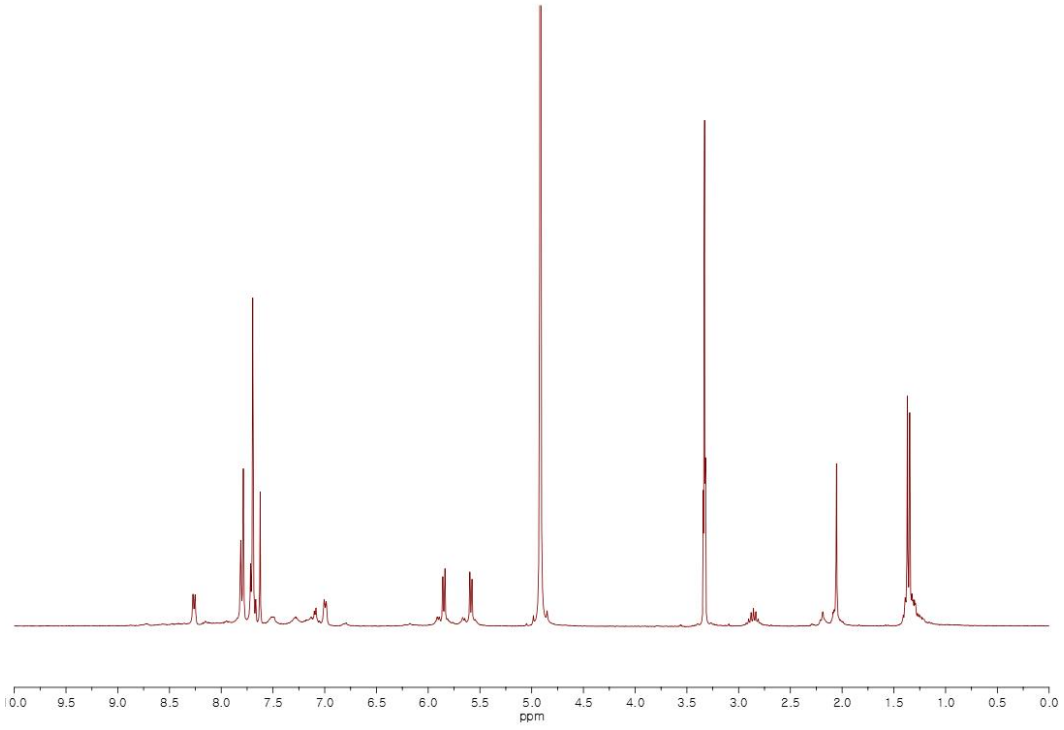

Figure 4.36 ^{1}H NMR spectrum showing formation of only **13** when reaction was carried out in the presence of pyrene (2.0 eq) (CD_3OD [8.0 mM], 300 MHz)

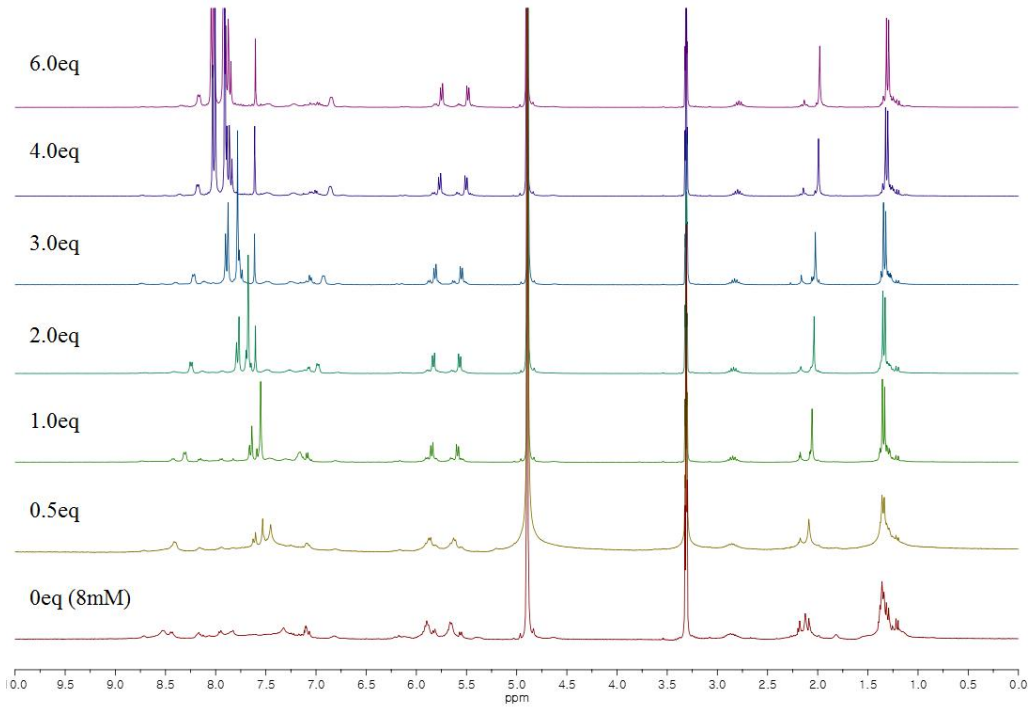

Figure 4.37 ^{1}H NMR spectra of mixture **13+14** showing increasing proportion of **13** upon addition of pyrene from 0 eq to 6.0 eq (CD_3OD [8.0 mM], 300 MHz)

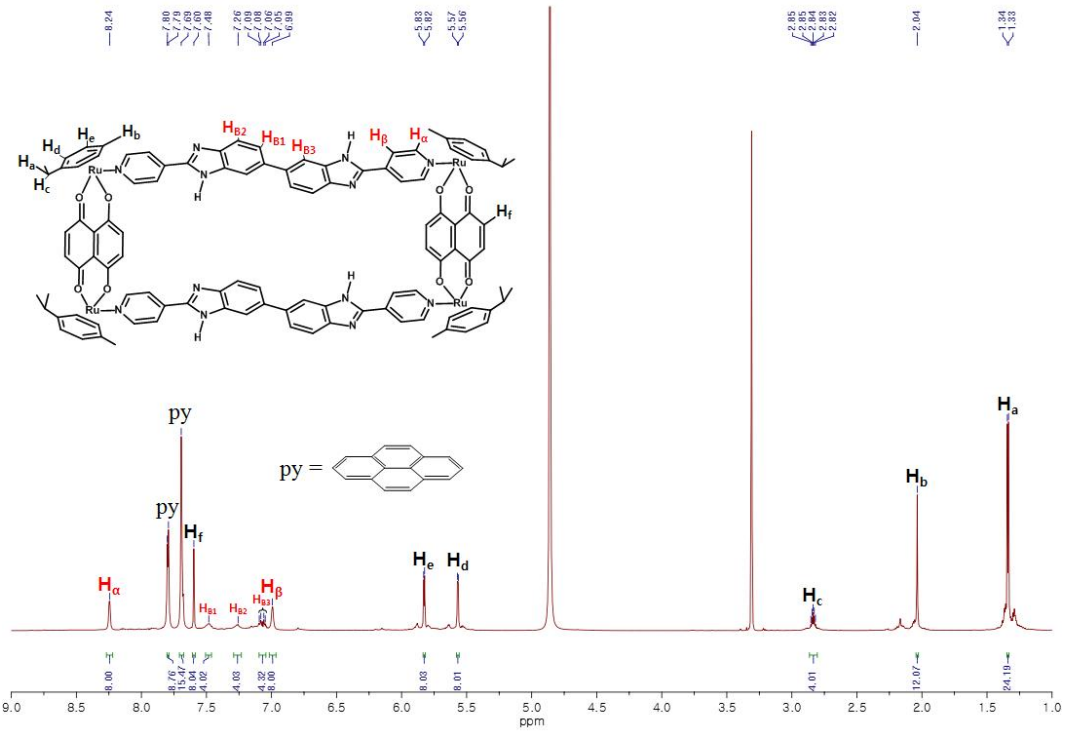

Figure 4.38 ^{1}H NMR spectrum of **13** with 2eq pyrene (CD_3OD [8.0 mM], 800 MHz)

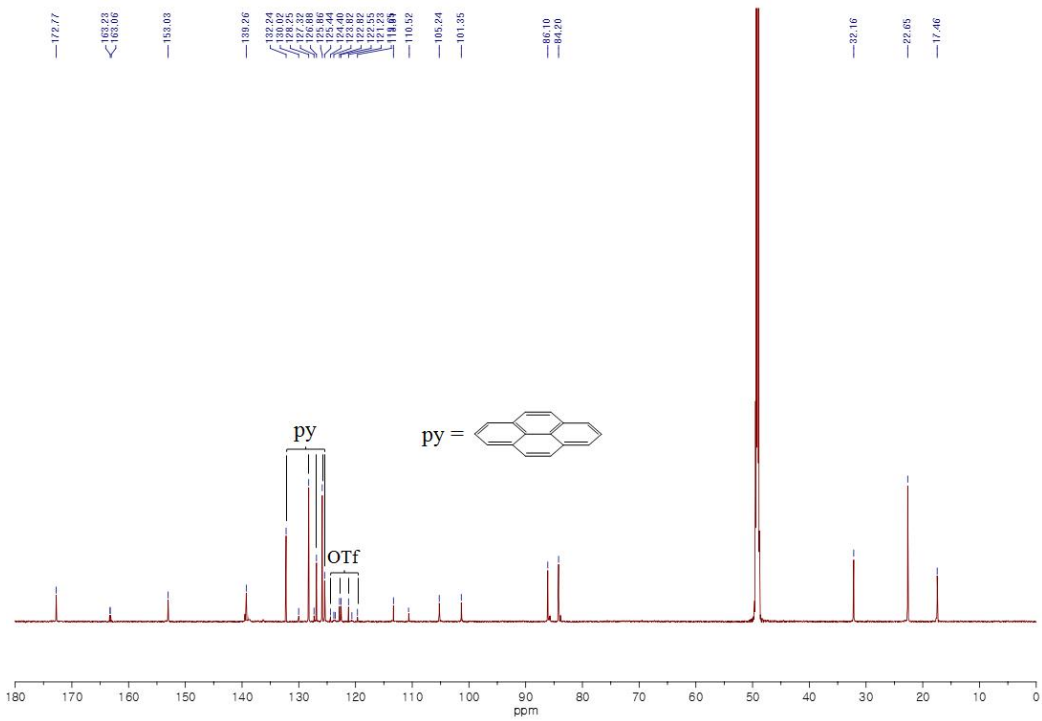

Figure 4.39 ^{13}C NMR spectrum of **13** with 2eq pyrene (CD_3OD [8.0 mM], 200 MHz)

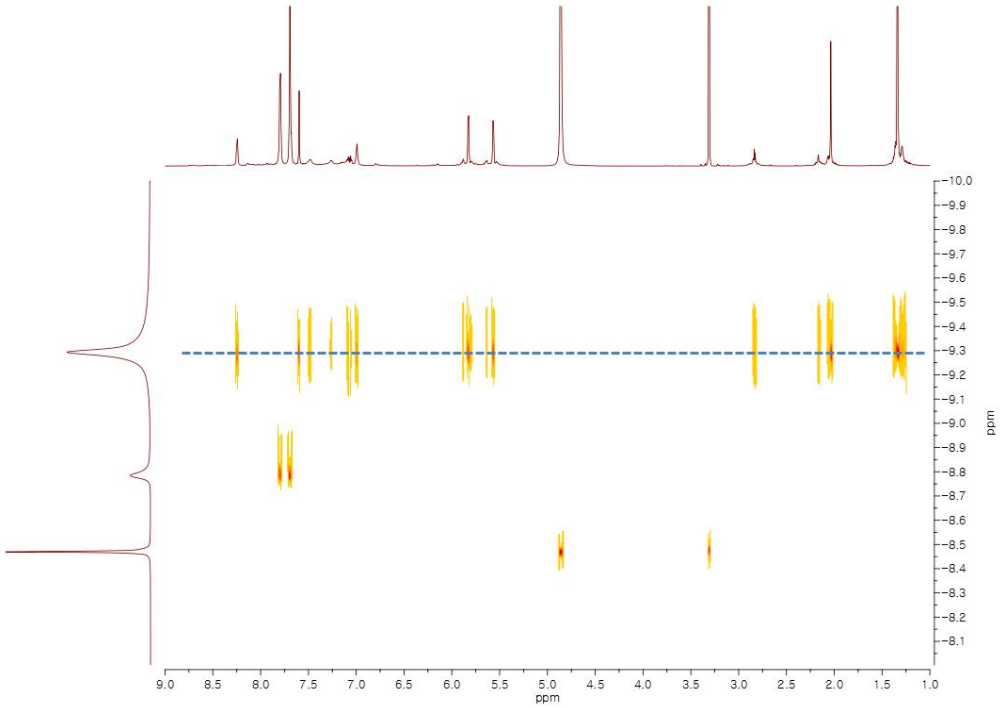

Figure 4.40 ^{1}H-DOSY NMR spectrum of **13** with 2eq pyrene (CD_3OD [8.0 mM], 298 K, 800 MHz)

Diffusion coefficient: 5.2×10^{-10} m^2/sec

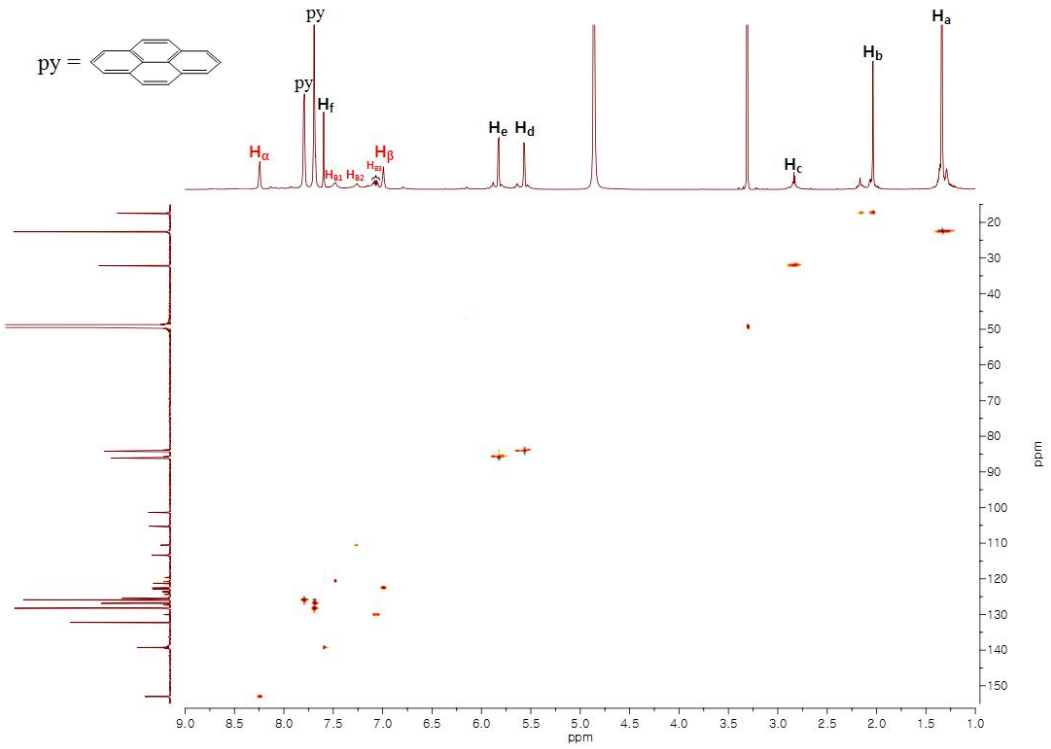

Figure 4.41 ^{1}H-^{13}C HSQC NMR spectrum of **13** with 2eq pyrene (CD_3OD [8.0 mM], 298 K, 800 MHz)

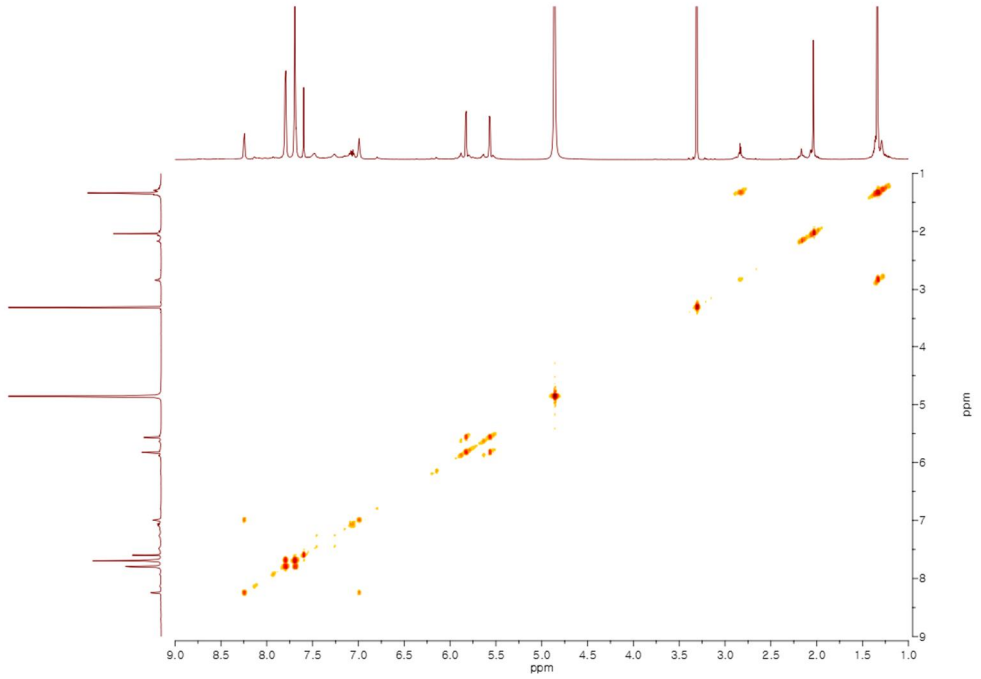

Figure 4.42 ^{1}H-^{1}H COSY NMR spectrum of **13** with 2eq pyrene (CD_3OD [8.0 mM], 298 K, 800 MHz)

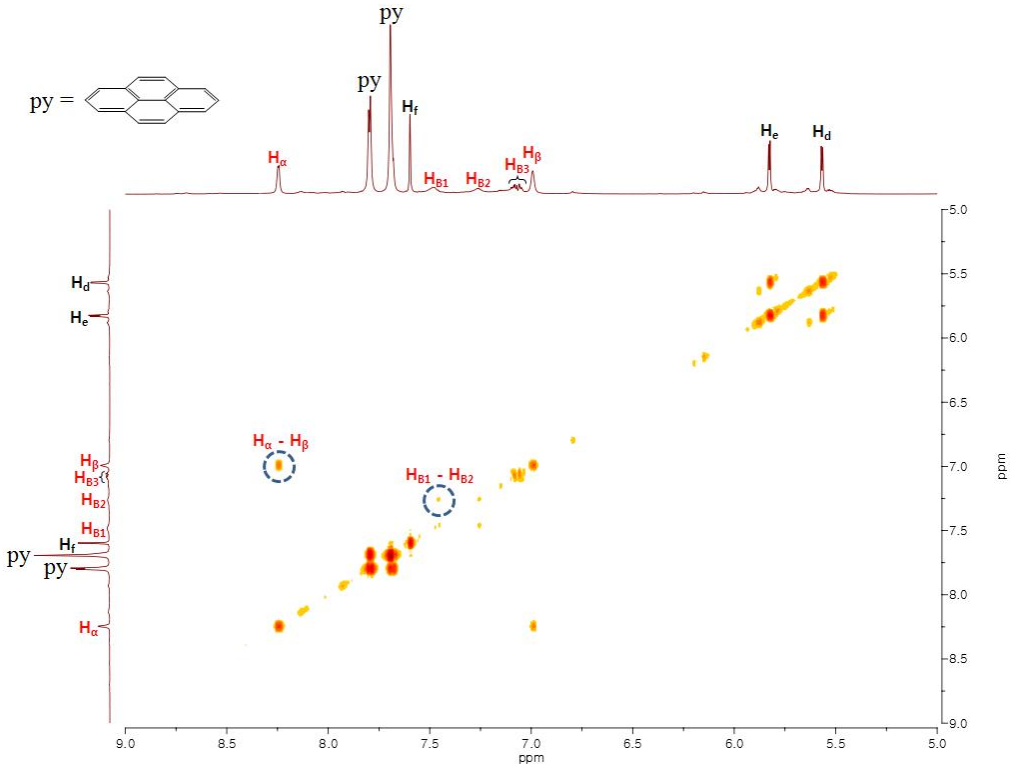

Figure 4.43 Expanded ^{1}H-^{1}H COSY NMR spectrum of **13** with 2eq pyrene (CD_3OD [8.0 mM], 298 K, 800 MHz)

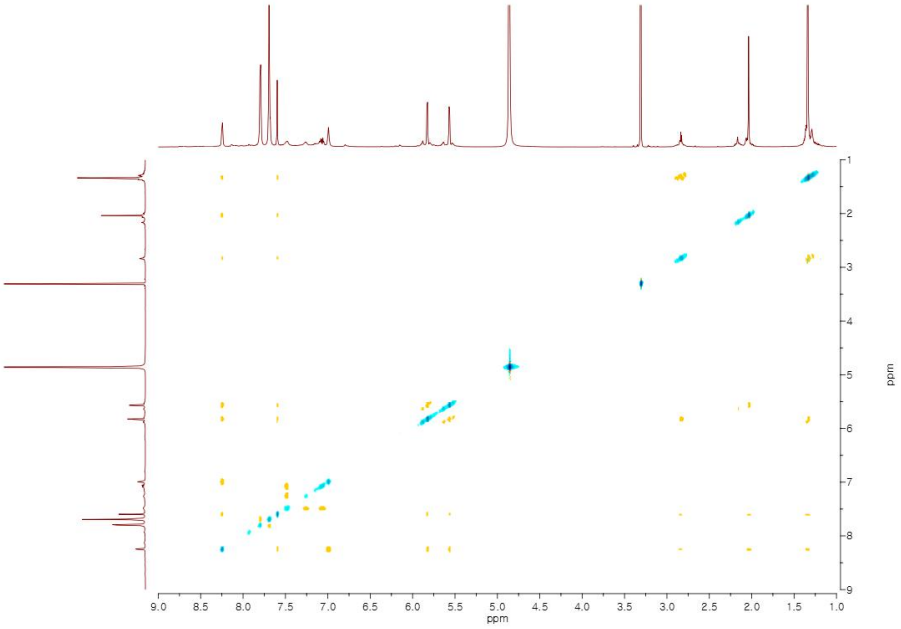

Figure 4.44 ^{1}H-^{1}H ROESY NMR spectrum of **13** with 2eq pyrene (CD_3OD [8.0 mM], 298 K, 800 MHz)

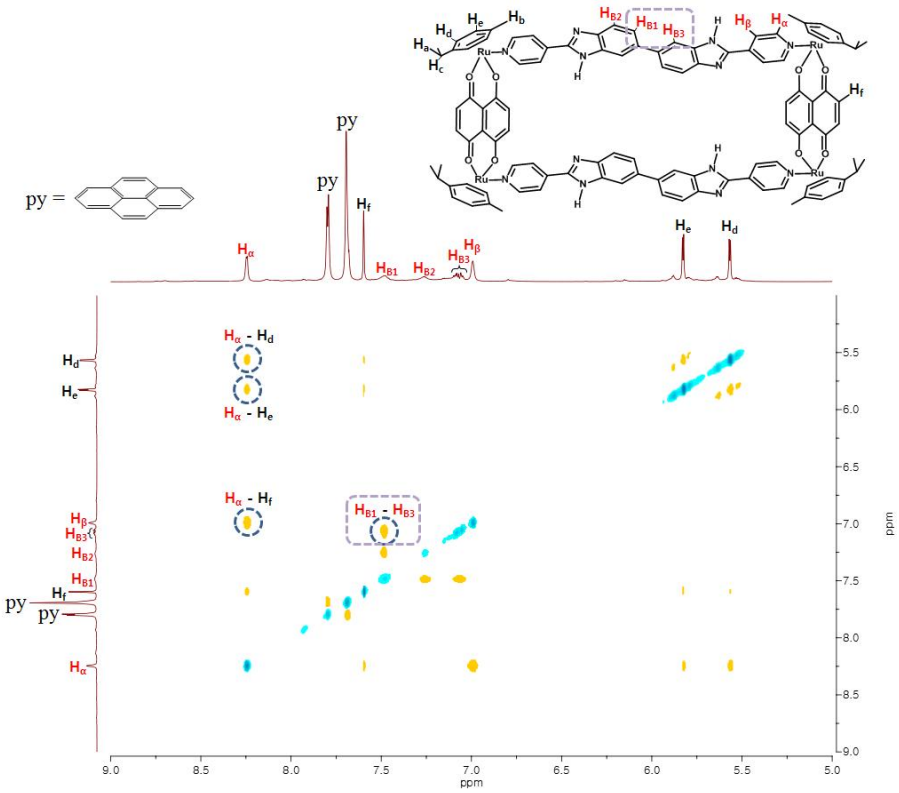

Figure 4.45 Expanded ^{1}H-^{1}H ROESY NMR spectrum of **13** with 2eq pyrene (CD_3OD [8.0 mM], 298 K, 800 MHz)

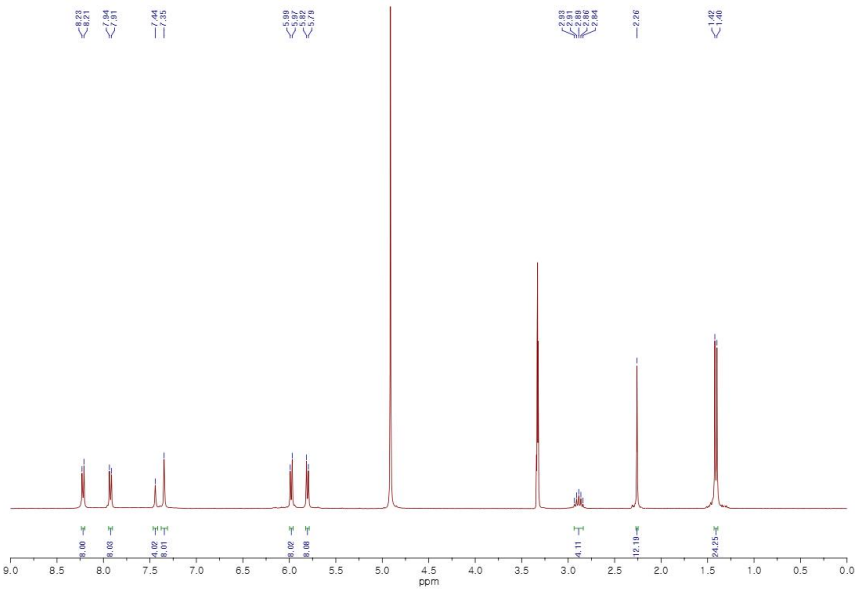

Figure 4.46 ^{1}H NMR spectrum of **15** (CD_3OD [8.0 mM], 300 MHz)

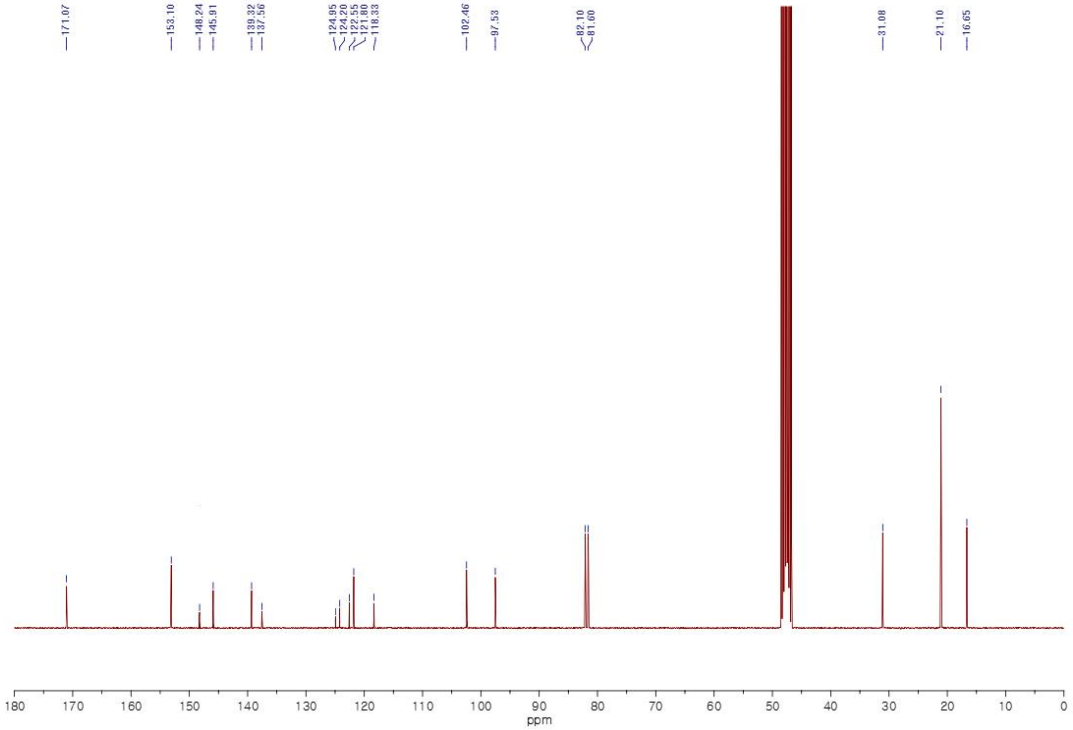

Figure 4.47 ^{13}C NMR spectrum of **15** (CD_3OD [8.0 mM], 75 MHz)

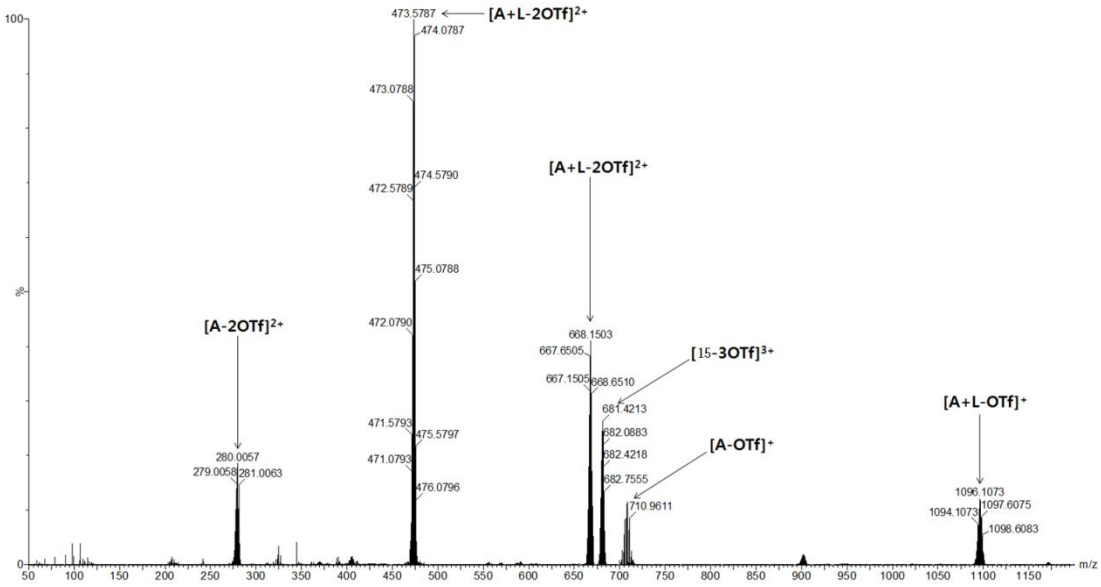

Figure 4.48 Full ESI mass spectrum of **15** (Reaction in CD_3OD [8.0 mM])

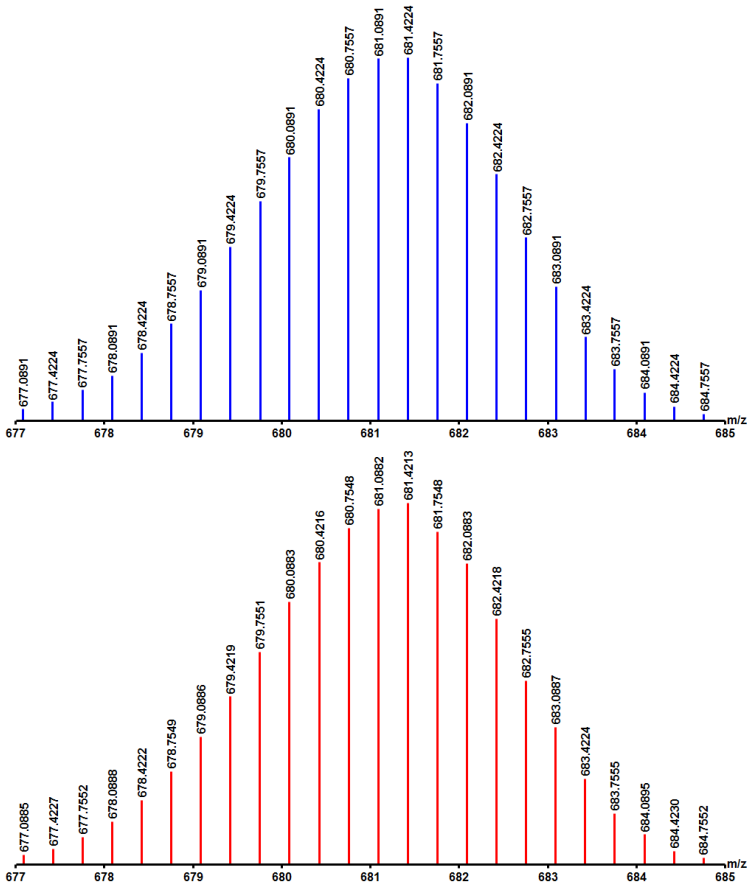

Figure 4.49 Calculated (blue) and experimental (red) ESI mass spectra of [**15**-3OTf]$^{3+}$. (Reaction in CD_3OD [8.0 mM])

4.4 Conclusions

This study synthesized a novel supramolecular topology of closed three–link chain through the coordination–driven self–assembly of two components. The self–assembly reaction between naphthalene–based acceptor **A7** and flexible benzimidazole–based donor **L6** allows the recognition of combining units through synergic NCIs, and thus results in the selective formation of the closed three–link chain **14**. The quantitative synthesis of **14** was achieved by 20 mM self–assembly reaction, while 1.0 mM reaction only resulted in the formation of the [2+2] rectangle **13**. Solvents such as nitromethane and acetonitrile were found to have no adverse effect on the formation of $[2+2]_3$ structure, which shows the thermodynamic stability of this framework. Addition of π–electron rich pyrene or self–assembly with shorter oxalate acceptor resulted in the isolation of [2+2] macrocycle **13**. Single–crystal X–ray diffraction analysis using synchrotron radiation was used to elucidate the topology of **14**–first ever reported structure of a closed three–link chain. Crystal structure reveals synergstic CH–π and π–π intercycler NCIs have major role in the selective and quantitaive formation of the closed three−link chain **14**. These results shows that the use of synergestic NCIs along with moderate flexibitiy of ligand is important and pivotal in the coordination−driven self–assembly for realizing complex and high–ordered supramolecular topologies.

4.5 References

1. (a) Sauvage, J. P.; Dietrich–Buchecker, C. Wiley–VCH Verlag GmbH **1999**. (b) Raymo, F. M.; Stoddart, J. F. *Chemical Reviews* **1999**, *99*, 1643−1663. (c) Stoddart, J. F. *Chemical Society Reviews* **2009**, *38*, 1802. (d) Gil-Ramírez, G.; Leigh, D. A.; Stephens, A. J. *Angewandte Chemie International Edition* **2015**, *54*, 6110–6150. (e) Forgan, R. S.; Sauvage, J.-P.; Stoddart, J. F. *Chemical Reviews* **2011**, *111*, 5434–5464. (f) Sauvage, J.-P. *Angewandte Chemie International Edition* **2017**, *56*, 11080–11093. (g) Fielden, S. D. P.; Leigh, D. A.; Woltering, S. L. *Angewandte Chemie International Edition* **2017**, *56*, 11166–11194.

2. (a) Raymo, F. M.; Stoddart, J. F. Wiley-VCH Verlag GmbH **2003**, 219–248. (b) Leigh, D. A.; Wong, J. K. Y.; Dehez, F.; Zerbetto, F. *Nature* **2003**, *424*, 174–179. (c) Meng, Z.; Han, Y.; Wang, L.-N.; Xiang, J.-F.; He, S.-G.; Chen, C.-F. *Journal of the American Chemical Society* **2015**, *137*, 9739–9745. (d) Gómez-López, M.; Preece, J. A.; Stoddart, J. F. *Nanotechnology* **1996**. (e) van Dongen, S. F. M.; Cantekin, S.; Elemans, J. A. A. W.; Rowan, A. E.; Nolte, R. J. M. *Chemical Society Reviews* **2014**, *43*, 99–122.

3. (a) Byrne, J. P.; Blasco, S.; Aletti, A. B.; Hessman, G.; Gunnlaugsson, T. *Angew. Chem., Int. Ed.,* **2016**, *55*, 8938–8943. (b) Ibukuro, F.; Fujita, M.; Yamaguchi, K.; Sauvage, J.-P. *Journal of the American Chemical Society* **1999**, *121*, 11014–11015. (c) West, K. R.; Ludlow, R. F.; Corbett, P. T.; Besenius, P.; Mansfeld, F. M.; Cormack, P. A. G.; Sherrington, D. C.; Goodman, J. M.; Stuart, M. C. A.; Otto, S. *Journal of the American Chemical Society* **2008**, *130*, 10834–10835.

4. (a) Nierengarten, J. F.; Dietrich-Buchecker, C. O.; Sauvage, J. P. *Journal of the American Chemical Society* **1994**, *116*, 375–376. (b) Westcott, A.; Fisher, J.; Harding, L. P.; Rizkallah, P.; Hardie, M. J. *Journal of the American Chemical*

Society **2008**, *130*, 2950–2951. (c) Sawada, T.; Yamagami, M.; Ohara, K.; Yamaguchi, K.; Fujita, M. *Angewandte Chemie International Edition* **2016**, *55*, 4519–4522. (d) Allen, C. D.; Link, A. J. *Journal of the American Chemical Society* **2016**, *138*, 14214–14217. (e) Wang, K.; Yee, C.-C.; Au-Yeung, H. Y. *Chemical Science* **2016**, *7*, 2787–2792. (f) Li, H.; Zhang, H.; Lammer, A. D.; Wang, M.; Li, X.; Lynch, V. M.; Sessler, J. L. *Nature Chemistry* **2015**, *7*, 1003–1008. (g) Fujita, M.; Fujita, N.; Ogura, K.; Yamaguchi, K. *Nature* **1999**, *400*, 52–55. (h) Hori, A.; Yamashita, K.; Kusukawa, T.; Akasaka, A.; Biradha, K.; Fujita, M. *Chemical Communications* **2004**, 16, 1798–1799.

5. (a) Beves, J. E.; Blight, B. A.; Campbell, C. J.; Leigh, D. A.; McBurney, R. T. *Angewandte Chemie International Edition* **2011**, *50*, 9260–9327. (b) Ayme, J. F.; Beves, J. E.; Campbell, C. J.; Leigh, D. A. *Chemical Society Reviews* **2013**, *42*, 1700-1712.

6. (a) Aricó, F.; Badjic, J. D.; Cantrill, S. J.; Flood, A. H.; Leung, K. C. F.; Liu, Y.; Stoddart, J. F. *Topics in Current Chemistry* **2005** 203–259. (b) Leung, K. C. F.; Aricó, F.; Cantrill, S. J.; Stoddart, J. F. *Journal of the American Chemical Society* **2005**, *127*, 5808-5810. (c) Griffiths, K. E.; Stoddart, J. F. *Pure and Applied Chemistry* **2008**, *80*, 485-506.

7. (a) Denis, M.; Goldup, S. M. *Nature Reviews Chemistry*. **2017**, *1*, 0061. (b) Crowley, J. D.; Goldup, S. M.; Lee, A. L.; Leigh, D. A.; McBurney, R. T. *Chemical Society Reviews*. **2009**, *38*, 1530-1541. (c) Aucagne, V.; Berná, J.; Crowley, J. D.; Goldup, S. M.; Hänni, K. D.; Leigh, D. A.; Lusby, P. J.; Ronaldson, V. E.; Slawin, A. M. Z.; Viterisi, A.; Walker DB. *Journal of the American Chemical Society* **2007**, *129*, 11950-11963. (d) Leigh, D. A.; Hanni, K. D. *Chemical Society Reviews* **2010**, *39*, 1240-1251. (e) Goldup, S. M.; Leigh, D. A.; Long, T.; McGonigal, P. R.; Symes, M. D.; Wu, J. *Journal of the American Chemical Society* **2009**, *131*, 15924-15929.

8. (a) Cougnon, F. B. L.; Jenkins, N. A.; Pantoş, G. D.; Sanders, J. K. M. *Angewandte Chemie International Edition* **2012**, *51*, 1443–1447. (b) Iwamoto, H.; Takizawa, W.; Itoh, K.; Hagiwara, T.; Tayama, E.; Hasegawa, E.; Haino, T. *The Journal of Organic Chemistry* **2013**, *78*, 5205–5217. (d) Hori, A.; Kumazawa, K.; Kusukawa, T.; Chand, D. K.; Fujita, M.; Sakamoto, S.; Yamaguchi, K. *Chemistry - A European Journal* **2001**, *7*, 4142–4149. (e) Ng, A. W. H.; Yee, C.-C.; Wang, K.; Au-Yeung, H. Y. *Beilstein Journal of Organic Chemistry* **2018**, *14*, 1846–1853. (f) Lincheneau, C.; Jean-Denis, B.; Gunnlaugsson, T. *Chemical Communications* **2014**, *50*, 2857-2860.

9. (a) Chichak, K. S. *Science (80-.)* **2004**, *304*, 1308–1312. (b) Cantrill, S. J.; Chichak, K. S.; Peters, A. J.; Stoddart, J. F. Nanoscale Borromean Rings. *Accounts of Chemical Research* **2005**, *38*, 1–9. (c) Mao, C.; Sun, W.; Seeman, N. C. *Nature* **1997**, *386*, 137–138. (d) Schalley, C. A. *Angewandte Chemie International Edition* **2004**, *43*, 4399–4401. (e) Meyer, C. D.; Forgan, R. S.; Chichak, K. S.; Peters, A. J.; Tangchaivang, N.; Cave, G. W. V.; Khan, S. I.; Cantrill, S. J.; Stoddart, J. F. *Chemistry - A European Journal* **2010**, *16*, 12570-12581. (f) Chichak, K. S.; Cantrill, S. J.; Stoddart, J. F. *Chemical Communications* **2005**, 27, 3391-3393.

10. (a) Wood, C. S.; Ronson, T. K.; Belenguer, A. M.; Holstein, J. J.; Nitschke, J. R. *Nature Chemistry* **2015**, *7*, 354–358. (b) Zhang, L.; Stephens, A. J.; Nussbaumer, A. L.; Lemonnier, J.-F.; Jurček, P.; Vitorica-Yrezabal, I. J.; Leigh, D. A. *Nature Chemistry* **2018**, *10*, 1083–1088.

11. Li, Q.; Wu, G.; Yang, Y.; An, R.; Li, J.; Liang, X.; Komiyama, M. *Chemical Communications* **2018**, *54*, 10156–10159.

12. (a) Zheng, Y.-R.; Yang, H.-B.; Ghosh, K.; Zhao, L.; Stang, P. J. *Chemistry - A European Journal* **2009**, *15*, 7203–7214. (b) Northrop, B. H.; Zheng, Y. R.; Ki-Whan, C. H. I.; Stang, P. J. *Accounts of Chemical Research* **2009**, *42*,

1554-1563. (c) Cook, T. R.; Stang, P. J. *Chemical Reviews* **2015**, *115*, 7001–7045. (d) Datta, S.; Saha, M. L.; Stang, P. J. *Accounts of Chemical Research* **2018**, *51*, 2047–2063. (e) Chakrabarty, R.; Mukherjee, P. S.; Stang, P. J. *Chemical Reviews* **2011**, *111*, 6810-6918. (f) Zheng, Y.-R.; Yang, H.-B.; Ghosh, K.; Zhao, L.; Stang, P. J. *Chemistry - A European Journal* **2009**, *15*, 7203–7214. (g) Singh, N.; Singh, J.; Kim, D.; Kim, D. H.; Kim, E. H.; Lah, M. S.; Chi, K. W. *Inorganic Chemistry* **2018**, *57*, 3521-3528.

13. (a) Acharyya, K.; Bhattacharyya, S.; Sepehrpour, H.; Chakraborty, S.; Lu, S.; Shi, B.; Li, X.; Mukherjee, P. S.; Stang, P. J. *Journal of the American Chemical Society* **2019**, *141*, 14565-14569. (b) Chang, X.; Zhou, Z.; Shang, C.; Wang, G.; Wang, Z.; Qi, Y.; Li, Z. Y.; Wang, H.; Cao, L.; Li, X.; et al. *Journal of the American Chemical Society* **2019**, *141*, 1757-1765. (c) Saha, R.; Devaraj, A.; Bhattacharyya, S.; Das, S.; Zangrando, E.; Mukherjee, P. S. *Journal of the American Chemical Society* **2019**, *141*, 8638–8645. (d) Howlader, P.; Mondal, B.; Purba, P. C.; Zangrando, E.; Mukherjee, P. S. *Journal of the American Chemical Society* **2018**, *140*, 7952-7960. (e) Li, S.; Huang, J.; Zhou, F.; Cook, T. R.; Yan, X.; Ye, Y.; Zhu, B.; Zheng, B.; Stang, P. J. *Journal of the American Chemical Society* **2014**, *136*, 5908–5911. (f) Yan, X.; Wang, M.; Cook, T. R.; Zhang, M.; Saha, M. L.; Zhou, Z.; Li, X.; Huang, F.; Stang, P. J. *Journal of the American Chemical Society* **2016**, *138*, 4580-4588.

14. (a) Neel, A. J.; Hilton, M. J.; Sigman, M. S.; Toste, F. D. *Nature* **2017**, *543*, 637-646. (b) Černý, J.; Hobza, P. *Physical Chemistry Chemical Physics*. **2007**, *9*, 5291-5303. (c) Waters, M. L. Aromatic Interactions. *Accounts of Chemical Research* **2013**, *46*, 873–873. (d) Claessens, C. G.; Stoddart, J. F. *Journal of Physical Organic Chemistry*. **1997**, *10*, 254-272. (e) Raynal, M.; Ballester, P.; Vidal-Ferran, A.; Van Leeuwen, P. W. N. M. *Chemical Society Reviews* **2014**, *43*, 1660-1733.

15. (a) Huang, S.-L.; Lin, Y.-J.; Li, Z.-H.; Jin, G.-X. *Angewandte Chemie International Edition* 2014, *53*, 11218–11222. (b) Lu, Y.; Zhang, H.-N.; Jin, G.-X. *Accounts of Chemical Research* **2018**, *51*, 2148–2158.

16. (a) Kim, T.; Singh, N.; Oh, J.; Kim, E.-H.; Jung, J.; Kim, H.; Chi, K.-W. *Journal of the American Chemical Society* **2016**, *138*, 8368–8371. (b) Song, Y. H.; Singh, N.; Jung, J.; Kim, H.; Kim, E.-H.; Cheong, H.-K.; Kim, Y.; Chi, K.-W. *Angewandte Chemie International Edition* **2016**, *55*, 2007–2011. (c) Lee, H.; Elumalai, P.; Singh, N.; Kim, H.; Lee, S. U.; Chi, K.-W. *Journal of the American Chemical Society* **2015**, *137*, 4674–4677 (d) Jo, J.-H.; Singh, N.; Kim, D.; Cho, S. M.; Mishra, A.; Kim, H.; Kang, S. C.; Chi, K.-W. *Inorganic Chemistry* **2017**, *56*, 8430–8438. (e) Shan, W.-L.; Lin, Y.-J.; Hahn, F. E.; Jin, G.-X. *Angewandte Chemie International Edition* **2019**, *58*, 5882–5886. (f) Li, S.; Huang, J.; Cook, T. R.; Pollock, J. B.; Kim, H.; Chi, K.-W.; Stang, P. J. *Journal of the American Chemical Society* **2013**, *135*, 2084–2087. (g) Guo, B.; Lin, Y.; Jin, G. *Chemistry - A European Journal* **2019**, *25*, 9721–9727. (h) Vajpayee, V.; Song, Y. H.; Cook, T. R.; Kim, H.; Lee, Y.; Stang, P. J.; Chi, K.-W. *Journal of the American Chemical Society* **2011**, *133*, 19646–19649. (i) Dang, L.-L.; Sun, Z.-B.; Shan, W.-L.; Lin, Y.-J.; Li, Z.-H.; Jin, G.-X. *Nature Chemistry* **2019**, *10*, 2057. (j) Kim, D. H.; Singh, N.; Oh, J.; Kim, E.-H.; Jung, J.; Kim, H.; Chi, K.-W. *Angewandte Chemie International Edition* **2018**, *57*, 5669–5673.

17. Singh, J.; Kim, D. H.; Kim, E.-H.; Singh, N.; Kim, H.; Hadiputra, R.; Jung, J.; Chi, K.-W. *Chem. Commun.* **2019**, *55*, 6866–6869.

18. Singh, M. P.; Sasmal, S.; Lu, W.; Chatterjee, M. N. *Synthesis (Stuttg).* **2000**, *2000*, 1380–1390.

19. Barry, N. P. E.; Furrer, J.; Therrien, B. *Helvetica Chimica Acta* **2010**, *93*, 1313–1328.

20. Sheldrick G. M. *Acta Crystallographica Section A Foundations of Crystallography* **2008**; A64:112–122.

21. (a) Speck, A. L. *Acta Crystallographica Section A Foundations of Crystallography* **2009**; D65:148–155. (b) Speck, A. L. *Acta Crystallographica Section A Foundations of Crystallography* **1990**; A46:194-201.